ANALYSIS AND DESIGN OF MASTER-SLAVE TELEOPERATION SYSTEMS(Dissertation_全文)

AUTHOR(S):

Yokokohji, Yasuyoshi

ANALYSIS AND DESIGN OF MASTER-SLAVE TELEOPERATION SYSTEMS

Yasuyoshi YOKOKOHJI

MAY 1991

ANALYSIS AND DESIGN OF MASTER-SLAVE TELEOPERATION SYSTEMS

Yasuyoshi YOKOKOHJI

MAY 1991

Abstract

In this paper, the analysis and design of master-slave teleoperation systems are discussed in order to build a superior master-slave system that can provide good maneuverability.

This paper consists mainly of two parts. In the first part, chapters 2 through 6, analysis and design of master-slave systems are discussed. In chapter 2, maneuverability of master-slave teleoperation systems is discussed, and new control schemes are proposed in chapter 3 in a simple one degree-of-freedom (DOF) case. Chapters 4 and 5 concern design of master-slave systems in the multiple DOF case. In chapter 4, a guide for designing master arms is proposed. Then, the control schemes proposed in chapter 3 are extended to the multiple DOF case in chapter 5. Chapter 6 shows experimental results using a designed master-slave system.

In the analysis of master-slave systems, it was found that compensation of dynamics of both the master arm and the slave arm is important to obtain good maneuverability. Since there is no specific desired trajectory in teleoperation, off-line computing of the arm dynamics is impossible and on-line compensation of dynamics is required. Concerning the multiple DOF case, the on-line compensation of arm dynamics becomes difficult because dynamics of multi-link mechanisms is complex. From the viewpoint of the mechanism, master and slave arms are equivalent to robot manipulators. Therefore, efficient computations of manipulator kinematics and dynamics for trajectory control are discussed in the second part, chapters 7 through 9. In chapter 7, efficient computational algorithms for kinematics and dynamics of robot manipulators are proposed. In chapter 8, application of DSP (Digital Signal Processor) to real time computation for dynamic control of robot manipulators is discussed. In chapter 9, link coordinate frame assignment for serial link manipulators is discussed for improving the computational efficiency.

Teleoperation is a very important approach to perform complicated task in ill-arranged environments. The result of this paper is applicable to improving the performance of current teleoperation systems and will also be useful for future telerobot systems.

ACKNOWLEDGMENT

I wish to express my gratitude to Professor Tsuneo Yoshikawa for his patient guidance and constant encouragement throughout this work. His valuable advice and detailed criticism have enabled me to complete this thesis.

I would also like to express my gratitude to Professor Hideo Hanafusa for his encouragement of my study at the Automation Research Laboratory, Kyoto University. His guidance had directed my research area to the field of robotics.

I also wish to my gratitude to Dr. Yoshihiko Nakamura for his valuable guidance and stimulating discussions at the Automation Research Laboratory.

I also wish to thank Dr. Toshiharu Sugie for his useful advice and discussions.

I would like to thank all members of the laboratory, especially Mr. Yasunao Okazaki and Mr. Kuniaki Hosohara for their helpful assistance to build up the experimental system and Mr. Hitoshi Hasunuma for his helpful and great assistance in the experiments.

Finally, I am grateful to my wife Mariko and to my parents Shigeki and Taeko Yokokohji for their support and encouragement.

Contents

ANALYSIS AND DESIGN OF MASTER-SLAVE TELEOPERATION SYSTEMS

Chapter 1

INTRODUCTION

1.1 Teleoperation and Robotics

"Teleoperation" is an indirect operation by a human operator in hazardous environments such as nuclear power plants, the bottom of the sea, and space where human operators cannot perform tasks directly. Instead of direct operation, the operator maneuvers a remote manipulator placed at a remote site.

The idea of teleoperation concept dates back to the 1940s when master-slave manipulators were designed at the Argonne National Laboratory to handle radioactive materials in hot-cells. *Master-slave manipulator* is a mechanism consisting of two arms. The operator can command the motion of the remote manipulator (called the *slave arm*) by moving the tip of an arm-shaped control device (called the *master arm*). The social needs such that the human operations in the extreme environments should be avoided are expanding year by year. For example, very recently, a manipulator mounted on the Space Shuttle played a significant role in the activities in space. This arm is controlled by an astronaut using joy-sticks inside the Shuttle[1].

On the other hand, "robotics" deals with the science of robots. A "robot" is a human-like mechanism controlled by computers which can

[1]Someone may insist that this kind of operation cannot be called "teleoperation", since the operator is located very close to the environment where the task is performed. In this paper, the author will classify this kind of situation as teleoperation because the operator cannot directly access the environment.

execute tasks automatically *without human intervention.* The idea of industrial robots come from the concept of "programmable artificial transfer" originally proposed by Devol in 1954. MH-1 is the first robot used for research and was developed by Ernst at MIT in 1961. The appearances of these robots were just like manipulators used for teleoperation, because robotics research was mainly focused on the manipulation area. Actually, the mechanical part of MH-1 was a slave manipulator and the master arm was replaced by a computer. In this sense, teleoperation is the origin of robotics[2].

Currently, the autonomy of robots is still poor. But they can work well enough in an arranged environment such as factories using a poor autonomy or sometimes without autonomy (teaching playback type). On the other hand, tasks in uncertain environments, such as a hazardous environment, requires a high level of perception, planning, and action, and it would be very difficult for autonomous robots to do such tasks using current technology. Teleoperation can be regarded as the replacement of the functions, perception, planning, and action, by humans normally performed by robots. **Fig.1.1** shows the prototype of a maintenance robot used in nuclear power plants and developed by a consortium of Japanese companies in the large-scale national R & D project "Advanced Robot Technology" promoted by the Agency of Industrial Science and Technology, Ministry of International Trade and Industry. In this case, the most complicated tasks such as the loosening of bolts of a valve unit are performed by master-slave type teleoperation. At the current stage, teleoperation replaces the use of robots which still have poor autonomous functions.

From a practical point of view, teleoperation is much more useful than robots in many situations. However, teleoperations have a serious short coming, that is, an operator is always necessary. Long operation time places a burden on the operator, especially simple iterative tasks cause a great deal of stress. *Telerobotics* is a new approach to overcome this problem by combining robotics technology and teleoperation. In the telerobotics approach, the operator and the robot working together improve upon the weak points and perform very complicated tasks.

[2]The development of electrically driven human limb prostheses started at the end of the 1940s is another important origin of robotics.

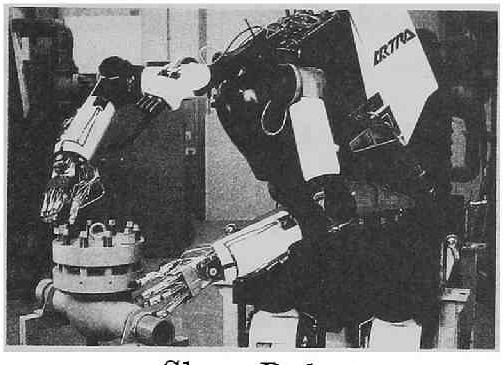

Slave Robot

Master Console

Figure 1.1: Maintenance robot for nuclear power plant: Large-scale National R & D Project "Advanced Robot Technology" promoted by the Agency of Industrial Science and Technology, Ministry of International Trade and Industry, Japan[1]

As mentioned above, teleoperation and robotics are closely related, and teleoperation was the origin of past robots; teleoperation is a substitution of robots; teleoperation will still be an important aspect to be fused with robotics (telerobotics) in the future.

1.2 Background of Teleoperation

1.2.1 History of Teleoperation

The needs of teleoperation was due to the handling of radioactive materials in hot-cells in the 1940s. At the beginning, the operator must command each joint movement of the remote manipulator by on/off switches for the motion at each joint. However, this kind of remote manipulator was very difficult for precise operations or compliant motions. The first master-slave manipulator was developed at the Argonne National Laboratory in 1949 by Geortz[24, 26, 29]. This manipulator could be used for many tasks in the hot cells as a general purpose manipulator. A slave manipulator in the hot cell was mechanically linked to a master arm, located at a safe site, by metal tapes and wires at each corresponding joint. This mechanical linkage not only enables the operator to transmit motion from the master arm to the slave arm, but also allows force reflections from the slave arm. However, this mechanical linkage was restricted by workspace and payload.

In 1954, Geortz developed the servo-type master-slave manipulator where the mechanical linkage was replaced by electric motors with servo-mechanisms[27, 28, 30]. The servo-type manipulator have no restriction of the distance, and the slave arm can be mounted on a moving table that allows the arm to access a wider area. Servo-mechanisms also enable the handling of much heavier objects or very precise positioning by changing the position or force scales between the master and slave.

In the 1960s, applications of teleoperation became great. For example, a manipulator and a video camera were attached to submarines for deep sea explorations. One of the famous examples is the CURV (cable-controlled underwater research vehicle) developed by the U.S. Navy. Space application had also started at the 1960s. The surveyor project of the U.S. is an example. Time delay problems appeared in

full relief throughout of the space applications, and the concept of supervisory control was proposed.

Currently, technology levels of computers, sensors, and actuators have been improved considerably. The applications for teleoperation, especially using the master-slave manipulator, are increasing in various situations such as nuclear power plants, maintenance of high voltage electric power supply lines, micro surgery, fire fighting, etc.[77]. But the basic technique is almost the same as that in the 1950's. In a sense, it is very surprising.

1.2.2 Several Topics of Teleoperation

Bilateral Servo

In the unilateral servo, where the actuators are mounted only at the slave arm joints, the mechanism can be simple and have low cost because the master arm has no actuators. Controlling of the slave manipulator by joy-sticks or a control box with on/off switches for each joint can be classified as a unilateral servo. A conventional position servo mechanism is implemented at the slave side and the reference positions are given by means of the master arm motions or joy-sticks or switches. Some tasks such as handling heavy objects can be performed well enough by the unilateral servo type.

In the unilateral servo, however, there is no force reflection from the remote manipulator to the operator side, and it is difficult to perform precise tasks and compliant motions. In 1952, Geortz[24] had already pointed out the importance of kinesthetic sense and tactile sense in various manipulations. From the experience of the mechanical type master-slave manipulators, he stressed the importance of force reflection in teleoperation and proposed the concept of a bilateral servo where actuators are also mounted at the joints of the master arm to reflect the force of the remote side to the operator[25].

The basic idea of the bilateral servo is to replace the mechanical linkage between the master and slave arms by servo control that has the function of force reflection. There are several ways to realize force reflection. One of the most intuitive ways is to attach force or torque sensors to the output of the actuators at both the master and slave, and

to implement a force servo mechanism to the master side that makes the force/torque of the master side track the force/torque of the slave side, while a conventional position servo mechanism is implemented at the slave side. Geortz called this the *Force Reflecting Servo.*

If there is no force/torque feedback loop at the master side, the force reflecting servo becomes just *Force Reflection.* In this case, no force/torque sensor is required at the master side. However, exact force reflection is not guaranteed. Besides, if we could neglect inertia of the slave side, the force/torque applied at the slave side is equivalent to the actuator driving force/torque generated by the position servo mechanism located at the slave side. Therefore, force reflection can also be realized by implementing the same position servo mechanism at the slave side to the master side, where the same input to the servo-mechanism is used. This type is called the *Symmetric Position Servo.* The symmetric position servo can be regarded as having both arms connected by a massless elastic rod. In the symmetric servo case, force sensors are not necessary at both arms and it is the most simple among the three types of bilateral servo listed above.

Isomorphic Configuration and Different Configuration

In mechanically linked master-slave systems, master arm and slave arm must have an isomorphic configuration, that is, they must have the same kinematic structures (the same link length and the same joint assignment), because the corresponding joints between master and slave arms are mechanically connected. The servo manipulators have also this restriction, as long as the servo mechanisms are assigned to each joint individually.

The necessity of the isomorphic configurations causes some limitations. Especially, the size of the master arm becomes large when the degree-of-freedom becomes six or more. Moreover, different kinds of master arms must be built for different types of slave arms.

Bejczy et al.[12] at Jet Propulsion Laboratory proposed generalized bilateral control and removed these limitations. They put a computer between the master arm and the slave arm for calculation of coordinate transformations where each arm joint position and force are transformed into hand tip position and force respectively with reference to

Cartesian coordinates. This transformation enables bilateral servo in Cartesian coordinates even when the arm configurations are different.

Different configuration is much more flexible than isomorphic configuration, and enables independent design of the master arm from that of the slave arm. However, there are other problems such as difficulty in imagining the slave arm posture which is important for avoiding obstacles in the remote environment. A more serious problem is the singularity point. Since the singularity point may be different between the master and slave, there is a possibility that the slave arm cannot move in the direction commanded by the operator.

Telepresence

The ideal state of teleoperation is that where the operator can use the system as if he or she were located in the remote environment. This state is called *Telepresence*[37]. In order to realize telepresence, it is necessary to deliver several sensations to the operator which would be perceived if he or she were in the remote environment.

If telepresence is realized, the operator would be able to use the teleoperation system based on his/her usual experiences. Therefore, rapid decision making would be possible, and it would be easy to become used to operating the system. Tachi[79, 80] proposed "tele-existence" which is similar in concept to telepresence. He stressed the importance of active interaction to the remote environment through a realistic display of sensations. For visual sensation, he pointed out the importance of not only changing the view of the remote environment according to the head motion of the operator, but also displaying the view of the slave arm so that the operator can see the slave arm in the same location where his/her arm would exist.

Force reflection by bilateral servo can be classified as the telepresence in the context of force display. However, the current technique is still far from satisfactory. Visual display is, of course, one of the important displays of sensations. However, if the system could display the force to the operator as if he/she were manipulating the object in the remote environment directly, it might be possible to perform some teleoperations without visual display, just as he/she can perform some tasks with closing their eyes.

So far, research into telepresence is focused mainly on visual display, and there is little research for improving bilateral servo control aimed at the realization of a "more realistic force display".

Supervisory Control

In teleoperation, the operator is necessary at all times. In particular, simple but iterative tasks place a great burden on the operator. The concept of *Supervisory Control* proposed by Ferrell and Sheridan[20] in 1967 solves the problem by combining teleoperation with robotics technology, and this concept is the origin of telerobotics. Supervisory control was originally proposed for solving the "move-and-wait" problems in teleoperation with time delay, but the effectiveness of supervisory control was stressed soon even for teleoperation without time delay.

In supervisory control, simple tasks are performed by the remote robot which has several sensors and a certain level of autonomy, and the operator just watches the operation as a supervisor and orders the next command, for example, "*pick up the object A and place it on the object B*", to the robot. Consequently, the operator need not send his motion by the master arm all the time.

However, even in the supervisory control system, a master-slave manipulator is necessary. For example, suppose that the slave robot made a mistake and an error occurred. In supervisory control, the operator can issue another command to the remote robot to correct the error. But if the error was unexpected, it would be difficult to correct this error by using the autonomous function of the remote robot. The only way to correct the error might be by manual control using master-slave manipulators. Sato and Hirai[76] proposed a concept of intelligent teleoperation systems based on a kinematic world model. They pointed out the importance of the intervention of the operator at various levels, such as the servo level, motion level and task level, etc. and the coordination of manual control and autonomous control.

If the autonomy and reliability of the remote robot was improved more, situations where the master-slave manipulator is used would become fewer, and, of course, that is desirable. However, if this rare situation happened, the task that must be done by the master-slave mode must be very complicated, because even a high autonomous robot could

not perform it. Therefore, improvement of maneuverability of master-slave systems is quite necessary for improving the reliability of total telerobot systems.

1.2.3 Problems of Teleoperation

Maneuverability and Stability

The most important problem of master-slave systems is maneuverability. Although several modifications were tested, so far, in order to improve the maneuverability, task efficiency was far below that of direct operations. Geortz evaluated that the operation time required for a mechanically linked master-slave manipulator was eight times longer, on the average, than the time required for direct operations, and there were some tasks which took more time and which were impossible to perform by teleoperation. There is another report that the maximum time in which operators could continue the teleoperation was two hours and its contents were equivalent to only twelve minutes of direct operation[45].

The bilateral servo which was developed to overcome the limitations of mechanical linked master-slave manipulators generated another problem of stability. To discuss system stability strictly requires considerations of dynamics of the operator himself who is grasping the master arm, and the dynamics of the object which interacts with the slave arm. Therefore the analysis of stability is difficult. Burnett[14] showed that the master slave system must be equivalent to the passive electrical network in order to remain stable with various kinds of environments.

Very recently, stability problems were discussed by several researchers. Raju[72, 73] treated dynamics of the operator and object as impedances and showed a sufficient condition of stability. Stabilization of the system sometimes spoils the maneuverability. Hannaford[34] also pointed out the importance of considering the operator and object dynamics and discussed trade-offs between performance and stability.

Even at present, maneuverability of the system is far from satisfactory. They still use "classical" types of bilateral servos and little information exists about designing new bilateral servos which can provide better maneuverability. One of the reasons is that maneuverability

is an intuitive measure and difficult to evaluate quantitatively.

Design Guide

The bilateral servo was proposed to replace the mechanical linkage between the master and slave by means of control, but its design manner was somewhat intuitive. It would be necessary to give a design guide for improving maneuverability when we want to design a new control scheme aimed at better maneuverability. It is also necessary to make clear what is the ideal state of master-slave systems.

Concerning the mechanical design of arms, different configurations enable the master and slave arms to be designed independently. Especially, many kinds of mechanisms were considered for a master arm that is important as an interface to human operators. However, there is no quantitative design guide, and the mechanical design of arms was also intuitive. Trial and error were necessary.

1.3 Background of Robotics: –Field of Manipulator Control–

1.3.1 Kinematics and Dynamics

A *robot* can be defined as an artificial human-like mechanism controlled by computers which is similar in function to a human being. It is very difficult to build a complete robot which functions like a human. Robotics research started to focus on each function, such as manipulation, locomotion, and vision.

Manipulation is one of the important fields of robotics because this field treats direct interactions with the physical world. *Robot manipulators* are spatial multi-link mechanisms, and this fact causes several problems for controlling robot manipulators. Two major problems in manipulator control are kinematics and dynamics[3]. *Kinematics* means the position, velocity, and acceleration relationships among the links of the manipulator. *Dynamics* means the relationships among joint torque/force, external force/moment, and link accelerations.

[3]Statics can be regarded as a stationary case of dynamics.

Kinematics is important in trajectory control because the tasks are usually given as the motion of the end-effector in Cartesian space, whereas the manipulator motion depends on the motion of each joint. The kinematics is often classified into *Direct Kinematics* (DK) and *Inverse Kinematics* (IK)[13]. DK means to find the position (including orientation), velocity, and acceleration of the end-effector from given joint variables, and its velocity and acceleration. On the other hand, IK means to find joint variables from a given position, velocity, and acceleration of the end-effector of the manipulator. DK is generally a straightforward solution and it has unique end-effector position, velocity, and acceleration corresponding to the given joint variables, whereas IK is a difficult problem because end-effector position becomes a nonlinear function of joint positions and the solution is not straightforward nor unique. Pieper[71] showed that the analytical IK solutions for some manipulators with kinematic characteristics such as the last three joint axes of 6 DOF manipulators intersect at one point.

Dynamics is important in analysis, simulation and highly accurate motion control of robot manipulators. The dynamics is also classified into *Direct Dynamics* (DD) and *Inverse Dynamics* (ID)[13]. DD means to find the joint acceleration of the manipulator from a given joint torque/force exerted at each joint, and is necessary for dynamic simulations. On the other hand, ID means to find joint torque/force required to generate a given joint acceleration. Robot manipulators are spatial linkage mechanisms that have very complicated dynamics where nonlinear terms and dynamic coupling exist at each joint. For the first formulation of manipulator dynamics, Kahn[46] showed the dynamic equation of open chain manipulators based on the Lagrangian formulation of the general linked mechanisms by Uicker[87].

1.3.2 Trajectory Control

Trajectory control is a fundamental problem of manipulation. Paul[70] discussed path planning of manipulators in Cartesian space using homogeneous transformation matrices. Tayler[85] proposed the *Bounded Deviation Path* which is a recursive solution of joint variables from the straight line of the end-effector in Cartesian space. The difficulty of path planning by IK comes from the fact that the relationship between

joint variables and the end-effector position (orientation) is nonlinear.

Whitney[91, 92] proposed the *Resolved Motion Rate Control* where he focused on the linear relationship between joint velocities and the end-effector velocity. In his method, the commanded hand tip velocity is resolved into joint velocities by multiplying the inverse of the Jacobian matrix which specifies linear relation between the joint velocity and the end-effector velocity.

The way to control the manipulator can be classified into two methods; one is to determine the joint position and the other is to determine the joint torque. Trajectory control is usually based on the former method including industrial robots in practical use. However, the former does not take manipulator dynamics into account, and position errors become large when the desired trajectory has a high speed or high acceleration. The latter method has the advantage not only of direct control of force/moment against the environment but also of exact consideration of the manipulator dynamics in the trajectory control. Takase[83] discussed the motion control in a task-oriented coordinate system by calculating joint torques from the dynamic model of a manipulator. Luh et al.[55] proposed the *Resolved Acceleration Control* where the command acceleration of the end-effector obtained by the servo compensation in Cartesian space is resolved into joint acceleration, and joint torques for generating the resolved joint accelerations are then obtained by computing ID problems.

Around the mid-1980's, the method to calculate joint torque for servoing the desired trajectory based on the dynamic model of the manipulator had been referred as *Dynamic Control* or *Computed Torque Method.* Khosla and Kanade[52] experimentally evaluated the effectiveness of feedforward compensation and computed torque method based on the dynamic model of the manipulator. An et al.[3] also confirmed the validity of the computed torque method by comparing to the conventional PD control. They concluded that if the dynamic model is very accurate and the computation of the joint torque can be executed in a high enough sampling rate, the computed torque method has a high performance for high velocity or high acceleration trajectory control.

1.3.3 Efficient Computational Algorithms

According to the formulation by Kahn[46], computational amounts required for ID are 66,271 multiplications and 51,548 additions in the case of 6 DOF manipulators. It takes 2.3[s] using a standard 16-bit microcomputer of 50[kflops] and is far from real time computation. Besides, since the order of the number of computations is $O(n^4)$, where n is DOF, the computational amount increases rapidly as n increases. Therefore, it was practically impossible to apply the computed torque method to real time control.

To avoid these difficulties, Horn and Raibert[42] developed the table-look-up method where each joint variable, its velocity, and its acceleration are divided into some appropriate sections and the joint torques corresponding to each section are computed beforehand and stored to memory. But this approach requires a huge amount of memory if the joint variables are divided into sections small enough in order to obtain high accuracy. Another problem is that it cannot deal with the change of dynamic parameters such as the case when the manipulator grasps an object in the middle of the task.

Difficulty of real time computation of the computed torque method was solved once and for all by the Newton-Euler method proposed by Luh et al.[54]. This algorithm computes the velocity and acceleration at each link recursively from the base link to the end link (forward process) and computes force and moment exerted at each link from the end link to the base link (backward process) based on the Newton-Euler equation. This recursive computation is very effective for the structure of serial link manipulators, and the number of computations becomes $O(n)$. Hollerbach[40] showed that the number of computations can be $O(n)$ by recursive algorithm even based on the Lagrangian formulation. Moreover, Silver[78] discussed about the equivalence between the Newton-Euler approach and the Lagrangian approach.

The improvement of the Newton-Euler method was studied by several researchers. Kanade et al.[47] customized the Newton-Euler algorithm for a particular robot manipulator in order to reduce the number of computations. Renaud[75] and Balafoutis et al.[10] proposed efficient algorithms based on the concept of an augmented body and tensor computation.

So far, many researchers focused on the efficient computation of ID, since it was the bottle-neck for realizing real time computation of the computed torque method. However, when the desired trajectory is specified by the trajectory of the end-effector in Cartesian space, not only ID, but also DK and IK computations are necessary. Orin et al.[67] proposed an efficient computational algorithm of Jacobian matrix. This algorithm is also recursive and its number of computations is $O(n)$. Hollerbach et al.[41] proposed an efficient algorithm of resolved acceleration control for 6 DOF rotational joint manipulators where their wrist joints intersect at one point (like the PUMA type). They combined the analytical solution of kinematics with the recursive ID algorithm and considered the duplication between kinematics and dynamics computations. Mudge et al.[60], Wang et al.[90] and Khalil et al.[51] also discussed the combination of kinematics and dynamics computations for general types of manipulators. However, they lacked the consideration of total efficiency of the computations which are necessary for resolved acceleration control.

1.3.4 Utilization of Special Computational Devices

The Newton-Euler algorithm proposed by Luh et al. can reduce the number of computations and the possibility to realize the computed torque method becomes great. However, the required number of computations is still large. For 6 DOF manipulators, for example, 657 multiplications and 544 additions are required and it takes about 24[ms] using a standard microprocessor of 50[kflops]. It is necessary for real time computation to use a computer which is faster (and, therefore, more expensive) than conventional microcomputers.

To avoid the high cost of computers, parallel computation was considered. Luh and Lin[56] proposed parallel computation of the Newton-Euler algorithm where each microprocessor was assigned for each link computation. Kasahara et al.[48] considered scheduling of parallel computations for ID to obtain the optimal performance for a given number of processors. Recently, special devices developed for parallel computation become popular and inexpensive, and the possibility of parallel

computation has become greater than before. Hashimoto et al.[36] modified the formulation of the Newton-Euler algorithm for parallel computations.

Recently, digital signal processors (DSP) have become considerably noticeable. DSP has hardware logic of arithmetic operations and can execute computations of vectors or matrices very fast. Although DSP is usually used for digital filters of voice or image data, it would also be applicable to manipulator control. Mayeda et al.[57] applied a floating-point DSP to inverse dynamics computation of manipulators with parallel or perpendicular joints. Takanashi[82] applied a floating-point DSP to the computation of stiffness control of robot manipulators.

The merit of DSP is that the computation by single DSP is fast enough for real time computation and parallel computation is not necessary. The difficulty of programming for DSP by assembly language is one of the problems. Very recently, new types of DSPs using high level languages such as C have become available and they will make the programming of DSPs easier in the future.

1.4 The Goal of this Paper and the Composition of Chapters

The goal of this paper is to analyze exactly master-slave teleoperation systems and to design a superior master-slave teleoperation system that provides good maneuverability. *Master-slave teleoperation system* is a set of master arm, slave arm and their control scheme. Hereafter, we call it *master-slave system* for simplicity.

This paper consists of two parts. In the first part, chapters 2 through 6, analysis and design of master-slave systems are discussed. Chapters 2 and 3 concern a simple one degree-of-freedom (DOF) case, and chapters 4 and 5 concern the design of master-slave systems in the multiple DOF case. Chapter 6 shows experimental results using a designed master-slave system.

In the analysis of master-slave systems, it was found that compensation of dynamics of both the master arm and the slave arm is important to obtain good maneuverability. In teleoperation, since no specific

desired trajectory is given in advance, off-line computing of the arm dynamics is impossible and on-line compensation of dynamics is required. Concerning the multiple DOF case, the on-line compensation of arm dynamics becomes difficult because dynamics of multi-link mechanisms is complex. From the viewpoint of the mechanism, master and slave arms are equivalent to robot manipulators. Therefore, efficient computations of manipulator kinematics and dynamics for trajectory control are discussed in the second part, chapters 7 through 9.

In chapter 2, maneuverability of master-slave systems is discussed. Maneuverability of master-slave systems is difficult to evaluate exactly, since "maneuverability" seems to be an intuitive sense for human operators. However, quantitative evaluation of the system performance is necessary to decide what kind of master-slave system is desirable and to evaluate the qualities of control schemes. In this chapter, a way to evaluate the maneuverability of master-slave systems is proposed. First, a one DOF system is analyzed taking the operator and object dynamics into account. Second, some ideal responses of the master-slave system are defined and the conditions to achieve these responses are derived. Third, a quantitative performance index is given in order to evaluate the maneuverability of the system. Last, stability of the master-slave system is discussed.

In chapter 3, bilateral control of master-slave manipulators for an ideal kinesthetic coupling is discussed in a one DOF systems. The way to control master-slave manipulators considerably affects the maneuverability of master-slave systems. The ideal state of master-slave systems can be regarded as the state where the operator can operate the system as if he were directly manipulating the object which actually exists at the remote site. In other words, the system must be coupled with the operator to give the ideal kinesthetic sense. So far, several researchers have applied their own definition of the ideal states of master-slave systems. However, there is no unanimous agreement about how close we can approach the ideal state or what kind of control scheme should be designed in order to achieve it. In this chapter, a control scheme is proposed which can achieve the ideal kinesthetic coupling with the operator and realize the three ideal responses which were defined in the previous chapter. Secondly, the stability of the system controlled by the proposed scheme is discussed by using the concept of passivity.

In chapter 4, a design guide for master arms for teleoperation is discussed. The amount of freedom to design the configuration of the master arm independently from that of the slave arm becomes great for multiple DOF arms of different configurations, and the quality of the master arm design has a considerable influence on the maneuverability of the master-slave system. In this chapter, a quantitative measure of the manipulating ability of master arms is proposed. This measure, which is obtained by extending the concept of dynamic manipulability, considers operator dynamics, since operator dynamics cannot be neglected when he manipulates the master arm. It is pointed out that the manipulability of master arms depends not only on the magnitude of the manipulability measure but also on the distribution of the manipulability measure and the directional property of the manipulability ellipsoid in the work space. A quantitative index to evaluate these properties is then proposed by comparing and evaluating the similarity of the manipulability ellipsoid produced between the two situations when the operator manipulates the master arm and when he has no load. It is shown that the relative position of the master arm to the operator is an important factor in the manipulability as well as the master arm design itself.

In chapter 5, the control scheme for realizing the ideal responses proposed in the chapter 3, is extended to the multiple DOF case. Most of the discussions about master-slave systems in the traditional studies were restricted in one DOF cases. They dealt with the problem to control the multiple DOF master-slave manipulators by applying one DOF controller at each joint for the isomorphic configuration arms, and at each direction of Cartesian coordinates for the different configuration arms. But this approach does not consider the arm dynamics such as the inertia coupling and nonlinear effects. In this chapter, we formulate the problem based on the same concept as in the one DOF case. First, the ideal responses of multiple DOF master-slave systems are defined. Second, new control schemes are proposed for different configurations and for isomorphic configuration arms. Third, the validity of the proposed control schemes are confirmed by simulations. Last, design guides of master and slave arms are discussed from various points of view.

In chapter 6, we discuss a prototype master-slave system which was

built for experiments, and show experimental results obtained by using this system. The master and slave arms were designed according to the design guides discussed in chapters 4 and 5. Experiments were done for a one DOF system by using only one joint of the arms. Validity of the control schemes proposed in chapter 3 for realizing the ideal responses is examined experimentally by comparing to several conventional control schemes.

In chapter 7, new computational algorithms for DK, IK and ID of robot manipulators are discussed. When the manipulator should follow the trajectory specified in Cartesian space, it requires not only ID calculation but also DK and IK calculation. In this chapter, efficient recursive algorithms for DK, IK and ID are formulated, so that they may include as many common physical values as possible. Next, it is shown that the total amount of calculation can be reduced by eliminating the duplication included in the algorithms of DK, IK, and ID.

In chapter 8, an application of DSP (Digital Signal Processor) to real time computation for dynamic control of robot manipulators is proposed. In order to perform dynamic control in real time with low cost, DSP is utilized for the main part of the computations of dynamic control. LSI technology is advancing very rapidly, and floating-point DSPs have recently become available commercially. In this chapter, a 32-bit floating-point DSP (μPD77230 developed by NEC Corp.) is used for the computation of the resolved acceleration control. It is confirmed that the total computational time for the resolved acceleration control except trigonometric functions becomes 1.06[ms] for general 6 DOF manipulators.

In chapter 9, the link coordinate frame assignment for serial link manipulators is discussed. For formulating the kinematics and dynamics of robot manipulators, it is usually necessary to assign a link coordinate frame to each link. The Denavit and Hartenberg method is well known as a way of link coordinate frame assignment. In this chapter, four types of link coordinate frame assignment are defined. It is shown that the number of computations for inverse dynamics can be reduced by only changing the assignment of the link frames. A concept of optimal link frame assignment is also proposed.

In chapter 10, some concluding remarks are given and further research topics are described.

Chapter 2

MANEUVERABILITY OF MASTER-SLAVE TELEOPERATION SYSTEMS

2.1 Introduction

Retrospecting to the previous studies about master-slave manipulators, unilateral control was taken over by bilateral control [25, 14] and isomorphic configurations of master and slave arms advanced to different configurations [12, 32, 6] accompanied with the progress of computers. As for control schemes, however, they still use somewhat "classical" ones such as symmetric position servo type, force reflection type, and force reflecting servo type. The maneuverability of the present master-slave systems seems still far from satisfactory.

It is true that the maneuverability of master-slave systems depends upon the quality of mechanical design of each arm. But the quality of control schemes also affects surely the maneuverability. However, serious discussions have been lacking about how to evaluate the maneuverability of the system exactly or quantitatively. The reason comes from the fact that the "maneuverability" of the system can be regarded as an intuitive property for human operators and it would be difficult to eval-

uate such an intuitive matter quantitatively. Raju[72, 74] evaluated the maneuverability of master-slave system experimentally. He also pointed out that there are various aspects for evaluating the performance of the system. Besides, theoretical analysis of master-slave system is complex since, strictly speaking, dynamics of both the operator and manipulated object should be taken into account. Hannaford[34] also pointed out the importance of consideration of the whole system including not only the arm dynamics but also the object and operator dynamics for analyzing the system stability.

In this chapter, we propose a way to evaluate the maneuverability of master-slave systems quantitatively. For this purpose, we first model the master-slave system in a simple one degree-of-freedom (DOF) case including the object and operator dynamics. Secondly, we define three ideal responses of master-slave systems by paying attention to the position and force responses of the master and slave arms. We then derive conditions to achieve those ideal responses. Thirdly, a quantitative performance index, which examines how close the actual responses is to the ideal one, is given in order to evaluate the maneuverability of the system. Lastly, we discuss the stability of the master-slave systems based on the concept of passivity.

2.2 Modeling in One DOF System

2.2.1 Modeling of Arms, Object and Operator

Generally, a master-slave system is composed of arms with multiple DOF. However, a one DOF system is considered in this chapter to make the problem simple.

The dynamics of master arm and slave arm is given by the following equations:

$$\tau_m + f_m = m_m \ddot{x}_m + b_m \dot{x}_m \tag{2.1}$$

$$\tau_s - f_s = m_s \ddot{x}_s + b_s \dot{x}_s \tag{2.2}$$

where x_m and x_s denote the displacements of the master and slave arms respectively. And m_m and m_s represent mass of master and slave arms, and b_m and b_s are viscous coefficients of the master and slave arms.

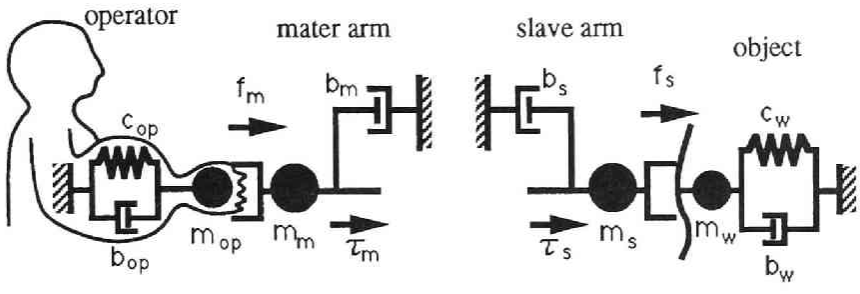

Figure 2.1: Master and slave arms, operator and object

On the other hand, f_m denotes the force that the operator applies to the master arm and f_s denotes the force that the slave arm applies to the object. Actuator driving forces of master and slave arms are represented by τ_m and τ_s respectively.

The dynamics of the object interacting with the slave arm is modeled by the following linear system.

$$f_m = m_w \ddot{x}_s + b_w \dot{x}_m + c_w x_s \tag{2.3}$$

where m_w, b_w and c_w denote mass, viscous coefficient and stiffness of the object respectively. As shown that the displacement of the object is represented by x_s in eq.(2.3), we assumed that the slave arm is contacting with the object completely or grasping the object firmly so that it does not depart from the object.

Lastly, it is also assumed that the dynamics of the operator can be represented approximately as a simple spring-damper-mass system.

$$\tau_{op} - f_m = m_{op} \ddot{x}_m + b_{op} \dot{x}_m + c_{op} x_m \tag{2.4}$$

where m_{op}, b_{op} and c_{op} denote mass, viscous coefficient, and stiffness of the operator respectively and τ_{op} means force generated by the operator's muscles. Similarly to eq.(2.3), the displacement of the operator is represented by x_m in eq.(2.4) because we assumed that the operator is grasping the master arm firmly and he never release the master arm during the operation. The parameters of the operator dynamics may

change according to the operational state. Therefore, these parameters are not constant values. For example, Akazawa et al. reported that b_{op} and c_{op} are proportional to the sum of the forces exerted by flexor and extensor muscles[2]. **Fig.2.1** shows the models of one DOF system.

2.2.2 Control Schemes of Master and Slave Arms

Let the control schemes for the master and slave arms be given by the following general expressions which determine actuator inputs, τ_m and τ_s:

$$\begin{aligned}\tau_m &= \left[K_{mpm} + K'_{mpm}\frac{d}{dt} + K''_{mpm}\frac{d^2}{dt^2} \quad K_{mfm} \right] \begin{bmatrix} x_m \\ f_m \end{bmatrix} \\ &\quad - \left[K_{mps} + K'_{mps}\frac{d}{dt} + K''_{mps}\frac{d^2}{dt^2} \quad K_{mfs} \right] \begin{bmatrix} x_s \\ f_s \end{bmatrix} \end{aligned} \tag{2.5}$$

$$\begin{aligned}\tau_s &= \left[K_{spm} + K'_{spm}\frac{d}{dt} + K''_{spm}\frac{d^2}{dt^2} \quad K_{sfm} \right] \begin{bmatrix} x_m \\ f_m \end{bmatrix} \\ &\quad - \left[K_{sps} + K'_{sps}\frac{d}{dt} + K''_{sps}\frac{d^2}{dt^2} \quad K_{sfs} \right] \begin{bmatrix} x_s \\ f_s \end{bmatrix} \end{aligned} \tag{2.6}$$

where K_{mpm}, K'_{mpm}, K''_{mpm} and K_{mfm} are the feedback gains of the master arm position, velocity, acceleration and force respectively, and K_{mps}, K'_{mps}, K''_{mps} and K_{mfs} are gains of the slave arm position, velocity, acceleration and force respectively to determine the actuator force of the master arm. Similarly, K_{spm}, K'_{spm}, K''_{spm}, K_{sfm}, K_{sps}, K'_{sps}, K''_{sps}, and K_{sfs} are the feedback gains of position, velocity, acceleration and force of the master and slave arms respectively for determining the actuator force of the slave arm. Eqs.(2.5) and (2.6) are extensions of the formulation by Fukuda et al.[22] and obtained by adding velocity and acceleration gains. The conventional control schemes such as symmetric position servo type, force reflection type and force reflecting servo type can be represented as the special cases of eqs.(2.5) and (2.6) by setting each gain properly. In eqs.(2.5) and (2.6), we suppose an ideal situation where time delay for data transmission between the master site and slave site is negligible.

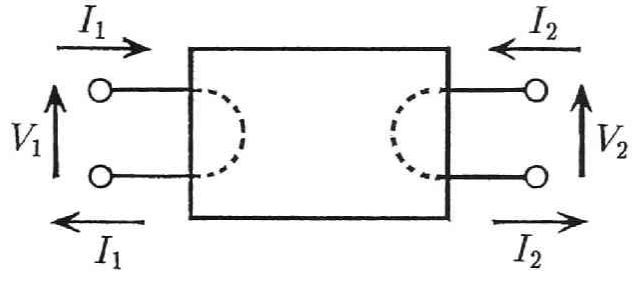

Figure 2.2: Two-terminal-pair network

2.2.3 Representation of the Master-Slave System by Two-Terminal-Pair Network

The concept of two-terminal pair network is usually used in electrical circuits. This concept is very useful to formulate the master-slave system. The impedance matrix $\boldsymbol{Z}$ is defined from the relations between current and voltage of the two-terminal-pair network shown in **Fig.2.2.**

$$V_1 = z_{11}I_1 + z_{12}I_2 \tag{2.7}$$

$$V_2 = z_{21}I_1 + z_{22}I_2 \tag{2.8}$$

$$\boldsymbol{Z} = \begin{bmatrix} z_{11} & z_{12} \\ z_{21} & z_{22} \end{bmatrix} \tag{2.9}$$

where I_1 and I_2 denote currents at each terminal pair, and V_1 and V_2 denote voltages between each terminal pair.

Let us consider a two-terminal-pair network which is connected to a power source and a load at each terminal pair shown in **Fig.2.3**. Regarding the power source as an operator, the load as an object and the two-terminal-pair network as a master-slave system, the whole system can be represented by the electric circuit in **Fig.2.3**. The correspondence between the modeling in the previous section and the circuit representation in **Fig.2.3** is given as follows:

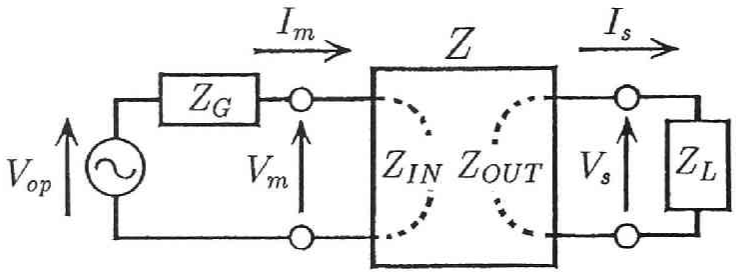

Figure 2.3: Connection of power source and load to two-terminal-pair network

velocity of the master arm $\dot{x}_m$	$\longleftrightarrow$	current I_m
velocity of the slave arm $\dot{x}_s$	$\longleftrightarrow$	current I_s
operator's force τ_{op}	$\longleftrightarrow$	voltage V_{op}
force at the master side f_m	$\longleftrightarrow$	voltage V_m
force at the slave side f_s	$\longleftrightarrow$	voltage V_s

Representing the master-slave system by a two-terminal-pair network is not a new concept. However, this framework where operator and object are considered as the power source and load connected to the network was shown by Raju[72][73]. This representation of the system by electric circuits does not change the nature of the problem. However, it enables a very compact formulation and gives a good prospects for deriving the equations.

Rewriting the actuator forces τ_m and τ_s into voltages T_m and T_s respectively in addition to the above correspondence, eqs.(2.1), (2.2), (2.5) and (2.6) are transformed from time domain into s-domain as follows:

$$T_m + V_m = (m_m s + b_m) I_m \triangleq Z_m I_m \tag{2.10}$$

$$T_s - V_s = (m_s s + b_s) I_s \triangleq Z_s I_s \tag{2.11}$$

$$\begin{aligned} T_m \;=\; & \left[\; K''_{mpm} s + K'_{mpm} + K_{mpm} \frac{1}{s} \quad K_{mfm} \;\right] \begin{bmatrix} I_m \\ V_m \end{bmatrix} \\ & - \left[\; K''_{mps} s + K'_{mps} + K_{mps} \frac{1}{s} \quad K_{mfs} \;\right] \begin{bmatrix} I_s \\ V_s \end{bmatrix} \end{aligned}$$

$$\triangleq \begin{bmatrix} P_m & Q_m \end{bmatrix} \begin{bmatrix} I_m \\ V_m \end{bmatrix} - \begin{bmatrix} R_m & S_m \end{bmatrix} \begin{bmatrix} I_s \\ V_s \end{bmatrix} \tag{2.12}$$

$$\begin{aligned} T_s &= \begin{bmatrix} K''_{spm}s + K'_{spm} + K_{spm}\frac{1}{s} & K_{sfm} \end{bmatrix} \begin{bmatrix} I_m \\ V_m \end{bmatrix} \\ &\quad - \begin{bmatrix} K''_{sps}s + K'_{sps} + K_{sps}\frac{1}{s} & K_{sfs} \end{bmatrix} \begin{bmatrix} I_s \\ V_s \end{bmatrix} \\ &\triangleq \begin{bmatrix} P_s & Q_s \end{bmatrix} \begin{bmatrix} I_m \\ V_m \end{bmatrix} - \begin{bmatrix} R_s & S_s \end{bmatrix} \begin{bmatrix} I_s \\ V_s \end{bmatrix} \end{aligned} \tag{2.13}$$

Eliminating T_m and T_s from eqs.(2.10), (2.11), (2.12) and (2.13), the following equation is obtained.

$$\begin{aligned} &\begin{bmatrix} Z_m - P_m & -R_m \\ -P_s & -(Z_s + R_s) \end{bmatrix} \begin{bmatrix} I_m \\ -I_s \end{bmatrix} \\ &= \begin{bmatrix} 1 + Q_m & -S_m \\ Q_s & -(1 + S_s) \end{bmatrix} \begin{bmatrix} V_m \\ V_s \end{bmatrix} \end{aligned} \tag{2.14}$$

Noting that I_1, I_2, V_1, and V_2 in **Fig.2.2** correspond to I_m, $-I_s$, V_m, and V_s in **Fig.2.3** respectively, each element of the impedance matrix of the master-slave system is given as follows:

$$z_{11} = \frac{(1 + S_s)(Z_m - P_m) + S_m P_s}{(1 + S_s)(1 + Q_m) - S_m Q_s} \triangleq \frac{N_{11}}{D_Z} \tag{2.15}$$

$$z_{12} = \frac{-(1 + S_s)R_m + S_m(Z_s + R_s)}{(1 + S_s)(1 + Q_m) - S_m Q_s} \triangleq \frac{N_{12}}{D_Z} \tag{2.16}$$

$$z_{21} = \frac{(1 + Q_m)P_s + Q_s(Z_m - P_m)}{(1 + S_s)(1 + Q_m) - S_m Q_s} \triangleq \frac{N_{21}}{D_Z} \tag{2.17}$$

$$z_{22} = \frac{(1 + Q_m)(Z_s + R_s) - Q_s R_m}{(1 + S_s)(1 + Q_m) - S_m Q_s} \triangleq \frac{N_{22}}{D_Z} \tag{2.18}$$

The determinant $|\boldsymbol{Z}|$ is given by

$$|\boldsymbol{Z}| = \frac{(Z_m - P_m)(Z_s + R_s) + P_s R_m}{(1 + S_s)(1 + Q_m) - S_m Q_s} \triangleq \frac{D_Y}{D_Z} \tag{2.19}$$

The admittance matrix is given by inverting $\boldsymbol{Z}$.

$$\begin{aligned} \boldsymbol{Y} = \boldsymbol{Z}^{-1} &= \begin{bmatrix} y_{11} & y_{12} \\ y_{21} & y_{22} \end{bmatrix} \\ &= \begin{bmatrix} \dfrac{N_{22}}{D_Y} & \dfrac{-N_{12}}{D_Y} \\ \dfrac{-N_{21}}{D_Y} & \dfrac{N_{11}}{D_Y} \end{bmatrix} \end{aligned} \tag{2.20}$$

Dynamics of the operator and object can also be represented as the form of impedance.

$$Z_L = m_w s + b_w + c_w \frac{1}{s} \tag{2.21}$$

$$Z_G = m_{op} s + b_{op} + c_{op} \frac{1}{s} \tag{2.22}$$

Eqs.(2.21) and (2.22) are obtained from the simple modeling of the operator and object in the previous section. Of course, Z_L and Z_G need not always be represented by eqs.(2.21) and (2.22). One can suppose a more appropriate form (for example, a higher orders system or a time variant system) as long as the dynamics of the operator and object is described as the general forms, Z_L and Z_G. We will use eqs.(2.21) and (2.22) only when Z_L and Z_G are evaluated numerically.

2.3 Ideal Responses of Master-Slave Systems

2.3.1 Definition of Ideal Responses

In this section, before evaluating the performance of the system, it is discussed what the ideal responses of master-slave systems should be. If the definition of the ideal response is valid, it would be possible to evaluate the performance of the system by examining how close the actual system response is to the ideal responses.

DEFINITION : The following three responses are defined as the ideal responses of master-slave systems.

Ideal response I : *When the operator applies operating force τ_{op} to the system, the* position *responses of both the master and slave arms, x_m and x_s, are exactly equal regardless of the object dynamics.*

Ideal response II : *When the operator applies operating force τ_{op} to the system, the* force *responses of both the master and slave arms, f_m and f_s, are exactly equal regardless of the object dynamics.*

Ideal response III : *When the operator applies operating force τ_{op} to the system, the* position and force *responses of the master and slave arms, x_m and x_s, and f_m and f_s, are absolutely equal respectively regardless of the object dynamics.*

The ideal response III coincides with the response when the operator operate the object directly. Therefore, if the ideal response III is achieved, the operator can operate the system as if he were manipulating the actual object himself. In this sense, the ideal response III can be regarded as a final ideal response for master-slave systems.

2.3.2 Conditions for Ideal Responses

The concept of the two-terminal-pair network is well used to design a electric filter. The master-slave system can also be regarded as a sort of mechanical filter between the operator and the object. Here we define some transmission coefficients in order to derive the conditions for the ideal responses.

First, we define the velocity transmission coefficient which specifies how the master side velocity (I_m) is transmitted to the slave side velocity (I_s).

$$T_i = \frac{I_m}{I_s} \tag{2.23}$$

From eqs.(2.15) through (2.18) and the relationship $V_s = Z_L I_s$, T_i is given by

$$T_i = \frac{z_{22} + Z_L}{z_{21}} = \frac{N_{22} + D_Z Z_L}{N_{21}}. \tag{2.24}$$

Since it is necessary for realizing the ideal response I that $T_i \equiv 1$ regardless of Z_L, the following conditions can be obtained.

[Conditions for ideal response I]

$$\text{(A)} \quad D_Z = 0 \tag{2.25}$$

$$\text{(B)} \quad N_{21} = N_{22} \neq 0 \tag{2.26}$$

Next, we define the force transmission coefficient, T_v, which shows how the master side force (V_s) is transmitted to the slave side force (V_s).

$$T_v = \frac{V_m}{V_s} \tag{2.27}$$

Similarly, from eq.(2.20) and the relationship $V_s = Z_L I_s$, T_v is given by

$$T_v = \frac{y_{22} + \dfrac{1}{Z_L}}{-y_{21}} = \frac{N_{11} Z_L + D_Y}{N_{21} Z_L}. \tag{2.28}$$

Since it is necessary for realizing the ideal response II that $T_v \equiv 1$ regardless of Z_L, the following conditions are obtained.

[Conditions for ideal response II]

$$\text{(C)} \quad D_Y = 0 \tag{2.29}$$

$$\text{(D)} \quad N_{21} = N_{11} \neq 0 \tag{2.30}$$

Especially when $Z_L = 0$, T_v cannot be defined by eq.(2.28), because $V_s = 0$ in this case. However it will be shown later that the conditions (C) and (D) are valid at this special case as well[1].

When the both conditions for the ideal response I and II are satisfied, the system realizes the ideal response III. Letting $x_m = x_s = x$ and $f_m = f_s = f$ in eqs.(2.3) and (2.4), it is clear that x and f become the response when the operator manipulates the object directly. In fact, the system impedance from the operator side corresponds to the input impedance given by

$$\begin{aligned} Z_{IN} &= z_{11} - \frac{z_{12} z_{21}}{z_{22} + Z_L} \\ &= \frac{D_Y + N_{11} Z_L}{N_{22} + D_Z Z_L}. \end{aligned} \tag{2.31}$$

[1] See the footnote in section 2.4.1.

And, substituting the conditions (A), (B), (C) and (D) to eq.(2.31), we get

$$Z_{IN} \equiv Z_L \tag{2.32}$$

which shows that the operator can feel the pure object dynamics through the system.

[Conditions for ideal response III]
All of conditions (A), (B), (C) and (D).

Because of the conditions (A) and (C), impedance matrix and admittance matrix cannot be defined when the system is realizing the ideal response III. In this case, T_i and T_v cannot be defined using z_{ij} and y_{ij} in eqs.(2.24) and (2.28), and this fact may contradict to the obtained conditions which derived from T_i and T_v. Here, let a new matrix called the chain matrix be defined. This matrix can be defined even when the condition (A) and (C) are satisfied. From **Fig.2.2**, let the following relations be considered:

$$V_1 = k_{11}V_2 + k_{12}(-I_2) \tag{2.33}$$

$$I_1 = k_{21}V_2 + k_{22}(-I_2) \tag{2.34}$$

The chain matrix is defined as:

$$\boldsymbol{K} \triangleq \begin{bmatrix} k_{11} & k_{12} \\ k_{21} & k_{22} \end{bmatrix} \tag{2.35}$$

The chain matrix is used when the output of a two-terminal-pair network is connected to the input of another two-terminal-pair network. In the case of master-slave systems, the chain matrix can be represented as follows:

$$\boldsymbol{K} = \frac{1}{z_{21}} \begin{bmatrix} z_{11} & |\boldsymbol{Z}| \\ 1 & z_{22} \end{bmatrix} = \begin{bmatrix} \dfrac{N_{11}}{N_{21}} & \dfrac{D_Y}{N_{21}} \\ \dfrac{D_Z}{N_{21}} & \dfrac{N_{22}}{N_{21}} \end{bmatrix} \tag{2.36}$$

Substituting the conditions (A) and (B) to eq.(2.36), we get $I_1 = -I_2$ from eq.(2.34) and consequently $T_i \equiv 1$. On the other hand, substituting the conditions (C) and (D) to eq.(2.36), we get $V_1 = V_2$ from

eq.(2.33) and consequently $T_v \equiv 1$. When the ideal response III is realized, that is, when all the conditions (A), (B), (C), and (D) are satisfied, the chain matrix becomes

$$\boldsymbol{K} = \begin{bmatrix} 1 & 0 \\ 0 & 1 \end{bmatrix}. \tag{2.37}$$

2.3.3 Consideration of Transmission Ratios of Position and Force

So far in this chapter, we have been assuming tacitly that the scales of position and force are identity between the master side and the slave side. Practically speaking, however, we may face the situation where the scale of the object should be different from that of the operator, such as the case when very heavy objects are handled and the case when very precise operations are required. It is possible to deal with this situation by setting the velocity and force transmission coefficients in eqs.(2.24) and (2.28) not to one but $T_i = \zeta_p$ and $T_v = \zeta_f$ respectively. The values ζ_p and ζ_f are arbitrary determined transmission ratios of velocity and force. It is possible to derive the conditions of the ideal responses when these ζ_p and ζ_f are considered. Especially, eq.(2.32) showing the ideal situation can be rewritten by the following equation.

$$Z_{IN} = \frac{\zeta_f}{\zeta_p} Z_L \tag{2.38}$$

Of course, it is possible to make the discussion more general by introducing ζ_p and ζ_f. Hereafter, however, we will consider only when $\zeta_p = 1$ and $\zeta_f = 1$ to simplify the discussion.

2.3.4 Design Guide of Control Schemes Realizing the Ideal Responses

In this section, we discuss the design of control schemes which can realize the ideal responses defined previously. In eqs.(2.5) and (2.6), we took the acceleration signals of master and slave arms into account for a general form of control schemes besides position, velocity, and force signals. Compared to the measurement of position and velocity, however,

the acceleration measurement is rather difficult because accelerometers should be attached at the arm tip and the measured data may include some noises. Therefore, it would be desirable if the acceleration is not necessary for constructing control schemes.

However, one can find easily that it is impossible to satisfy the condition (C) when the acceleration signals are not used in eqs.(2.12) and (2.13), in other words, when $K''_{mpm} = K''_{mps} = K''_{spm} = K''_{sps} = 0$ in P_m, R_m, P_s, and R_s. Consequently, the following proposition is obtained.

PROPOSITION : *In the framework of eqs.(2.5) and (2.6), any control scheme cannot realize the ideal response II nor III unless the acceleration signals are used.*

2.4 Evaluation of Maneuverability

2.4.1 Performance Index of Maneuverability

A high performance master-slave system means that it provides high maneuverability and it enables stable operations. However, qualitative expressions such like "high maneuverability" and "stable operations" are not enough to evaluate the performance of the system. In this section, a quantitative performance index for maneuverability is given based on the concept of the ideal responses introduced in the previous section.

Let $G_{mp}(s)$, $G_{sp}(s)$, $G_{mf}(s)$, and $G_{sf}(s)$ be transfer functions of the master-slave system from the operator's force τ_{op} (V_{op}) to the master side displacement x_m (I_m/s), slave side displacement x_s (I_s/s), master side force f_m (V_m), and slave side force f_s (V_s) respectively. These four transfer functions are given by

$$G_{mp}(s) = \frac{s[N_{22} + D_Z Z_L]}{s^2[D_Y + N_{11}Z_L + N_{22}Z_G + D_Z Z_L Z_G]}, \tag{2.39}$$

$$G_{sp}(s) = \frac{s[N_{21}]}{s^2[D_Y + N_{11}Z_L + N_{22}Z_G + D_Z Z_L Z_G]}, \tag{2.40}$$

$$G_{mf}(s) = \frac{s[D_Y + N_{11}Z_L]}{s^2[D_Y + N_{11}Z_L + N_{22}Z_G + D_Z Z_L Z_G]}, \tag{2.41}$$

$$G_{sf}(s) = \frac{s^2[N_{21}Z_L]}{s^2[D_Y + N_{11}Z_L + N_{22}Z_G + D_Z Z_L Z_G]}. \tag{2.42}$$

By using these transfer functions, one can evaluate how well the actual system realizes the ideal responses. Here, we propose the following performance index for evaluating the maneuverability of master-slave systems.

[Performance index of maneuverability]
If the following equality of the position response, J_p, and the equality of the force response, J_f, between the master and slave arms are small, it is evaluated that the system has high maneuverability.

$$J_p = \int_0^{\omega_{max}} F(G_{mp}(j\omega), G_{sp}(j\omega))W(\omega)d\omega \tag{2.43}$$

$$J_f = \int_0^{\omega_{max}} F(G_{mf}(j\omega), G_{sf}(j\omega))W(\omega)d\omega \tag{2.44}$$

where $F()$ is an appropriate function which evaluates the difference between two transfer functions, $W()$ is a weighting function of frequency, and ω_{max} is the maximum frequency of the manipulation band of human operators.

When the system realizes the ideal response I, J_p becomes zero, and when the system realizes the ideal response II, J_f becomes zero. Consequently, if both J_p and J_f are close to zero, the response of that system is close to the ideal response III. Concrete examples of J_p and J_f are shown as follows:

$$J_p = \int_0^{\omega_{max}} |G_{mp}(j\omega) - G_{sp}(j\omega)| \left| \frac{1}{1 + j\omega T} \right| d\omega, \tag{2.45}$$

$$J_f = \int_0^{\omega_{max}} |G_{mf}(j\omega) - G_{sf}(j\omega)| \left| \frac{1}{1 + j\omega T} \right| d\omega. \tag{2.46}$$

In this case, $F()$ is just the absolute value of simple subtraction and $W()$ is the gain of the first-order-lag for the purpose of attaching much importance toward the static characteristics and the low frequency domain. The value T is the time constant.

A difficulty with eqs.(2.43) and (2.44) in evaluating the maneuverability of the system is that the performance indices J_p and J_f are functions of Z_L and Z_G. This means that, even if a control scheme is determined, the indices J_p and J_f may change according to Z_L and Z_G. Therefore, it may be better to consider another index which does not contain Z_L and Z_L so that one can evaluate the system performance regardless of Z_L and Z_L. On the other hand, it may make sense that Z_G is taken into the consideration for the performance index, since the maneuverability is just for the operator and the operator dynamics Z_G can be a standard for performance evaluation.

Now let us consider two special cases when $Z_L = 0$ and $Z_L = \infty$. The case when $Z_L = 0$[2] means the situation with no object and the slave arm is free in the space. On the other hand, the case when $Z_L = \infty$ means the situation where the slave arm is completely constrained by a rigid environment and cannot move. In these special cases, the subtractions of two transfer functions become as follows:

[$Z_L = 0$]

$$G_{mp}(s) - G_{sp}(s) = \frac{s[N_{22} - N_{21}]}{s^2[D_Y + N_{22}Z_G]} \tag{2.47}$$

$$G_{mf}(s) - G_{sf}(s) = \frac{s[D_Y]}{s^2[D_Y + N_{22}Z_G]} \tag{2.48}$$

[$Z_L = \infty$]

$$G_{mp}(s) - G_{sp}(s) = \frac{D_Z}{s[N_{11} + D_Z Z_G]} \tag{2.49}$$

$$G_{mf}(s) - G_{sf}(s) = \frac{s[N_{11} - N_{21}]}{s[N_{11} + D_Z Z_G]} \tag{2.50}$$

Making eqs.(2.47),(2.48),(2.49) and (2.50) be zero corresponds exactly to the conditions (B), (C), (A) and (D) respectively. And one can get the performance indices which do not contain Z_L by substituting these eqs.(2.47) through (2.50) into eqs.(2.45) and (2.46).

[2] In the case of $Z_L = 0$, substituting the condition (C) and (D) into eqs.(2.41) and (2.42), $G_{mf}(s) = 0$ and $G_{sf} = 0$ are obtained. It means that $f_m = f_s = 0$ and the ideal response II is realized. Therefore the conditions (C) and (D) are valid even in this case.

2.4.2 Numerical Examples of Performance Evaluation

Let us evaluate the performance of the conventional control schemes such as symmetric position servo type, force reflection type, and force reflecting servo type by using the proposed index when the parameters of master and slave arms are concretely given, for example, by

$$m_m = m_s = 2.0[\mathrm{kg}],\ b_m = b_s = 0.2[\mathrm{Ns/m}].$$

The following three kinds of object are considered.

[case 1]: $m_w = 1.0[\mathrm{kg}],\ b_w = 2.0[\mathrm{Ns/m}],\ c_w = 10.0[\mathrm{N/m}]$
[case 2]: $m_w = 10[\mathrm{kg}],\ b_w = 50[\mathrm{Ns/m}],\ c_w = 1000[\mathrm{N/m}]$
[case 3]: $m_w = 1.0 \times 10^4[\mathrm{kg}],\ b_w = 2.0 \times 10^4[\mathrm{Ns/m}],$
$c_w = 4.0 \times 10^4[\mathrm{N/m}]$

In case 1, a relatively soft object is supposed. In case 2, a relatively hard one is supposed. In case 3, a nearly rigid one is supposed. To simplify the problem, the parameters of the operator are fixed at constant values as follows:

$$m_{op} = 1.0[\mathrm{kg}],\ b_{op} = 20.0[\mathrm{Ns/m}],\ c_{op} = 10.0[\mathrm{N/m}]$$

The gains for each control scheme are set as follows. The gains which are not shown below are set zero.

[Symmetric Position Servo Type]:
$K_{mpm} = K_{mps} = -500[\mathrm{N/m}],\ K'_{mpm} = -50[\mathrm{Ns/m}],$
$K_{spm} = K_{sps} = 500[\mathrm{N/m}],\ K'_{sps} = 50[\mathrm{Ns/m}]$

[Force Reflection Type]:
$K_{mfs} = 1.0,\ K_{spm} = K_{sps} = 500[\mathrm{N/m}],$
$K'_{sps} = 50[\mathrm{Ns/m}]$

[Force Reflecting Servo Type]:
$K_{mfm} = 2.5,\ K_{mfs} = 3.5,$
$K_{sps} = K_{spm} = 500[\mathrm{N/m}],\ K'_{sps} = 50[\mathrm{Ns/m}]$

Fig.2.4 shows the values of J_p and J_f defined by eqs.(2.45) and (2.46) for the cases 1, 2 and 3, in addition to the special cases when $Z_L = 0$ and ∞. We set $\omega_{max} = 100[\mathrm{Hz}]$ and $1/T = 50[\mathrm{Hz}]$. Symmetric

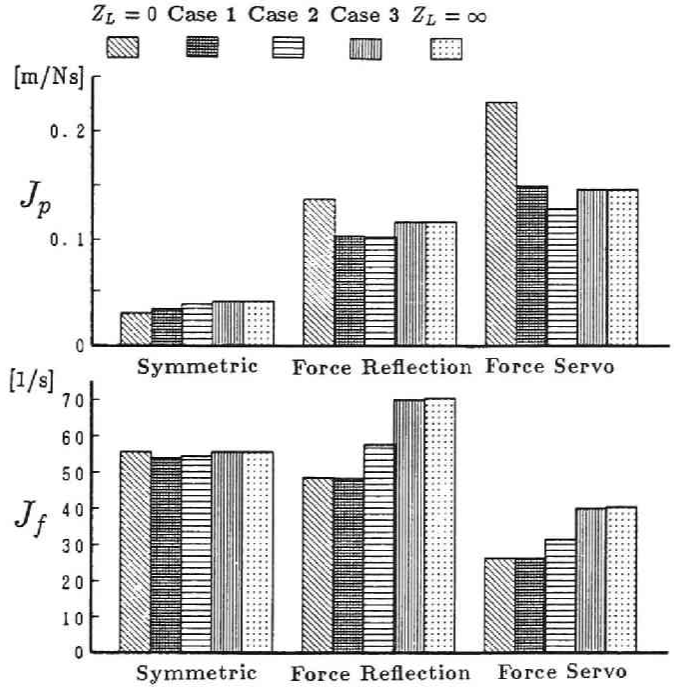

Figure 2.4: Example of performance index for maneuverability

position servo type is good for position response but poor for force response. Force reflecting servo type has worse J_p than symmetric position servo type but J_f is better in every case. As for force reflection type, both J_p and J_f become worse than symmetric position servo type, especially when the object has high impedance.

This numerical result is just one example for particular gains and we cannot conclude which control scheme is the best. But the result of the proposed quantitative evaluation for the conventional control schemes seem to agree with our intuition. As mentioned before, J_p and J_f may change according to the object parameters. If we could know the range of the object parameter in advance, we could evaluate J_p and J_f by using a representative parameter among this object parameter range. If we cannot specify the object parameter range, we can evaluate J_p and J_f by setting Z_L at zero and infinity. Of course, it is very

important to identify the operator's parameters in order to obtain a valid evaluation result. However actual parameters such as b_{op} and c_{op} will fluctuate according to the task, and it would be necessary to choose an appropriate representative value.

Eqs.(2.45) and (2.46) evaluate just an absolute difference between the two transfer functions. It is also possible to evaluate a relative difference with the ideal response as follows:

$$J_p = \int_0^{\omega max} \left| \frac{G_{mp}(j\omega) - G_{sp}(j\omega)}{G_{0p}(j\omega)} \right| \left| \frac{1}{1 + j\omega T} \right| d\omega \qquad (2.51)$$

$$J_f = \int_0^{\omega max} \left| \frac{G_{mf}(j\omega) - G_{sf}(j\omega)}{G_{0f}(j\omega)} \right| \left| \frac{1}{1 + j\omega T} \right| d\omega \qquad (2.52)$$

where $G_{0p}(s)$ and $G_{0f}(s)$ are transfer functions of the ideal response III and given by

$$G_{0p}(s) = \frac{1}{s[Z_L + Z_G]}, \qquad (2.53)$$

$$G_{0f}(s) = \frac{s[Z_L]}{s[Z_L + Z_G]}. \qquad (2.54)$$

Evaluation by eqs.(2.51) and (2.52) which use relative differences may match to our intuition better than by eqs.(2.45) and (2.46) where the absolute difference is used. It should be noted, however, that G_{0f} and G_{0p} become zero when $Z_L = 0$ and ∞ and J_f and J_f of eqs.(2.51) and (2.52) cannot be used in these cases.

2.5 Evaluation of Stability

2.5.1 Linear Systems Case

In order to evaluate strictly the stability of the system, it is necessary to consider whole system including the operator and object. From eqs.(2.39) through (2.42), the characteristic equation of four transfer functions, $G_{mp}(s)$, $G_{sp}(s)$, $G_{mf}(s)$, and $G_{sf}(s)$, are given by

$$H(s) = s^2[D_Y + N_{11}Z_L + N_{22}Z_G + D_Z Z_L Z_G]. \qquad (2.55)$$

In order to make the system stable, all the roots of eq.(2.55) should be in the left half side of the complex plane regardless of parameters of the operator and object. Since $H(s)$ contains many parameters, however, it is difficult to obtain a general condition for stability.

2.5.2 Passivity of the System

The characteristic equation approach is applicable only to the case when the dynamics of the operator and object can be represented by linear systems described in eqs.(2.3) and (2.4). Strictly speaking, however, the operator dynamics may be nonlinear and every object cannot be treated as a linear system. In this subsection, we discuss the system stability for more wide range of the operator and object dynamics based on the concept of passivity.

Raju[72][73] showed that the positive definiteness of the impedance matrix of the master-slave system is a sufficient condition of stability. However, this condition cannot be applied in the case when the condition (A) is satisfied because the impedance matrix cannot be defined. Colgate et al.[15] showed that the necessary and sufficient condition for the system which may interact to any passive environments to be stable is that the system itself must be passive. In the case of master-slave systems, the condition for the total system to be stable is that the master-slave system itself must be passive if the operator and environment can be regarded as passive systems. Anderson et al.[4] also checked the stability of the master-slave systems with time-delay by passivity of the system.

However, strictly speaking, the operator is not passive because he has a power source of muscles and may generate the energy outside. Colgate et al. mentioned that, even if the system interacting with an environment has an active term, the system stability is guaranteed unless the active term is in some way state-dependent. In the case of master-slave system, the operator himself is obviously passive when $\tau_{op} = 0$, therefore, we set the following assumption about τ_{op}; "*The operator does not generate τ_{op} that cause the system to be unstable.*" Dudragne et al.[19] gave a similar assumption in order to use the concept of passivity for stability distinction.

Let us show the system stability using the concept of passivity of

electric circuits. First, vectors are defined as $\boldsymbol{V} \triangleq [\ V_m \quad V_s\ ]^T$ and $\boldsymbol{I} \triangleq [\ I_m \quad -I_s\ ]^T$. The system is defined to be passive when the power P consumed by the system satisfies the following equation[53]:

$$\begin{aligned} P &= \mathrm{Re}(V_m^* I_m - V_s^* I_s) \\ &= \left(\frac{\boldsymbol{V}+\boldsymbol{I}}{2}\right)^* \left(\frac{\boldsymbol{V}+\boldsymbol{I}}{2}\right) - \left(\frac{\boldsymbol{V}-\boldsymbol{I}}{2}\right)^* \left(\frac{\boldsymbol{V}-\boldsymbol{I}}{2}\right) \\ &= \boldsymbol{a}^*\boldsymbol{a} - \boldsymbol{b}^*\boldsymbol{b} \\ &= \boldsymbol{a}^*(\boldsymbol{E}_2 - \boldsymbol{S}^*\boldsymbol{S})\boldsymbol{a} \geq 0 \end{aligned} \tag{2.56}$$

where * denotes conjugate transpose. The matrix $\boldsymbol{S}$ in eq.(2.56) is called the scattering matrix. The scattering matrix specifies the relation between the input wave to the system $\boldsymbol{a} \triangleq (\boldsymbol{V}+\boldsymbol{I})/2$ and the output wave from the system $\boldsymbol{b} \triangleq (\boldsymbol{V}-\boldsymbol{I})/2$.

$$\boldsymbol{b} = \boldsymbol{S}\boldsymbol{a} \tag{2.57}$$

From eq.(2.56), the passivity of the system can be checked by the following equation:

$$||\boldsymbol{S}|| = \max_{\boldsymbol{x}} \frac{||\boldsymbol{S}\boldsymbol{x}||}{||\boldsymbol{x}||} = \max \lambda^{1/2}(\boldsymbol{S}^*\boldsymbol{S}) \leq 1 \tag{2.58}$$

in other words, the system is passive if the maximum singularity value of $\boldsymbol{S}$ is less than 1[4].

The scattering matrix $\boldsymbol{S}$ of the master-slave system is given by

$$\begin{aligned} \boldsymbol{S} &= \frac{1}{D_Y + N_{11} + N_{22} + D_Z} \\ &\times \begin{bmatrix} D_Y + N_{11} - N_{22} - D_Z & 2N_{12} \\ 2N_{21} & D_Y - N_{11} + N_{22} - D_Z \end{bmatrix} \end{aligned} \tag{2.59}$$

The system stability is guaranteed if the maximum singularity value of $\boldsymbol{S}$ in eq.(2.59) is less than 1.

2.6 Conclusion

The main results of this chapter can be summarized as follows:

- A simple one degree of freedom system model of the master-slave system has been discussed where both the operator dynamics and object dynamics have been taken into account.
- Three ideal responses have been defined and the conditions to achieve these ideal responses have been derived. It has been shown that acceleration signals must be used in the control schemes in order to realize the ideal responses.
- A quantitative performance index for maneuverability has been given based on the concept of the ideal responses by evaluating how well the actual system realizes the ideal responses.
- The stability of the system is discussed based on the concept of network passivity.

It becomes possible to evaluate the performance of the system maneuverability quantitatively by using the result of this chapter. It could also be a design guide for new control schemes to provide good maneuverability.

Chapter 3

BILATERAL CONTROL OF MASTER-SLAVE MANIPULATORS FOR IDEAL KINESTHETIC COUPLING

3.1 Introduction

Master-slave systems have been applied to many areas since the 1960's when the first master-slave manipulator was developed. However, there was little improvement about the control scheme. Very recently, several studies analyzed master-slave systems strictly and new control schemes aimed at the improvement of maneuverability were proposed. Dudragne et al.[19] paid their attention to the system passivity and proposed a new control scheme by extending the symmetric position servo type. There are other new control schemes such as a modification of force reflecting servo type by Nagai and Matsushima[64], the virtual internal model scheme by Furuta et al.[23], adaptive control by Fujii et al.[21], and parallel control type by Miyasaki et al.[59]. Some of these control schemes are not clear in the point of the system stability or the quality of the total system response. Especially, these studies

lack the discussion about how to improve the maneuverability.

It is important to specify an ideal response of master-slave systems for designing control schemes. In order that the operator can perceive the remote object as if he were manipulating it directly, the system must be coupled with the operator to give the ideal kinesthetic sense. Dudragne et al. mentioned that the system should give a response just like a virtual rod connecting the operator and remote site which has infinitely small mass and infinitely large stiffness[19], and specified an ideal response as the case when the hybrid matrix has a special value. The latter fact was also shown by Hannaford[35]. But they did not exactly discuss to what extent the actual responses can be realized the ideal response. Tachi et al.[81] proposed the impedance type control scheme where an appropriate impedance model is realized at each arm in order to improve the maneuverability, and they mentioned that the smaller a desired impedance is set, the closer the system response is to the ideal one. Kazerooni[49] proposed a concept of "Telefunctioning", the extension of telepresence by including appropriate functions between the master and slave sides.

In this chapter, we design a new control scheme which provides ideal kinesthetic coupling. First, we design new control schemes to realize the ideal responses defined in chapter 2. Next, we discuss the system stability when the designed control schemes are used based on the system passivity. Last, we confirm the validity of the proposed control schemes by simulations.

3.2 Design of Control Schemes Realizing the Ideal Responses

3.2.1 Modeling in One DOF System

The dynamics of the master arm and the slave arm is given by the following equations.

$$\tau_m + f_m = m_m \ddot{x}_m + b_m \dot{x}_m \tag{3.1}$$

$$\tau_s - f_s = m_s \ddot{x}_s + b_s \dot{x}_s \tag{3.2}$$

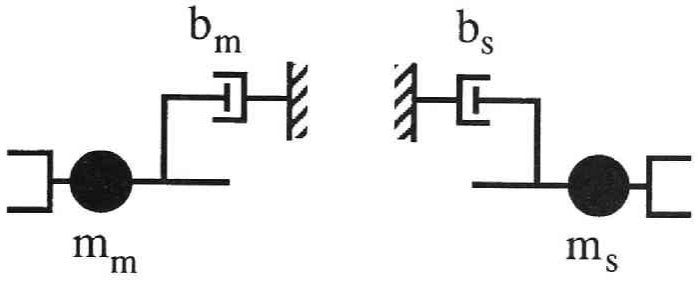

Figure 3.1: Master and slave arms

where x_m and x_s denote the displacements of the master and slave arms respectively. And m_m and m_s represent mass of the master and slave arms, and b_m and b_s are the viscous coefficients of the master and slave arms. On the other hand, f_m denotes the force that the operator applies to the master arm and f_s denotes force that the slave arm applies to the object. The actuator driving forces of the master and slave arms are represented by τ_m and τ_s respectively. **Fig.3.1** shows the model of master and slave arms.

The dynamics of the object which the slave arm manipulates is modeled by the following liner system.

$$f_s = m_w \ddot{x}_s + b_w \dot{x}_s + c_w x_s \tag{3.3}$$

where m_w, b_w, and c_w denote mass, viscous coefficient, and stiffness of the object respectively.

The dynamics of the operator is also assumed to be represented by

$$\tau_{op} - f_m = m_{op} \ddot{x}_m + b_{op} \dot{x}_m + c_{op} x_m \tag{3.4}$$

where m_{op}, b_{op} and c_{op} denote mass, viscous coefficient, and stiffness of the operator respectively and τ_{op} means force generated by the operator's muscles.

3.2.2 Control Scheme Realizing the Ideal Response III

In this section, we design control schemes which realize the ideal responses based on the results obtained in the previous chapter. First,

we design a control scheme realizing the ideal response III.

Let the following basic form of control schemes be considered:

$$\tau_m = m_m u_m + b_m \dot{x}_m - k_{mf}\left(\frac{f_s - f_m}{2}\right) - \frac{f_m + f_s}{2} \tag{3.5}$$

$$\tau_s = m_s u_s + b_s \dot{x}_s - k_{sf}\left(\frac{f_s - f_m}{2}\right) + \frac{f_m + f_s}{2} \tag{3.6}$$

where k_{mf} and $k_{sf} \geq 0$ are force gains, and u_m and u_s are new input vectors. Eqs.(3.5) and (3.6) satisfy the condition (A) derived in chapter 2 unless force signals are used in the new inputs u_m and u_s. We assume that physical parameters of each arm, such as m_m, m_s, b_m and b_s, are correctly known so that the exact parameters can be used in the control schemes. Substituting eqs.(3.5) and (3.6) into eqs.(3.1) and (3.2) respectively, the following equations are obtained:

$$\ddot{x}_m = u_m - \frac{1}{m_m}(1 + k_{mf})\left(\frac{f_s - f_m}{2}\right) \tag{3.7}$$

$$\ddot{x}_s = u_s - \frac{1}{m_s}(1 + k_{sf})\left(\frac{f_s - f_m}{2}\right) \tag{3.8}$$

Adding both sides of eqs.(3.7) and (3.8), we obtain

$$\ddot{x}_m + \ddot{x}_s = u_m + u_s - \left(\frac{1 + k_{mf}}{m_m} + \frac{1 + k_{sf}}{m_s}\right)\left(\frac{f_s - f_m}{2}\right) \tag{3.9}$$

Here, if

$$\ddot{x}_m + \ddot{x}_s = u_m + u_s \tag{3.10}$$

can be satisfied, we get

$$f_m - f_s = 0 \tag{3.11}$$

from eq.(3.9) and it means that at least the ideal response II is realized. It is clear that acceleration signals are necessary in the control schemes to realize eq.(3.10). Next, subtracting both sides of eq.(3.8) from eq.(3.7) and considering eq.(3.11), we get

$$\ddot{x}_m - \ddot{x}_s = u_m - u_s \tag{3.12}$$

where $e \triangleq x_m - x_s$ denotes the position error between the two arms. Eq.(3.12) shows that the behavior of $\ddot{e}$ can be specified by $u_m - u_s$. Here, we set $u_m - u_s$ as follows:

$$u_m - u_s = -k_1\dot{e} - k_2 e \tag{3.13}$$

Then, we get

$$\ddot{e} + k_1\dot{e} + k_2 e = 0 \tag{3.14}$$

and e converges into zero asymptotically by appropriate gains k_1 and k_2, and the ideal response III can be realized in the steady state. From eqs.(3.10) and (3.13), u_m and u_s are given by the following equations:

$$u_m = \frac{1}{2}(\ddot{x}_m + \ddot{x}_s) - \frac{1}{2}k_1\dot{e} - \frac{1}{2}k_2 e \tag{3.15}$$

$$u_s = \frac{1}{2}(\ddot{x}_m + \ddot{x}_s) + \frac{1}{2}k_1\dot{e} + \frac{1}{2}k_2 e \tag{3.16}$$

Consequently, the control scheme is given as follows:

$$\begin{aligned} \tau_m &= m_m[\ddot{x}_{ms} + k_1(\dot{x}_{ms} - \dot{x}_m) + k_2(x_{ms} - x_m)] \\ &\quad + b_m\dot{x}_m - k_{mf}(f_{ms} - f_m) - f_{ms} \end{aligned} \tag{3.17}$$

$$\begin{aligned} \tau_s &= m_s[\ddot{x}_{ms} + k_1(\dot{x}_{ms} - \dot{x}_s) + k_2(x_{ms} - x_s)] \\ &\quad + b_s\dot{x}_s + k_{sf}(f_{ms} - f_s) + f_{ms} \end{aligned} \tag{3.18}$$

where $x_{ms} \triangleq (x_m + x_s)/2$ and $f_{ms} \triangleq (f_m + f_s)/2$. Eqs.(3.17) and (3.18) can be interpreted as the dynamic control where the desired trajectory is the middle point of both arms x_{ms}, and the forces of both arms are simultaneously controlled to follow the averaged force f_{ms}. Force gains k_{mf} and k_{fs} are not required in this case because these terms in eqs.(3.17) and (3.18) are zero from eq.(3.11).

We assumed that arm parameters m_m, m_s, b_m and b_s are exactly known. However, it should be noted that these parameters may actually contain some identification errors, and not only these parameter errors but also noises of the acceleration and force signals and the computation delays may cause the system to be unstable. Several

Figure 3.2: Ideal state of master-slave system

researchers discussed the robustness of the computed torque law for trajectory control of manipulators with respect to the uncertainty of the dynamics parameters where the controller provides an arbitrary small tracking error capability for the particular class of the desired trajectories by choosing appropriate feed-back gains[31][68]. In the case of master-slave systems, the parameter uncertainty or time delay of the computation spoils the achievement of eq.(3.10), and the robustness of the controller should be considered for the future.

It is obvious that this control scheme satisfies the conditions of the ideal response III obtained in subsection 2.3.2, because we can get

$$\begin{array}{ll} P_m = \frac{m_m}{2}(s - k_1 - k_2/s) + b_m & Q_m = \frac{1}{2}(k_{mf} - 1) \\ R_m = -\frac{m_m}{2}(s + k_1 + k_2/s) & S_m = \frac{1}{2}(k_{mf} + 1) \\ P_s = \frac{m_s}{2}(s + k_1 + k_2/s) & Q_s = \frac{1}{2}(k_{sf} + 1) \\ R_s = \frac{m_s}{2}(-s + k_1 + k_2/s) - b_s & S_s = \frac{1}{2}(k_{sf} - 1) \end{array}$$

from eqs.(3.17) and (3.18).

3.2.3 Control Schemes Realizing the Ideal Responses I and II

In the previous subsection, we discussed a new control scheme which can realize the ideal response III. We can interpret that this control scheme cancels the dynamics of the master and slave arms which actually exists between the operator and object. It means that this control scheme requires the arm controller a high performance. In this section, we discuss a way to reduce the burden on the controller by allowing the existence of arm dynamics as a certain type of impedance. Applying the control scheme of eqs.(3.17) and (3.18) corresponds to achieving

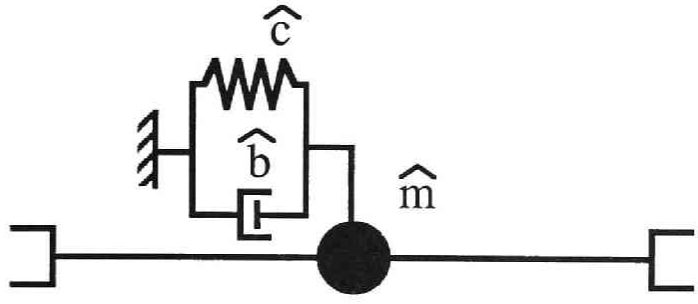

Figure 3.3: Intervenient impedance model

the state shown in **Fig.3.2** from the actual system shown in **Fig.3.1**, where the master side and the slave side are connected by a virtually rigid and weightless bar if $e = 0$ at the initial state. Here, we try to make the dynamics of master and slave arms act as a certain kind of impedance shown in **Fig.3.3**. Since this impedance seemingly intervenes between the operator and the object, we call it the *intervenient impedance*. The existence of this intervenient impedance requires the operator to exert force toward the system even if there is no load at the slave side. Consequently the movements of the master and slave arms are restricted so that the burden on the arm controller is reduced. The state of **Fig.3.3** can be described by the following equation by setting $x_m = x_s = x$.

$$f_m - f_s = \hat{m}\ddot{x} + \hat{b}\dot{x} + \hat{c}x \tag{3.19}$$

where $\hat{m}$, $\hat{b}$, and $\hat{c}$ are the mass, coefficient of viscous friction, and stiffness of the intervenient impedance respectively. Since x_m and x_s may not coincide all the time, we consider the following equation:

$$f_m - f_s = \hat{m}\ddot{x}_{ms} + \hat{b}\dot{x}_{ms} + \hat{c}x_{ms} \tag{3.20}$$

We set the following equation corresponding to eq.(3.14).

$$\ddot{e} + k_1\dot{e} + k_2 e = \lambda\frac{f_m + f_s}{2} \tag{3.21}$$

where $\lambda > 0$ is a positive constant. Substituting eq.(3.20) into eqs.(3.7) and (3.8), and substituting u_m and u_s which are obtained by considering

eq.(3.21), into eqs.(3.5) and (3.6) respectively, we get the following control scheme:

$$\begin{aligned}\tau_m &= m_m[\ddot{x}_{ms} + k_1(\dot{x}_{ms} - \dot{x}_m) + k_2(x_{ms} - x_m)] \\ &\quad + b_m\dot{x}_m - \frac{(1+k_{mf})}{2}[\widehat{m}\ddot{x}_{ms} + \widehat{b}\dot{x}_{ms} + \widehat{c}x_{ms}] \\ &\quad + \frac{\lambda}{2}m_m f_{ms} - k_{mf}(f_{ms} - f_m) - f_{ms} \qquad (3.22)\end{aligned}$$

$$\begin{aligned}\tau_s &= m_s[\ddot{x}_{ms} + k_1(\dot{x}_{ms} - \dot{x}_s) + k_2(x_{ms} - x_s)] \\ &\quad + b_s\dot{x}_s - \frac{(1+k_{sf})}{2}[\widehat{m}\ddot{x}_{ms} + \widehat{b}\dot{x}_{ms} + \widehat{c}x_{ms}] \\ &\quad - \frac{\lambda}{2}m_s f_{ms} + k_{sf}(f_{ms} - f_s) + f_{ms} \qquad (3.23)\end{aligned}$$

If $\lambda = 0$ in eqs.(3.22) and (3.23), e converges into zero by appropriate gains k_1, k_2 similarly to eq.(3.14) and the state of eq.(3.20) becomes the state of eq.(3.19). Since the control scheme of eqs.(3.22) and (3.23) where $\lambda = 0$ guarantees the convergence of e into 0, this control scheme is one of the examples of the control schemes realizing the ideal response I. It is also easy to show that this control scheme satisfies the conditions for ideal response I. Especially when $\widehat{c} = 0$, this particular intervenient impedance can be regarded as a model of mechanical master-slave manipulator where the viscous friction of the transmission wires is considered. Besides, when $\widehat{b} = 0$, the intervenient impedance becomes an ideal model of a mechanical master-slave manipulator, where there is no friction. Moreover, when $\widehat{m} = 0$, this control scheme coincides with that of eqs.(3.17) and (3.18). Therefore one can regard the control scheme of eqs.(3.17) and (3.18) as the special case when the intervenient impedance is set at zero. On the other hand, when $\widehat{m}$, k_{mf}, and k_{sf} are set so that $\widehat{m} = 2m_m/(1+k_{mf}) = 2m_s/(1+k_{sf})$, the acceleration terms in both eqs.(3.17) and (3.18) become zero and the control scheme becomes the special case where no acceleration signal is used.

On the other hand, when $\widehat{m} = \widehat{b} = \widehat{c} = 0$ in eqs.(3.22) and (3.23), this control scheme realizes the ideal response II. Moreover, when $m_m = m_s = m$, $\lambda = 2/m$, $k_{mf} = k_{sf} = 0$, the control scheme becomes the special case where no force signal is used.

Consequently, eqs.(3.22) and (3.23) are general forms of the control schemes for realizing three ideal responses. Especially, when $\lambda \neq 0$ and $\hat{c} = 0$ in eqs.(3.22) and (3.23), the corresponding intervenient impedance can be regarded as a model of a mechanical master-slave manipulator where the stiffness of the transmission wires is also considered.

3.2.4 Special Cases of Object

Let the following two special cases of the object be considered; the cases when the object impedance is zero $Z_L = 0$ and infinite $Z_L = \infty$.

$Z_L = 0$:

This case corresponds to the case when $m_w = b_w = c_w = 0$ in eq.(3.3). This is one of the special cases of the object, but it happens very often such that when the operator moves the slave arm from a point to another without handling any object.

In this case, from eq.(3.3), the following equation always satisfies.

$$f_s = 0 \tag{3.24}$$

When the control schemes of eqs.(3.17) and (3.18) are applied, eq.(3.11) is realized. Consequently, we get

$$f_m = 0. \tag{3.25}$$

Since there is no object at the slave side, eq.(3.25) is an ideal situation for the operator. However, eq.(3.25) means that the master arm have to move in the same acceleration as that of the operator's without the force interaction with the operator, and this situation seems against the principle of causality. This problem appears due to the inexactness of the sensor placement.

Fig.3.4 shows the sensor placement at the master arm. The force sensor is placed at the tip of the master arm, and the accelerometer is placed at the tip of the force sensor so that the accelerometer can sense the acceleration of the operator even if $f_m = 0$. In the above analysis, we implicitly assumed that mass of the tip part from the force sensor, including the gripper and accelerometer, is negligible.

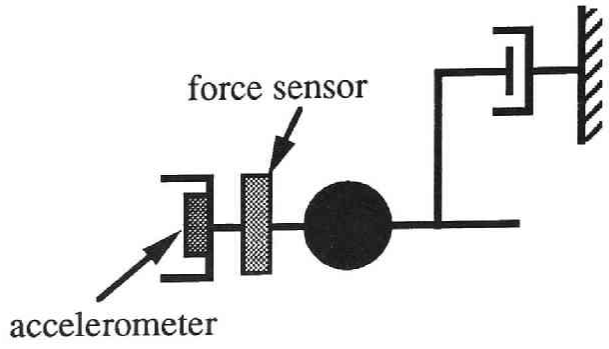

Figure 3.4: Sensor placement at master arm

When the acceleration is measured at the joint, we cannot cancel out all the dynamics of arms but have to set the intervenient mass $\widehat{m}$ at nonzero. However, theoretically speaking, we can set $\widehat{m}$ close to zero as much as we want.

$Z_L = \infty$:

When at least one among m_w, b_w, and c_w becomes infinite in eq.(3.3), Z_L becomes ∞. This case corresponds to the situation when the slave arm contacts to the rigid object fixed on the base.

This is also one of the special cases of objects. It also happens often in teleoperation as well as the case when $Z_L = 0$. And this is a very critical situation for manipulator control where a sudden transition from the free motion to the constraint motion causes sometimes the system to be unstable. In this case,

$$\ddot{x}_s = \dot{x}_s = x_s = 0 \tag{3.26}$$

must be satisfied all the time, and eq.(3.2) becomes

$$f_s = \tau_s \tag{3.27}$$

Even in this case, we can derive eqs.(3.11) and (3.14) from eqs.(3.1), (3.17), (3.18), (3.26), and (3.27).

3.3 Discussion about Stability

We discuss the stability of the system when the proposed control schemes are applied. In order to evaluate the stability of the system strictly, it is necessary to consider whole system including the operator and object. As for the control schemes of eqs.(3.17) and (3.18), the system stability can be shown from the characteristic equations (2.55) of four transfer functions shown in chapter 2. However, this approach is applicable only when the dynamics of the operator and object can be regarded as linear systems shown in eqs.(3.3) and (3.4). In chapter 2, we have discussed the system stability based on the concept of passivity where we can treat more wide range of operators and objects. In this section, we show the system stability when the general form of control scheme eqs.(3.22) and (3.23) is applied based on the concept of passivity.

From section 2.5.2 in chapter 2, the passivity of the system can be checked by the following equation:

$$||\boldsymbol{S}|| = \max_{\boldsymbol{x}} \frac{||\boldsymbol{S}\boldsymbol{x}||}{||\boldsymbol{x}||} = \max \lambda^{1/2}(\boldsymbol{S}^*\boldsymbol{S}) \leq 1 \tag{3.28}$$

where $\boldsymbol{S}$ is the scattering matrix of the master-slave system and given by

$$\begin{aligned} \boldsymbol{S} &= \frac{1}{D_Y + N_{11} + N_{22} + D_Z} \\ &\times \begin{bmatrix} D_Y + N_{11} - N_{22} - D_Z & 2N_{12} \\ 2N_{21} & D_Y - N_{11} + N_{22} - D_Z \end{bmatrix} \end{aligned} \tag{3.29}$$

Eq.(3.28) means that the system is passive if the maximum singularity value of $\boldsymbol{S}$ is less than 1. Substituting the parameters in eqs.(3.22) and (3.23) to eq.(3.29), we get

$$\begin{aligned} \boldsymbol{S} &= \frac{1}{((s + k_1 + k_2/2) + \frac{1}{2}\lambda)((\widehat{m}s + \widehat{b} + \widehat{c}/2) + 2)} \\ &\times \begin{bmatrix} \alpha & \beta \\ \beta & \alpha \end{bmatrix} \end{aligned} \tag{3.30}$$

$$\begin{aligned} \alpha &= (s + k_1 + k_2/s)(\widehat{m}s + \widehat{b} + \widehat{c}/s) - \lambda \\ \beta &= 2(s + k_1 + k_2/s) - \frac{1}{2}(\widehat{m}s + \widehat{b} + \widehat{c}/s) \end{aligned}$$

From eq.(3.30), the singularity values of $\boldsymbol{S}$ are given as follows:

$$\sigma_1 = \frac{|(\widehat{m}s + \widehat{b} + \widehat{c}/s) - 2|}{|(\widehat{m}s + \widehat{b} + \widehat{c}/s) + 2|} \leq 1 \tag{3.31}$$

$$\sigma_2 = \frac{|(s + k_1 + k_2/s) - \frac{1}{2}\lambda|}{|(s + k_1 + k_2/s) + \frac{1}{2}\lambda|} \leq 1 \tag{3.32}$$

and both of them never over 1. Consequently, the system stability by applying the proposed control schemes of eqs.(3.22) and (3.23) has been guaranteed under the assumption that the object is passive and the operator is passive when $\tau_{op} = 0$.

3.4 Simulation

In this section, we confirm the validity of the proposed control scheme by simulations. The parameters of the master and slave arms are chosen as follows:

$$m_m = m_s = 2.0[\text{kg}], \quad b_m = b_s = 0.2[\text{Ns/m}]$$

and the object parameter is set as:

$$m_w = 3.0[\text{kg}], \quad b_w = 1.0[\text{Ns/m}], \quad c_w = 100.0[\text{N/m}]$$

The parameter of the operator is set the constant values for simplification as follows:

$$m_{op} = 1.0[\text{kg}], \quad b_{op} = 2.0[\text{Ns/m}], \quad c_{op} = 10.0[\text{N/m}]$$

The following three cases of control schemes are compared.

[Case 1]: Eqs.(3.17) and (3.18)
$k_1 = 20[1/\text{s}], k_2 = 100[1/\text{s}^2], k_{mf} = k_{sf} = 0$

[Case 2]: Force reflecting servo type
$K_{mfm} = 2.5, K_{mfs} = 3.5$
$K_{sps} = K_{spm} = 500[\text{N/m}], K'_{sps} = 50[\text{Ns/m}]$

[Case 3]: Eq.(3.22) and (3.23)
$k_1 = 20[1/\mathrm{s}], k_2 = 100[1/\mathrm{s}^2], \widehat{m} = 2.0[\mathrm{kg}]$
$\widehat{b} = 1.0[\mathrm{kg/s}], \widehat{c} = 0.0[\mathrm{kg/s}^2], \lambda = 0.1[1/\mathrm{kg}], k_{mf} = k_{sf} = 0$

Fig.3.5~3.7 show the responses of x_m, x_s, f_m and f_s respectively when sinusoidal input $\tau_{op} = 5 - 5\cos(4\pi t)[\mathrm{N}]$ is exerted. Sampling time is 1[ms]. In each figure, the maximum inputs of both arm actuators are shown. While the case 2 has delay of response and steady error, the case 1 almost realizes the ideal response III, although the actuator inputs are smaller. It should be noted that the case 2 becomes unstable when the gains are set larger in order to suppress the errors. The case 3 shows the effect of the intervenient impedance. The actuator input at the slave arm was reduced due to the existence of the intervenient impedance.

3.5 Conclusion

The main results obtained in this chapter can be summarized as follows:

- New control schemes of master-slave manipulators have been proposed which can realize the ideal responses previously defined. These control schemes take the arm dynamics into account by using acceleration signals. Especially, the control scheme that can achieve the ideal response III provides the ideal kinesthetic coupling.

- It has been shown by using the concept of network passivity that the proposed control scheme guarantees the system stability.

- The validity of the proposed control schemes has been confirmed by simulations.

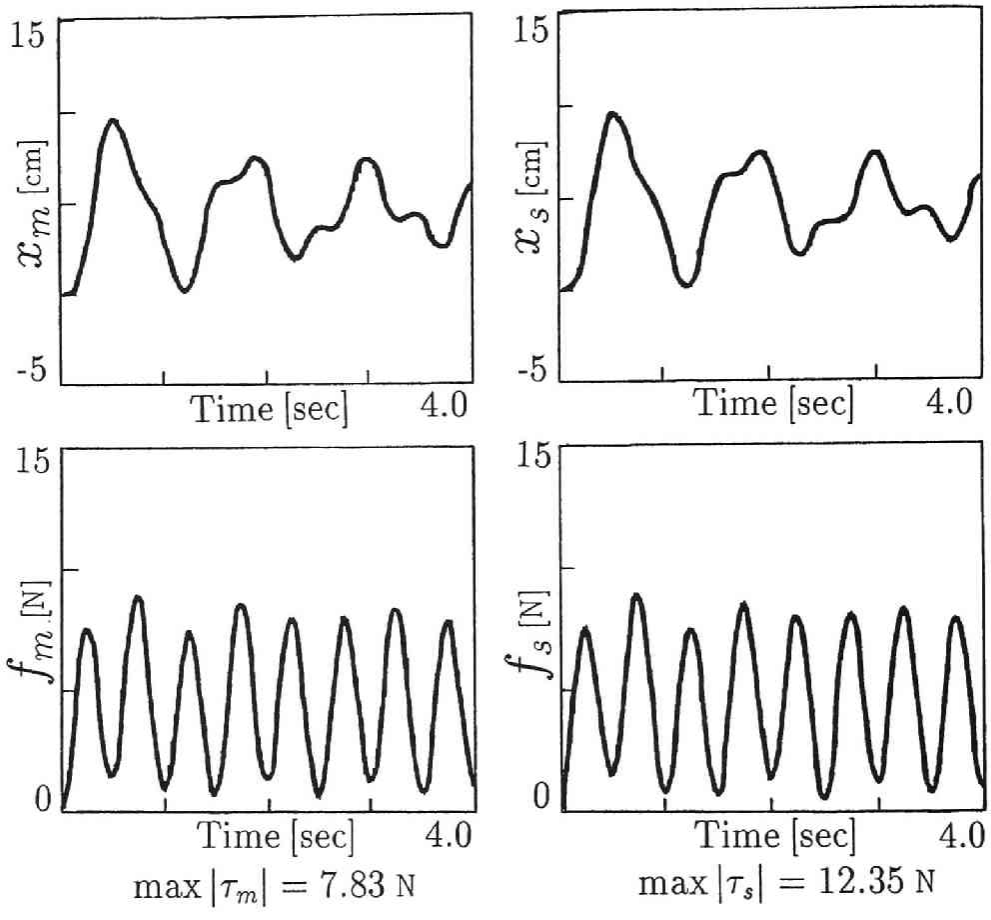

Figure 3.5: Simulation result (case 1)

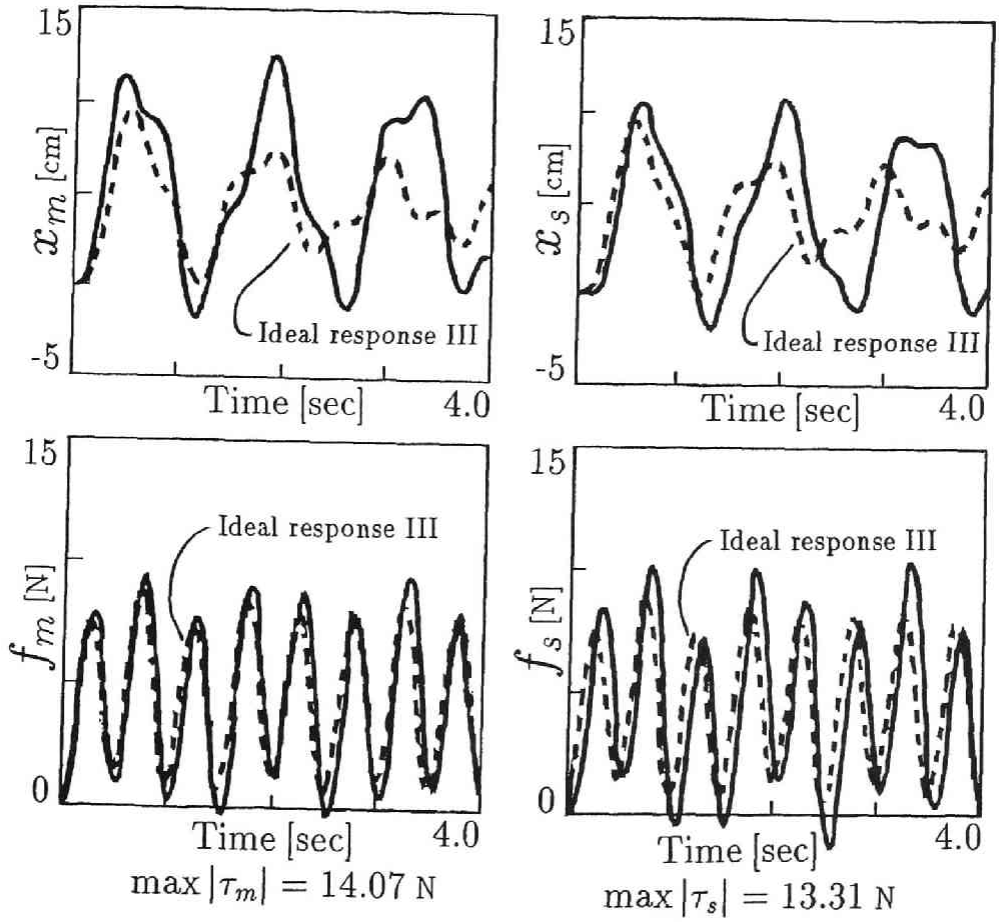

Figure 3.6: Simulation result (case 2)

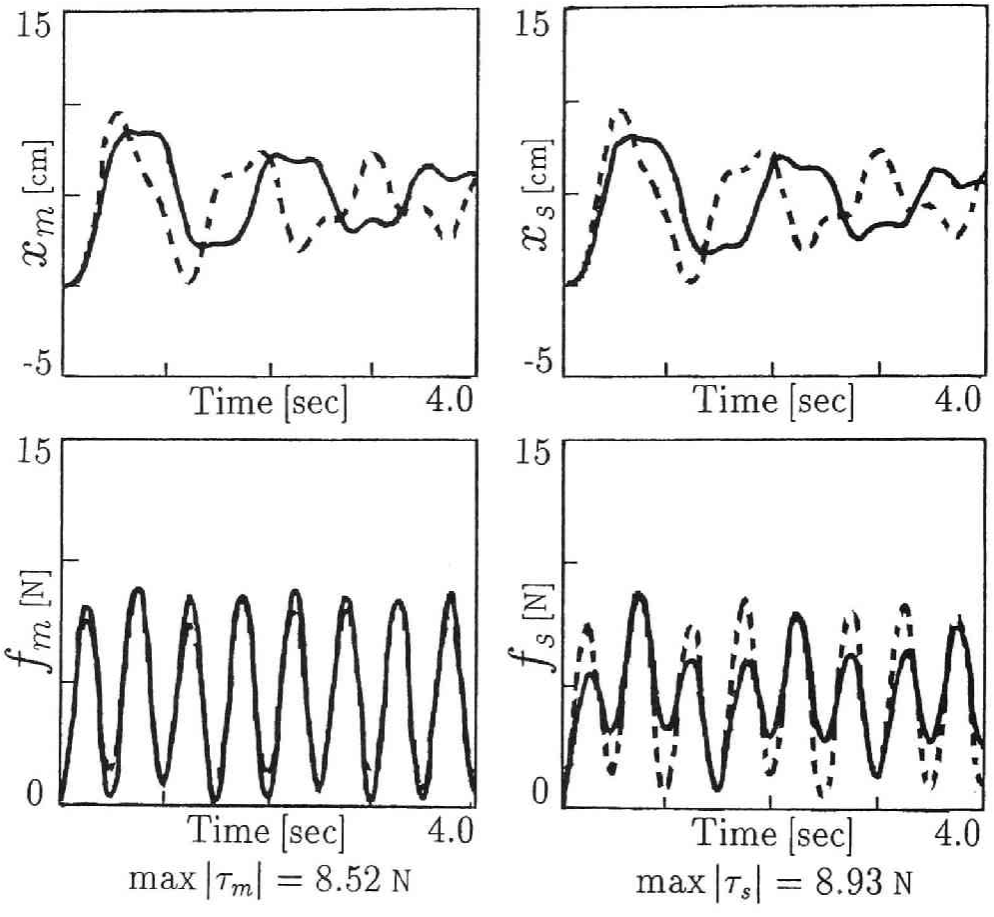

Figure 3.7: Simulation result (case 3)

Chapter 4

DESIGN GUIDE OF MASTER ARMS CONSIDERING OPERATOR DYNAMICS

4.1 Introduction

The design of master-slave systems has two aspects; one is the design of control schemes and the other is the mechanical design of arms. In chapter 3, we have discussed the control design of one DOF master-slave systems. Before extending the discussion of the controller design into the multiple DOF case, we discuss the mechanical design of multiple DOF arms and especially focus on the design of master arms.

The design of the master arm is very important as a man/machine interface of the teleoperation system and the quality of master arm design affects considerably the maneuverability of the system. In the early model of master-slave systems, the isomorphic configuration arms were used and the master arm should have the same configuration as that of the slave arm. Therefore, the amount of freedom in designing master arms was restricted. Recently, the performance of computers has improved and it becomes practicable to compute the coordinate transformation in real time. Under this situation, the isomorphic con-

figuration type has been taken over by the different configuration type and the amount of freedom in designing the configuration of the master arm independently from that of the slave arm has become greater. So far, several master arm designs aimed at high maneuverability for operators were proposed. For example, polar coordinates type was proposed by Bejczy et al.[11], Cartesian coordinates type by Inoue et al.[43], parallel link type using direct-drive motors by Hirai and Sato[38][76] and homogeneous inertia type by Ioi et al.[44]. However these designs were somewhat intuitive and there were little discussion about quantitative evaluation of the master arm manipulability. In this chapter, we use the term of "manipulability" as a measure of the easiness to manipulate the arm, whereas "maneuverability" means the measure of total performance of the master-slave systems.

The generalized inertia matrix[7] or the generalized inverse inertia matrix[39][8], can be a candidate for a measure of the master arm manipulability. These matrices represent the equivalent inertia of the arm at the hand tip, and one can evaluate the easiness for the operator to move the master arm based on these matrices. This evaluation, however, does not consider the dynamics of the operator himself and such properties of the operator as he can easily exert force in a certain direction but cannot in another direction. Another problem is that the standard of the manipulability evaluation is not clear.

In this chapter, a measure of the master arm manipulability is proposed considering the operator dynamics by extending the concept of the dynamic manipulability[88]. Furthermore, we point out that it is important for evaluating the master arm manipulability to consider not only the scalar value of the manipulability measure but also the directional property of the manipulability. We propose a new index to evaluate the directional property of the manipulability. Numerical examples are shown where several master arms are evaluated by using the proposed measure.

4.2 Dynamic Manipulability

In this section, we briefly introduce the concept of the dynamic manipulability proposed by Yoshikawa[88] before we discuss the master

arm maneuverability. Consider an n DOF robotic arm and let $\boldsymbol{q} \in \boldsymbol{R}^n$ be the joint vector. The notation $\boldsymbol{R}^n$ means n-dimensional Euclidean space. Let the task vector be represented by $\boldsymbol{r} \in \boldsymbol{R}^m$ $(m \leq n)$ where m is the dimension of the task vector. Since the end-effector position (and orientation) is usually chosen as the task vector $\boldsymbol{r}$, we hereafter assume that $\boldsymbol{r}$ represents end-effector position (including orientation if necessary). The kinematic relation between $\boldsymbol{q}$ and $\boldsymbol{r}$ is given by a nonlinear function $\boldsymbol{F}_r(\cdot)$.

$$\boldsymbol{r} = \boldsymbol{F}_r(\boldsymbol{q}) \tag{4.1}$$

Taking the first and second order time derivatives of eq.(4.1), the following equations are obtained.

$$\dot{\boldsymbol{r}} = \boldsymbol{J}(\boldsymbol{q})\dot{\boldsymbol{q}} \tag{4.2}$$

$$\ddot{\boldsymbol{r}} = \boldsymbol{J}(\boldsymbol{q})\ddot{\boldsymbol{q}} + \dot{\boldsymbol{J}}(\boldsymbol{q})\dot{\boldsymbol{q}} \tag{4.3}$$

where $\dot{\boldsymbol{r}}$ denotes the end-effector velocity[1], $\dot{\boldsymbol{q}} = d\boldsymbol{q}/dt$ is the joint velocity vector and $\boldsymbol{J}(\boldsymbol{q}) \in \boldsymbol{R}^{m \times n}$ is the Jacobian matrix. On the other hand, the dynamic equation of a robotic arm is generally given by

$$\boldsymbol{\tau} = \boldsymbol{M}(\boldsymbol{q})\ddot{\boldsymbol{q}} + \boldsymbol{h}(\boldsymbol{q}, \dot{\boldsymbol{q}}) + \boldsymbol{g}(\boldsymbol{q}) \tag{4.4}$$

where $\boldsymbol{\tau} \in \boldsymbol{R}^n$ is the joint driving force vector, $\boldsymbol{M}(\boldsymbol{q}) \in \boldsymbol{R}^{n \times n}$ is the inertia matrix, $\boldsymbol{h}(\boldsymbol{q}, \dot{\boldsymbol{q}}) \in \boldsymbol{R}^n$ represents the centrifugal and Coriolis forces, and $\boldsymbol{g}(\boldsymbol{q}) \in \boldsymbol{R}^n$ represents the effect of gravity. If we neglect the term of square of velocity and the gravity effect in eqs.(4.3) and (4.4) in order to simplify the problem, we get the relation between the end-effector acceleration and the joint driving force as follows:

$$\ddot{\boldsymbol{r}} = \boldsymbol{J}\boldsymbol{M}^{-1}\boldsymbol{\tau} = \boldsymbol{J}\boldsymbol{M}^{-1}\boldsymbol{T}_\tau^{-1}\hat{\boldsymbol{\tau}} \triangleq \boldsymbol{G}\hat{\boldsymbol{\tau}} \tag{4.5}$$

In eq.(4.5), $\boldsymbol{T}_\tau = \mathrm{diag}(1/\tau_{i_{max}})$, and $\hat{\boldsymbol{\tau}}$ is the normalized joint driving force vector which satisfies $\|\hat{\boldsymbol{\tau}}\| \leq 1$, where $\tau_{i_{max}}$ represents the maximum value of the i-th joint driving force and $\|\cdot\|$ denotes the Euclidean norm.

[1]Sometimes, the end-effector velocity is defined by a new velocity vector which orientational component is angular velocity vector instead of the orientational component of $\dot{\boldsymbol{r}} = d\boldsymbol{r}/dt$. In this chapter, we will use $\dot{\boldsymbol{r}}$ for the notation of the end-effector velocity for convenience, assuming that it also includes this new definition.

The dynamic manipulability[88] is defined as follows:

$$w_d = \sqrt{\det \boldsymbol{G}\boldsymbol{G}^T} \tag{4.6}$$

where the superscript ^{T} denotes the transpose. The dynamic manipulability w_d measures the degree of realizable acceleration of the end-effector under the restriction of $\|\hat{\boldsymbol{\tau}}\| \leq 1$ and w_d is proportional to the volume of the ellipsoid (the dynamic manipulability ellipsoid) in $\boldsymbol{R}^m$ which is made from all the sets of the realizable end-effector accelerations $\ddot{\boldsymbol{r}}$ by the joint driving force satisfying $\|\hat{\boldsymbol{\tau}}\| \leq 1$.

Here, we neglected the term of the square of velocity (the Coriolis and centrifugal forces) and the effect of gravity in the above formulations. Of course, we can cope with these terms by defining a new joint driving force vector $\boldsymbol{\tau}' = \boldsymbol{\tau} - \boldsymbol{h}(\boldsymbol{q}, \dot{\boldsymbol{q}}) - \boldsymbol{g}(\boldsymbol{q})$, and a new end-effector acceleration $\ddot{\boldsymbol{r}}' = \ddot{\boldsymbol{r}} - \dot{\boldsymbol{J}}\dot{\boldsymbol{q}}$.

4.3 Manipulability of Master Arms for Human Operator

4.3.1 Definition of Manipulability Measure of Master Arms

As shown in **Fig.4.1**, we will suppose a situation where the operator is manipulating a master arm by gripping the end-effector of the master arm. We assume that the operator is gripping the master arm tight so that the end-effector position (and orientation) of the master arm always coincides with that of the operator hand. We also assume for the simplification that the master arm does not generate any joint driving force. Later, we will comment on the case when the master arm generates the joint driving force.

If we regard the arm of the operator as a robotic arm, the supposed state shown in **Fig.4.1** can be treated as the motion of a robotic arm (the operator) grasping another robotic arm (the master arm) as a payload which does not generate any joint driving force. Assuming that the operator arm and the master arm are n DOF and n' DOF respectively, and denoting the common position (and orientation) vector of

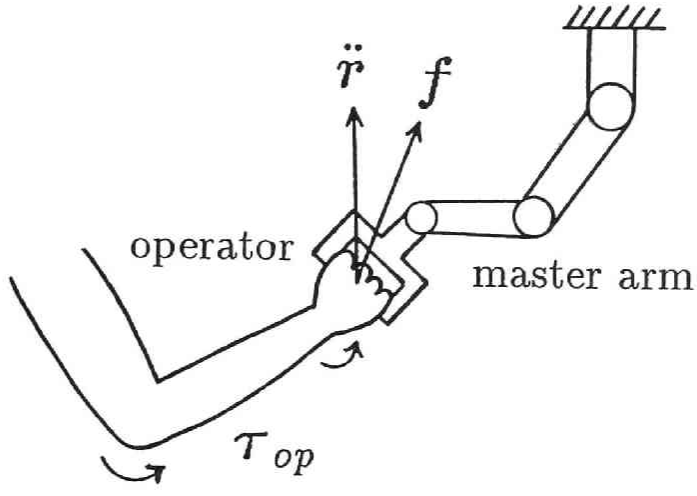

Figure 4.1: Operator arm holding a master arm

the two end-effectors by $\boldsymbol{r} \in \boldsymbol{R}^m$ ($m \leq n,\ m \leq n'$), the supposed state is given by the following equations:

$$\boldsymbol{\tau}_{op} = \boldsymbol{M}_{op}(\boldsymbol{q}_{op})\ddot{\boldsymbol{q}}_{op} + \boldsymbol{J}_{op}^T(\boldsymbol{q}_{op})\boldsymbol{f} \tag{4.7}$$

$$\ddot{\boldsymbol{r}} = \boldsymbol{J}_m(\boldsymbol{q}_m)\boldsymbol{M}_m^{-1}(\boldsymbol{q}_m)\boldsymbol{J}_m^T(\boldsymbol{q}_m)\boldsymbol{f} \tag{4.8}$$

Here we have also neglected the term of the square of velocity and the gravity effect for the simplification. In eqs.(4.7) and (4.8), $\boldsymbol{\tau}_{op} \in \boldsymbol{R}^n$ is the joint driving torque vector of the operator, and $\boldsymbol{q}_{op} \in \boldsymbol{R}^n$ and $\boldsymbol{q}_m \in \boldsymbol{R}^{n'}$ are the joint position vectors of the operator and the master arm respectively. And $\boldsymbol{M}_{op}(\boldsymbol{q}_{op}) \in \boldsymbol{R}^{n\times n}$ and $\boldsymbol{M}_m(\boldsymbol{q}_m) \in \boldsymbol{R}^{n'\times n'}$ are the inertia matrices of the operator and the master arm respectively, and $\boldsymbol{J}_{op}(\boldsymbol{q}_{op}) \in \boldsymbol{R}^{m\times n}$ and $\boldsymbol{J}_m(\boldsymbol{q}_m) \in \boldsymbol{R}^{m\times n'}$ are the Jacobian matrices of the operator and the master arm respectively. Hereafter, these matrices will be written as $\boldsymbol{M}_{op}$, $\boldsymbol{M}_m$, $\boldsymbol{J}_{op}$ and $\boldsymbol{J}_m$. The vector $\boldsymbol{f} \in \boldsymbol{R}^m$ represents the force (and moment) that the operator applies to the end-effector of the master arm, and its definition must correspond to the definition of $\dot{\boldsymbol{r}}$.

Multiplying both side of eq.(4.7) by $\boldsymbol{J}_{op}\boldsymbol{M}_{op}^{-1}$ and considering $\ddot{\boldsymbol{r}} = \boldsymbol{J}_{op}\ddot{\boldsymbol{q}}_{op}$ ($\dot{\boldsymbol{J}}_{op}\dot{\boldsymbol{q}}_{op}$ was neglected) and eliminating $\ddot{\boldsymbol{r}}$ furthermore by using

eq.(4.8), we get the following equation:

$$\boldsymbol{J}_{op}\boldsymbol{M}_{op}^{-1}\boldsymbol{\tau}_{op} = (\boldsymbol{J}_{op}\boldsymbol{M}_{op}^{-1}\boldsymbol{J}_{op}^{T} + \boldsymbol{J}_{m}\boldsymbol{M}_{m}^{-1}\boldsymbol{J}_{m}^{T})\boldsymbol{f} \tag{4.9}$$

If there exists $(\boldsymbol{J}_{op}\boldsymbol{M}_{op}^{-1}\boldsymbol{J}_{op}^{T} + \boldsymbol{J}_{m}\boldsymbol{M}_{m}^{-1}\boldsymbol{J}_{m}^{T})^{-1}$, we can solve the force vector $\boldsymbol{f}$ from eq.(4.9). Substituting this $\boldsymbol{f}$ back to eq.(4.8), we finally obtain the following equation.

$$\begin{aligned}\ddot{\boldsymbol{r}} &= \boldsymbol{J}_{m}\boldsymbol{M}_{m}^{-1}\boldsymbol{J}_{m}^{T}(\boldsymbol{J}_{op}\boldsymbol{M}_{op}^{-1}\boldsymbol{J}_{op}^{T} + \boldsymbol{J}_{m}\boldsymbol{M}_{m}^{-1}\boldsymbol{J}_{m}^{T})^{-1}\boldsymbol{J}_{op}\boldsymbol{M}_{op}^{-1}\boldsymbol{\tau}_{op} \\ &= \boldsymbol{J}_{m}\boldsymbol{M}_{m}^{-1}\boldsymbol{J}_{m}^{T}(\boldsymbol{J}_{op}\boldsymbol{M}_{op}^{-1}\boldsymbol{J}_{op}^{T} + \boldsymbol{J}_{m}\boldsymbol{M}_{m}^{-1}\boldsymbol{J}_{m}^{T})^{-1}\boldsymbol{J}_{op}\boldsymbol{M}_{op}^{-1}\boldsymbol{T}_{\tau_{op}}^{-1}\hat{\boldsymbol{\tau}} \\ &\triangleq \widetilde{\boldsymbol{G}}\hat{\boldsymbol{\tau}}\end{aligned} \tag{4.10}$$

where $\boldsymbol{T}_{\tau_{op}} = \mathrm{diag}(1/\tau_{op_{i\,max}})$ and $\tau_{op_{i\,max}}$ represents the maximum value of the i-th joint torque of the operator. In eq.(4.10), if the inertia of the master arm becomes close to zero, then $\boldsymbol{J}_{m}\boldsymbol{M}_{m}^{-1}\boldsymbol{J}_{m}^{T} \longrightarrow \infty$ and the matrix $\boldsymbol{J}_{m}\boldsymbol{M}_{m}^{-1}\boldsymbol{J}_{m}^{T}(\boldsymbol{J}_{op}\boldsymbol{M}_{op}^{-1}\boldsymbol{J}_{op}^{T} + \boldsymbol{J}_{m}\boldsymbol{M}_{m}^{-1}\boldsymbol{J}_{m}^{T})^{-1}$ becomes close to the unity matrix. Consequently, the matrix $\widetilde{\boldsymbol{G}}$ defined in eq.(4.10) becomes close to the following matrix:

$$\boldsymbol{G}_{op} \triangleq \boldsymbol{J}_{op}\boldsymbol{M}_{op}^{-1}\boldsymbol{T}_{\tau_{op}}^{-1} \tag{4.11}$$

which corresponds to the case when the operator has no load. In this sense, eq.(4.10) is a sort of extension of eq.(4.5). Hence, when the robotic arm is grasping another arm as a payload, the dynamic manipulability is defined in the same way as eq.(4.6) by the following equation:

$$\tilde{w}_{d} = \sqrt{\det\widetilde{\boldsymbol{G}}\widetilde{\boldsymbol{G}}^{T}} \tag{4.12}$$

Now, let us consider the condition when the matrix $(\boldsymbol{J}_{op}\boldsymbol{M}_{op}^{-1}\boldsymbol{J}_{op}^{T} + \boldsymbol{J}_{m}\boldsymbol{M}_{m}^{-1}\boldsymbol{J}_{m}^{T})^{-1}$ exists. Since the matrix $(\boldsymbol{J}_{op}\boldsymbol{M}_{op}^{-1}\boldsymbol{J}_{op}^{T} + \boldsymbol{J}_{m}\boldsymbol{M}_{m}^{-1}\boldsymbol{J}_{m}^{T})$ is transformed as:

$$\begin{aligned}&(\boldsymbol{J}_{op}\boldsymbol{M}_{op}^{-1}\boldsymbol{J}_{op}^{T} + \boldsymbol{J}_{m}\boldsymbol{M}_{m}^{-1}\boldsymbol{J}_{m}^{T}) \\ &= \begin{bmatrix} \boldsymbol{J}_{op} & \boldsymbol{J}_{m} \end{bmatrix} \begin{bmatrix} \boldsymbol{M}_{op} & \mathbf{O} \\ \mathbf{O} & \boldsymbol{M}_{m} \end{bmatrix}^{-1} \begin{bmatrix} \boldsymbol{J}_{op} & \boldsymbol{J}_{m} \end{bmatrix}^{T},\end{aligned} \tag{4.13}$$

the matrix $(\boldsymbol{J}_{op}\boldsymbol{M}_{op}^{-1}\boldsymbol{J}_{op}^{T}+\boldsymbol{J}_{m}\boldsymbol{M}_{m}^{-1}\boldsymbol{J}_{m}^{T})$ is positive definite if and only if rank $\left(\left[\begin{array}{cc}\boldsymbol{J}_{op} & \boldsymbol{J}_{m}\end{array}\right]\right) = m$. On the other hand, when rank $\left(\left[\begin{array}{cc}\boldsymbol{J}_{op} & \boldsymbol{J}_{m}\end{array}\right]\right)$ $< m$, both the operator and the master arm are at the singularity and the singular direction (the direction in which the end-effector cannot move at an arbitrary velocity) coincide mutually. In this case, one cannot obtain $\boldsymbol{f}$ from $\boldsymbol{\tau}_{op}$ and cannot define $\widetilde{\boldsymbol{G}}$. However, it would be reasonable to set the dynamic manipulability to zero in this case from the original meaning of the manipulability, because the operator cannot accelerate his hand in arbitrary directions when both his arm and the master arm are at the singularity point. In the neighborhood of the singularity point, the more it is close at the singularity point, the more $\tilde{w}_d$ becomes close to zero.

From the above discussion, we define the manipulability measure of master arms as follows:

[Manipulability of master arms]

$$\tilde{w}_d = \begin{cases} \sqrt{\det \widetilde{\boldsymbol{G}}\widetilde{\boldsymbol{G}}^{T}} & \text{if rank} \left[\begin{array}{cc}\boldsymbol{J}_{op} & \boldsymbol{J}_{m}\end{array}\right] = m \\ 0 & \text{if rank} \left[\begin{array}{cc}\boldsymbol{J}_{op} & \boldsymbol{J}_{m}\end{array}\right] < m \end{cases} \tag{4.14}$$

The matrix $\widetilde{\boldsymbol{G}}$ contains $\boldsymbol{J}_{op}$, $\boldsymbol{M}_{op}$, and $\boldsymbol{T}_{\tau_{op}}$. It means that the dynamics of the operator arm is considered in this measure.

4.3.2 Consideration of the Joint Driving Force of Master Arms

In the above discussion, we assumed that the master arm does not generate any force or torque at its joints. This assumption corresponds, for example, to the case of the unilateral servo control or the case when no external force is applied to the slave arm from the environment under the force reflection type bilateral control (no force feedback loop in the master arm side).

We can also apply our discussion to master arms with the joint driving force under a certain control scheme, if we can obtain the equivalent inertia of the master arm. Consider force reflecting servo type bilateral

control, for example. Assume that the master arm is controlled by force feedback with the gain matrix $\boldsymbol{K}_f \in \boldsymbol{R}^{n' \times n'}$ in joint space as follows:

$$\boldsymbol{\tau}_m = \boldsymbol{K}_f \boldsymbol{J}_m^T (\boldsymbol{f} - \boldsymbol{f}_s) \tag{4.15}$$

where $\boldsymbol{\tau}_m \in \boldsymbol{R}^{n'}$ is the joint driving force vector of the master arm and $\boldsymbol{f}_s \in \boldsymbol{R}^m$ is the force vector applying at the slave side. When $\boldsymbol{f}_s = \boldsymbol{0}$, that is, when no external force applies at the slave side, the inertia of the master arm becomes equivalently $(\boldsymbol{E} + \boldsymbol{K}_f)^{-1} \boldsymbol{M}_m$ and we can regard it as a new inertia matrix, where $\boldsymbol{E} \in \boldsymbol{R}^{m \times m}$ is unity matrix.

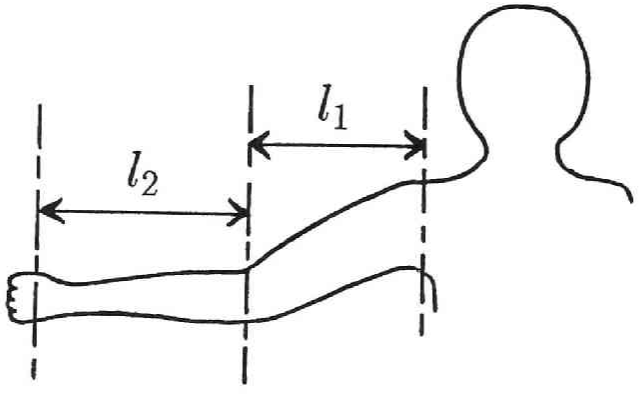

Figure 4.2: Operator arm model in the horizontal plane

Table 4.1: Parameters of operator arm model

	link 1	link 2
l_i [m]	0.25	0.30
l_{g_i} [m]	0.125	0.15
m_i [kg]	1.5	1.5
$\hat{I}_i$ [kgm^2]	0.0078	0.0113
$\tau_{i_{max}}$ [Nm]	15	10

4.3.3 Numerical Example

We will evaluate several types of master arm by the proposed measure of manipulability. To simplify the problem, we suppose that the operator arm is a two-link manipulator in a horizontal plane as shown in **Fig.4.2**. The parameters of the operator arm are given in **Table 4.1**.

We will compare three types of master arms such as (i) articulated type, (ii) Cartesian coordinates type, and (iii) homogeneous inertia type. All of them are 2 DOF planner manipulators. Therefore, we can set as $n = n' = m = 2$ and $\boldsymbol{r} = [\ r_x \quad r_y\ ]^T$, where r_x and r_y are x and y coordinates of the end-effector in the horizontal plane.

Concerning the type (i), we will use the parameter in Table 1, that is, we supposed an articulated type master arm which is identical with the operator arm. Besides, in this type, it is necessary to determine the relative position between the operator and the master arm. We will choose two cases such as (ia) the case when the position of the first joint of each arm is apart just sum of the length of link 1 and 2, $l_1 + l_2$, (we call it "opposite origin"), and (ib) the case when the first joint coincides at one point ("same origin"). Furthermore, there is another option whether the arm posture is elbow up or down. We set the posture of the operator arm to the elbow down supposing the right arm. As for the posture of the master arm, we can choose both elbow up and down. Consequently, we get four cases by changing the posture and the position of the master arm origin as shown in **Fig.4.3**, that is, (ia–1) **posture I**, (ia–2) **posture II**, (ib–1) **posture III**, (ib–2) **posture IV**, where the posture of the operator is set to **posture IV**.

On the other hand, master arms of both type (ii) and (iii) can be represented as follows:

$$\boldsymbol{J}_m = \boldsymbol{E}_2 \tag{4.16}$$

$$\boldsymbol{M}_m = \begin{bmatrix} m_x & 0 \\ 0 & m_y \end{bmatrix} \tag{4.17}$$

where $\boldsymbol{E}_2$ is 2×2 unity matrix. As for the type (ii), we will choose two cases such as (ii–1) $m_x = 0.5$[kg], $m_y = 2.5$[kg], and (ii–2) $m_x = 2.5$[kg], $m_y = 0.5$ [kg]. As for the type (iii), we set $m_x = m_y = 1.5$ [kg], that is, we suppose an ideally homogeneous inertia arm which keeps the same inertia at any posture.

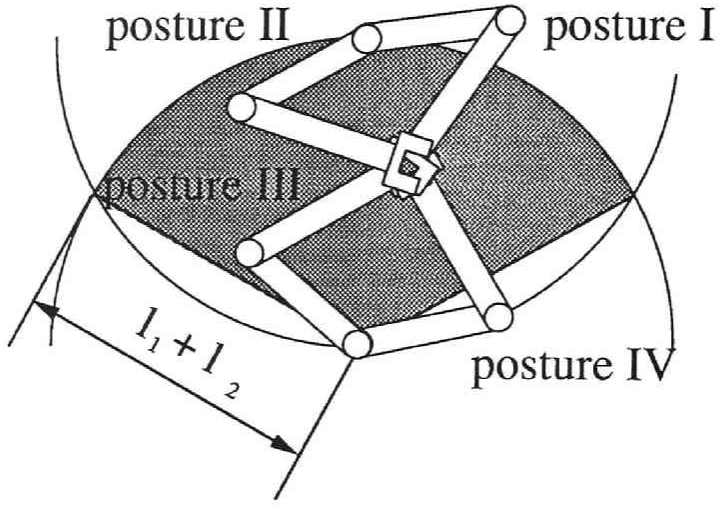

Figure 4.3: Arm postures and work space in a plane

The manipulability will be evaluated in a fan-shaped area shown in **Fig.4.3** which is approximated to the common work space between the operator and the master in the case (ia).

In **Figs.4.4** through **4.10**, distribution maps both of the dynamic manipulability ellipsoid and the value of the measure $\tilde{w}_d$ are shown. In order to compare the manipulability among those arms, we will regard the dynamic manipulability of the operator when he has no load shown in **Fig.4.11** as a criterion of the evaluation. As can been seen from **Fig.4.11**, the dynamic manipulability of the operator with no load makes uniformly a concentric circular distribution.

In the evaluation of the manipulability of master arms, it is important not only how much the maximum value of $\tilde{w}_d$ is in the work space but also how well the distribution of $\tilde{w}_d$ and the directional property of the ellipsoid are similar to that of the operator without any load. If we concerned only the maximum value of $\tilde{w}_d$, (ia) and (ii) have the largest value. However, if we concerned the distributions of the value $\tilde{w}_d$, (ib) and (iii) have a uniformed distribution and we can expect a good manipulability from these cases of master arms. In other words,

it can be expected that incongruous feeling of manipulation is small for operators over the whole working space in these cases.

4.4 Evaluation of Directional Property of Manipulability

4.4.1 Index for Evaluation of Directional Property

As we pointed out in the previous section, the manipulability of master arms for the operator depends on not only how much the proposed measure is but also how this measure is distributed in the working space of the arm and what the shape and the directional property of the manipulability ellipsoid is. As a standard of these evaluations, the dynamic manipulability of the operator himself would be suitable. It corresponds to the situation when he accelerate his own arm without any load. If the distribution of the manipulability measure of the master arm and the directional property of the manipulability ellipsoid are similar to those of the dynamic manipulability of the operator himself, he may be able to manipulate the master arm in a natural feeling.

In this section, we discuss a way to evaluate the similarity between the manipulability of master arms and the dynamic manipulability of the operator without any load. Here, we again represent the relations of eqs.(4.11) and (4.10) as:

$$\ddot{\boldsymbol{r}} = \boldsymbol{G}_{op}\hat{\boldsymbol{\tau}} \tag{4.18}$$

$$\ddot{\tilde{\boldsymbol{r}}} = \widetilde{\boldsymbol{G}}\hat{\boldsymbol{\tau}} \tag{4.19}$$

Eqs.(4.18) and (4.19) give the acceleration of the operator hand (and the end-effector of the master arm) by the normalized joint torque $\|\hat{\boldsymbol{\tau}}\| \leq 1$. These two equations mean that $\ddot{\boldsymbol{r}}$ and $\ddot{\tilde{\boldsymbol{r}}}$ are different vectors even by the same joint torque $\hat{\boldsymbol{\tau}}$.

Since it is desirable that the acceleration $\ddot{\tilde{\boldsymbol{r}}}$ when the operator is gripping the master arm is similar to the acceleration $\ddot{\boldsymbol{r}}$ when he has no load, we will consider the following integral of the inner product of

these two vectors, $\ddot{\boldsymbol{r}}^T\ddot{\hat{\boldsymbol{r}}}$, assuming that $\hat{\boldsymbol{\tau}}$ is distributed uniformly on the surface of the n-dimensional hyper sphere $\|\hat{\boldsymbol{\tau}}\| = 1$.

$$\xi(\boldsymbol{G}_{op}, \widetilde{\boldsymbol{G}}) = \int_{S_n} \ddot{\boldsymbol{r}}^T \ddot{\hat{\boldsymbol{r}}} d\Omega_n = \int_{S_n} \hat{\boldsymbol{\tau}}^T \boldsymbol{G}_{op}^T \widetilde{\boldsymbol{G}} \hat{\boldsymbol{\tau}} d\Omega_n \tag{4.20}$$

where $d\Omega_n$ denotes the infinitesimal n-dimensional hyper solid angle from the center of n-dimensional hyper sphere (see **Appendix 1**), and $\int_{S_n}$ denotes the integration over the whole of the hyper sphere. Here, we can show that $\int_{S_n} \hat{\boldsymbol{\tau}}\hat{\boldsymbol{\tau}}^T d\Omega_n = \Pi(n)\boldsymbol{E}_n$, where $\boldsymbol{E}_n$ is $n \times n$ unity matrix and $\Pi(\cdot)$ is a scalar function of n. The reason is as follows. The off-diagonal part of the matrix $\int_{S_n} \hat{\boldsymbol{\tau}}\hat{\boldsymbol{\tau}}^T d\Omega_n$ represents the correlation between the i-th and j-th elements of $\hat{\boldsymbol{\tau}}$, and the diagonal part represents the self-correlation. Integrating $\hat{\boldsymbol{\tau}}\hat{\boldsymbol{\tau}}^T$ over the whole of hyper sphere, there is no correlation between the different elements of $\hat{\boldsymbol{\tau}}$ and self-correlations of each element are equal mutually because of the symmetrical property of the hyper sphere (see **Appendix 2**).

Denoting the trace of matrix as tr(), generally $\mathrm{tr}(\boldsymbol{AB}) = \mathrm{tr}(\boldsymbol{BA})$ for matrices $\boldsymbol{A}$ and $\boldsymbol{B}$, and $\alpha = \mathrm{tr}(\alpha)$ for a scalar α. From these facts, we get

$$\begin{aligned}
\xi(\boldsymbol{G}_{op}, \widetilde{\boldsymbol{G}}) &= \int_{S_n} \mathrm{tr}(\hat{\boldsymbol{\tau}}^T \boldsymbol{G}_{op}^T \widetilde{\boldsymbol{G}} \hat{\boldsymbol{\tau}}) d\Omega_n \\
&= \int_{S_n} \mathrm{tr}(\widetilde{\boldsymbol{G}} \hat{\boldsymbol{\tau}}\hat{\boldsymbol{\tau}}^T \boldsymbol{G}_{op}^T) d\Omega_n \\
&= \mathrm{tr}\left(\widetilde{\boldsymbol{G}} \int_{S_n} \hat{\boldsymbol{\tau}}\hat{\boldsymbol{\tau}}^T d\Omega_n \boldsymbol{G}_{op}^T\right) \\
&= \Pi(n)\mathrm{tr}(\widetilde{\boldsymbol{G}} \boldsymbol{G}_{op}^T)
\end{aligned} \tag{4.21}$$

A massless master arm, that is the case when $\widetilde{\boldsymbol{G}} = \boldsymbol{G}$, can be regarded as an ideal master arm. Therefore, we propose the following index which is a relative evaluation by regarding the case of $\widetilde{\boldsymbol{G}} = \boldsymbol{G}$ as a standard of the evaluation.

[Similarity between the master arm operation and no load]

$$\rho = \frac{\xi(\boldsymbol{G}_{op}, \widetilde{\boldsymbol{G}})}{\xi(\boldsymbol{G}_{op}, \boldsymbol{G}_{op})} = \frac{\mathrm{tr}(\widetilde{\boldsymbol{G}} \boldsymbol{G}_{op}^T)}{\mathrm{tr}(\boldsymbol{G}_{op} \boldsymbol{G}_{op}^T)} \tag{4.22}$$

The index value ρ is less than 1 (see **Appendix 3**), and one can evaluate that the more the index ρ is close to 1, the better manipulability the master arm has.

4.4.2 Numerical Example

In **Figs.4.4**(c) through **4.10**(c), the similarity index ρ is given for each case. These examples show that the distribution of ρ reflects well the similarity of the ellipsoid to that of **Fig.4.11**, and the area of maximum value of $\tilde{w}_d$ does not always corresponds to the area of maximum value of ρ. Especially in case (ib–2), $\rho = 0.5$ is achieved over the whole working area and we can conclude that this case has the best manipulability among these examples. The master arm of this case (ib-2) corresponds to the exoskeleton type. It should be noted that only the proposed index is not the design factor of master arms. Compactness, easiness to set up, and safety are other factors, and obviously the exoskeleton type has disadvantages against these factors. The homogeneous inertia type in case (iii) also shows good manipulability. However its directional property of the ellipsoid is different a little from that of the operator without any load. This difference is reflected in the value of ρ.

It should be noted that not only the arm design itself but also the relative position of the arm to the operator is very important factor for evaluating the manipulability of master arms. For example, comparing between cases (ib–1) and (ib–2), the case (ib–1) becomes worse than the case (iii) by only changing the elbow position from the case (ib–2) which is much better than case (iii).

4.5 Conclusion

The main results of this chapter are summarized as follows:

- We have pointed out that the consideration of operator dynamics is important for evaluating the manipulability of master arms, and we have proposed a measure of the manipulability of master arms by extending the concept of the dynamic manipulability.

- We have regarded the dynamic manipulability of the operator himself without any load as a standard for evaluating the manipulability of master arms, and we have proposed an index of the similarity between the manipulability ellipsoid of the master arm and the dynamic manipulability ellipsoid of the operator without any load. The manipulability measure itself evaluates only the volume of the ellipsoid, whereas this index also evaluates the directional property of the ellipsoid.

- We have pointed out that the relative position of master arm to the operator is an important factor for evaluating the manipulability of master arms as well as the arm design itself.

The proposed measure and index can be a design guide of master arms. The discussion in this chapter is applicable to the problem determining from which direction and position the teaching operator should grasp the robot arm in the direct teaching.

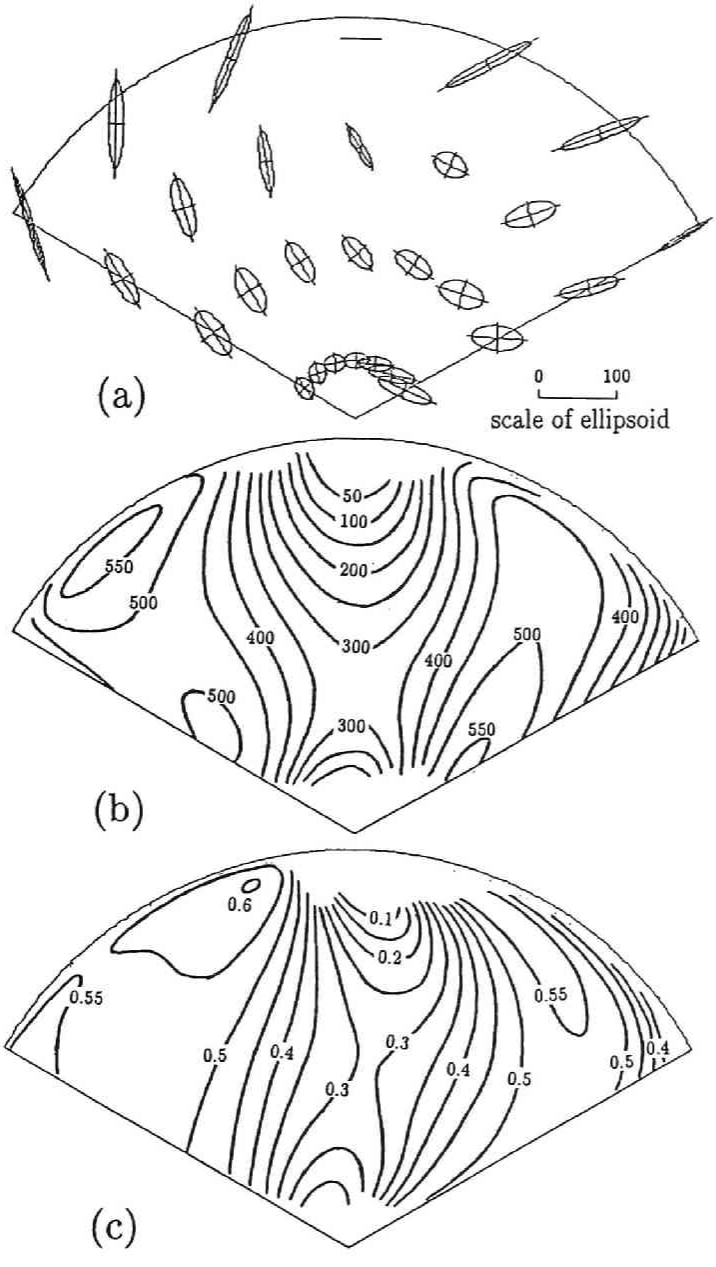

Figure 4.4: Manipulability of master arm: case (ia-1)
(a) Manipulability ellipsoid,
(b) Manipulability measure $\tilde{w}_d$,
(c) Similarity index ρ

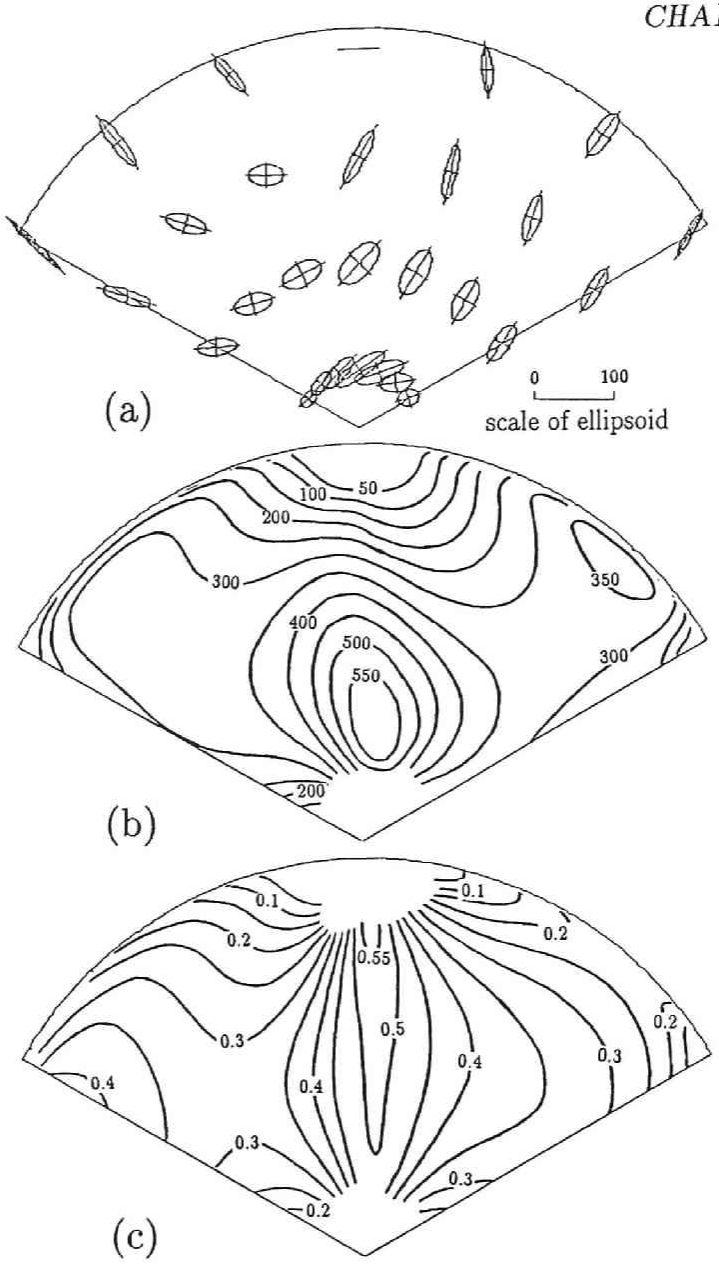

Figure 4.5: Manipulability of master arm: case (ia-2)

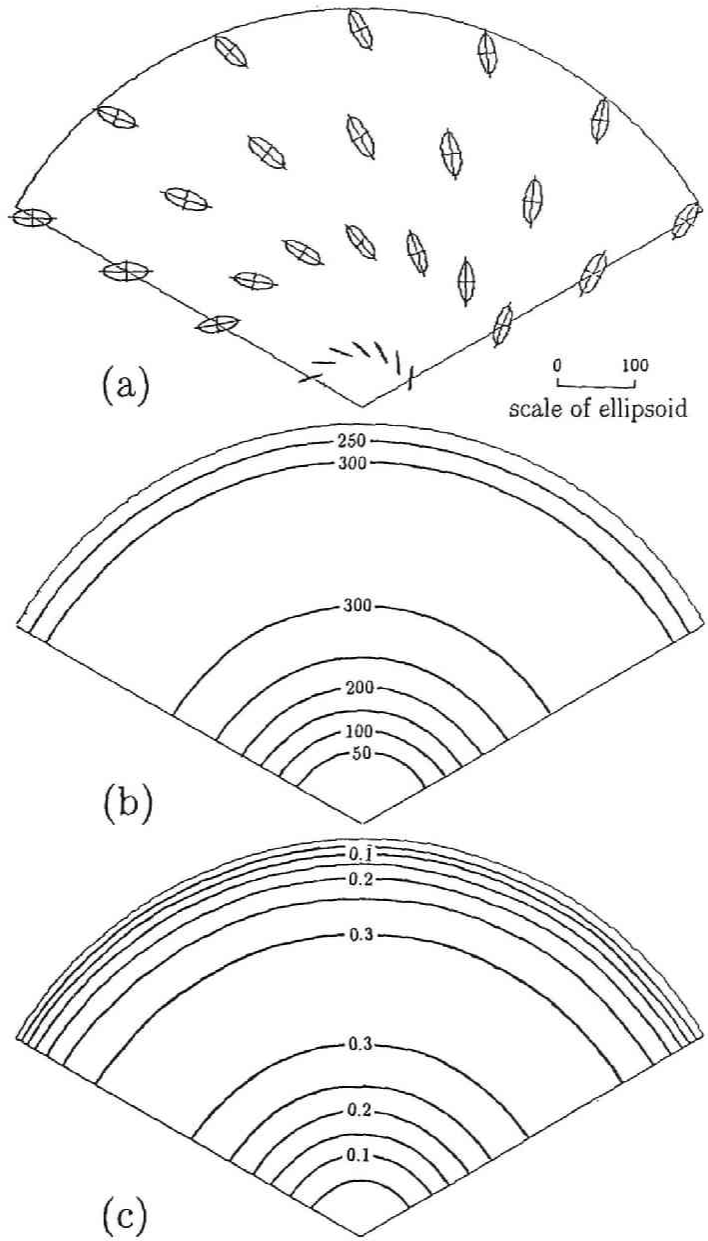

Figure 4.6: Manipulability of master arm: case (ib-1)

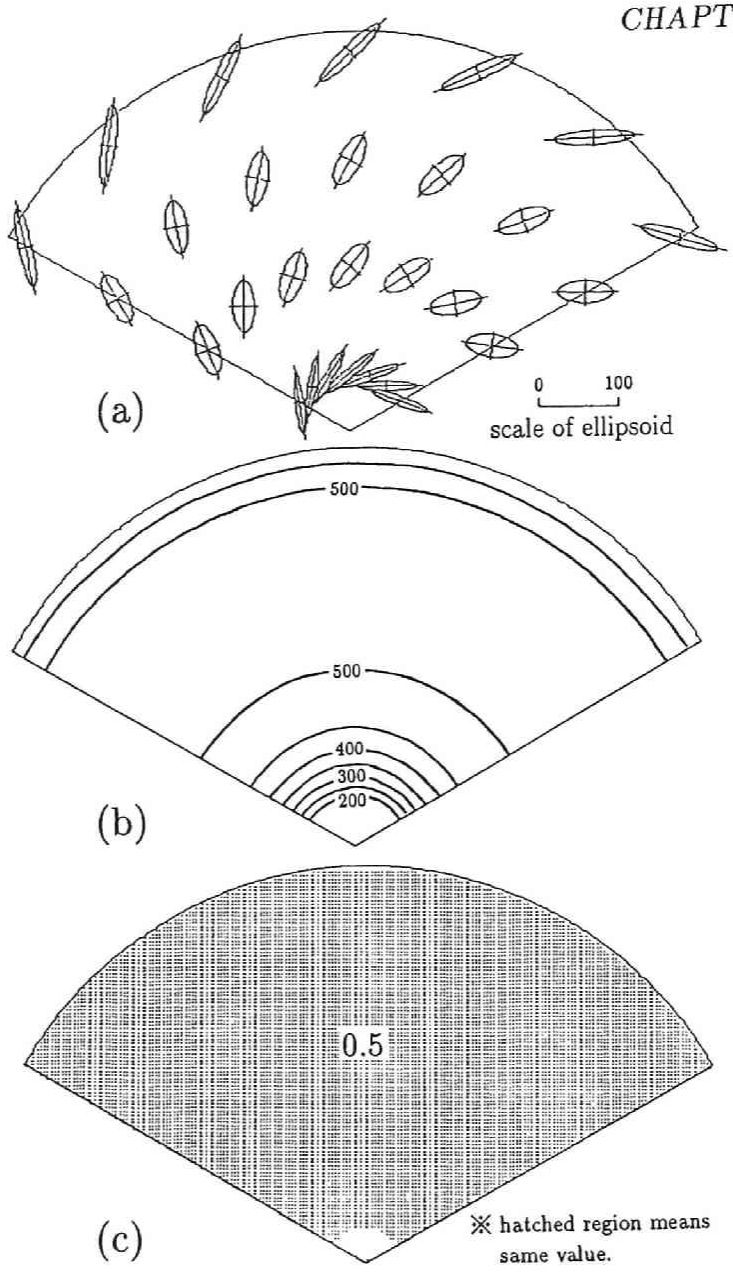

Figure 4.7: Manipulability of master arm: case (ib-2)

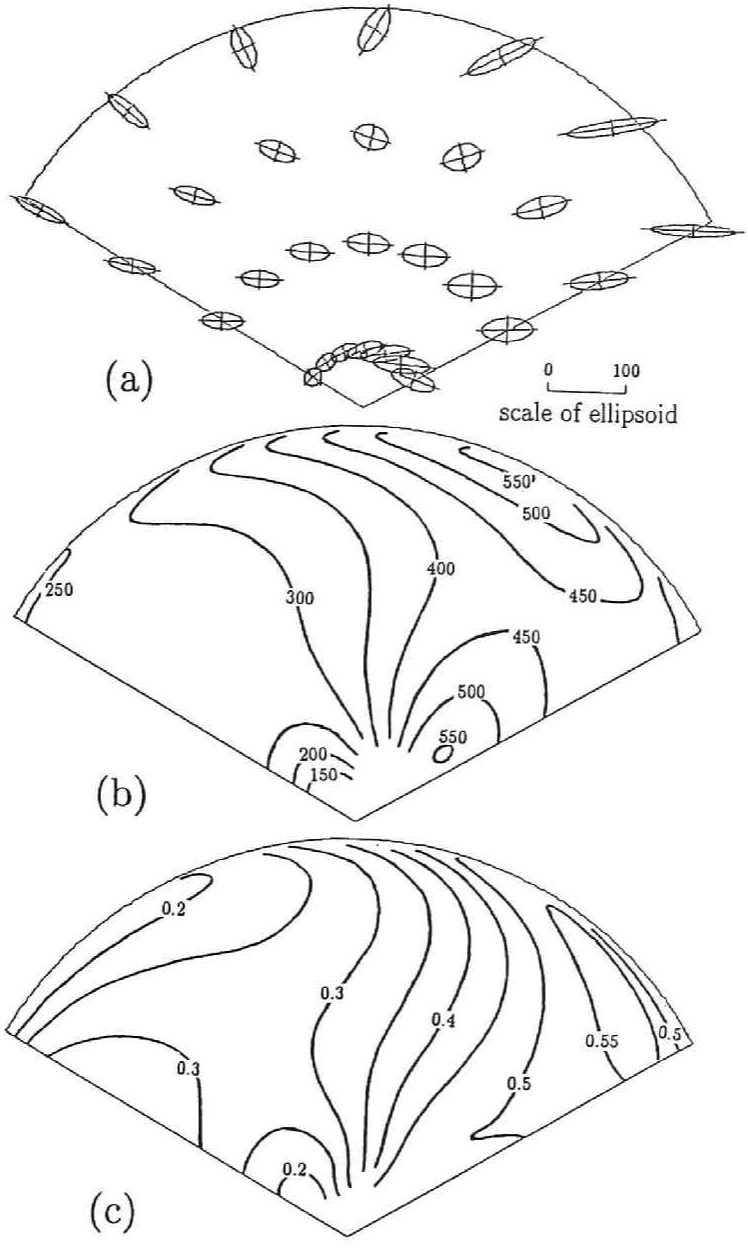

Figure 4.8: Manipulability of master arm: case (ii-1)

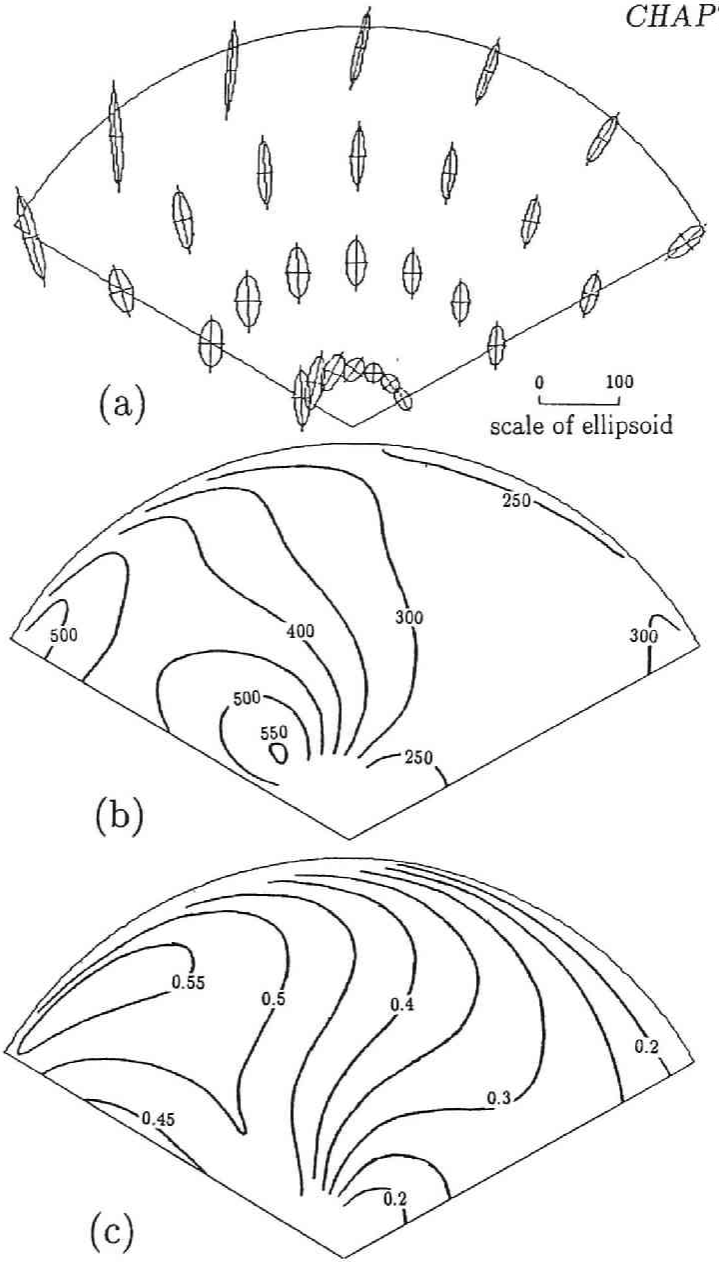

Figure 4.9: Manipulability of master arm: case (ii-2)

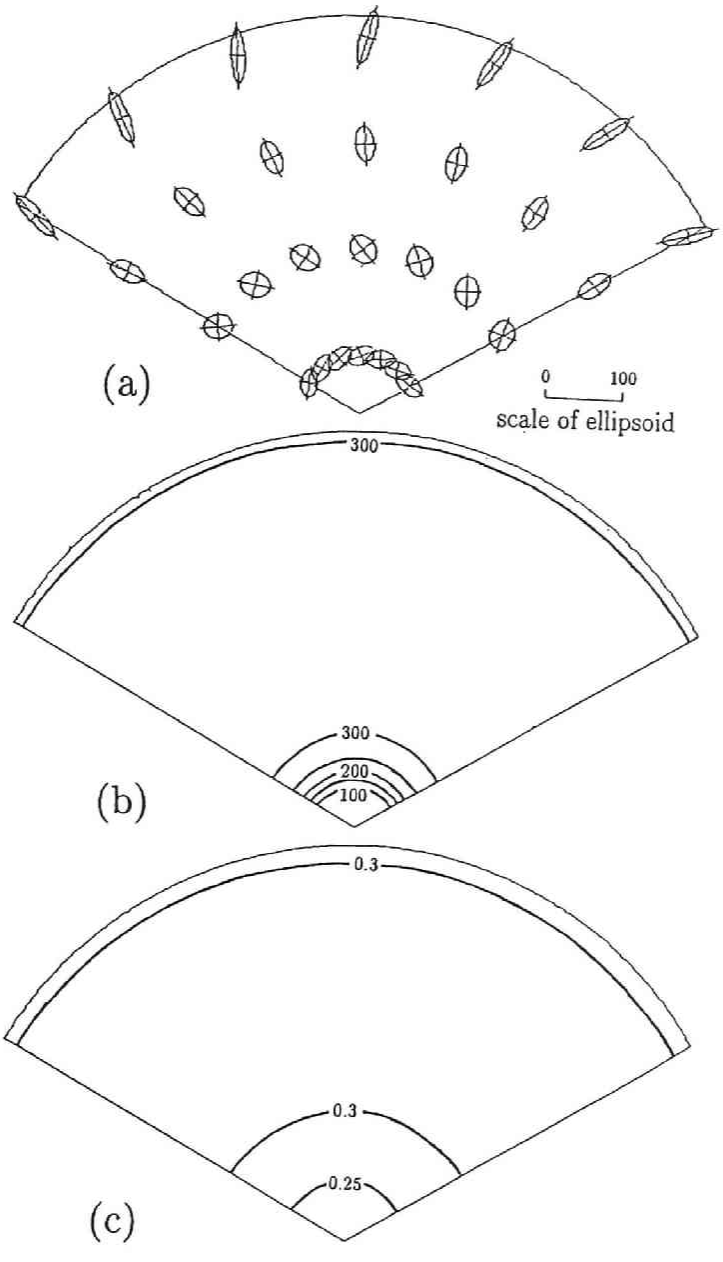

Figure 4.10: Manipulability of master arm: case (iii)

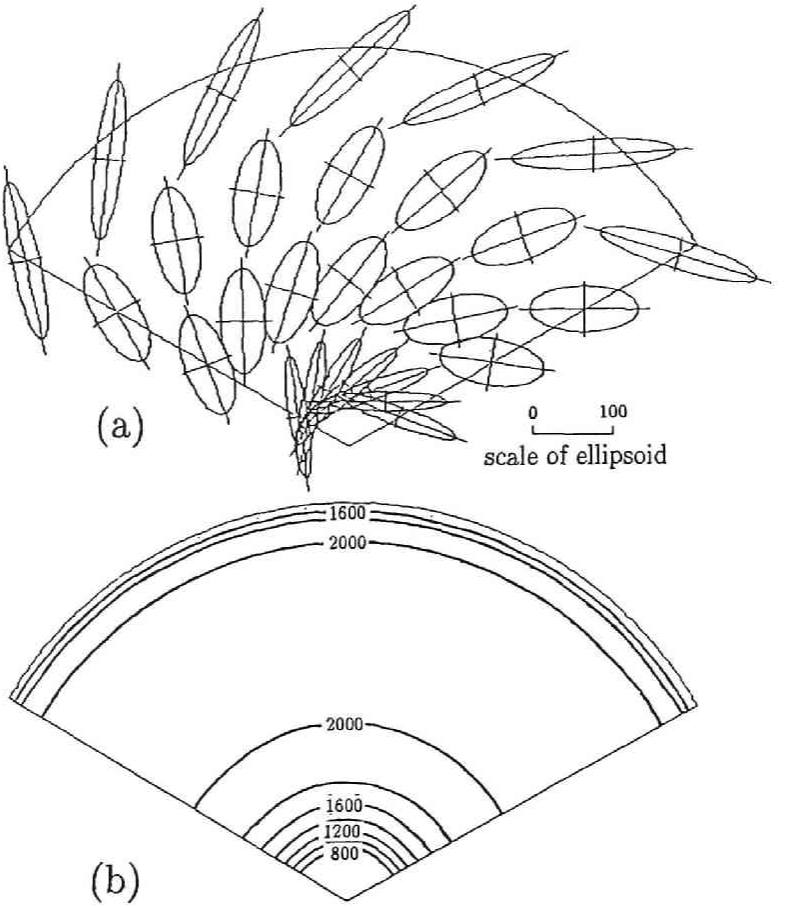

Figure 4.11: Dynamic manipulability of operator arm without loads

Appendix

1. Hyper solid angle

A spatial extent surrounded by a cone is called the *solid angle*. Denoting the area cut off by the cone from the spherical surface with a radius of r which center is at the vertex of that cone by ΔS, the solid angle is defined as:

$$\Omega = \Delta S / r^2 \tag{A.1}$$

Concerning a sphere with a unity radius, Ω corresponds just to the cut-off surface of the sphere.

We extend it to n-dimensional space. Supposing a hyper cone in n-dimensional space and denoting the area cut off by the hyper cone from the hyper spherical surface with a radius of r which center is at the vertex of the cone by ΔS_n, the *hyper solid angle* is defined by

$$\Omega_n = \Delta S_n / r^{n-1}. \tag{A.2}$$

The hyper stereo angle corresponds to radian when $n = 2$ and to the solid angle (steradian) when $n = 3$.

2. Integral $\int_{S_n} \hat{\boldsymbol{\tau}} \hat{\boldsymbol{\tau}}^T d\Omega_n$

First, let us consider when $n = 2$ and 3. Hereafter we will shorten as $S_\theta = \sin\theta$ and $C_\theta = \cos\theta$.

(i) when $n = 2$

From **Fig.4.12**, we can set

$$\hat{\boldsymbol{\tau}} = \begin{bmatrix} S_\theta \\ C_\theta \end{bmatrix}. \tag{A.3}$$

Therefore,

$$\begin{aligned} \int_{S_2} \hat{\boldsymbol{\tau}} \hat{\boldsymbol{\tau}}^T d\Omega_2 &= \int_0^{2\pi} \begin{bmatrix} S_\theta^2 & S_\theta C_\theta \\ S_\theta C_\theta & C_\theta^2 \end{bmatrix} d\theta \\ &= \begin{bmatrix} \pi & 0 \\ 0 & \pi \end{bmatrix}. \end{aligned} \tag{A.4}$$

(ii) when $n = 3$

From **Fig.4.13**, we can set

$$\hat{\boldsymbol{\tau}} = \begin{bmatrix} C_\phi S_\theta \\ C_\phi C_\theta \\ S_\phi \end{bmatrix}. \tag{A.5}$$

Therefore,

$$\begin{aligned} \int_{S_3} \hat{\boldsymbol{\tau}}\hat{\boldsymbol{\tau}}^T d\Omega_3 &= \int_0^{2\pi}\int_{-\pi/2}^{\pi/2} \begin{bmatrix} C_\phi^2 S_\theta^2 & C_\phi^2 S_\theta C_\theta & C_\phi S_\phi S_\theta \\ C_\phi^2 S_\theta C_\theta & C_\phi^2 C_\theta^2 & C_\phi S_\phi C_\theta \\ C_\phi S_\phi S_\theta & C_\phi S_\phi C_\theta & S_\phi^2 \end{bmatrix} C_\phi d\phi d\theta \\ &= \begin{bmatrix} 4\pi/3 & 0 & 0 \\ 0 & 4\pi/3 & 0 \\ 0 & 0 & 4\pi/3 \end{bmatrix}. \end{aligned} \tag{A.6}$$

Here, we denote $\hat{\boldsymbol{\tau}}$ of n-dimension by $\hat{\boldsymbol{\tau}}_n$. We will show that if $\int_{S_{n-1}} \hat{\boldsymbol{\tau}}_{n-1}\hat{\boldsymbol{\tau}}_{n-1}^T d\Omega_{n-1} = \Pi(n-1)\boldsymbol{E}_{n-1}$ is achieved, then $\int_{S_n} \hat{\boldsymbol{\tau}}_n\hat{\boldsymbol{\tau}}_n^T d\Omega_n = \Pi(n)\boldsymbol{E}_n$ can be achieved. Denoting the i-th element of $\hat{\boldsymbol{\tau}}_n$ by $\hat{\tau}_{n,i}$, each element of $\hat{\boldsymbol{\tau}}_n$ is given by

$$\hat{\tau}_{n,i} = \begin{cases} \hat{\tau}_{n-1,i} C_\phi & (i < n) \\ S_\phi & (i = n) \end{cases} \quad -\pi/2 \le \phi \le \pi/2 \tag{A.7}$$

and we can divide the integration as:

$$\int_{S_n} \hat{\boldsymbol{\tau}}_n\hat{\boldsymbol{\tau}}_n^T d\Omega_n = \int_{-\pi/2}^{\pi/2}\int_{S_{n-1}} \hat{\boldsymbol{\tau}}_n\hat{\boldsymbol{\tau}}_n^T d\Omega_{n-1} W(\phi) d\phi \tag{A.8}$$

where $W(\phi)$ is the weighting function of ϕ. Now, from

$$\int_{-\pi/2}^{\pi/2}\int_{S_{n-1}} C_\phi S_\phi \hat{\tau}_{n-1,i} d\Omega_{n-1} W(\phi) d\phi = 0 \quad (1 \le i \le n-1) \tag{A.9}$$

and

$$\int_{-\pi/2}^{\pi/2}\int_{S_{n-1}} C_\phi^2 \hat{\tau}_{n-1,i}\hat{\tau}_{n-1,j} d\Omega_{n-1} W(\phi) d\phi = 0 \quad (1 \le i, j \ (i \ne j) \le n-1), \tag{A.10}$$

the off-diagonal elements of the integration become zero. Since all of the diagonal elements are equal from the symmetrical property, we get

$$\int_{S_n} \widehat{\boldsymbol{\tau}}_n \widehat{\boldsymbol{\tau}}_n^T d\Omega_n = \Pi(n) \boldsymbol{E}_n. \tag{A.11}$$

The scalar function $\Pi(n)$ is given by

$$\Pi(n) = S_n/n \tag{A.12}$$

where S_n is the surface area of an n-dimensional hyper sphere with a unity radius. The reason is as follows. Considering that

$$\begin{aligned} \mathrm{tr}(\int_{S_n} \widehat{\boldsymbol{\tau}}\widehat{\boldsymbol{\tau}}^T d\Omega_n) &= \int_{S_n} \mathrm{tr}(\widehat{\boldsymbol{\tau}}\widehat{\boldsymbol{\tau}}^T) d\Omega_n = \int_{S_n} \|\widehat{\boldsymbol{\tau}}\|^2 d\Omega_n \\ &= \int_{S_n} d\Omega_n = S_n, \end{aligned} \tag{A.13}$$

we can get eq.(A.12) from the symmetry.

The surface area of n-dimensional hyper sphere with a unity radius is given by

$$S_n = \frac{\pi^{n/2}}{\Gamma(n/2)} = \begin{cases} (2\pi)^{n/2}/[2 \cdot 4 \cdot 6 \cdots n-2] & n = \textit{even number} \\ 2(2\pi)^{(n-1)/2}/[1 \cdot 3 \cdot 5 \cdots n-2] & n = \textit{odd number} \end{cases} \tag{A.14}$$

where $\Gamma(\cdot)$ is the Gamma function. Therefore $\Pi(n)$ is given by

$$\Pi(n) = S_n/n = \frac{\pi^{n/2}}{\Gamma((n/2)+1)} = \begin{cases} (2\pi)^{n/2}/[2 \cdot 4 \cdot 6 \cdots n] & n = \textit{even number} \\ 2(2\pi)^{(n-1)/2}/[1 \cdot 3 \cdot 5 \cdots n] & n = \textit{odd number} \end{cases} \tag{A.15}$$

and it shows that $\Pi(n)$ represents the volume of n-dimensional hyper sphere with a unity radius.

3. Proof of $\rho < 1$

Setting $\boldsymbol{W}_{op} \triangleq \boldsymbol{J}_{op}\boldsymbol{M}_{op}^{-1}\boldsymbol{J}_{op}^T$ and $\boldsymbol{W}_m \triangleq \boldsymbol{J}_m\boldsymbol{M}_m^{-1}\boldsymbol{J}_m^T$, we get

$$\widetilde{\boldsymbol{G}} = \boldsymbol{W}_m(\boldsymbol{W}_{op} + \boldsymbol{W}_m)^{-1}\boldsymbol{G}_{op} \tag{A.16}$$

and

$$\ddot{\tilde{\boldsymbol{r}}} = \boldsymbol{W}_m(\boldsymbol{W}_{op} + \boldsymbol{W}_m)^{-1}\ddot{\boldsymbol{r}}. \tag{A.17}$$

Taking the norm of both sides of eq.(A.17), we obtain

$$\begin{aligned} \|\ddot{\tilde{\boldsymbol{r}}}\| &= \|\boldsymbol{W}_m(\boldsymbol{W}_{op} + \boldsymbol{W}_m)^{-1}\ddot{\boldsymbol{r}}\| \\ &\leq \lambda_{max}(\boldsymbol{W}_m(\boldsymbol{W}_{op} + \boldsymbol{W}_m)^{-1})\|\ddot{\boldsymbol{r}}\| \end{aligned} \tag{A.18}$$

where $\lambda_{max}(\cdot)$ denotes the maximum eigenvalue of the matrix. Since $\boldsymbol{W}_{op} > 0$, $\boldsymbol{W}_m > 0$, and $\boldsymbol{W}_{op} + \boldsymbol{W}_m > \boldsymbol{W}_m$, we get $\lambda_{max}(\boldsymbol{W}_m(\boldsymbol{W}_{op} + \boldsymbol{W}_m)^{-1}) < 1$, therefore, we obtain

$$\|\ddot{\tilde{\boldsymbol{r}}}\| < \|\ddot{\boldsymbol{r}}\|. \tag{A.19}$$

This result is obvious from the physical point of view such as the acceleration of hand with loads is always less than the acceleration without loads under the same joint torque. Consequently, we get

$$\ddot{\boldsymbol{r}}^T\ddot{\tilde{\boldsymbol{r}}} < \ddot{\boldsymbol{r}}^T\ddot{\boldsymbol{r}} \tag{A.20}$$

and finally

$$\xi(\boldsymbol{G}_{op}, \widetilde{\boldsymbol{G}}) < \xi(\boldsymbol{G}_{op}, \boldsymbol{G}_{op}). \tag{A.21}$$

Eq.(A.21) proofs $\rho < 1$.

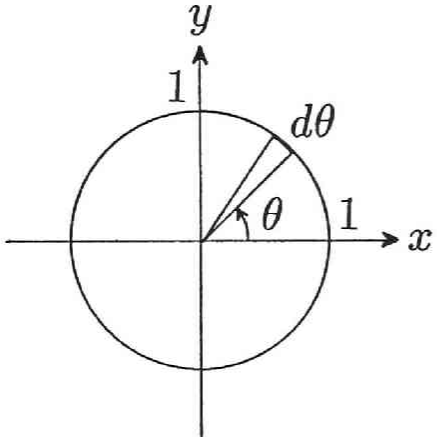

Figure 4.12: Circle ($n = 2$)

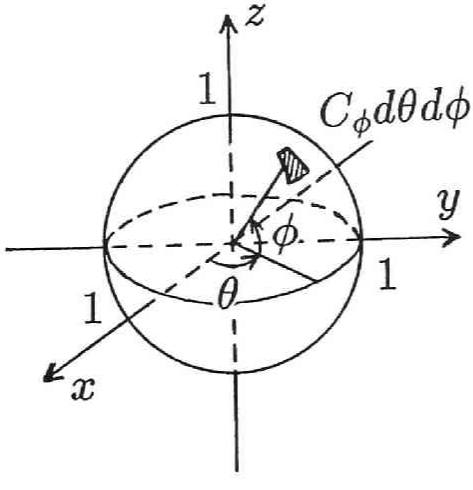

Figure 4.13: Sphere ($n = 3$)

Chapter 5

CONTROL OF MULTIPLE DOF MASTER-SLAVE MANIPULATORS

5.1 Introduction

The use of master-slave manipulators is an intuitive way to perform dexterous tasks in the environments where human operator cannot do himself. However, the maneuverability of the present master-slave systems seems still far from satisfactory. Certainly, the bilateral control is a good way for operators to interact remotely with the environment by a kinesthetic coupling. The problem is how this kinesthetic coupling with the environment can be more "realistic". In chapter 3, we have discussed new control schemes of master-slave manipulators which achieve an ideal kinesthetic coupling in one DOF case. By the proposed scheme, the operator can feel the object through the master-slave system as though he were manipulating the object directly by himself.

In this chapter, the discussion is extended to the multiple DOF case. Concerning the previous studies of multiple DOF master-slave systems, Handlykken and Turner[32] developed 6 DOF different configuration master-slave system and applied the force feedback bilateral control in Cartesian space. Arai et al.[6] proposed a force feedback bilateral control for different configuration arms in the joint space us-

ing coordinate transformations between the master and slave arm joint space. Miyazaki et al.[58] extended the symmetric position servo type into the multiple DOF case and showed the asymptotic stability of this control law. Furuta et al.[23] applied a virtual internal model following control to master-slave manipulators. Dudragne[19] proposed a new control scheme by extending the symmetric position servo type bilateral control considering the passivity of the system and extended to the multiple DOF case. But they did not discuss exactly how the ideal kinesthetic coupling can be realized.

In this chapter, new control schemes which can realize the ideal responses are proposed in two cases; different configuration arms and isomorphic configurations arms. Next, the validity of the proposed control schemes is examined by simulations. Last, design guides of master and slave arms are discussed from several aspects. Design problem for the intervenient impedance in the multiple DOF case are also discussed. It is shown that these design guides are also applicable to choosing the parameters of the intervenient impedance.

5.2 Definition of Ideal Responses

In chapter 3, we have discussed the ideal responses of master-slave systems and derived their conditions in the one DOF case. Here we again show the definition of the ideal responses for the multiple DOF case.

DEFINITION : The following three responses are defined as the ideal responses of the master-slave system.

Ideal response I : *The responses of* position *of the hand tip of the master arm and the slave arm are exactly equal regardless of the object dynamics.*

Ideal response II : *The responses of* force *at the hand tip of the master arm and the slave arm are exactly equal regardless of the object dynamics.*

Ideal response III : *Both the responses of* position *of the hand tip and the responses of* force *at the hand tip are absolutely equal*

between the master arm and the slave arm regardless of the object dynamics.

If the ideal response III is realized, the operator can feel the object through the master-slave system as though he were manipulating it directly by himself. Therefore it can be said that the ideal response III performs the ideal kinesthetic coupling.

In the one DOF case, we derived conditions to realize these ideal responses by using linear circuit theory in chapter 2. We showed that the acceleration signals of both arms are necessary in addition to the position, velocity, and force signals for composing a control scheme which realizes the ideal response III. In chapter 3, we have designed control schemes that realize ideal responses based on the result of chapter 2. If the control scheme which realizes ideal response III is applied, the arm dynamics existing between the operator and object are canceled completely.

For extending the discussion to the multiple DOF case, the circuit theory cannot be applied straightforwardly because the system becomes nonlinear and multivariable. In the following section, we design control schemes for the multiple DOF case based on the design process in one DOF case discussed in chapter 3.

5.3 Control of Different Configuration Arms

5.3.1 Control Scheme Realizing the Ideal Response III

Most of the discussions about master-slave systems in the traditional studies were restricted in one DOF cases. They dealt with the problem to control multiple DOF master-slave manipulators by applying one DOF controller at each joint for the isomorphic configuration arms, and at each direction of Cartesian coordinates for the different configuration arms. But this approach does not consider the arm dynamics such as the inertia coupling and nonlinear effects, and these dynamic effects may spoil the maneuverability and sometimes it may cause instability of the system. Here, we formulate the problem based on the same

concept as in the one DOF case, and propose a new control scheme for the ideal kinesthetic coupling (ideal response III) which is applicable to the different configuration arms.

First, dynamic equations of master and slave arms are given by

$$\boldsymbol{\tau}_m = \boldsymbol{M}_m(\boldsymbol{q}_m)\ddot{\boldsymbol{q}}_m + \boldsymbol{h}_m(\boldsymbol{q}_m, \dot{\boldsymbol{q}}_m) - \boldsymbol{J}_m^T(\boldsymbol{q}_m)\boldsymbol{f}_m \tag{5.1}$$

$$\boldsymbol{\tau}_s = \boldsymbol{M}_s(\boldsymbol{q}_s)\ddot{\boldsymbol{q}}_s + \boldsymbol{h}_s(\boldsymbol{q}_s, \dot{\boldsymbol{q}}_s) + \boldsymbol{J}_s^T(\boldsymbol{q}_s)\boldsymbol{f}_s \tag{5.2}$$

where $\boldsymbol{q}_m$, $\boldsymbol{q}_s \in \boldsymbol{R}^n$ are joint displacement vectors of master and slave arms, $\boldsymbol{\tau}_m$, $\boldsymbol{\tau}_s \in \boldsymbol{R}^n$ are joint driving force/torque vectors of each arm, $\boldsymbol{M}_m(\boldsymbol{q}_m)$, $\boldsymbol{M}_s(\boldsymbol{q}_s) \in \boldsymbol{R}^{n\times n}$ are inertia matrices, $\boldsymbol{h}_m(\boldsymbol{q}_m, \dot{\boldsymbol{q}}_m)$ and $\boldsymbol{h}_s(\boldsymbol{q}_s, \dot{\boldsymbol{q}}_s) \in \boldsymbol{R}^n$ are terms of centrifugal and Coriolis force and gravitational force of each arm respectively. And $\boldsymbol{J}_m(\boldsymbol{q}_m)$ and $\boldsymbol{J}_s(\boldsymbol{q}_s) \in \boldsymbol{R}^{n\times n}$ are the Jacobian matrices. Here, n denotes the number of DOF and $\boldsymbol{R}^n$ denotes an n-dimensional Euclidean space. We assume that both arms have different configurations but the same DOF, and they have no redundancy, that is, the dimension of the control variable is also n. The vector $\boldsymbol{f}_m \in \boldsymbol{R}^n$ means the force that the operator applies to the master arm, and $\boldsymbol{f}_s \in \boldsymbol{R}^n$ means the force that the slave arm exerts to the object. Hereafter, the inertia matrices and the Jacobian matrices will be written as $\boldsymbol{M}_m$, $\boldsymbol{M}_s$, $\boldsymbol{J}_m$, and $\boldsymbol{J}_s$ respectively. Also, the vectors $\boldsymbol{h}_m(\boldsymbol{q}_m, \dot{\boldsymbol{q}}_m)$ and $\boldsymbol{h}_s(\boldsymbol{q}_s, \dot{\boldsymbol{q}}_s)$ will be written by $\boldsymbol{h}_m$ and $\boldsymbol{h}_s$.

Let us start from the following form of control scheme.

$$\begin{aligned}\boldsymbol{\tau}_m &= \boldsymbol{M}_m\boldsymbol{J}_m^{-1}[\boldsymbol{u}_m - \dot{\boldsymbol{J}}_m\dot{\boldsymbol{q}}_m] + \boldsymbol{h}_m \\ &\quad - \boldsymbol{J}_m^T[\boldsymbol{K}_{mf}\left(\frac{\boldsymbol{f}_s - \boldsymbol{f}_m}{2}\right) + \frac{\boldsymbol{f}_m + \boldsymbol{f}_s}{2}]\end{aligned} \tag{5.3}$$

$$\begin{aligned}\boldsymbol{\tau}_s &= \boldsymbol{M}_s\boldsymbol{J}_s^{-1}[\boldsymbol{u}_s - \dot{\boldsymbol{J}}_s\dot{\boldsymbol{q}}_s] + \boldsymbol{h}_s \\ &\quad - \boldsymbol{J}_s^T[\boldsymbol{K}_{sf}\left(\frac{\boldsymbol{f}_s - \boldsymbol{f}_m}{2}\right) - \frac{\boldsymbol{f}_m + \boldsymbol{f}_s}{2}]\end{aligned} \tag{5.4}$$

where $\boldsymbol{K}_{mf}$ and $\boldsymbol{K}_{sf} \in \boldsymbol{R}^{n\times n}$ are gain matrices of force, and $\boldsymbol{u}_m$ and $\boldsymbol{u}_s \in \boldsymbol{R}^n$ are input vectors defined anew. Since the above equations consist of $\boldsymbol{M}_m$, $\boldsymbol{M}_s$, $\boldsymbol{h}_m$, and $\boldsymbol{h}_s$, we will assume that dynamic parameters of each arm are exactly known. Eqs.(5.3) and (5.4) are natural extensions of eqs.(3.5) and (3.6) in chapter 3.

Substituting eqs.(5.3), (5.4) into eqs.(5.1), (5.2), the following equations are obtained.

$$\ddot{\boldsymbol{x}}_m = \boldsymbol{u}_m - \boldsymbol{W}_m(\boldsymbol{E} + \boldsymbol{K}_{mf}) \left(\frac{\boldsymbol{f}_s - \boldsymbol{f}_m}{2} \right) \tag{5.5}$$

$$\ddot{\boldsymbol{x}}_s = \boldsymbol{u}_s - \boldsymbol{W}_s(\boldsymbol{E} + \boldsymbol{K}_{sf}) \left(\frac{\boldsymbol{f}_s - \boldsymbol{f}_m}{2} \right) \tag{5.6}$$

where $\boldsymbol{x}_m$ and $\boldsymbol{x}_s \in \boldsymbol{R}^n$ are position(and orientation) vectors of each hand tip. Each hand tip acceleration and joint acceleration has a relation such as $\ddot{\boldsymbol{x}}_m = \boldsymbol{J}_m \ddot{\boldsymbol{q}}_m + \dot{\boldsymbol{J}}_m \dot{\boldsymbol{q}}_m$ or $\ddot{\boldsymbol{x}}_s = \boldsymbol{J}_s \ddot{\boldsymbol{q}}_s + \dot{\boldsymbol{J}}_s \dot{\boldsymbol{q}}_s$. The matrices $\boldsymbol{W}_m \triangleq \boldsymbol{J}_m \boldsymbol{M}_m^{-1} \boldsymbol{J}_m^T$ and $\boldsymbol{W}_s \triangleq \boldsymbol{J}_s \boldsymbol{M}_s^{-1} \boldsymbol{J}_s^T \in \boldsymbol{R}^{n \times n}$ are the generalized inverse inertia matrices. The matrix $\boldsymbol{E}$ denotes $n \times n$ unity matrix. Adding eqs.(5.5) and (5.6), we get

$$\ddot{\boldsymbol{x}}_m + \ddot{\boldsymbol{x}}_s = \boldsymbol{u}_m + \boldsymbol{u}_s - [\boldsymbol{W}_m(\boldsymbol{E} + \boldsymbol{K}_{mf}) + \boldsymbol{W}_s(\boldsymbol{E} + \boldsymbol{K}_{sf})] \left(\frac{\boldsymbol{f}_s - \boldsymbol{f}_m}{2} \right) \tag{5.7}$$

Here, if

$$\ddot{\boldsymbol{x}}_m + \ddot{\boldsymbol{x}}_s = \boldsymbol{u}_m + \boldsymbol{u}_s \tag{5.8}$$

were achieved and if the matrix $[\boldsymbol{W}_m(\boldsymbol{E} + \boldsymbol{K}_{mf}) + \boldsymbol{W}_s(\boldsymbol{E} + \boldsymbol{K}_{sf})]$ is a non-singular matrix, then we get

$$\boldsymbol{f}_m - \boldsymbol{f}_s = \boldsymbol{0} \tag{5.9}$$

from eq.(5.7) and it means at least the ideal response II has been realized. Next, subtracting eq.(5.6) from eq.(5.5) and considering eq.(5.9), we get

$$\ddot{\boldsymbol{x}}_m - \ddot{\boldsymbol{x}}_s = \boldsymbol{u}_m - \boldsymbol{u}_s \tag{5.10}$$

Let $\boldsymbol{e}_y \triangleq \boldsymbol{x}_m - \boldsymbol{x}_s$ be the error vector between master and slave arms. Eq.(5.10) means that the behavior of $\ddot{\boldsymbol{e}}_y$ can be specified by $\boldsymbol{u}_m - \boldsymbol{u}_s$. Here, we set as

$$\boldsymbol{u}_m - \boldsymbol{u}_s = -\boldsymbol{K}_1 \dot{\boldsymbol{e}}_y - \boldsymbol{K}_2 \boldsymbol{e}_y \tag{5.11}$$

where $\boldsymbol{K}_1$ and $\boldsymbol{K}_2 \in \boldsymbol{R}^{n \times n}$ are gain matrices for velocity and position, respectively. From eqs.(5.10) and (5.11), we obtain

$$\ddot{\boldsymbol{e}}_y + \boldsymbol{K}_1 \dot{\boldsymbol{e}}_y + \boldsymbol{K}_2 \boldsymbol{e}_y = \boldsymbol{0} \tag{5.12}$$

and appropriate gain matrices, $\boldsymbol{K}_1$ and $\boldsymbol{K}_2$, guarantee an asymptotic convergence of $\boldsymbol{e}_y$ to zero. Consequently, the ideal response III can be realized in steady state. From eqs.(5.8) and (5.11), the input vectors $\boldsymbol{u}_m$ and $\boldsymbol{u}_s$ are given by the following equations:

$$\boldsymbol{u}_m = \frac{1}{2}(\ddot{\boldsymbol{x}}_m + \ddot{\boldsymbol{x}}_s) - \frac{1}{2}\boldsymbol{K}_1\dot{\boldsymbol{e}}_y - \frac{1}{2}\boldsymbol{K}_2\boldsymbol{e}_y \tag{5.13}$$

$$\boldsymbol{u}_s = \frac{1}{2}(\ddot{\boldsymbol{x}}_m + \ddot{\boldsymbol{x}}_s) + \frac{1}{2}\boldsymbol{K}_1\dot{\boldsymbol{e}}_y + \frac{1}{2}\boldsymbol{K}_2\boldsymbol{e}_y \tag{5.14}$$

Finally, control scheme which can realize the ideal response III is obtained as:

$$\begin{aligned}\boldsymbol{\tau}_m &= \boldsymbol{M}_m\boldsymbol{J}_m^{-1}[\ddot{\boldsymbol{x}}_{ms} + \boldsymbol{K}_1(\dot{\boldsymbol{x}}_{ms} - \dot{\boldsymbol{x}}_m) + \boldsymbol{K}_2(\boldsymbol{x}_{ms} - \boldsymbol{x}_m) \\ &\quad - \dot{\boldsymbol{J}}_m\dot{\boldsymbol{q}}_m] + \boldsymbol{h}_m - \boldsymbol{J}_m^T[\boldsymbol{K}_{mf}(\boldsymbol{f}_{ms} - \boldsymbol{f}_m) + \boldsymbol{f}_{ms}]\end{aligned} \tag{5.15}$$

$$\begin{aligned}\boldsymbol{\tau}_s &= \boldsymbol{M}_s\boldsymbol{J}_s^{-1}[\ddot{\boldsymbol{x}}_{ms} + \boldsymbol{K}_1(\dot{\boldsymbol{x}}_{ms} - \dot{\boldsymbol{x}}_s) + \boldsymbol{K}_2(\boldsymbol{x}_{ms} - \boldsymbol{x}_s) - \dot{\boldsymbol{J}}_s\dot{\boldsymbol{q}}_s] \\ &\quad + \boldsymbol{h}_s + \boldsymbol{J}_s^T[\boldsymbol{K}_{mf}(\boldsymbol{f}_{ms} - \boldsymbol{f}_s) + \boldsymbol{f}_{ms}]\end{aligned} \tag{5.16}$$

where $\boldsymbol{x}_{ms} \triangleq (\boldsymbol{x}_m + \boldsymbol{x}_s)/2$ and $\boldsymbol{f}_{ms} \triangleq (\boldsymbol{f}_m + \boldsymbol{f}_s)/2$. The control scheme of eqs.(5.15) and (5.16) can be regarded as a combination of the resolved acceleration control which makes each arm follow $\boldsymbol{x}_{ms}$, the middle point of both arms, as the desired trajectory and force control which makes actual exerting force of each arm follow $\boldsymbol{f}_{ms}$, the average of force at the both sides, as the desired force command.

We assumed that we can calculate $\boldsymbol{M}_m$, $\boldsymbol{M}_s$, $\boldsymbol{h}_m$, and $\boldsymbol{h}_s$ accurately. Several methods to identify the dynamic parameters of manipulators were proposed[9, 50]. In practice, however, the identified values of dynamic parameters may have a certain amount of error. It should be noted that these identification errors may cause the system to be unstable. Several researchers discussed the robustness of the computed torque law for trajectory control of manipulators with respect to the uncertainty of the dynamics parameters where the controller provides an arbitrary small tracking error capability for the particular class of the desired trajectories by choosing appropriate feed-back gains[31][68]. In the case of master-slave systems, the parameter uncertainty or time

delay of the computation spoils the achievement of eq.(5.8), and the robustness of the controller should be considered for the future.

The resolved acceleration control law generates the joint driving force based on the on-line compensation of the manipulator dynamics. Concerning the multiple DOF case, the on-line compensation of arm dynamics becomes difficult because dynamics of multi-link mechanisms is complex and requires many computations. Another method to compensate the manipulator dynamics is the feedforward scheme that compensates for the manipulator dynamics in the feedforward path according to the desired trajectory. If the desired trajectory can be given in advance, the feedforward compensation can be realized by the off-line computation where the performance of the computer is not so serious. In controlling the master-slave manipulators, however, there is no specific desired trajectory. Consequently, the on-line computation is only the way to compensate for the manipulator dynamics of the master and slave arms.

5.3.2 Control Scheme Realizing the Ideal Response I and II

In the previous subsection, we discussed a new control scheme which can realize the ideal response III. We can interpret that this control scheme eliminates the dynamics of master and slave arms completely which exists between the operator and the object. In this section, we discuss other control schemes which do not eliminate arm dynamics completely but allow the existence of arm dynamics as a certain type of impedance. Here, we try to make the dynamics of master and slave arms act as an impedance shown in **Fig.5.1**. We call call it the intervenient impedance as discussed in one DOF case. The state of **Fig.5.1** can be described by the following equation.

$$\boldsymbol{f}_m - \boldsymbol{f}_s = \widehat{\boldsymbol{M}}\ddot{\boldsymbol{x}} + \widehat{\boldsymbol{B}}\dot{\boldsymbol{x}} + \widehat{\boldsymbol{C}}\boldsymbol{x} \tag{5.17}$$

where $\widehat{\boldsymbol{M}} \triangleq \mathrm{diag}(\hat{m}_1, \cdots, \hat{m}_n)$, $\widehat{\boldsymbol{B}} \triangleq \mathrm{diag}(\hat{b}_1, \cdots, \hat{b}_n)$, and $\widehat{\boldsymbol{C}} \triangleq \mathrm{diag}(\hat{c}_1, \cdots, \hat{c}_n)$ denote matrices which elements represent mass, viscosity, and stiffness of the intervenient impedance in each direction of Cartesian coordinates respectively. And $\boldsymbol{x}$ means the position vector of

intervenient impedance. Actually $\boldsymbol{x}_m$ and $\boldsymbol{x}_s$ may not always coincide, therefore we will consider the following equation.

$$\boldsymbol{f}_m - \boldsymbol{f}_s = \widehat{\boldsymbol{M}}\ddot{\boldsymbol{x}}_{ms} + \widehat{\boldsymbol{B}}\dot{\boldsymbol{x}}_{ms} + \widehat{\boldsymbol{C}}\boldsymbol{x}_{ms} \tag{5.18}$$

Moreover we set the following equation corresponding to eq.(5.12).

$$\ddot{\boldsymbol{e}}_y + \boldsymbol{K}_1\dot{\boldsymbol{e}}_y + \boldsymbol{K}_2\boldsymbol{e}_y = \boldsymbol{\Lambda}\frac{\boldsymbol{f}_m + \boldsymbol{f}_s}{2} \tag{5.19}$$

where $\boldsymbol{\Lambda} \triangleq \mathrm{diag}(\lambda_1, \cdots, \lambda_n)$ is a coefficient matrix corresponding to λ in eq.(3.21) in chapter 3. The following control scheme is obtained which achieves both eqs.(5.18) and (5.19).

$$\begin{aligned}\boldsymbol{\tau}_m \;=\; & \boldsymbol{M}_m\boldsymbol{J}_m^{-1}[\ddot{\boldsymbol{x}}_{ms} + \boldsymbol{K}_1(\dot{\boldsymbol{x}}_{ms} - \dot{\boldsymbol{x}}_m) + \boldsymbol{K}_2(\boldsymbol{x}_{ms} - \boldsymbol{x}_m) \\ & - \dot{\boldsymbol{J}}_m\dot{\boldsymbol{q}}_m] + \boldsymbol{h}_m \\ & - \boldsymbol{J}_m^T\frac{(\boldsymbol{E} + \boldsymbol{K}_{mf})}{2}[\widehat{\boldsymbol{M}}\ddot{\boldsymbol{x}}_{ms} + \widehat{\boldsymbol{B}}\dot{\boldsymbol{x}}_{ms} + \widehat{\boldsymbol{C}}\boldsymbol{x}_{ms}] \\ & + \boldsymbol{M}_m\boldsymbol{J}_m^{-1}\frac{\boldsymbol{\Lambda}}{2}\boldsymbol{f}_{ms} - \boldsymbol{J}_m^T[\boldsymbol{K}_{mf}(\boldsymbol{f}_{ms} - \boldsymbol{f}_m) + \boldsymbol{f}_{ms}]\end{aligned} \tag{5.20}$$

$$\begin{aligned}\boldsymbol{\tau}_s \;=\; & \boldsymbol{M}_s\boldsymbol{J}_s^{-1}[\ddot{\boldsymbol{x}}_{ms} + \boldsymbol{K}_1(\dot{\boldsymbol{x}}_{ms} - \dot{\boldsymbol{x}}_s) + \boldsymbol{K}_2(\boldsymbol{x}_{ms} - \boldsymbol{x}_s) - \dot{\boldsymbol{J}}_s\dot{\boldsymbol{q}}_s] \\ & + \boldsymbol{h}_s - \boldsymbol{J}_s^T\frac{(\boldsymbol{E} + \boldsymbol{K}_{sf})}{2}[\widehat{\boldsymbol{M}}\ddot{\boldsymbol{x}}_{ms} + \widehat{\boldsymbol{B}}\dot{\boldsymbol{x}}_{ms} + \widehat{\boldsymbol{C}}\boldsymbol{x}_{ms}] \\ & - \boldsymbol{M}_s\boldsymbol{J}_s^{-1}\frac{\boldsymbol{\Lambda}}{2}\boldsymbol{f}_{ms} + \boldsymbol{J}_s^T[\boldsymbol{K}_{sf}(\boldsymbol{f}_{ms} - \boldsymbol{f}_s) + \boldsymbol{f}_{ms}]\end{aligned} \tag{5.21}$$

When we set $\boldsymbol{\Lambda} = \boldsymbol{o}$ in eqs.(5.20) and (5.21), $\boldsymbol{e}_y$ converges into zero asymptotically from eq.(5.19). And in a steady state, the system response by eq.(5.18) becomes that of eq.(5.17). Therefore, the control scheme of eqs.(5.20) and (5.21) when $\boldsymbol{\Lambda} = \boldsymbol{o}$ is an example of control schemes realizing the ideal response I. On the other hand, when we set $\widehat{\boldsymbol{M}} = \widehat{\boldsymbol{B}} = \widehat{\boldsymbol{C}} = \boldsymbol{o}$, the system response becomes the ideal response II. In this sense, the control scheme of eqs.(5.15) and (5.16) can be regarded as a special case of eqs.(5.20) and (5.21) when the intervenient impedance is set at zero. Eqs.(5.20) and (5.21) are general form of control schemes which realize the ideal response I or II or III.

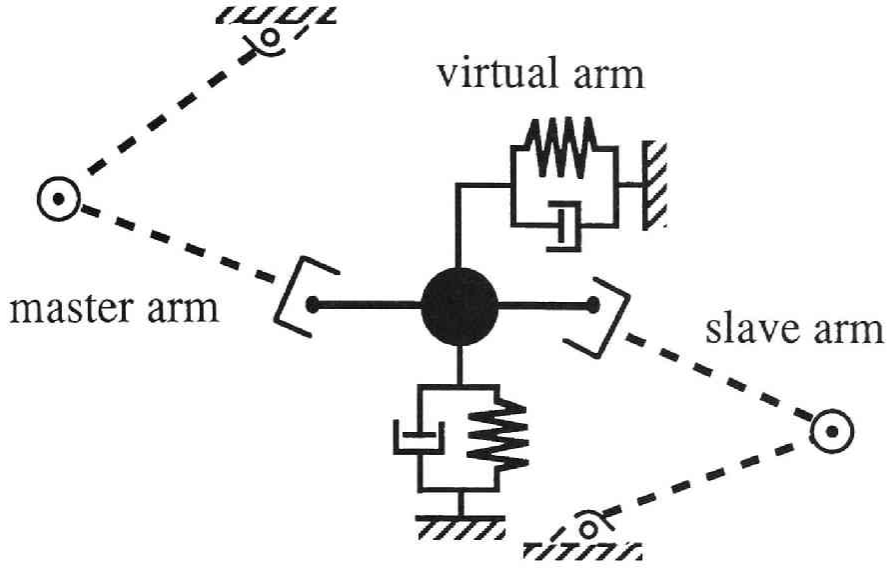

Figure 5.1: Intervenient impedance model in Cartesian space

5.4 Control of Isomorphic Configuration Arms

5.4.1 Control Scheme Realizing the Ideal Response III

A serious problem in the multiple DOF case is singularity points where the control schemes using the Jacobian inverse matrix cannot be applied. In order to avoid this problem, we next focus on the isomorphic configuration arms and formulate new control schemes where the joint space is used instead of the Cartesian space. Since this scheme does not use the inverse of Jacobian, there is no problem at the singularity point or around it.

Early models of master-slave manipulators used isomorphic configuration arms. By applying a one DOF servo controller to each joint, the controller could be simple. But those method neglected the consideration of arm dynamics such as the coupling inertia effects and Coriolis force and centrifugal force. The control scheme to be proposed

takes the arm dynamics exactly into account and it is different from the conventional methods where an one DOF controller is applied to each corresponding joint.

First, let the following basic form be considered corresponding to eqs.(5.3) and (5.4).

$$\boldsymbol{\tau}_m = \boldsymbol{M}_m\boldsymbol{\eta}_m + \boldsymbol{h}_m - \frac{1}{2}(\boldsymbol{J}_m^T\boldsymbol{f}_m + \boldsymbol{J}_s^T\boldsymbol{f}_s) - \boldsymbol{\Gamma}_{mf}\frac{1}{2}(\boldsymbol{J}_s^T\boldsymbol{f}_s - \boldsymbol{J}_m^T\boldsymbol{f}_m) \quad (5.22)$$

$$\boldsymbol{\tau}_s = \boldsymbol{M}_s\boldsymbol{\eta}_s + \boldsymbol{h}_s + \frac{1}{2}(\boldsymbol{J}_m^T\boldsymbol{f}_m + \boldsymbol{J}_s^T\boldsymbol{f}_s) - \boldsymbol{\Gamma}_{sf}\frac{1}{2}(\boldsymbol{J}_s^T\boldsymbol{f}_s - \boldsymbol{J}_m^T\boldsymbol{f}_m) \quad (5.23)$$

where $\boldsymbol{\eta}_m$ and $\boldsymbol{\eta}_s \in \boldsymbol{R}^n$ are new input vectors in the joint space and $\boldsymbol{\Gamma}_{mf}$ and $\boldsymbol{\Gamma}_{sf} \in \boldsymbol{R}^{n\times n}$ are gain matrices of force in the joint space. Hereafter, we will regard eqs.(5.1) and (5.2) as the equations of motion of the isomorphic configuration arms. Isomorphic configuration means that the kinematic parameters are equal between the master and slave arms but the dynamic parameters need not be equal. Substituting eqs.(5.22) and (5.23) to eqs.(5.1) and (5.2), the following equations are obtained.

$$\ddot{\boldsymbol{q}}_m = \boldsymbol{\eta}_m - \boldsymbol{M}_m^{-1}(\boldsymbol{E} + \boldsymbol{\Gamma}_{mf})\left(\frac{\boldsymbol{J}_s^T\boldsymbol{f}_s - \boldsymbol{J}_m^T\boldsymbol{f}_m}{2}\right) \quad (5.24)$$

$$\ddot{\boldsymbol{q}}_s = \boldsymbol{\eta}_s - \boldsymbol{M}_s^{-1}(\boldsymbol{E} + \boldsymbol{\Gamma}_{sf})\left(\frac{\boldsymbol{J}_s^T\boldsymbol{f}_s - \boldsymbol{J}_m^T\boldsymbol{f}_m}{2}\right) \quad (5.25)$$

Adding both side of eqs.(5.25) and (5.25), we get

$$\ddot{\boldsymbol{q}}_m + \ddot{\boldsymbol{q}}_s = \boldsymbol{\eta}_m + \boldsymbol{\eta}_s - [\boldsymbol{M}_m^{-1}(\boldsymbol{E} + \boldsymbol{\Gamma}_{mf}) + \boldsymbol{M}_s^{-1}(\boldsymbol{E} + \boldsymbol{\Gamma}_{sf})]\left(\frac{\boldsymbol{J}_s^T\boldsymbol{f}_s - \boldsymbol{J}_m^T\boldsymbol{f}_m}{2}\right) \quad (5.26)$$

Here, in the same way as eq.(5.8), if

$$\boldsymbol{\eta}_m + \boldsymbol{\eta}_s = \ddot{\boldsymbol{q}}_m + \ddot{\boldsymbol{q}}_s \quad (5.27)$$

were achieved, then we get the following equation, since $[\boldsymbol{M}_m^{-1}(\boldsymbol{E} + \boldsymbol{K}_{mf}) + \boldsymbol{M}_s^{-1}(\boldsymbol{E} + \boldsymbol{K}_{sf})]$ is always a non-singular matrix.

$$\boldsymbol{J}_s^T\boldsymbol{f}_s - \boldsymbol{J}_m^T\boldsymbol{f}_m = \boldsymbol{o} \quad (5.28)$$

Next, subtracting eq.(5.25) from eq.(5.25) and considering eq.(5.28), we get

$$\ddot{\boldsymbol{q}}_m - \ddot{\boldsymbol{q}}_s = \boldsymbol{\eta}_m - \boldsymbol{\eta}_s. \tag{5.29}$$

Let $\boldsymbol{e} \triangleq \boldsymbol{q}_m - \boldsymbol{q}_s$ be the joint error vector between the master and slave arms. Eq.(5.29) means that the behavior of $\ddot{\boldsymbol{e}}$ can be specified by $\boldsymbol{\eta}_m - \boldsymbol{\eta}_s$. Here, we set as

$$\boldsymbol{\eta}_m - \boldsymbol{\eta}_s = -\boldsymbol{\Gamma}_1\dot{\boldsymbol{e}} - \boldsymbol{\Gamma}_2\boldsymbol{e} \tag{5.30}$$

where $\boldsymbol{\Gamma}_1$ and $\boldsymbol{\Gamma}_2 \in \boldsymbol{R}^{n\times n}$ are gain matrices for velocity and position in the joint space respectively. From eqs.(5.29) and (5.30), we obtain

$$\ddot{\boldsymbol{e}} + \boldsymbol{\Gamma}_1\dot{\boldsymbol{e}} + \boldsymbol{\Gamma}_2\boldsymbol{e} = \boldsymbol{o} \tag{5.31}$$

and appropriate gain matrices, $\boldsymbol{\Gamma}_1$ and $\boldsymbol{\Gamma}_2$, guarantee an asymptotic convergence of $\boldsymbol{e}$ to zero. Since the master and slave arms have the same configurations, both the hand tip positions coincide when $\boldsymbol{e} = \boldsymbol{o}$. Therefore at least the ideal response I has been realized. Moreover, when $\boldsymbol{e} = \boldsymbol{o}$, the Jacobian matrices of both arms become the same one.

$$\boldsymbol{J}_m = \boldsymbol{J}_s \triangleq \boldsymbol{J}_{ms} \tag{5.32}$$

and eq.(5.28) becomes

$$\boldsymbol{J}_{ms}^T(\boldsymbol{f}_s - \boldsymbol{f}_m) = \boldsymbol{o} \tag{5.33}$$

When $\boldsymbol{J}_{ms}$ is a non-singular matrix, we get

$$\boldsymbol{f}_s - \boldsymbol{f}_s = \boldsymbol{o} \tag{5.34}$$

and finally ideal response III has been realized. From eqs.(5.27) and (5.30), the control scheme is formulated as:

$$\begin{aligned}\boldsymbol{\tau}_m \;=\; & \boldsymbol{M}_m[\ddot{\boldsymbol{q}}_{ms} + \boldsymbol{\Gamma}_1(\dot{\boldsymbol{q}}_{ms} - \dot{\boldsymbol{q}}_m) + \boldsymbol{\Gamma}_2(\boldsymbol{q}_{ms} - \boldsymbol{q}_m)] + \boldsymbol{h}_m \\ & - \boldsymbol{\Gamma}_{mf}\left(\frac{\boldsymbol{J}_m^T\boldsymbol{f}_m + \boldsymbol{J}_s^T\boldsymbol{f}_s}{2} - \boldsymbol{J}_m^T\boldsymbol{f}_m\right) - \frac{\boldsymbol{J}_m^T\boldsymbol{f}_m + \boldsymbol{J}_s^T\boldsymbol{f}_s}{2}\end{aligned} \tag{5.35}$$

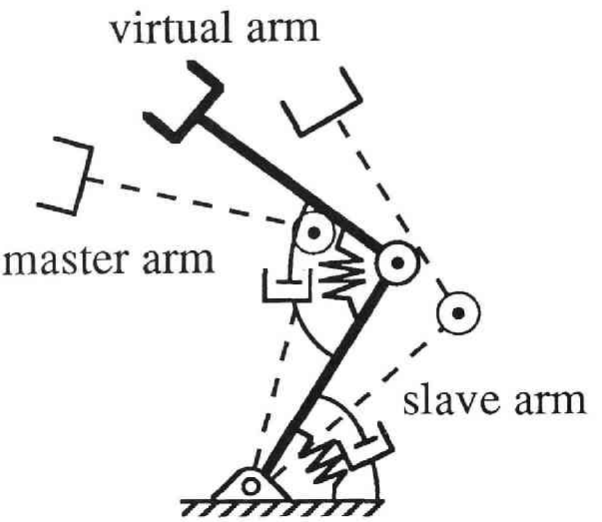

Figure 5.2: Intervenient impedance model in joint space

$$\begin{aligned}\boldsymbol{\tau}_s &= \boldsymbol{M}_s[\ddot{\boldsymbol{q}}_{ms} + \boldsymbol{\Gamma}_1(\dot{\boldsymbol{q}}_{ms} - \dot{\boldsymbol{q}}_s) + \boldsymbol{\Gamma}_2(\boldsymbol{q}_{ms} - \boldsymbol{q}_s)] + \boldsymbol{h}_s \\ &\quad + \boldsymbol{\Gamma}_{sf}\left(\frac{\boldsymbol{J}_m^T\boldsymbol{f}_m + \boldsymbol{J}_s^T\boldsymbol{f}_s}{2} - \boldsymbol{J}_s^T\boldsymbol{f}_s\right) + \frac{\boldsymbol{J}_m^T\boldsymbol{f}_m + \boldsymbol{J}_s^T\boldsymbol{f}_s}{2}\end{aligned} \tag{5.36}$$

where $q_{ms} \triangleq (q_m + q_s)/2$. It should be noted that eqs.(5.35) and (5.36) can be applied even when arm is in the singularity posture since they do not contain the Jacobian inverse matrix whereas eqs.(5.15) and (5.16) does. Moreover it should be noted that eqs.(5.31) and (5.33) are achieved whichever arms are in singularity or not. Especially, eq.(5.33) means that, when arms are in singularity, corresponding elements between $\boldsymbol{f}_m$ and $\boldsymbol{f}_s$ except in the singularity direction are equal, and it is equivalent to eq.(5.34) when arms are not singular.

5.4.2 Control Scheme Realizing the Ideal Response I and II

In this section, we discuss the intervenient impedance in the isomorphic configuration case. Let a virtual arm shown in **Fig.5.2** be considered as an intervenient impedance model. This virtual arm has the same configuration as that of the master and slave arms and its joint angle is $\boldsymbol{q}_{ms}$, the average of joint angles of the both arms. The dynamics of the virtual arm can be described as follows:

$$\boldsymbol{J}_m^T \boldsymbol{f}_m - \boldsymbol{J}_s^T \boldsymbol{f}_s = \widetilde{\boldsymbol{M}}(\boldsymbol{q}_{ms})\ddot{\boldsymbol{q}}_{ms} + \tilde{\boldsymbol{h}}(\boldsymbol{q}_{ms}, \dot{\boldsymbol{q}}_{ms}) + \widetilde{\boldsymbol{B}}\dot{\boldsymbol{q}}_{ms} + \widetilde{\boldsymbol{C}}\boldsymbol{q}_{ms} \quad (5.37)$$

$$\ddot{\boldsymbol{e}} + \boldsymbol{\Gamma}_1\dot{\boldsymbol{e}} + \boldsymbol{\Gamma}_2\boldsymbol{e} = \tilde{\boldsymbol{\Lambda}}\frac{\boldsymbol{J}_m^T\boldsymbol{f}_m + \boldsymbol{J}_s^T\boldsymbol{f}_s}{2} \quad (5.38)$$

where $\widetilde{\boldsymbol{M}}(\boldsymbol{q}_{ms})$ denotes inertia matrix of the intervenient virtual arm and $\tilde{\boldsymbol{h}}(\boldsymbol{q}_{ms}, \dot{\boldsymbol{q}}_{ms})$ denotes Coriolis and centrifugal force vector of the virtual arm. And $\widetilde{\boldsymbol{B}} \triangleq \mathrm{diag}(\tilde{b}_1, \cdots, \tilde{b}_n)$ and $\widetilde{\boldsymbol{C}} \triangleq \mathrm{diag}(\tilde{c}_1, \cdots, \tilde{c}_n)$ denote the matrices which element represents the parameter of viscous coefficient and stiffness at each joint of the intervenient virtual arm. And $\tilde{\boldsymbol{\Lambda}} \triangleq \mathrm{diag}(\tilde{\lambda}_1, \cdots, \tilde{\lambda}_n)$ is a coefficient matrix which corresponds to $\boldsymbol{\Lambda}$ in eq.(5.19). Eqs.(5.37) and (5.38) correspond to eqs.(5.18) and (5.19). In the same way as the different configuration case, the control scheme which achieves both eqs.(5.37) and (5.38) is given by

$$\begin{aligned}
\boldsymbol{\tau}_m \;=\; & \boldsymbol{M}_m[\ddot{\boldsymbol{q}}_{ms} + \boldsymbol{\Gamma}_1(\dot{\boldsymbol{q}}_{ms} - \dot{\boldsymbol{q}}_m) + \boldsymbol{\Gamma}_2(\boldsymbol{q}_{ms} - \boldsymbol{q}_m)] + \boldsymbol{h}_m \\
& - \frac{(\boldsymbol{E} + \boldsymbol{\Gamma}_{mf})}{2}[\widetilde{\boldsymbol{M}}\ddot{\boldsymbol{q}}_{ms} + \tilde{\boldsymbol{h}} + \widetilde{\boldsymbol{B}}\dot{\boldsymbol{q}}_{ms} + \widetilde{\boldsymbol{C}}\boldsymbol{q}_{ms}] \\
& + \boldsymbol{M}_m\frac{1}{2}\tilde{\boldsymbol{\Lambda}}\left(\frac{\boldsymbol{J}_m^T\boldsymbol{f}_m + \boldsymbol{J}_s^T\boldsymbol{f}_s}{2}\right) \\
& - \boldsymbol{\Gamma}_{mf}\left(\frac{\boldsymbol{J}_m^T\boldsymbol{f}_m + \boldsymbol{J}_s^T\boldsymbol{f}_s}{2} - \boldsymbol{J}_m^T\boldsymbol{f}_m\right) - \frac{\boldsymbol{J}_m^T\boldsymbol{f}_m + \boldsymbol{J}_s^T\boldsymbol{f}_s}{2},
\end{aligned} \quad (5.39)$$

$$\begin{aligned}
\boldsymbol{\tau}_s \;=\; & \boldsymbol{M}_s[\ddot{\boldsymbol{q}}_{ms} + \boldsymbol{\Gamma}_1(\dot{\boldsymbol{q}}_{ms} - \dot{\boldsymbol{q}}_s) + \boldsymbol{\Gamma}_2(\boldsymbol{q}_{ms} - \boldsymbol{q}_s)] + \boldsymbol{h}_s \\
& - \frac{(\boldsymbol{E} + \boldsymbol{\Gamma}_{sf})}{2}[\widetilde{\boldsymbol{M}}\ddot{\boldsymbol{q}}_{ms} + \tilde{\boldsymbol{h}} + \widetilde{\boldsymbol{B}}\dot{\boldsymbol{q}}_{ms} + \widetilde{\boldsymbol{C}}\boldsymbol{q}_{ms}]
\end{aligned}$$

Table 5.1: Parameters of master and slave arms, and operator arm

	Master & Slave		Operator	
	link 1	link 2	link 1	link 2
l_i [m]	1.0	1.0	1.0	1.0
m_i [kg]	2.0	2.0	1.0	1.0
l_{g_i} [m]	0.5	0.5	0.5	0.5
$\hat{I}_i$ [kgm^2]	1.0	1.0	0.5	0.5
b_i [Nms/rad]	–	–	0.5	0.5
c_i [Nm/rad]	–	–	1.0	1.0

$$
\begin{aligned}
&- \boldsymbol{M}_s \frac{1}{2} \tilde{\boldsymbol{\Lambda}} \left(\frac{\boldsymbol{J}_m^T \boldsymbol{f}_m + \boldsymbol{J}_s^T \boldsymbol{f}_s}{2} \right) \\
&+ \boldsymbol{\Gamma}_{sf} \left(\frac{\boldsymbol{J}_m^T \boldsymbol{f}_m + \boldsymbol{J}_s^T \boldsymbol{f}_s}{2} - \boldsymbol{J}_s^T \boldsymbol{f}_s \right) + \frac{\boldsymbol{J}_m^T \boldsymbol{f}_m + \boldsymbol{J}_s^T \boldsymbol{f}_s}{2}.
\end{aligned}
\tag{5.40}
$$

In eqs.(5.39) and (5.40), the ideal response I can be realized when $\tilde{\boldsymbol{\Lambda}} = \mathbf{o}$. And the ideal response II can be realized when $\widetilde{\boldsymbol{M}} = \widetilde{\boldsymbol{B}} = \widetilde{\boldsymbol{C}} = \mathbf{o}$, $\tilde{\boldsymbol{h}} = \mathbf{o}$. Moreover, if we set $\boldsymbol{\Gamma}_{mf} = 2\boldsymbol{M}_m \widetilde{\boldsymbol{M}}^{-1} - \boldsymbol{E}$, $\boldsymbol{\Gamma}_{sf} = 2\boldsymbol{M}_s \widetilde{\boldsymbol{M}}^{-1} - \boldsymbol{E}$ in the case when $\tilde{\boldsymbol{\Lambda}} = \mathbf{o}$, the control scheme of eqs.(5.39) and (5.40) becomes a special case where no acceleration signals are used. If both the inertia matrices satisfy $\boldsymbol{M}_m = \boldsymbol{M}_s \triangleq \boldsymbol{M}_{ms}$ when $\boldsymbol{e} = \mathbf{o}$ and if we set $\boldsymbol{\Gamma}_{mf} = \boldsymbol{\Gamma}_{sf} = \mathbf{o}$ and $\tilde{\boldsymbol{\Lambda}} = 2\boldsymbol{M}_{ms}^{-1}$, the control scheme becomes a special case where no force signals are used.

5.4.3 Discussion about Sensor Placement

In section 3.2.4, we discussed the sensor placement in the one DOF case, where it was shown that the accelerometer must be placed at the tip of the force sensor in order to satisfy the principle of causality when the ideal response III is realized without any constraints at the slave side. In the case of isomorphic configuration arms, what we need is not the acceleration at the hand tip but the acceleration at each joint.

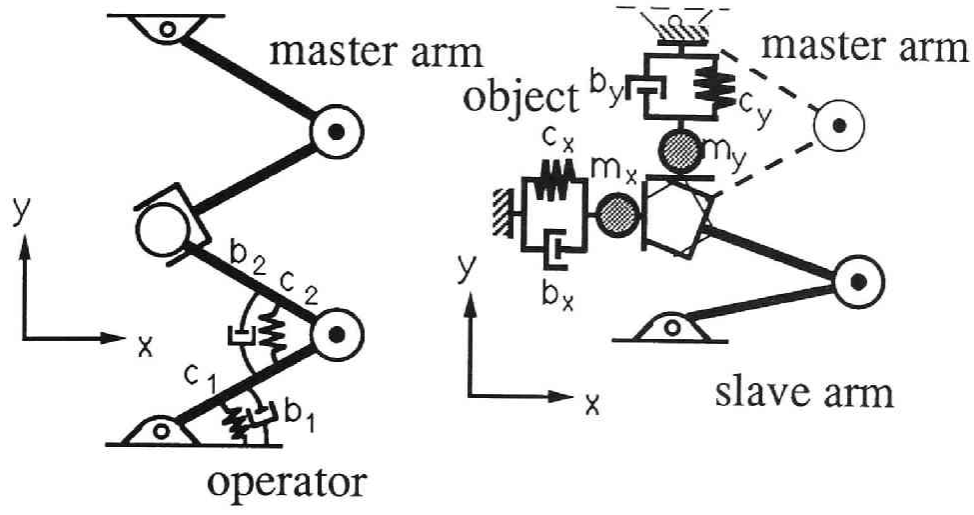

Figure 5.3: Initial postures of master and slave arms

The joint acceleration can be obtained from the hand tip acceleration by solving the inverse kinematics problem. But we are again faced with the singularity problem where the hand tip acceleration cannot be resolved uniquely into the joint accelerations. In this sense, realization of the control scheme eqs.(5.35) and (5.36) is rather difficult. One of the solutions would be to place the accelerometer at each joint and set a small intervenient inertia in the control scheme of eqs.(5.39) and (5.40).

5.5 Simulation

In this section, we show several numerical simulations in the multiple DOF case in order to confirm the validity of the proposed control schemes.

Isomorphic configuration arms of 2 DOF as shown in **Table 5.1** are used for simulation in a two dimensional plane. First, we set different initial postures for the master and slave arms as shown in **Fig.5.3** so that the control scheme for different configurations can be applied. The environment is a set of independent spring-damper-mass systems in x and y directions shown in **Fig.5.3**. The tip of the slave arm is just

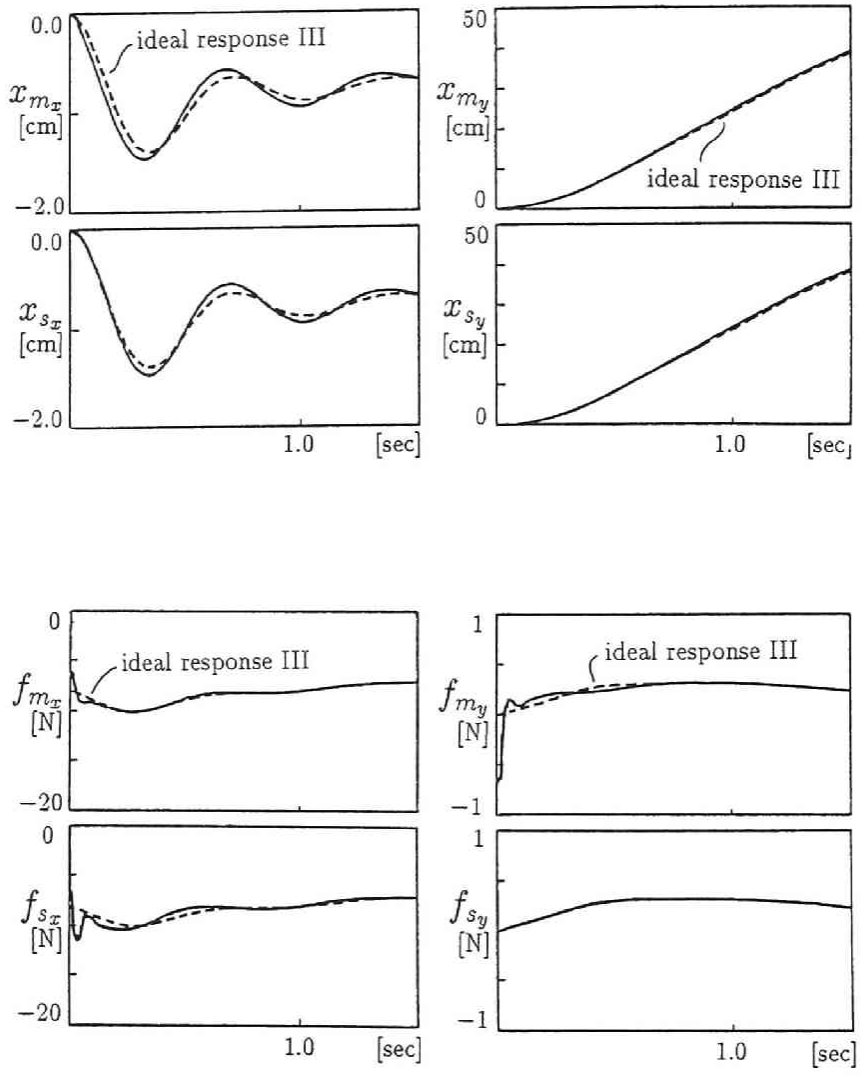

Figure 5.4: Simulation result by proposed control scheme for different configuration arms

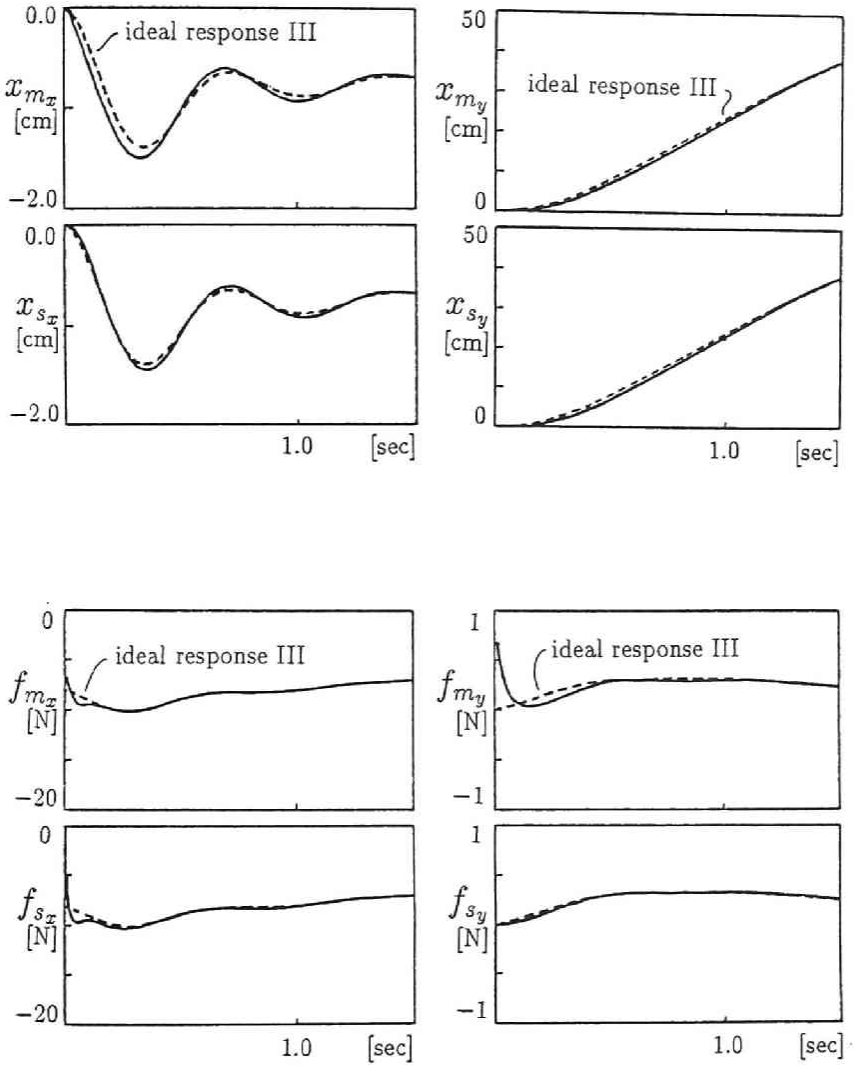

Figure 5.5: Simulation result by proposed control scheme for isomorphic configuration arms

attaching to the environment in the initial state. Parameters of the environment are given as follows:

$$m_x = 10[\text{kg}] \quad b_x = 50[\text{Ns/m}] \quad c_x = 1000[\text{N/m}]$$
$$m_y = 0[\text{kg}] \quad b_y = 1[\text{Ns/m}] \quad c_y = 0[\text{N/m}]$$

As the operator model, we also use a 2 DOF arm shown in **Fig.5.3**. At each joint of the operator, a rotational spring and a damper are attached. Parameters of the operator are also given in **Table 5.1**.

Fig.5.4 shows the responses of $\boldsymbol{x}_m$, $\boldsymbol{x}_s$, $\boldsymbol{f}_m$, and $\boldsymbol{f}_s$ under the control scheme of eqs.(5.15) and (5.16) when the operator continued to exert a constant joint torque which is equivalent to the hand tip force $[\ -10 \quad 1\ ]^T$[N] at the initial posture. Control parameters are $\boldsymbol{K}_1 = \text{diag}(20)[1/\text{s}]$, $\boldsymbol{K}_2 = \text{diag}(100)[1/\text{s}^2]$, and $\boldsymbol{K}_{mf} = \boldsymbol{K}_{sf} = \boldsymbol{0}$. We added identification errors of $+10\%$ and -10% to the dynamic parameters of master and slave arms respectively which are used in eqs.(5.15) and (5.16). The sampling time is 10[msec].

Next, in order to apply the control scheme for isomorphic configuration arms, we change the initial posture and base position of the master and slave arms so that the both arms coincide with the operator's initial posture. **Fig.5.5** shows the responses of the system under the control scheme of eqs.(5.35) and (5.36). The control parameters are $\boldsymbol{\Gamma}_1 = \text{diag}(20)[1/\text{s}]$, $\boldsymbol{\Gamma}_2 = \text{diag}(100)[1/\text{s}^2]$, and $\boldsymbol{\Gamma}_{mf} = \boldsymbol{\Gamma}_{sf} = \boldsymbol{0}$. These simulation results show the validity of the proposed control schemes.

5.6 Design Guide of Master-Slave Arms

In the previous sections, we focused on the design of control schemes for master-slave manipulators. But there are other aspects which should be considered, such as workspace and singularity points which depend on the arm design. In this section, we focus on the arm design for master-slave manipulators. Here, the arm design includes determination of the relative position between the operator and master arm, and between the master arm and slave arm[1]. The quality of arm design influences

[1]Relative position between the master and slave arms is not the physical distance between two arms but the distance with respect to the common reference base

considerably to the maneuverability of the system as well as the quality of control scheme does. As we designed each controller for different configuration arms and isomorphic configuration arms, the arm design and the controller design have a tight relation.

Certainly, dynamic property of the master and slave arms can be changed by the control schemes. If the ideal response III is achieved, the arm dynamics is completely canceled and it doesn't matter what kind of arm is used. However, the workspace and singularity points cannot be changed by the control scheme. The discussion of arm design is also applicable to the determination of intervenient impedance. One can set a suitable dynamic property of the intervenient impedance as a virtual arm based on the result of this section.

5.6.1 Design Guide of Master Arms from the Viewpoint of Manipulability for Operator

In this subsection, we discuss a design guide of master arms from the viewpoint of maneuverability for operators. Let the situation shown in **Fig.5.6** be considered, where the operator is manipulating the master arm by gripping the end tip of the master arm. In chapter 4, we have proposed a measure of master arm manipulability by extending the concept of dynamic manipulability measure as follows:

$$\widetilde{w}_d = \begin{cases} \sqrt{\det \widetilde{\boldsymbol{G}} \widetilde{\boldsymbol{G}}^T} & \text{if } \operatorname{rank}[\ \boldsymbol{J}_{op} \quad \boldsymbol{J}_m\ ] = n \\ 0 & \text{if } \operatorname{rank}[\ \boldsymbol{J}_{op} \quad \boldsymbol{J}_m\ ] < n \end{cases} \tag{5.41}$$

$$\widetilde{\boldsymbol{G}} \triangleq \boldsymbol{J}_m \boldsymbol{M}_m^{-1} \boldsymbol{J}_m^T (\boldsymbol{J}_{op} \boldsymbol{M}_{op}^{-1} \boldsymbol{J}_{op}^T + \boldsymbol{J}_m \boldsymbol{M}_m^{-1} \boldsymbol{J}_m^T)^{-1} \boldsymbol{J}_{op} \boldsymbol{M}_{op}^{-1} \boldsymbol{T}_{\tau_{op}}^{-1} \tag{5.42}$$

$$\boldsymbol{T}_{\tau_{op}} = \operatorname{diag}(1/\tau_{op_{i\,max}}) \tag{5.43}$$

where $\boldsymbol{J}_{op} \in \boldsymbol{R}^{n_{op} \times n_{op}}$, $\boldsymbol{M}_{op} \in \boldsymbol{R}^{n_{op} \times n_{op}}$ are the Jacobian matrix and inertia matrix of the operator respectively, regarding his arm as an n_{op} DOF robotic arm. And $\tau_{op_{i_{max}}}$ represents the maximum value of the i-th joint torque of the operator. The measure of $\widetilde{w}_d$ represents the

coordinates. Therefore, in the case of isomorphic configuration arms, the relative position is always zero although the slave arm is existing at remote site far from the master arm.

degree of realizable acceleration of the operator hand tip holding the master arm under the restriction of maximum joint torque. The value of $\widetilde{w}_d$ is proportional to the volume of ellipsoid in $\boldsymbol{R}^n$ which can be made from all the set of realizable acceleration vectors of the operator hand tip holding the master arm. Therefore if the value of $\widetilde{w}_d$ is large, the manipulability of master arm is high at that point.

However the measure of $\widetilde{w}_d$ evaluates only the volume of ellipsoid and it cannot evaluate such a directional property that the operator can move his arm easily in a certain direction but cannot in another direction. Then we proposed the following index which evaluates similarity between the dynamic manipulability ellipsoid of the operator holding the master arm and the dynamic manipulability ellipsoid of the operator holding nothing. This index is based on the idea that an ideal master arm is a massless arm so that the operator does not feel the existence of the master arm.

$$\rho_m = \frac{\mathrm{tr}(\widetilde{\boldsymbol{G}}\boldsymbol{G}_{op}^T)}{\mathrm{tr}(\boldsymbol{G}_{op}\boldsymbol{G}_{op}^T)} \tag{5.44}$$

$$\boldsymbol{G}_{op} \triangleq \boldsymbol{J}_{op}\boldsymbol{M}_{op}^{-1}\boldsymbol{T}_{\tau_{op}}^{-1} \tag{5.45}$$

where $\boldsymbol{G}_{op}$ corresponds to $\widetilde{\boldsymbol{G}}$ when $\boldsymbol{M}_m = \mathbf{o}$. The index value ρ_m is in the range of $0 < \rho_m < 1$ and it can be said that the more the index ρ_m is close to 1, the better manipulability the master arm has.

Here we will apply the proposed index to the evaluation of inertia term of the intervenient impedance. If we set $\boldsymbol{\Lambda} = \mathbf{o}(\widetilde{\boldsymbol{\Lambda}} = \mathbf{o})$ or sufficiently small in eqs.(5.20) and (5.21) (eqs.(5.39) and (5.40)), the total system behave as if only the intervenient impedance, which is described by eq.(5.18) (eq.(5.37)), exists between the operator and environment. Therefore, the above discussion can be applied to the evaluation of the inertia term of intervenient impedance by supposing that the operator holds the intervenient impedance as a virtual arm.

In the discussion of chapter 4, the best type of master arm is the isomorphic configuration type which just align with the operator's arm as shown in **Fig.5.7(a)**. This result can be straightforwardly applied to the case of intervenient impedance. This type of intervenient impedance can be realized easily in the case of isomorphic configuration arms.

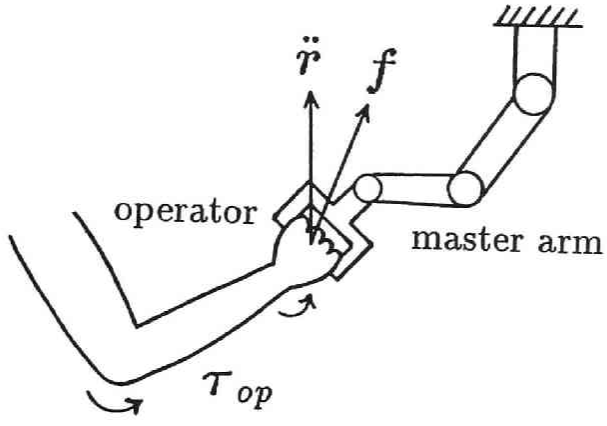

Figure 5.6: Operator arm holding a master arm

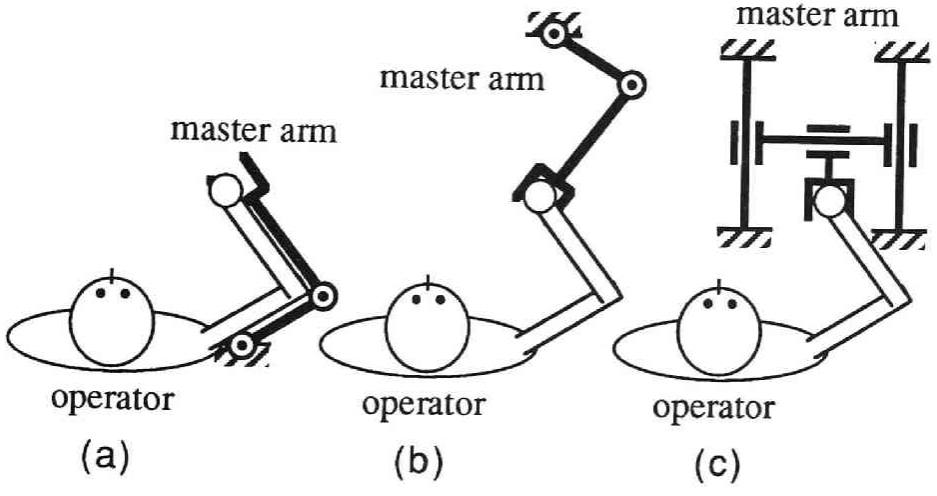

Figure 5.7: Variation of operator and master arm

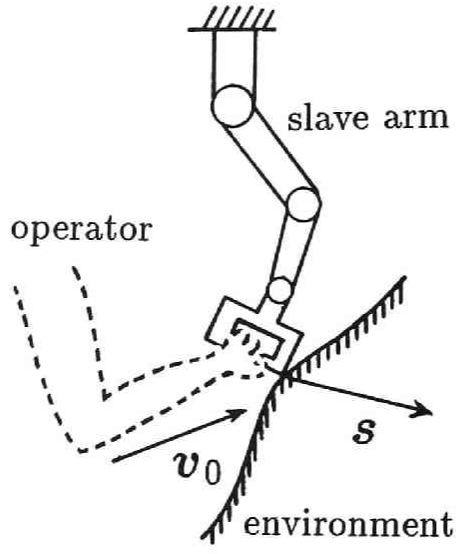

Figure 5.8: Slave arm interacting with environment

5.6.2 Design Guide of Slave Arms from the Viewpoint of Interaction with Environments

Next we discuss a design guide of slave arms from the viewpoint of the interaction with environments. First, suppose the situation where the slave arm runs into the environment. The relation between the impulse and hand tip velocity is given by

$$\boldsymbol{v} - \boldsymbol{v}_0 = -\boldsymbol{W}_s \boldsymbol{s} \tag{5.46}$$

$$\boldsymbol{W}_s \triangleq \boldsymbol{J}_s \boldsymbol{M}_s^{-1} \boldsymbol{J}_s^T \tag{5.47}$$

where $\boldsymbol{v}_0$ is the approaching velocity of the hand tip and $\boldsymbol{v}$ is the rebound velocity from the environment. The impulse that the slave arm applies to the environment is represented by $\boldsymbol{s}$. If the collision is perfectly non-elastic and $\boldsymbol{W}_s$ is non-singular, the impulse $\boldsymbol{s}$ can be obtained from $\boldsymbol{v}_0$.

$$\boldsymbol{s} = \boldsymbol{W}_s^{-1} \boldsymbol{v}_0 \tag{5.48}$$

When the arm is in singularity point, $\boldsymbol{W}_s^{-1}$ does not exist. This state is a sort of statically indeterminate situations and $\boldsymbol{s}$ cannot be obtained

from only $\boldsymbol{v}_0$. Next, let the situation shown in **Fig.5.8** be considered where the operator holds the slave arm directly and the slave arm collides with the environment. In this case, the generalized inverse inertia matrix is given as follows:

$$\widetilde{\boldsymbol{W}} \triangleq \boldsymbol{W}_{op}(\boldsymbol{W}_{op} + \boldsymbol{W}_s)^{-1}\boldsymbol{W}_s \tag{5.49}$$

$$\boldsymbol{W}_{op} \triangleq \boldsymbol{J}_{op}\boldsymbol{M}_{op}^{-1}\boldsymbol{J}_{op}^T \tag{5.50}$$

In the same way as in the previous subsection, if the shape of ellipsoid made from $\widetilde{\boldsymbol{W}}$ is similar to the ellipsoid made from $\boldsymbol{W}_{op}$, the impulse against the environment and the direction of rebound after the collision would be similar to the case when the operator arm itself collides with the environment. Then the operator's strange feel could be minimized even at the unexpected collision.

In order to evaluate the similarity of the ellipsoid, we can use the same equation as eq.(5.44).

$$\rho_s = \frac{\mathrm{tr}(\widetilde{\boldsymbol{W}}\boldsymbol{W}_{op}^T)}{\mathrm{tr}(\boldsymbol{W}_{op}\boldsymbol{W}_{op}^T)} \tag{5.51}$$

The index value, ρ_s is also in the range of $0 < \rho_s < 1$, and the more ρ_s is close to 1, the better the slave arm is.

In the above discussion, we supposed that the operator holds the slave arm directly. Of course, the operator cannot hold the slave arm directly which exists in the remote site. But these discussion can also be applied to the determination of intervenient impedances by supposing that the virtual arm collides with the environment and the operator holds this virtual arm directly. Similarly the isomorphic configuration arm of exoskeleton type which aligns with the operator arm shows a good evaluation of ρ_s.

In the multiple DOF case, it is difficult to choose many parameters of the intervenient impedance appropriately, whereas one DOF intervenient impedance has only three parameters. The indices ρ_m and ρ_s shown above would be design guides to choose the inertia term of the intervenient impedance.

5.6.3 Design Guide from the Viewpoint of Workspace

Next, we discuss a design guide of arms from the viewpoint of workspace. Master-slave systems are composed by the operator, master arm and slave arm. Therefore, workspace of the system is determined by the intersection of these workspace.

$$\Psi_{mss} = \Psi_{op} \cap \Psi_m \cap \Psi_s \tag{5.52}$$

where Ψ_{mss}, Ψ_{op}, Ψ_m, and Ψ_s represent the workspaces of master-slave system, operator, master arm, and slave arm respectively. Obviously, expansion of the workspace of only one arm does not affect efficiently to the expansion of the workspace of the total system. Of course, the relative position between the operator and the master arm and between the master and slave arms affect to Ψ_{mss}. When we want to use fully the original workspace of the operator, the master and slave arms must have a wider workspace than that of the operator's.

In the same way, singularity points of master-slave systems are given by

$$\Phi_{mss} = \Phi_{op} \cup \Phi_m \cup \Phi_s \tag{5.53}$$

where Φ_{mss} denotes all the set of singularity points of the master-slave system. And Φ_{op}, Φ_m, and Φ_s denote all the set of singularity points of operator, master arm, and slave arm in Ψ_{mss}. Among the singularity points of the system, serious ones are singularity points of the master and slave arms. At these points, the operator cannot move his arm in all directions while he can move in all direction originally. This singularity point may spoil the maneuverability for the operator.

5.6.4 Design Examples of Master-Slave Arms

Considering the above discussions, we designed experimental master-slave arms shown in **Fig.5.9**. Both the master and slave arms have 3 DOF and they have isomorphic configurations. Its arm configurations were determined by projecting the human arm configuration onto a horizontal plane.

There are several variations of relative position between the operator and master arm, and between the master arm and slave arm. One way

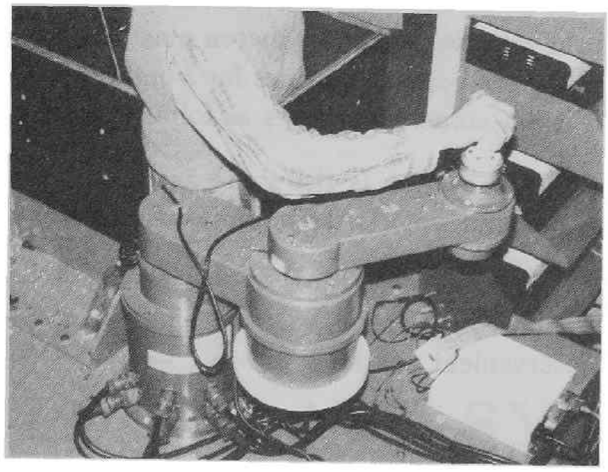

Master Arm

Slave Arm

Figure 5.9: Experimental arms

is that the operator holds the master arm so that his arm is just on the master arm and the relative position between master arm slave arms set to zero. In this case, the control schemes for isomorphic configurations can be used and it has some advantages as follows:

- Workspace of the system is the same as the original workspace of the operator and singularity points of the system are also the same as the operator's ones.
- The index values , ρ_m and ρ_s, can be made large by setting appropriate intervenient virtual arm.

5.7 Conclusion

The main results of this chapter can be summarized as follows:

- The concept of ideal kinesthetic coupling has been extended to the multiple DOF case. Control schemes realizing the ideal responses have been proposed for two cases; different configurations and isomorphic configurations.
- The validity of the proposed control schemes has been confirmed by simulations.
- Design guides of the master and slave arms have been discussed from several aspects such as the manipulability for the operator, interaction with the environments, and the workspace. These guides can also be used for determining the inertia parameters of the intervenient impedances.

Chapter 6

EXPERIMENTAL RESULTS BY A MASTER-SLAVE SYSTEM

6.1 Introduction

In this chapter, we discuss a prototype master-slave system which was built for experiments, and show experimental results obtained by using this system. The master and slave arms are 3 DOF planar type manipulators with direct-drive motors at each joint. They were designed according to the design guides discussed in chapters 4 and 5.

Experiments were done for a one DOF system by using only one joint of the arms. Validity of the control schemes proposed in chapter 3 for realizing the ideal responses is examined experimentally by comparing to several conventional control schemes.

6.2 Design of Experimental Arm

6.2.1 Policy of Arm Design

The following policies are adopted for designing the master and slave arms.

(i) Direct-drive motors are used because of their good controllability of torque;

(ii) Planar 3 DOF arms (2 DOF for position, 1 DOF for orientation) are selected as the master and slave arms to simplify the mechanism;

(iii) Configurations of master and slave arms are isomorphic so that they can be used as an exoskeleton type manipulator;

(iv) Motor size must be chosen so that the system can perform tasks with fast and quick motions by the operator.

If we follow the policy (iv), total weight of the arm may become large. However, we do not care so much about making the arm lighter, since the dynamics compensation is possible by control.

6.2.2 Choice of the Motor Size

According to the policy (iv), we first estimate the performance of human arms. Human arm is modeled as a planar 3 DOF arm as shown in **Fig.6.1**. Parameters of the estimated model are shown in **Table 6.1**. For estimating the arm model, we just set m_1 and m_2 from the roughly measured values of several men. Inertia and location of the center of gravity of each link are determined by assuming that mass of each link is uniformly distributed. The maximum torque at each joint is about half of the actually measured value. **Fig.6.2** shows the dynamic manipulability ellipsoid and dynamic manipulability measure[88] obtained from the parameters in **Table 6.1**. From **Fig.6.2**, maximum acceleration of the hand tip is about 100m/s^2. We actually measured the maximum acceleration by holding an accelerometer and it was $100 \sim 170\text{m/s}^2$. Considering that the estimated maximum torque is about half of the measured value, it shows the validity of the estimated model in **Table 6.1**.

According to the policy (iii), the configurations of the experimental arms are determined so that they have the same configuration as that of the human arm model in **Table 6.1**. We use the frameless motors (built-in DD series) produced by SHIN MEIWA Industry Co. Ltd. This series has a variety of sizes and have a good linearity of torque-current relation.

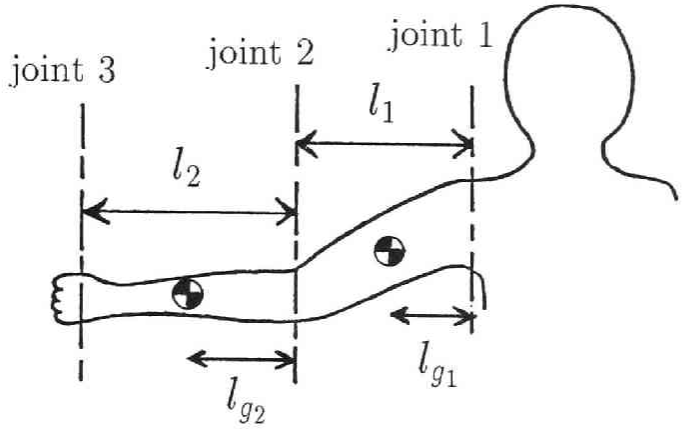

Figure 6.1: Operator arm model in a horizontal plane

Table 6.1: Parameters of the operator arm model

	link 1	link 2	wrist
l_i [m]	0.25	0.30	—
l_{g_i} [m]	0.125	0.15	—
m_i [kg]	1.5	1.5	—
$\widehat{I}_i$ [kgm^2]	0.0078	0.0113	—
$\tau_{i_{max}}$ [Nm]	15	10	6

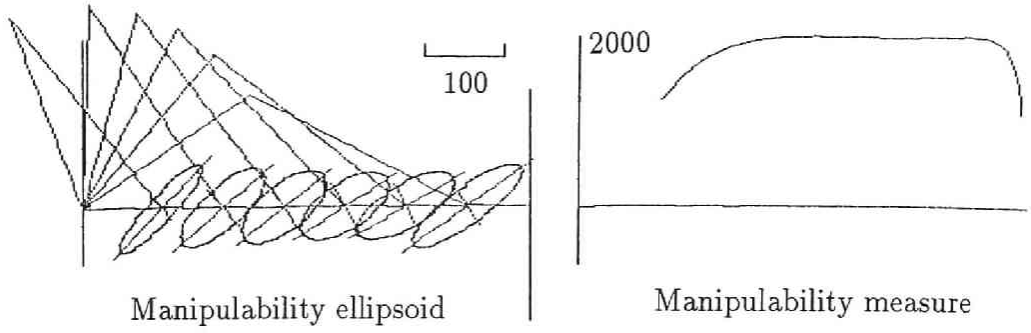

Figure 6.2: Dynamic manipulability of human arm

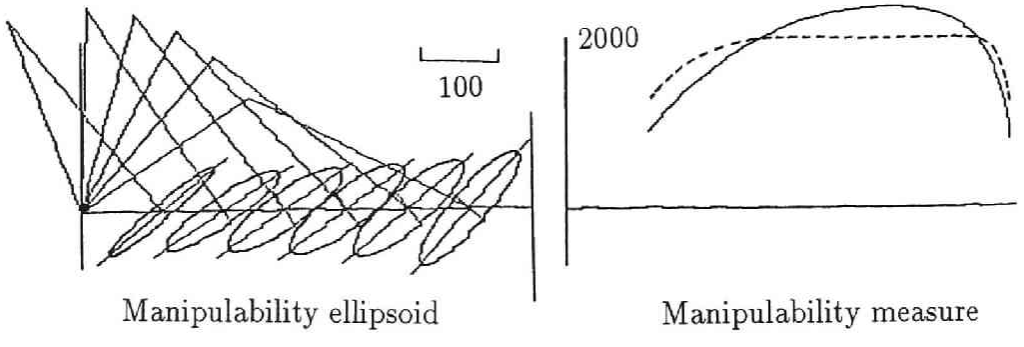

Figure 6.3: Dynamic manipulability of the designed arm

Table 6.2: Specifications of the motors

	joint 1	joint 2	joint 3
motor type	B18-64	B18-38	B09-25
instantaneous max. torque (Nm)	109	62	5.3
rating torque (Nm)	36	21	1.9
torque ripple*1 (%)	0.3	0.3	0.3
max. rotational speed (rpm)	120	120	500
rotor inertia (kgm^2)	2.5×10^{-3}	1.5×10^{-3}	7.8×10^{-5}
weight*2 (kg)	8.3	5.4	1.0

*1: ripple of cogging torque *2: in frameless case

In order to cope with quick motions of human, it is desirable that the dynamic manipulability of the designed arm coincides with that of the operator as close as possible. We will choose the motor size of each joint so that the dynamic manipulability becomes similar to that in **Fig.6.2**. First, the motor whose maximum torque is around 6[Nm] is chosen for the wrist joint (joint 3). For elbow and shoulder joints (joints 1 and 2), however, the maximum acceleration of the tip would be smaller than that of human, even if the motors which have the same maximum torque as that in **Table 6.1** were used, because the weight of arm may be much heavier than human arm. **Fig.6.3** shows the dynamic manipulability of the designed arm using appropriate motors where mass and inertia of the wrist motor, the mass and inertia of each link estimated from the material (aluminum), and the mass and inertia of motors at joints 1 and 2 corresponding to the chosen motor size were taken into account. Specifications of the chosen motors are shown in **Table 6.2**.

Fig.6.4 shows the dimensions of the designed arms and **Table 6.3** shows their specifications. Although the basic design is used for both the master and slave arms, we changed the link assignments upside-down between the master and slave arms so that the operator can grip the tip of master arm and the slave arm can easily reach objects on the base table.

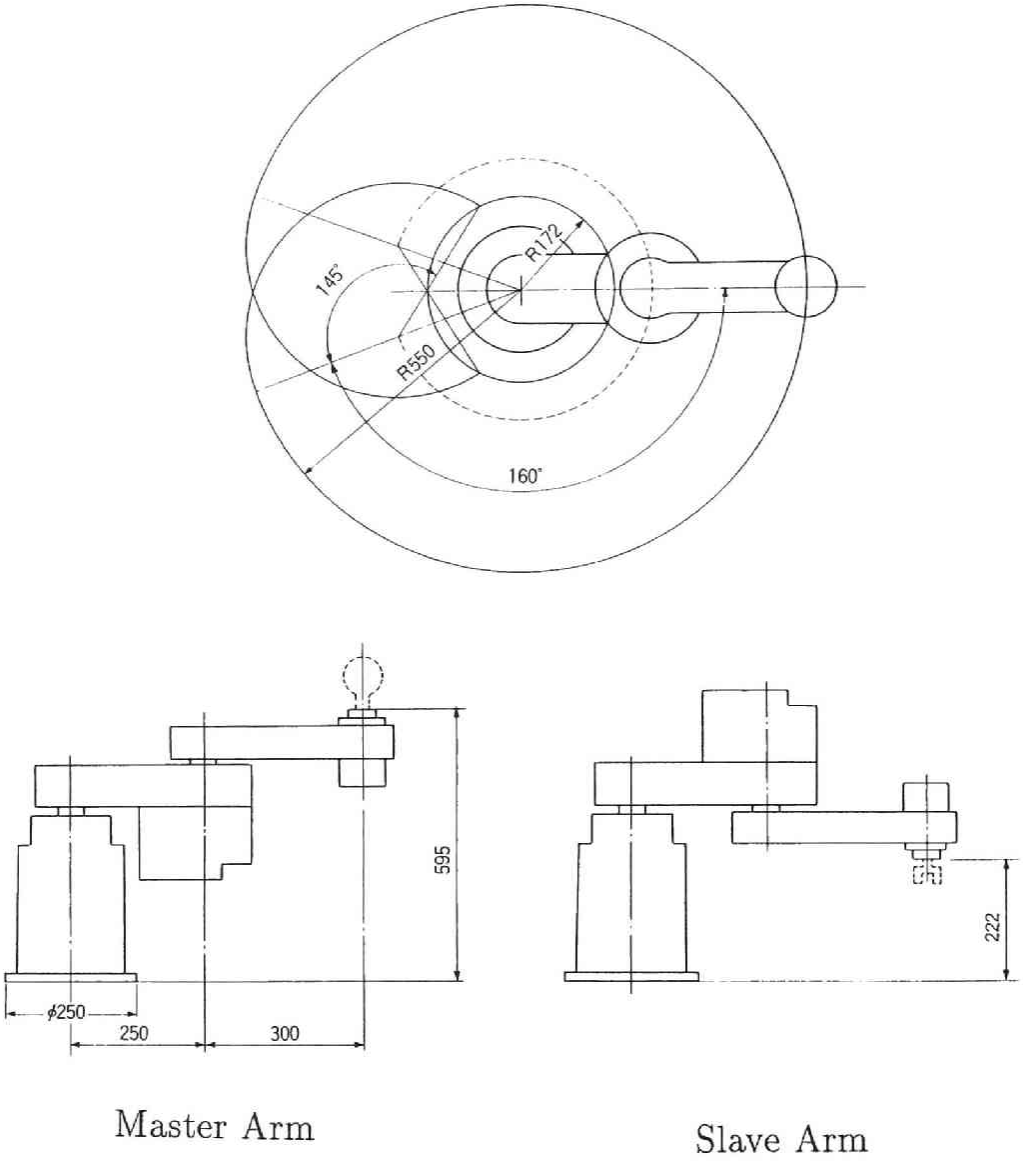

Figure 6.4: Experimental master and slave arms

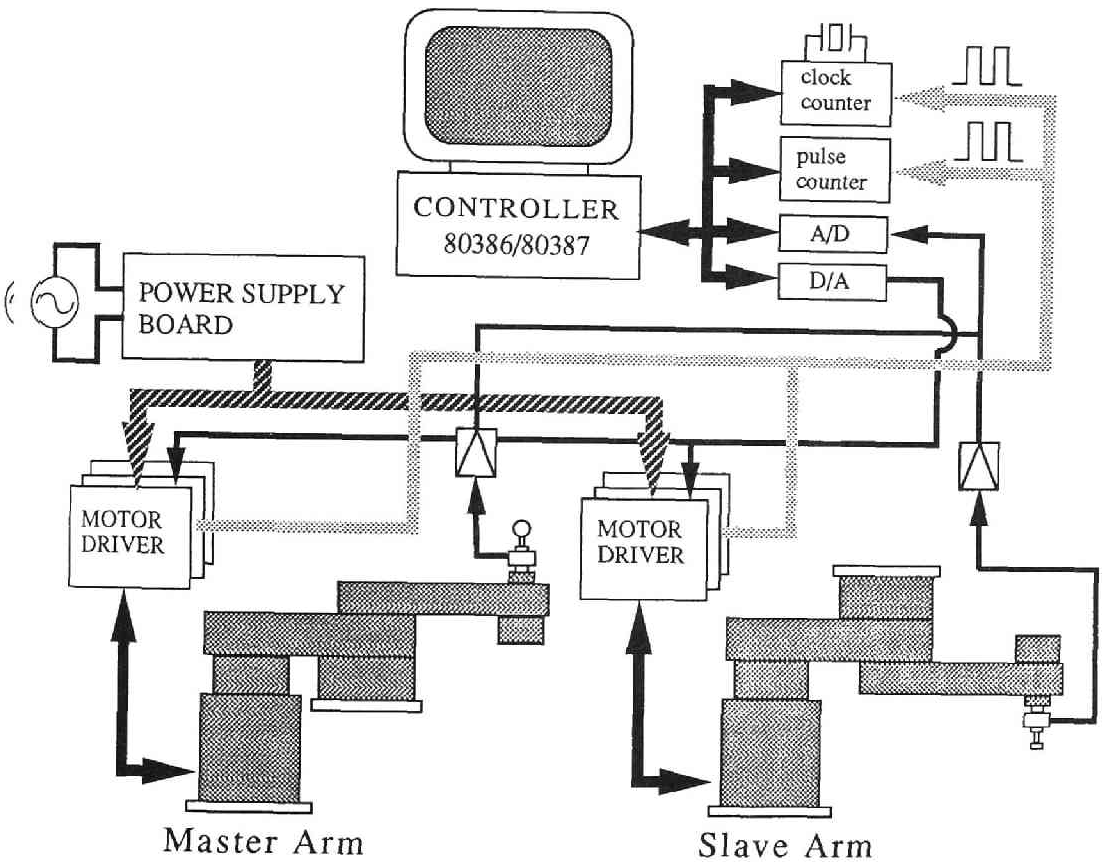

Figure 6.5: Schematic of experimental master-slave system "RATSU-WAN"

Table 6.3: Specifications of the designed DD-arm

DOF	3	
link length	link 1	250mm
	link 2	300mm
motion range	joint 1	±160°
	joint 2	±160°
	joint 3	no restriction
resolution	joint 1	2.7arc sec
	joint 2	2.7arc sec
	joint 3	64.8arc sec
maximum velocity at the tip		9m/sec
maximum payload		2kg

6.3 Experiment

6.3.1 Experimental System

We constructed a master-slave system using the two DD-arms discussed above. **Figs.6.5** and **6.6** show the schematic and overview of the experimental system respectively. We name this experimental master-slave system "RATSU-WAN" that means outstanding ability in Japanese. Each motor is independently driven by a motor driver. Electric power is supplied to each motor driver from the power-supply board in which an emergency brake and circuit breakers are built. Controller is a personal computer with 32-bit 80386/80387 CPU (20MHz), and the torque command is sent to each motor driver through a D/A converter. Encoder pulse signal of each joint can be obtained from an output terminal of each motor driver. These pulse signals are sent to a pulse counter board which is built in the personal computer.

Velocity information at each joint is obtained by combining the following two methods in order to get sufficient resolution in both low velocity region and high velocity region; counting the number of clock pulses during the interval of the encoder pulses and taking the difference of encoder pulse counter in each sampling period. To make the

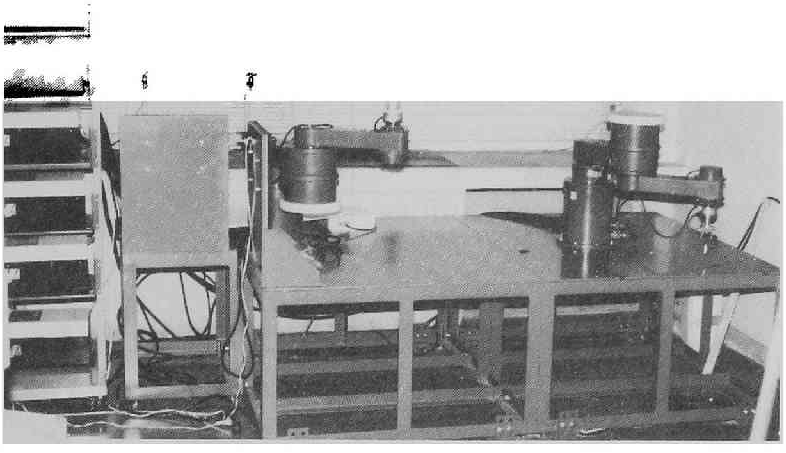

Figure 6.6: Overview of experimental master-slave system "RATSU-WAN"

deference operation exact, we set the sampling period exactly constant by using a timer interrupt procedure.

A six-axis force/torque sensor produced by OMRON Co. Ltd. is attached to the tip of each arm. Its specification is shown in **Table 6.4**. Force/torque signals are amplified and sent to the personal computer through an A/D converter.

6.3.2 Tasks in the Experiment

We experiment with a one DOF system where only the elbow joint (joint 2) of each arm is used. The shoulder joint is mechanically fixed. The wrist joint is not fixed so that the operator can always grip the arm tip firmly. **Fig.6.7** shows the experimental set up of one DOF system.

The following three tasks are used in the experiment.

[Task 1]

There is no object at the slave side. The operator maneuvers the system so that the tip of the slave arm follows a lighted LED on the table as shown in **Fig.6.8**. There are three LEDs on the table and the lighted one is changed periodically.

Table 6.4: Specifications of the force/torque sensor

rating load	F_x, F_y, F_z	10kgf
	M_x, M_y, M_z	80kgfcm
linearity		±0.3%
hysteresis		±0.3%
temperature drifting		±0.2%/°C
resolution		±0.1%
coupling		less than ±10%
allowable over-load		500%

[Task 2]

An aluminum plate is firmly fixed on the table by cramps as shown in **Fig.6.9**. The operator makes the slave arm collide with the plate and push the plate. Since the tip of the slave arm is also made of aluminum, the contact becomes the most critical one, "hard contact"[33].

[Task 3]

A sponge is set at the slave side as shown in **Fig.6.10**. The operator push the sponge through the system and examines how well he can feel the impedance of the sponge.

6.3.3 Control Schemes

We tried three conventional control schemes; symmetric position servo type, force reflection type, and force reflecting servo type. These control schemes and the values of gains are as follows:

[Symmetric position servo type]

$$\begin{aligned} \tau_m &= K_v(\dot{x}_s - \dot{x}_m) + K_p(x_s - x_m) \\ \tau_s &= K_v(\dot{x}_m - \dot{x}_s) + K_p(x_m - x_s) \end{aligned}$$

$$K_v = 163.5[\mathrm{Ns/m}], \quad K_p = 1406.1[\mathrm{N/m}]$$

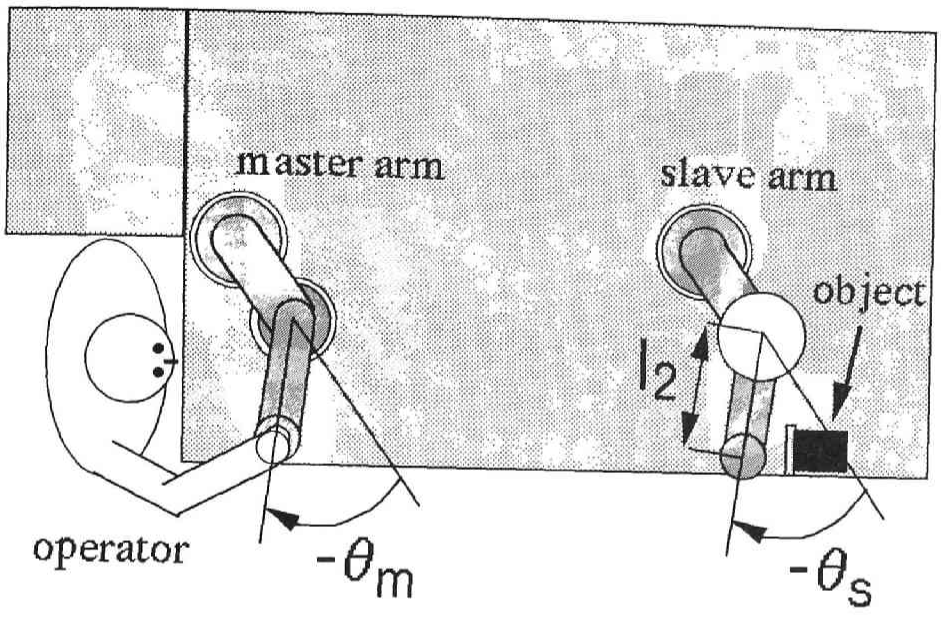

Figure 6.7: One DOF experimental system

[Force reflection type]

$$\begin{aligned} \tau_m &= f_s \\ \tau_s &= K_v(\dot{x}_m - \dot{x}_s) + K_p(x_m - x_s) \end{aligned}$$

$$K_v = 163.5[\mathrm{Ns/m}], \quad K_p = 1406.1[\mathrm{N/m}]$$

[Force reflecting servo type]

$$\begin{aligned} \tau_m &= f_s + K_f(f_s - f_m) \\ \tau_s &= K_v(\dot{x}_m - \dot{x}_s) + K_p(x_m - x_s) \end{aligned}$$

$$K_v = 163.5[\mathrm{Ns/m}], \quad K_p = 1406.1[\mathrm{N/m}], \quad K_f = 0.3$$

where $x_m = l_2 \times \theta_m$ and $x_s = l_2 \times \theta_s$ are equivalent hand tip displacements of the master and slave arms, θ_m and θ_s denote the joint angles, and $l_2 = 0.3[\mathrm{m}]$ is the link length. The equivalent driving forces at the tip τ_m and τ_s are finally converted to the joint torques.

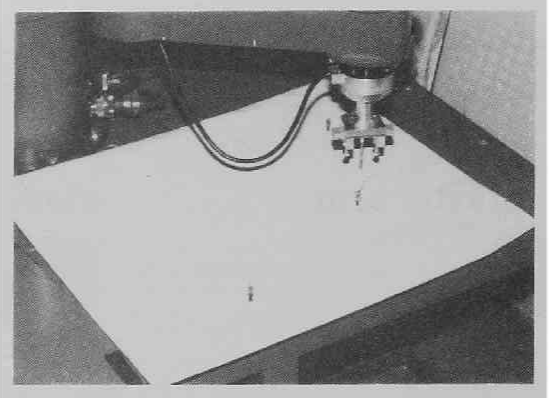

Figure 6.8: Task 1

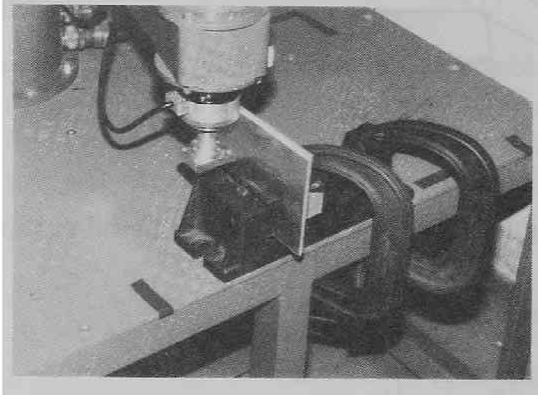

Figure 6.9: Task 2

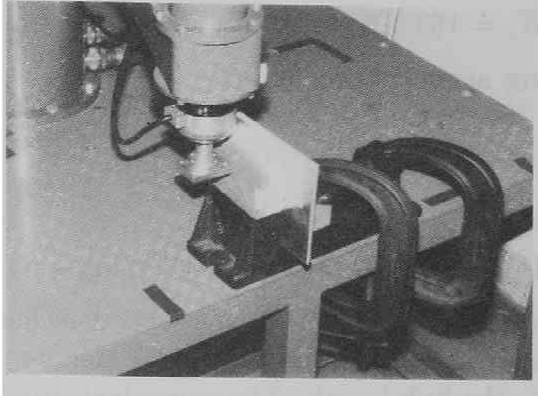

Figure 6.10: Task 3

The proposed control scheme in chapter 3 can be represented by the following form:

[Proposed type]

$$\begin{aligned} \tau_m &= \kappa\bar{M}\ddot{x}_{ms} + K_v(\dot{x}_s - \dot{x}_m) + K_p(x_s - x_m) + f_{ms} \\ \tau_s &= \kappa\bar{M}\ddot{x}_{ms} + K_v(\dot{x}_m - \dot{x}_s) + K_p(x_m - x_s) - f_{ms} \end{aligned}$$

$$K_v = 163.5[\mathrm{Ns/m}], \quad K_p = 1406.1[\mathrm{N/m}]$$

where $\bar{M}$ is the equivalent mass obtained from inertia around the joint 2 and its identified value is 5.48[kg], and κ denotes the coefficient of dynamics compensation. The above control scheme corresponds to eqs.(3.22) and (3.23) when $m_m = m_s = \bar{M}$, $k_1 = 2K_v/\bar{M}$, $k_2 = 2K_p/\bar{M}$, $b_m = b_s = 0$, $\lambda = 0$, $k_{mf} = k_{sf} = 0$, $\widehat{m} = 2(\bar{M} - \kappa\bar{M})$ and $\widehat{b} = \widehat{c} = 0$. And it can realize the ideal response I.

When $\kappa = 1.0$, the above scheme cancels all of the arm dynamics and it realizes the ideal response III. When $0 \leq \kappa < 1.0$, the intervenient inertia $\widehat{m} = 2(\bar{M} - \kappa\bar{M})$ is realized and the system response becomes the ideal response I.

Acceleration signals of the both arms are obtained by numerically differentiating the velocity signals. The differentiated data is pass trough a digital filter whose cut-off frequency is 19.8Hz. As discussed in subsection 3.2.4, it is impossible to set $\kappa = 1.0$ because the acceleration is measured at the joint. Theoretically, we can set κ as close to 1.0 as we want. However, $\kappa = 0.8$ was the actual upper bound to keep the good responses due to the delay of acceleration signals. Therefore, we examined three cases when $\kappa = 0.0$, $\kappa = 0.5$, and $\kappa = 0.8$ in the experiments. Especially when $\kappa = 0.5$, the intervenient inertia becomes just the same as that of the original arm, and the apparent inertia for the operator becomes the same value as that in case of the force reflection type. Sampling time was 1.68msec for all cases.

6.3.4 Experimental Results

From **Figs.6.11** through **6.22** show experimental results for three tasks under the conventional three control schemes and the proposed schemes with different values of κ.

In **Task 1**, as shown in **Fig.6.11**, there are some over-shoot of the slave arm position response with respect to that of the master when the conventional schemes are applied. In this task, the force of the master side becomes just the force error because no force is applied at the slave side. But small force at the slave side can be seen due to the inertia of the tip part of the slave arm. In **Fig.6.13**, we can see the difference of the maximum force at the master side among the three conventional schemes. The operator feels large inertia when the symmetric position servo type is applied and he can maneuver the system easier when force reflection type and force reflecting servo type are applied.

In the case of proposed schemes, the position responses of the master and slave arms shown in **Fig.6.12** are almost equal, since they satisfy the condition of the ideal response I irrespective of the values of κ. When $\kappa = 0.0$ in the proposed control scheme, the operator feels the intervened inertia which has twice amount of inertia of the original arm. And the apparent inertia becomes very heavy as well as the case of symmetric position servo. However, by canceling the dynamics of the two arms by setting $\kappa = 0.5$ and $\kappa = 0.8$, the force at the master side becomes smaller and the system response becomes near the ideal response III.

In **Task 2**, there is more remarkable difference between the conventional control schemes and the proposed scheme. In every case of the conventional schemes, large position error appears when the slave makes contact with the object. Since all of the conventional schemes generate the force of the slave arm based on the position errors between the master and slave, it is necessary to make the feedback gain infinitely large in order to make the position error zero. Practically, however, large gains may cause instability of the system. Especially in the case of force reflecting servo, the force response sometimes became oscillatory and the system became nearly unstable.

In all the cases of proposed schemes, the position error between the master and slave arms is almost zero even when the slave arm collide with the object, because they satisfy the condition of the ideal response I. The operator can feel a "rigid wall" realistically by the proposed schemes. Theoretically speaking, the force error at the contact state becomes zero in all the cases when $\kappa = 0.0$, $\kappa = 0.5$, and $\kappa = 0.8$, because the system has no acceleration under the constraint by the

object. However, the actual force response in **Fig.6.18** has large error even in the steady contact state. This kind of error also occurs in the case of conventional schemes as shown in **Fig.6.17**. These force errors are caused by insufficient adjustment of the motor drivers. We believe that these force errors will be solved by adjusting the motor drivers properly.

It should be noted that, even by the conventional schemes, the operator can perceive the instant of the contact from the sound and impulse of the contact reflected to the master arm. It means that there is a possibility to make the operator feel the the object more realistically by modifying the reflected force signal and by providing other information such as sound. This point should be studied in the future.

In **Task 3**, the operator exerted force periodically against the sponge. And we checked how realistically the dynamic response of the object is reflected to the operator. In the case of symmetric position servo, dynamic property of the sponge is completely hidden in the dynamics of the master and slave arms, and the operator cannot feel the characteristic of the sponge. This fact can be seen from **Fig.6.21** where the phase of force responses is different between the master and slave. The responses are improved by the force reflection type and improved more by the force reflecting servo type. However, the difference of force responses is still large due to the operator's motion in high frequency.

On the other hand, when $\kappa = 0.0$ in the proposed control scheme, the operator cannot feel the object realistically as well as the symmetric position servo type, since both of the arm inertia intervene between the operator and object. However, when $\kappa = 0.5$ and $\kappa = 0.8$, the difference of force response becomes smaller due to the cancellation of the dynamics of two arms. Especially when $\kappa = 0.8$, the operator could feel a delicate instant of contact with the sponge.

6.4 Conclusion

The main results of this chapter are summarized as follows:

- We designed experimental 3 DOF arms with direct-drive motors based on the design guides shown in chapters 4 and 5.

- A master-slave system was constructed using the designed arms and a 32-bit personal computer.
- In the experiment, the control schemes proposed in chapter 3 for realizing the ideal responses were compared to the conventional control schemes in the one DOF case. The validity of the proposed control schemes was confirmed experimentally.

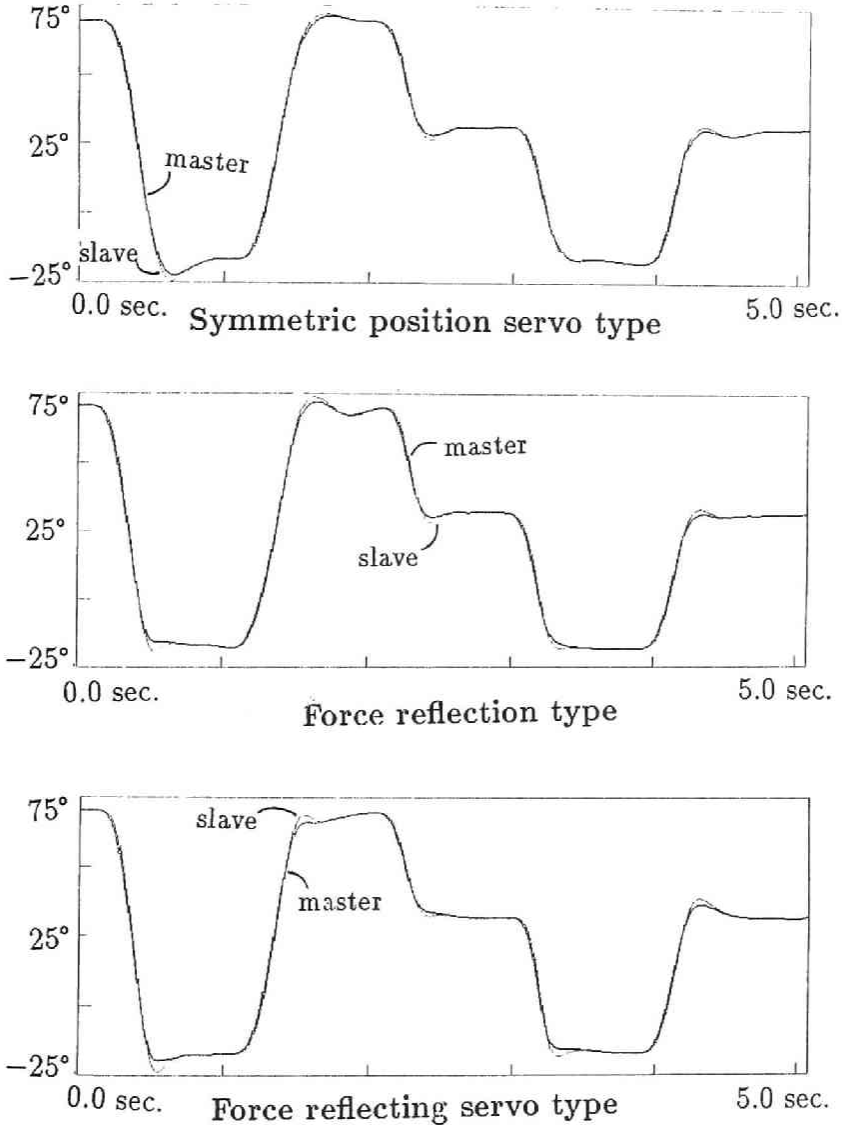

Figure 6.11: Experimental results: Position responses by the conventional schemes in Task 1

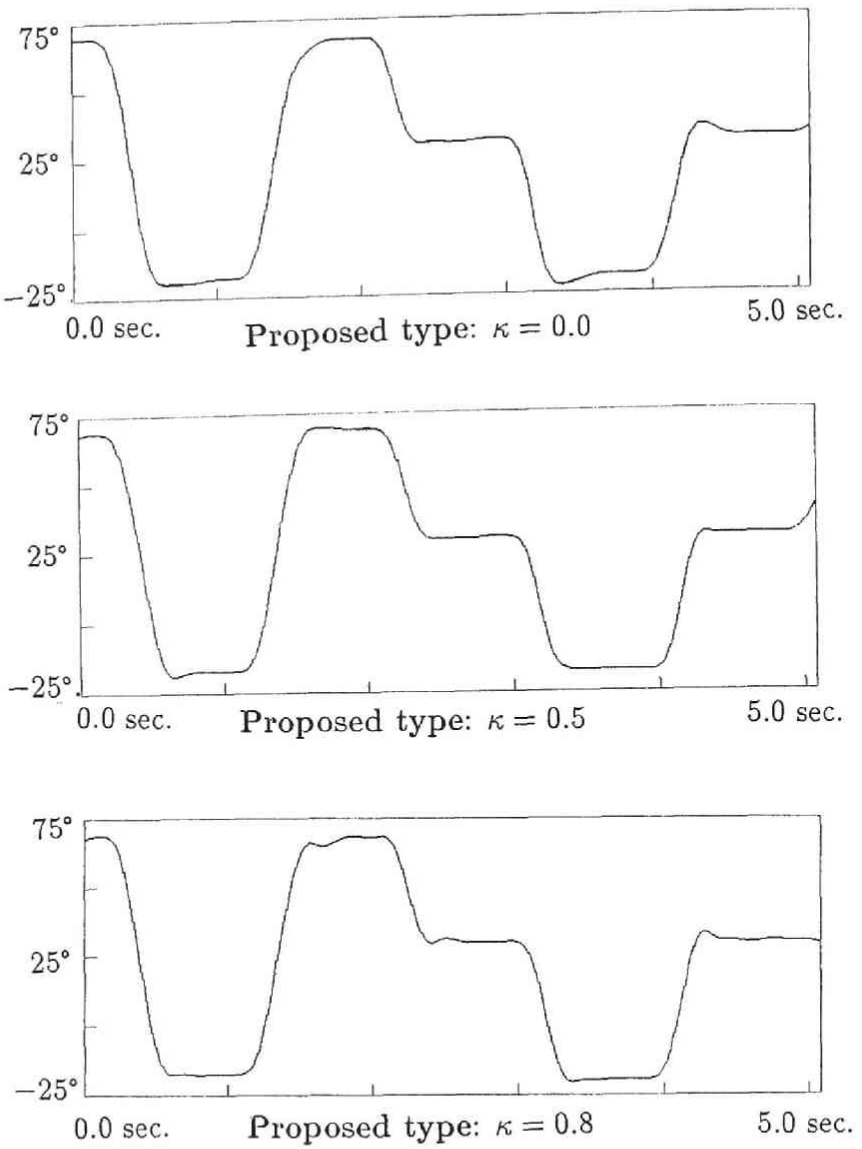

Figure 6.12: Experimental results: Position responses by the proposed schemes in Task 1

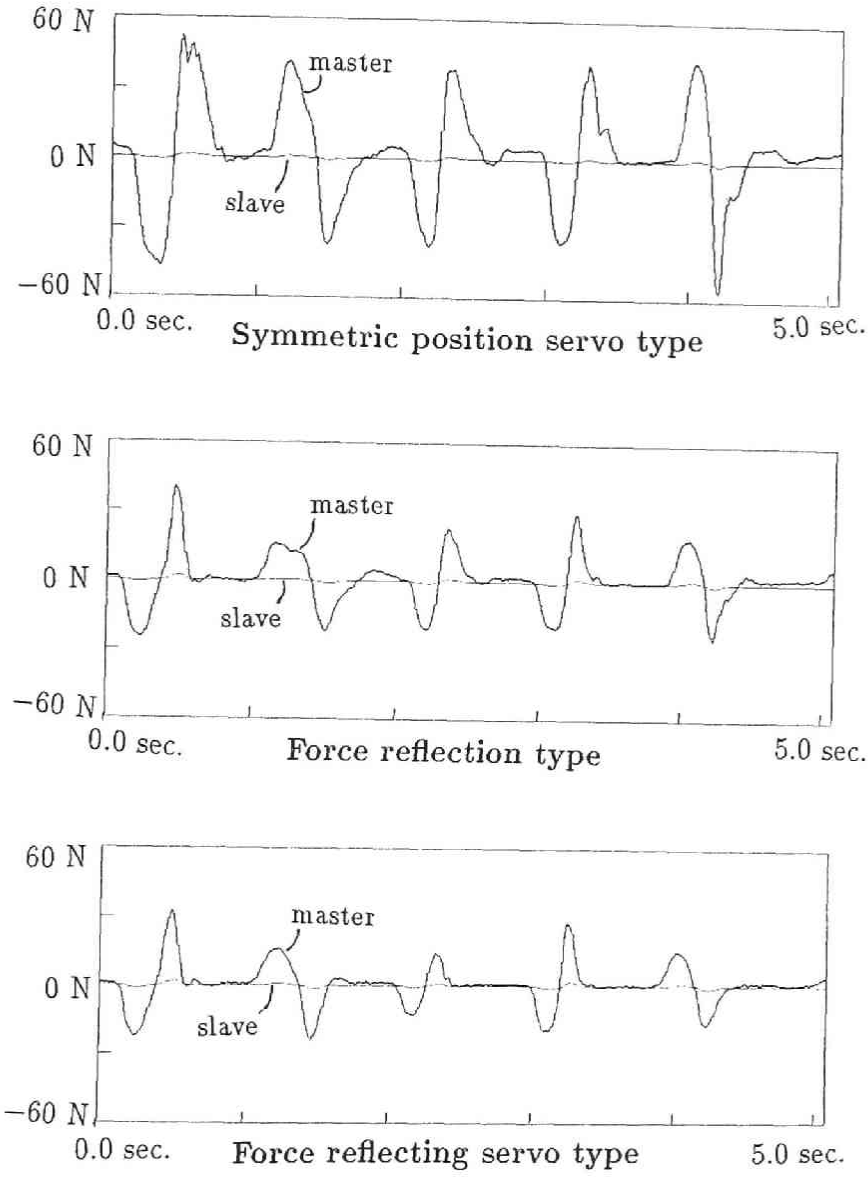

Figure 6.13: Experimental results: Force responses by the conventional schemes in Task 1

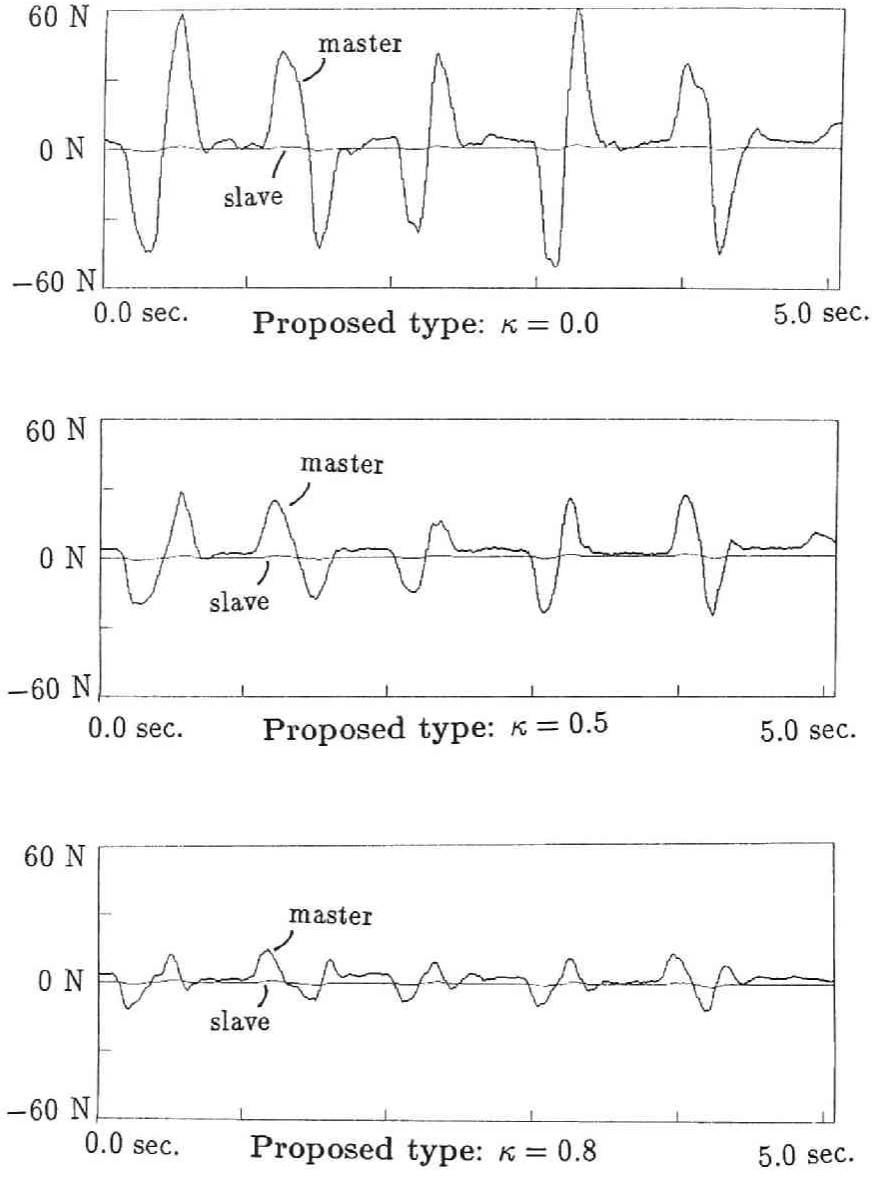

Figure 6.14: Experimental results: Force responses by the proposed schemes in Task 1

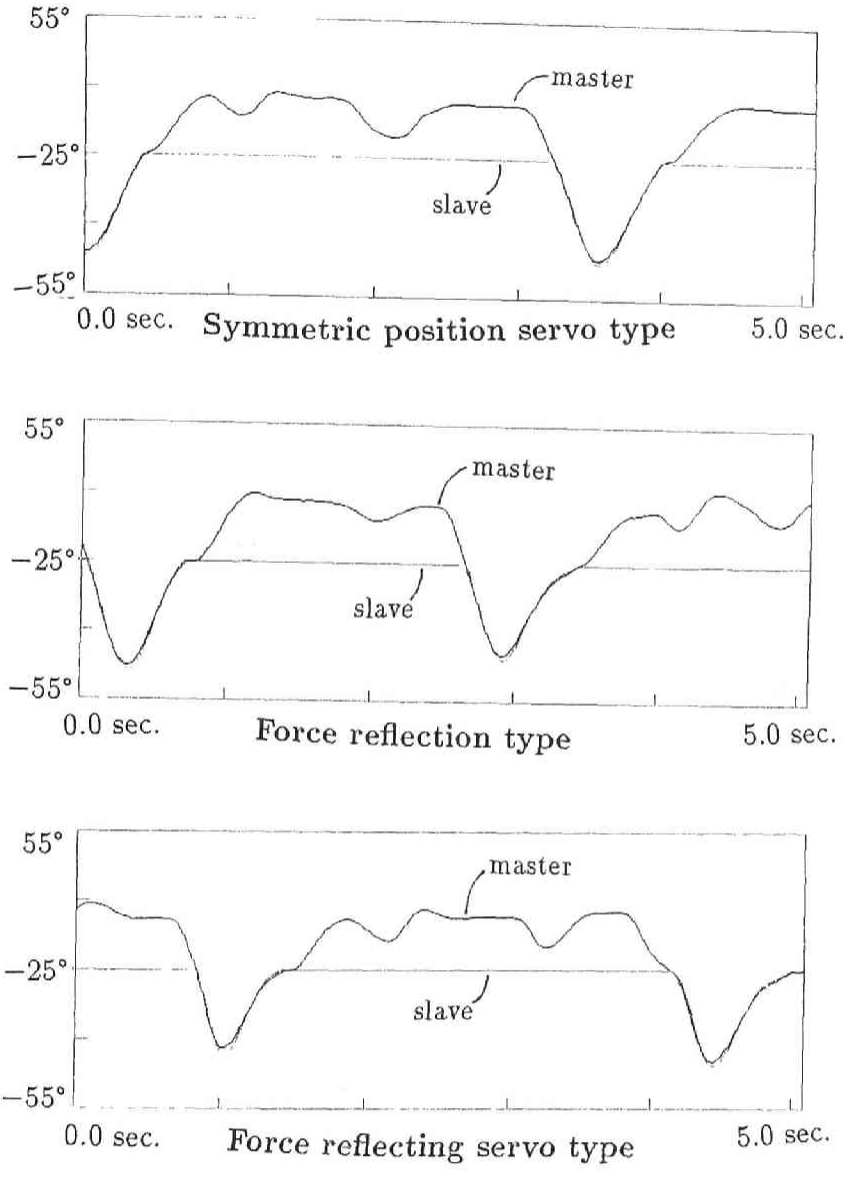

Figure 6.15: Experimental results: Position responses by the conventional schemes in Task 2

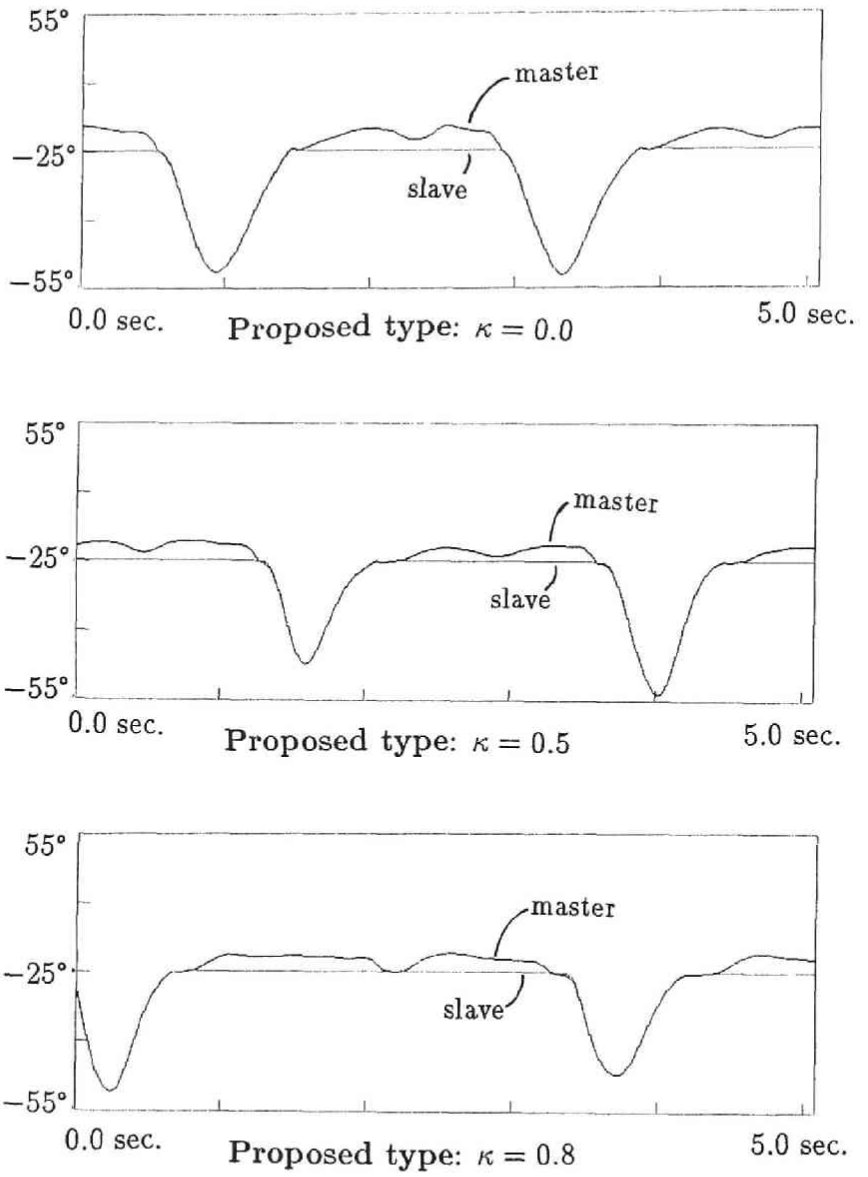

Figure 6.16: Experimental results: Position responses by the proposed schemes in Task 2

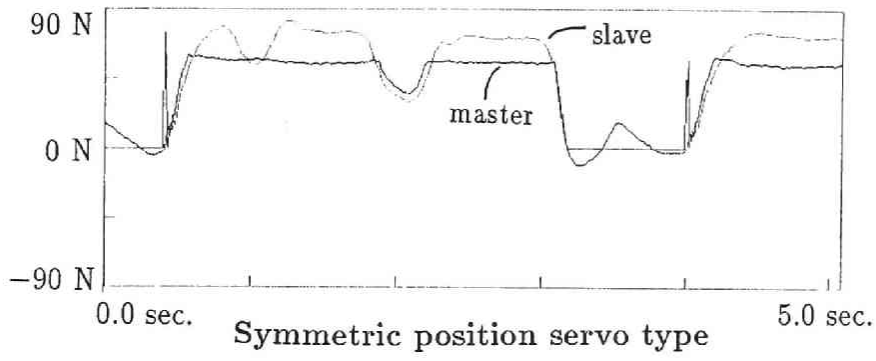

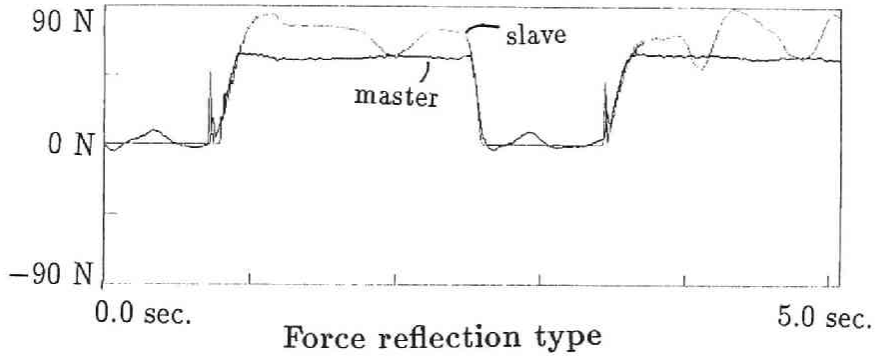

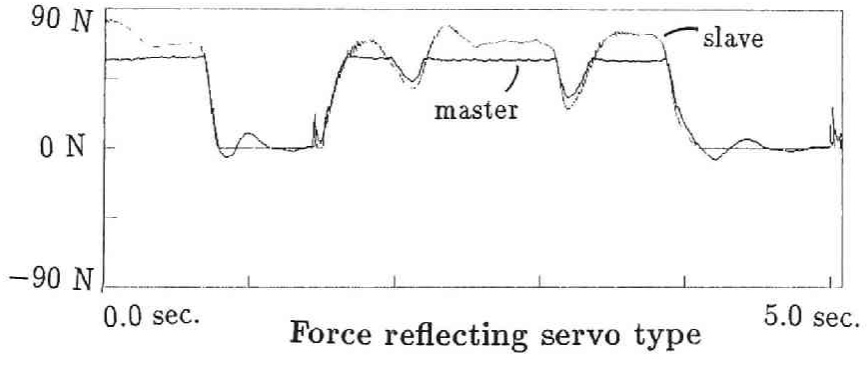

Figure 6.17: Experimental results: Force responses by the conventional schemes in Task 2

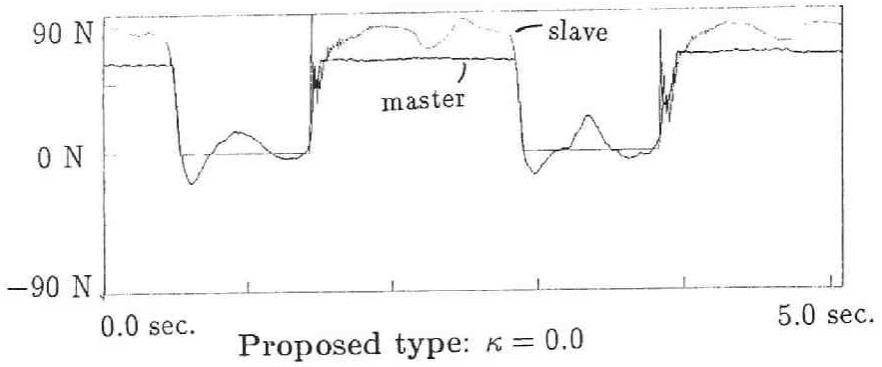

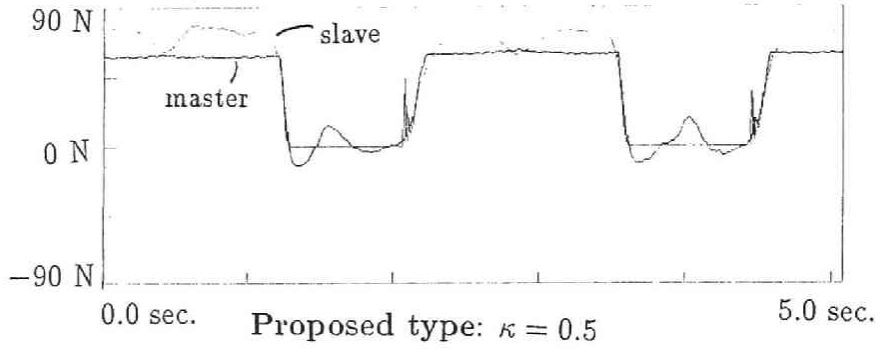

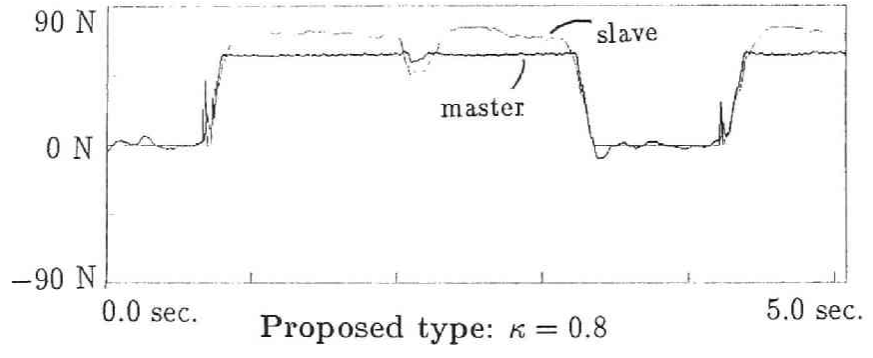

Figure 6.18: Experimental results: Force responses by the proposed schemes in Task 2

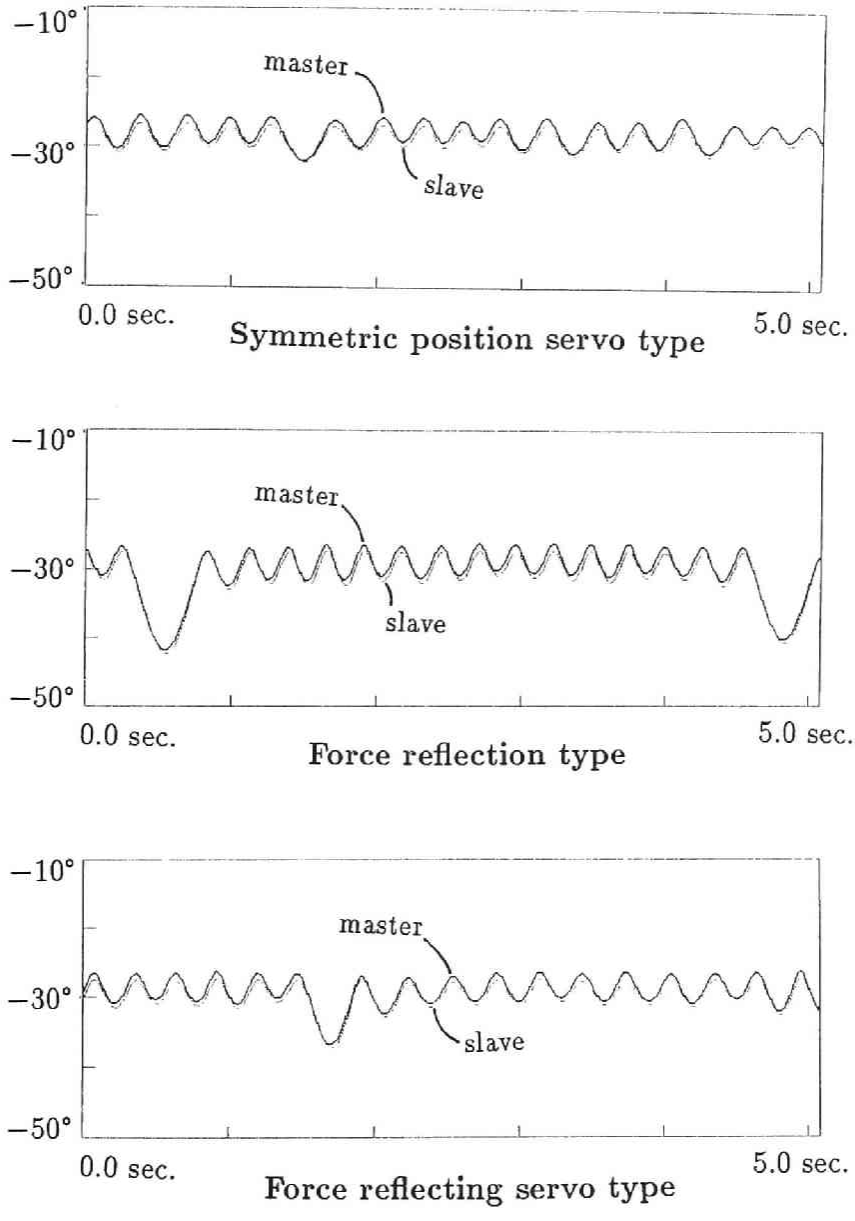

Figure 6.19: Experimental results: Position responses by the conventional schemes in Task 3

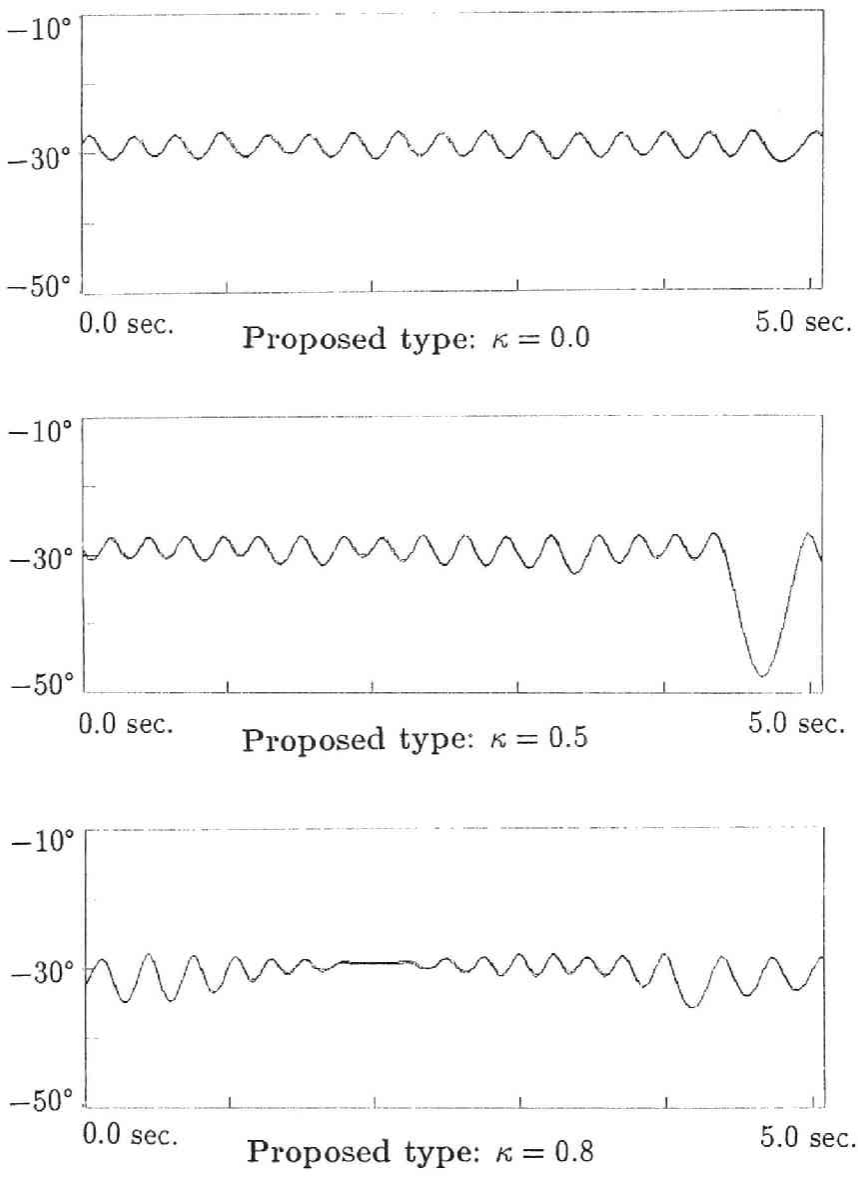

Figure 6.20: Experimental results: Position responses by the proposed schemes in Task 3

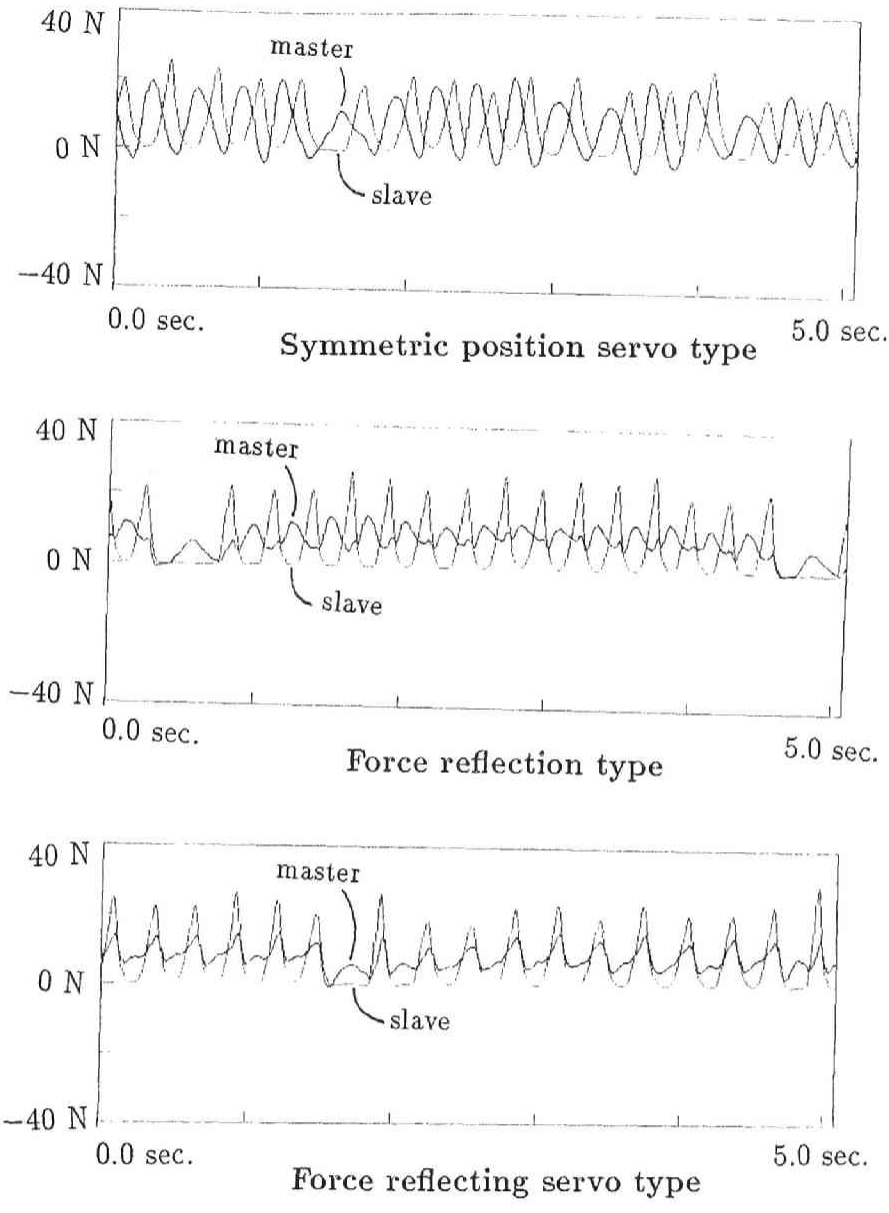

Figure 6.21: Experimental results: Force responses by the conventional schemes in Task 3

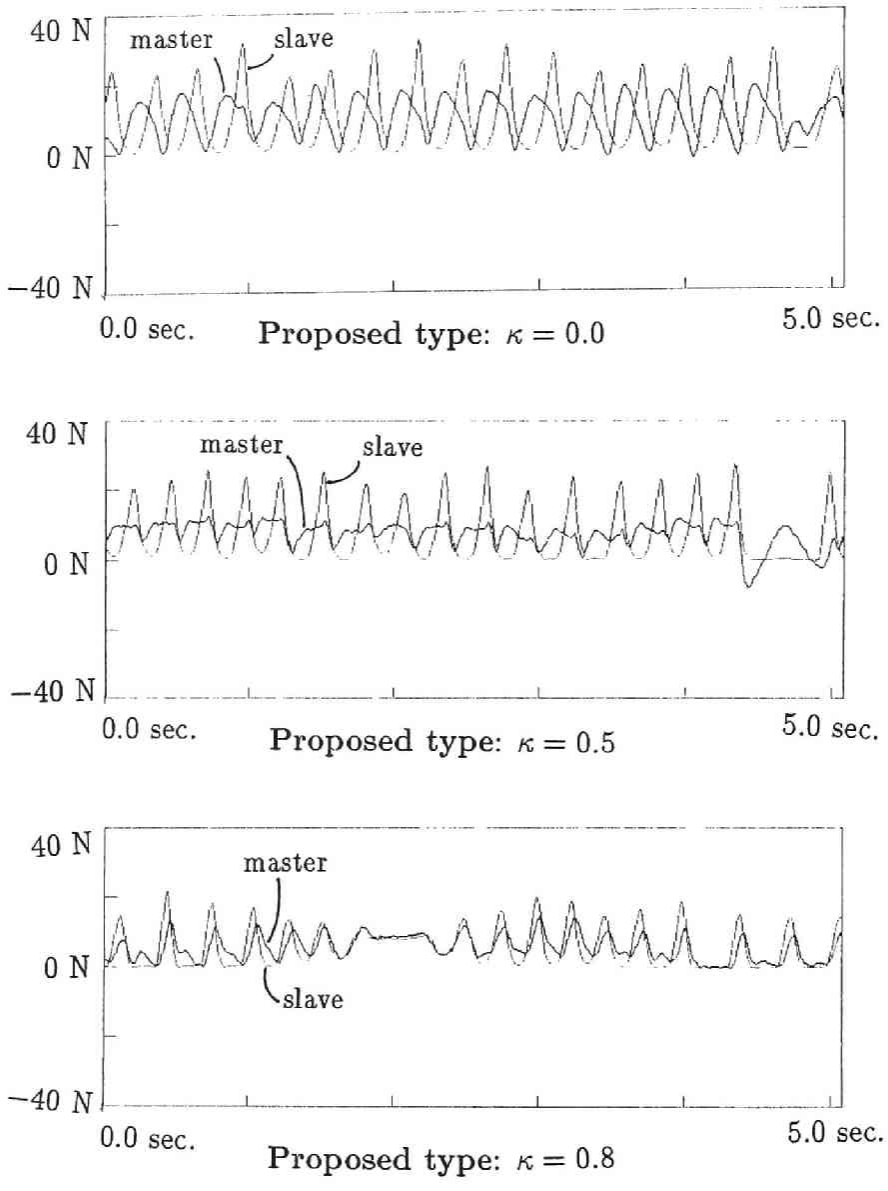

Figure 6.22: Experimental results: Force responses by the proposed schemes in Task 3

Chapter 7

UNIFIED COMPUTATION OF KINEMATICS AND DYNAMICS FOR ROBOT MANIPULATORS

7.1 Introduction

The dynamic control is one of the methods which realize a fast and accurate control of the motion and force of robot manipulators[83][89]. The dynamic control method generates the joint driving force based on the explicit consideration of the manipulator dynamics. However, it has been difficult to perform the dynamic control in real time by using presently available microcomputers since it requires a huge amount of computation.

Another method to compensate for the manipulator dynamics is the feedforward scheme that compensates for the manipulator dynamics in the feedforward path using the desired trajectory, whereas the dynamic control (alias Computed-Torque Scheme) uses the dynamics in the feedback loop for linearization and decoupling[52]. Khosla[52] compared the performance experimentally between the dynamic control and feedforward dynamics compensation and showed that there is no remarkable difference if the dynamic model is accurate enough. If

the desired trajectory is given in advance, the feedforward compensation can be realized by an off-line computation for which the performance of the computer is not so serious. In controlling the master-slave manipulators, however, there is no specific desired trajectory. Consequently, the on-line computation is the only way to compensate for the manipulator dynamics of the master and slave arms.

In order to realize the real time control, the computation speed must be improved, and the formulation of an efficient algorithm is an important approach. So far, studies on the efficient computations of robot manipulators have been focused mainly on the inverse dynamics (ID) problem, and the recursive computational schemes based on the Newton-Euler equation by Luh et al.[54] and based on the Lagrangian equation by Hollerbach[40] are well known.

However, the dynamic control in Cartesian space requires not only ID computation but also direct kinematics (DK) and inverse kinematics (IK) computations. Luh et al.[55] proposed the resolved acceleration control which is a formulation of dynamic control in Cartesian space. Thomas et al.[86] proposed a unified computational approach for the inertia matrix and Coriolis and centrifugal force term based on the computation of the Jacobian matrix, but they did not consider so much about the computational efficiency. Concerning the efficient algorithms for DK and IK, Orin et al.[67] proposed an efficient algorithm of the Jacobian matrix, and Takase[84] showed a vector formulation with respect to the base coordinates.

These computational algorithms may certainly be efficient individually. However, these computations may include computational duplication among them, and the total computation of DK, IK, and ID may not be the most efficient in the case when all of DK, IK and ID computations are necessary. Concerning the idea of unifying kinematics and dynamics computations, Hollerbach et al.[41] showed a customized algorithm for RPPRPR type rotational joint manipulators where their wrist joints intersects at one point such as the PUMA type. They combined the closed solutions of DK and IK with the recursive algorithm for ID. For general case, Mudge et al.[60] yielded algorithms for the Jacobian matrix and the term of squared velocity from the forward computation part of the ID algorithm, and showed an approach which unifies the ID computation also. Wang et al.[90] showed an efficient al-

gorithm for computing the Jacobian matrix and ID. These approaches are based on the idea to eliminate the duplication among DK, IK, and ID computations, but these studies do not consider all of the kinematic computations which are necessary for the dynamic control in Cartesian space.

In this chapter, we clarify the total computational complexity for the dynamic trajectory control and force control of robot manipulators, and discuss the possibility of the real time computation of the uncustomized and versatile algorithms. First of all, all the algorithms of DK, IK and ID which are necessary for dynamic control are represented in a unified recursive way in order to show the duplication explicitly. Especially ID and the term related to the derivative of the Jacobian matrix are formulated so that they may include as many common calculations as possible. The total computational complexity is reduced by eliminating the duplication of the algorithms. It is shown that 42% of multiplications and 33% of additions are reduced compared to the case without eliminating the duplication. The proposed algorithm, called the *unified computation of kinematics and dynamics*, is an efficient formulation of not only ID but also DK and IK without customizing.

The uncustomized algorithms are certainly less efficient than the customized one from the viewpoint of the computational complexity. However the uncustomized algorithms can be applied to any type of manipulators without changing the algorithms. This feature is very important when many types of slave arms and master arms are controlled by the same controller. This algorithm would be useful not only for master-slave systems but also for general purpose controllers or dynamic simulators for any kind of robot manipulators.

7.2 Nomenclature

Symbols used in this chapter are defined as follows:

${}^{j}\boldsymbol{A}_i \in \boldsymbol{R}^{3\times 3}$	:	rotation matrix
$\boldsymbol{p}_i^* \in \boldsymbol{R}^3$	:	position vector from the origin of the $(i-1)$-th link frame to the origin of the i-th link frame

α_i	:	twist angle, the Denavit-Hartenberg parameter
d_i	:	joint distance, the Denavit-Hartenberg parameter
a_i	:	link length, the Denavit-Hartenberg parameter
θ_i	:	joint angle, the Denavit-Hartenberg parameter
n	:	number of DOF
$\boldsymbol{q} \in \boldsymbol{R}^n$	:	joint variable vector
$\boldsymbol{r} \in \boldsymbol{R}^6$	:	manipulation variable vector which describes position and orientation of the end-effector $\boldsymbol{r} = [\ \boldsymbol{r}_p^T \quad \boldsymbol{r}_o^T\ ]^T$
$\boldsymbol{r}_p \in \boldsymbol{R}^3$	:	position vector of the hand tip (the origin of the n-th link frame)
$\boldsymbol{r}_o \in \boldsymbol{R}^3$	:	orientational vector of the hand tip (orientation of the n-th link frame)
${}^0\boldsymbol{A}_n \in \boldsymbol{R}^{3\times 3}$	:	orientational matrix of the hand tip ${}^0\boldsymbol{A}_n = {}^0\boldsymbol{A}_1 {}^1\boldsymbol{A}_2 \cdots {}^{n-1}\boldsymbol{A}_n$
$\boldsymbol{r}_d \in \boldsymbol{R}^6$	:	desired trajectory of the hand tip
$\boldsymbol{v}_i' \in \boldsymbol{R}^3$	:	linear velocity vector of the i-th link converted to the origin of the n-th link frame
$\boldsymbol{\omega}_i \in \boldsymbol{R}^3$	:	angular velocity vector of the i-th link
$\dot{\tilde{\boldsymbol{v}}}_i \in \boldsymbol{R}^3$	:	linear acceleration vector of the gravity center of the i-th link
$\boldsymbol{J} \in \boldsymbol{R}^{6\times n}$	:	Jacobian matrix
$\boldsymbol{\beta}_i \in \boldsymbol{R}^3$	:	the i-th column linear velocity element vector
$\boldsymbol{\gamma}_i \in \boldsymbol{R}^3$	:	the i-th column angular velocity element vector
$\boldsymbol{J}_p \in \boldsymbol{R}^{3\times n}$	:	$[\boldsymbol{\beta}_1 \boldsymbol{\beta}_2 \cdots \boldsymbol{\beta}_n]$; linear block of the Jacobian matrix
$\boldsymbol{J}_o \in \boldsymbol{R}^{3\times n}$	:	$[\boldsymbol{\gamma}_1 \boldsymbol{\gamma}_2 \cdots \boldsymbol{\gamma}_n]$; angular block of the Jacobian matrix
$\boldsymbol{h}_i \in \boldsymbol{R}^3$	:	position vector from the origin of the i-th link frame to the origin of the n-th link frame

m_i	:	mass of the i-th link
$\hat{\boldsymbol{I}}_i \in \boldsymbol{R}^{3\times3}$	:	inertia matrix of the i-th link about its gravity center
$\hat{\boldsymbol{s}}_i \in \boldsymbol{R}^3$	:	position vector from the origin of the i-th link frame to the gravity center of the i-th link
$\hat{\boldsymbol{t}}_i \in \boldsymbol{R}^3$	:	position vector from the origin of the n-th link frame to the gravity center of the i-th link
$\boldsymbol{F}_i \in \boldsymbol{R}^3$	:	total force vector exerted on the i-th link at the gravity center of the i-th link
$\boldsymbol{N}_i \in \boldsymbol{R}^3$	:	total moment vector exerted on the i-th link at the gravity center of the i-th link
$\boldsymbol{F}'_i \in \boldsymbol{R}^3$	:	total force vector exerted on the i-th link which exerting point is converted to the origin of the n-th link frame
$\boldsymbol{N}'_i \in \boldsymbol{R}^3$	:	total moment vector exerted on the i-th link which exerting point is converted to the origin of the n-th link frame
$\boldsymbol{f}_i \in \boldsymbol{R}^3$	:	force vector exerted on the i-th link by the $(i-1)$-th link at the origin of the $(i-1)$-th link frame
$\boldsymbol{n}_i \in \boldsymbol{R}^3$	:	moment vector exerted on the i-th link by the $(i-1)$-th link at the origin of the $(i-1)$-th link frame
$\boldsymbol{\tau} \in \boldsymbol{R}^n$	:	joint driving force/torque vector
τ_i	:	force/torque of the i-th joint
b_i	:	viscous friction coefficient of the i-th joint
$\tilde{\boldsymbol{g}} \in \boldsymbol{R}^3$	:	gravity acceleration vector
$\boldsymbol{z}_i \in \boldsymbol{R}^3$	:	unit vector in the direction of the z-axis of the i-th link frame
$\boldsymbol{E}_3 \in \boldsymbol{R}^{3\times3}$	:	3×3 unity matrix

The definition of the link frames is conformed to the Denavit-Hartenberg notation[18][69]. We assume that each link of the manipulator is connected serially. There are four parameters which specify the kinematic relation of each link such as α_i, d_i, a_i and θ_i as shown in **Fig.7.1**. These parameters are called the link parameters. When the i-th joint is a rotational joint, α_i, d_i and a_i are constant, and θ_i becomes

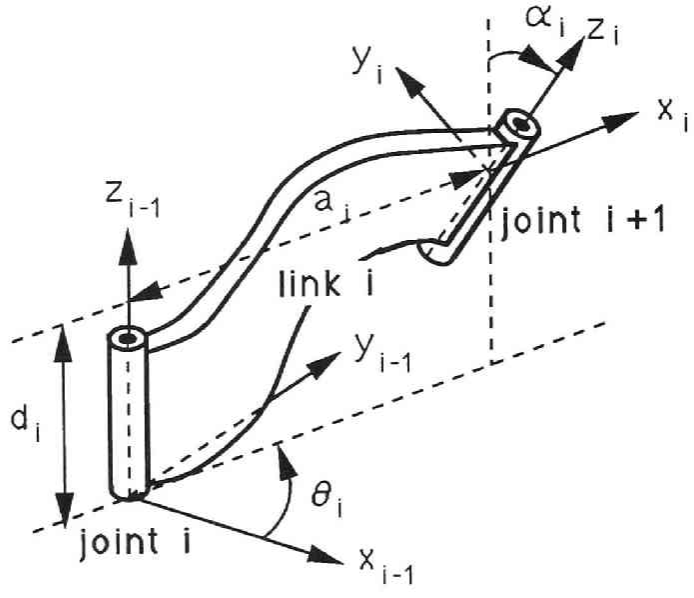

Figure 7.1: Link parameters by Denavit-Hartenberg notation

a variable. On the other hand, when the i-th joint is a prismatic joint, α_i, a_i and θ_i are constant, and d_i becomes a variable. We define the element of the joint variable vector $\boldsymbol{q} \triangleq [\ q_1 \cdots q_n\ ]^T$ as follows:

$$q_i = \begin{cases} \theta_i & \text{(ifR)} \\ d_i & \text{(ifP)} \end{cases} \tag{7.1}$$

where (ifR) means the case when the joint is rotational and (ifP) means the case when the joint is prismatic.

The coordinate transformation matrix from the i-th link coordinates to the $(i-1)$-th link coordinates is denoted as follows:

$$^{i-1}\boldsymbol{A}_i = \begin{bmatrix} \cos\theta_i & -\sin\theta_i\cos\alpha_i & \sin\theta_i\sin\alpha_i \\ \sin\theta_i & \cos\theta_i\cos\alpha_i & -\cos\theta_i\sin\alpha_i \\ 0 & \sin\alpha_i & \cos\alpha_i \end{bmatrix} \tag{7.2}$$

A vector with reference to the i-th link coordinates is transformed to the vector with reference to the $(i-1)$-th link coordinates by multiplying $^{i-1}\boldsymbol{A}_i$ from the left side. The position vector from the $(i-1)$-th link

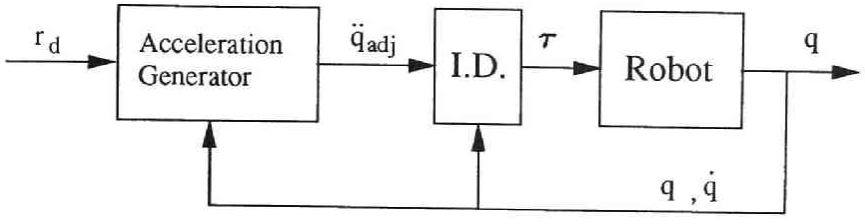

Figure 7.2: Block diagram of dynamic control

frame to the i-th link frame with reference to the i-th link coordinates is represented as follows:

$$ {}^{i}\boldsymbol{p}_i^* = [\ a_i \quad d_i \sin\alpha_i \quad d_i \cos\alpha_i\ ]^T \tag{7.3} $$

Hereafter the left-super-script of vectors denotes the link coordinates which describes the vector and when the vector is represented with reference to the base coordinates, the super-script becomes 0.

7.3 Necessary Computations for Dynamic Control

The block diagram of the dynamic control is shown in **Fig.7.2**. The acceleration generator block generates the joint acceleration vector $\ddot{\boldsymbol{q}}_{adj}$ and the ID block calculates the joint driving force/torque $\boldsymbol{\tau}$ which realizes the specified joint acceleration at the current state $\boldsymbol{q}$ and $\dot{\boldsymbol{q}}$. In order to calculate $\ddot{\boldsymbol{q}}_{adj}$, we use the resolved acceleration control proposed by Luh et al.[55] and the adjusted acceleration vector of the hand tip is given as follows:

$$ \ddot{\boldsymbol{r}}_{adj} = \ddot{\boldsymbol{r}}_d + \boldsymbol{K}_1(\dot{\boldsymbol{r}}_d - \dot{\boldsymbol{r}}) + \boldsymbol{K}_2(\boldsymbol{r}_d - \boldsymbol{r}) \tag{7.4} $$

where $\boldsymbol{K}_1$ and $\boldsymbol{K}_2$ are gain matrices. If these constant matrices are chosen so that eq.(7.4) becomes asymptotically stable, the hand tip

vector $\boldsymbol{r}$ will converge into the desired vector $\boldsymbol{r}_d$. The joint acceleration vector $\ddot{\boldsymbol{q}}_{adj}$ can be obtained by transforming this vector $\ddot{\boldsymbol{r}}_{adj}$ into the joint space as follows.

First, we will define the manipulation variable $\boldsymbol{r}$ in eq.(7.4) by its derivative $\dot{\boldsymbol{r}}$[61].

$$\dot{\boldsymbol{r}} \triangleq [\ {}^0\boldsymbol{v}_n^T \quad {}^0\boldsymbol{\omega}_n^T\ ]^T \tag{7.5}$$

The relation between $\dot{\boldsymbol{r}}$ and $\dot{\boldsymbol{q}}$ can be described by using the Jacobian matrix as follows:

$$\dot{\boldsymbol{r}} = \boldsymbol{J}\dot{\boldsymbol{q}} \tag{7.6}$$

By differentiating eq.(7.6) with respect to time, we obtain

$$\ddot{\boldsymbol{r}} = \boldsymbol{J}\ddot{\boldsymbol{q}} + \dot{\boldsymbol{J}}\dot{\boldsymbol{q}}. \tag{7.7}$$

Substituting eq.(7.4) into eq.(7.7), and assuming that $n = 6$ and $\boldsymbol{J}$ is nonsingular for simplification, we obtain the following equation:

$$\ddot{\boldsymbol{q}}_{adj} = \boldsymbol{J}^{-1}(\ddot{\boldsymbol{r}}_d + \boldsymbol{K}_1(\dot{\boldsymbol{r}}_d - \dot{\boldsymbol{r}}) + \boldsymbol{K}_2(\boldsymbol{r}_d - \boldsymbol{r}) - \dot{\boldsymbol{J}}\dot{\boldsymbol{q}}) \tag{7.8}$$

For calculating $\ddot{\boldsymbol{q}}_{adj}$ in eq.(7.8), if the algebraic solutions such as the Gaussian elimination are applied instead of the direct calculation of $\boldsymbol{J}^{-1}$, the computational complexity can be reduced considerably.

To deal with the case when $n > 6$ and the case of the singularity, one can apply the pseud inverse $\boldsymbol{J}^{\#}$[62] and singularity robust inverse $\boldsymbol{J}^{*}$[63] respectively instead of $\boldsymbol{J}^{-1}$ in eq.(7.8). The manipulation variable $\boldsymbol{r}$ in eqs.(7.4) and (7.8) is the time integration of $\dot{\boldsymbol{r}}$ defined in eq.(7.5). While the integration of the translational component of $\dot{\boldsymbol{r}}$ means the position of the hand tip, the integration of the rotational component has no clear physical meaning. However, what we need in eq.(7.8) is not $\boldsymbol{r}$ itself but just the error vector $\boldsymbol{r}_d - \boldsymbol{r}$. Luh et al.[55] specified the orientation component of the desired trajectory by the orientation matrix ${}^0\boldsymbol{A}_{nd}$. And from the error matrix

$$\Delta{}^0\boldsymbol{A}_n \triangleq {}^0\boldsymbol{A}_{nd}\,{}^0\boldsymbol{A}_n^T = \begin{bmatrix} \Delta n_x & \Delta o_x & \Delta a_x \\ \Delta n_y & \Delta o_y & \Delta a_y \\ \Delta n_z & \Delta o_z & \Delta a_z \end{bmatrix}, \tag{7.9}$$

they defined orientational component ${}^0\boldsymbol{e}_o$ of the error vector $\boldsymbol{r}_d - \boldsymbol{r}$ as follows:

$${}^0\boldsymbol{e}_o \triangleq 1/2[\ \Delta o_z - \Delta a_y \quad \Delta a_x - \Delta n_z \quad \Delta n_y - \Delta o_x\ ]^T \tag{7.10}$$

The error vector defined in eq.(7.10) has the same direction as the equivalent rotation axis of $\Delta^0\boldsymbol{A}_{nd}$ from the desired orientation ${}^0\boldsymbol{A}_{nd}$ to the current orientation ${}^0\boldsymbol{A}_n$, and its norm is equal to $\sin\phi$ where ϕ denotes the equivalent rotation angle.

By this formulation, the error vector $\boldsymbol{r}_d - \boldsymbol{r}$ can be obtained by calculating ${}^0\boldsymbol{r}_p$ (the position component of $\boldsymbol{r}$) for position component of $\boldsymbol{r}_d - \boldsymbol{r}$ and ${}^0\boldsymbol{A}_n$ for orientation component of $\boldsymbol{r}_d - \boldsymbol{r}$. Comparing with the Euler angles or the roll-pitch-yaw angles[69], this representation of the orientation is advantageous because it has no singularity caused by the mathematical representation and requires no inverse trigonometric functions.

From the above discussion, the required computation for the dynamic control can be summarized as follows:

(i) computation of $\boldsymbol{r}$, that is, ${}^0\boldsymbol{r}_p$ and ${}^0\boldsymbol{A}_n$,

(ii) computation of $\dot{\boldsymbol{r}}$,

(iii) computation of $\boldsymbol{J}$,

(iv) computation of $\dot{\boldsymbol{J}}\dot{\boldsymbol{q}}$,

(v) computation of $\ddot{\boldsymbol{q}}_{adj}$ in eq.(7.8) as an algebraic equation,

(vi) computation of inverse dynamics.

The computation (v) depends on whether system is redundant or not and the control strategy. Furthermore, it is a pure algebraic computation and has little physical relationship to the other computations. For these reasons, we will neglect (v) in this chapter. In the next section, we discuss the computations (i) through (iv) and (vi). The computation (i), (ii) and (iii) are classified into DK, the computation (iv) into IK, and the computation (vi) into ID.

7.4 Unified Computation of Kinematics and Dynamics

7.4.1 Computation of DK

Computation of ${}^0\boldsymbol{r}_p$ and ${}^0\boldsymbol{A}_n$

In this subsection, we show the algorithms to compute the position vector ${}^0\boldsymbol{r}_p$ and the orientation matrix ${}^0\boldsymbol{A}_n$. First, the matrix ${}^0\boldsymbol{A}_n$ can be calculated by the following recursive procedure:

$$ {}^0\boldsymbol{A}_i = {}^0\boldsymbol{A}_{i-1}\,{}^{i-1}\boldsymbol{A}_i \tag{7.11} $$

where the initial condition is ${}^0\boldsymbol{A}_0 = \boldsymbol{E}_3$. The vector ${}^0\boldsymbol{r}_p$ can be obtained by the following equations iterating from $i = n$ to 1.

$$ {}^0\boldsymbol{p}_i^* = {}^0\boldsymbol{A}_i\,{}^i\boldsymbol{p}_i^* \tag{7.12} $$

$$ {}^0\boldsymbol{h}_{i-1} = {}^0\boldsymbol{h}_i + {}^0\boldsymbol{p}_i^* \tag{7.13} $$

where the initial condition of eq.(7.13) is ${}^0\boldsymbol{h}_n = \mathbf{o}$, and ${}^0\boldsymbol{r}_p$ is obtained by the terminal condition ${}^0\boldsymbol{r}_p = {}^0\boldsymbol{h}_0$. The computational process is shown in **Fig.7.3**(a).

Computation of $\boldsymbol{J}$

As for the computation of the Jacobian matrix, we use the algorithm proposed by Orin and Schrader[67]. Let the Jacobian matrix be represented as follows:

$$ \boldsymbol{J} = \begin{bmatrix} {}^0\boldsymbol{\beta}_1 & {}^0\boldsymbol{\beta}_2 & \cdots & {}^0\boldsymbol{\beta}_n \\ {}^0\boldsymbol{\gamma}_1 & {}^0\boldsymbol{\gamma}_2 & \cdots & {}^0\boldsymbol{\gamma}_n \end{bmatrix} \tag{7.14} $$

Then, ${}^0\boldsymbol{\beta}_i$ and ${}^0\boldsymbol{\gamma}_i$ are computed as follows:

$$ {}^0\boldsymbol{\gamma}_i = \begin{cases} {}^0\boldsymbol{z}_{i-1} = {}^0\boldsymbol{A}_{i-1}\,{}^{i-1}\boldsymbol{z}_{i-1} & \text{(ifR)} \\ \mathbf{o} & \text{(ifP)} \end{cases} \tag{7.15} $$

$$ {}^0\boldsymbol{\beta}_i = \begin{cases} {}^0\boldsymbol{\gamma}_i \times {}^0\boldsymbol{h}_{i-1} & \text{(ifR)} \\ {}^0\boldsymbol{z}_{i-1} & \text{(ifP)} \end{cases} \tag{7.16} $$

where ${}^{i-1}\boldsymbol{z}_{i-1}$ is a constant vector $[\ 0 \quad 0 \quad 1\ ]^T$. Relations of these vectors are shown in **Fig.7.4**. The computational process of the Jacobian matrix is shown in **Fig.7.3**(b).

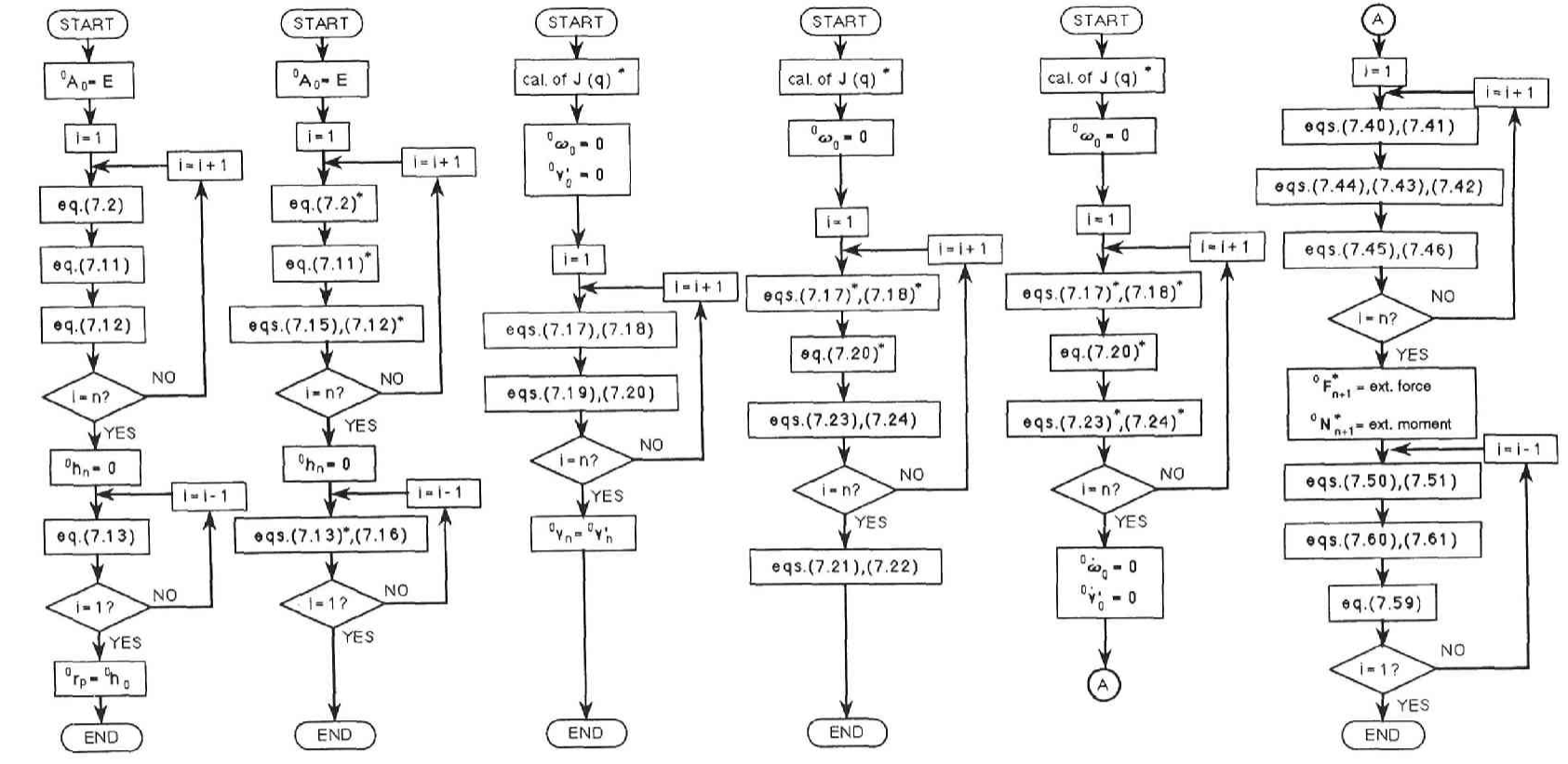

Figure 7.3: Flow charts of algorithms for DK, IK and ID

Computation of $\dot{\boldsymbol{r}}$

The velocity vector $\dot{\boldsymbol{r}} = [\ {}^0\boldsymbol{v}_n^T \quad {}^0\boldsymbol{\omega}_n^T\ ]^T$ is computed as follows. First, let the following values be defined:

$$ {}^0\tilde{\boldsymbol{\beta}}_i = {}^0\boldsymbol{\beta}_i \dot{q}_i \tag{7.17} $$

$$ {}^0\tilde{\boldsymbol{\gamma}}_i = {}^0\boldsymbol{\gamma}_i \dot{q}_i \tag{7.18} $$

Considering eq.(7.6), the translational and rotational components of $\dot{\boldsymbol{r}}$, ${}^0\boldsymbol{v}_n$ and ${}^0\boldsymbol{\omega}_n$, are calculated by the following recursive procedure:

$$ {}^0\boldsymbol{v}'_i = {}^0\boldsymbol{v}'_{i-1} + {}^0\tilde{\boldsymbol{\beta}}_i \tag{7.19} $$

$$ {}^0\boldsymbol{\omega}_i = {}^0\boldsymbol{\omega}_{i-1} + {}^0\tilde{\boldsymbol{\gamma}}_i \tag{7.20} $$

where the initial conditions are ${}^0\boldsymbol{v}'_n = \mathbf{o}$ and ${}^0\boldsymbol{\omega}_0 = \mathbf{o}$. The vector ${}^0\boldsymbol{v}'_i$ represents the linear velocity of the i-th link which reference point is converted to the hand tip as shown in **Fig.7.5**. The vector ${}^0\boldsymbol{v}_n$ can be obtained from ${}^0\boldsymbol{v}_n = {}^0\boldsymbol{v}'_n$. The computational process is shown in **Fig.7.3**(c).

7.4.2 Computation of IK

Computation of $\dot{\boldsymbol{J}}\dot{\boldsymbol{q}}$

The vector $\dot{\boldsymbol{J}}\dot{\boldsymbol{q}} \triangleq [\ {}^0\bar{\boldsymbol{v}}_n^T \quad {}^0\bar{\boldsymbol{\omega}}_n^T\ ]^T$ can be interpreted as the hand tip acceleration when $\ddot{\boldsymbol{q}} = \mathbf{o}$ from eq.(7.7). The translational and rotational components of this vector are calculated by the following equations:

$$ {}^0\bar{\boldsymbol{v}}_n = \sum_{i=1}^{n} {}^0\boldsymbol{\xi}_i \tag{7.21} $$

$$ {}^0\bar{\boldsymbol{\omega}}_n = \sum_{i=1}^{n} {}^0\boldsymbol{\eta}_i \tag{7.22} $$

where ${}^0\boldsymbol{\xi}_i$ and ${}^0\boldsymbol{\eta}_i$ are given by

$$ {}^0\boldsymbol{\xi}_i = ({}^0\boldsymbol{\omega}_{i-1} + {}^0\boldsymbol{\omega}_i) \times {}^0\tilde{\boldsymbol{\beta}}_i, \tag{7.23} $$

$$ {}^0\boldsymbol{\eta}_i = {}^0\boldsymbol{\omega}_{i-1} \times {}^0\tilde{\boldsymbol{\gamma}}_i. \tag{7.24} $$

In eqs.(7.23) and (7.24), the vectors ${}^0\tilde{\boldsymbol{\beta}}_i$ and ${}^0\tilde{\boldsymbol{\gamma}}_i$ are already obtained in the computation of $\dot{\boldsymbol{r}}$. The computational process is shown in **Fig.7.3**(d).

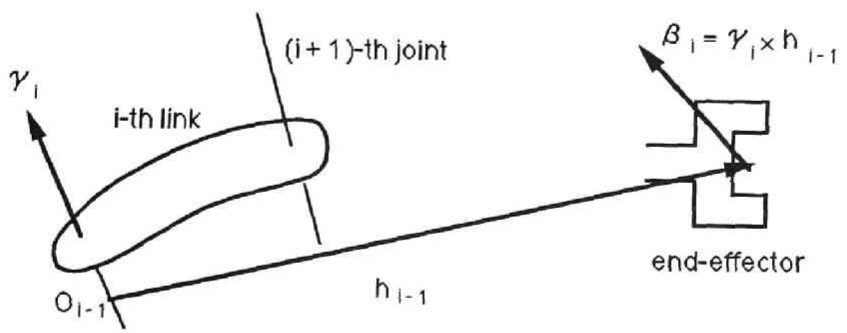

Figure 7.4: Relations of ${}^0\boldsymbol{\beta}_i$ and ${}^0\boldsymbol{\gamma}_i$ when the i-th joint is rotational

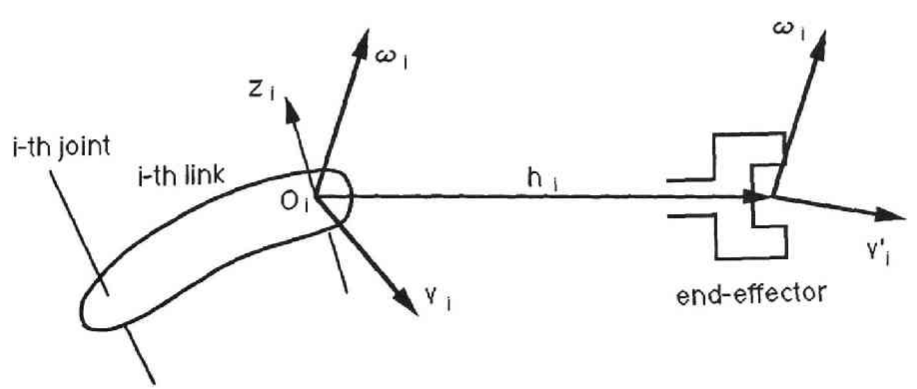

Figure 7.5: Translational velocity of the i-th link which reference point is converted to the hand tip

Proof of eqs.(7.21) and (7.22)

The vector $\dot{\boldsymbol{J}}\dot{\boldsymbol{q}}$ can be represented in general by the following equation[86]:

$$\dot{\boldsymbol{J}}\dot{\boldsymbol{q}} = \dot{\boldsymbol{q}}^T \boldsymbol{H} \dot{\boldsymbol{q}} \tag{7.25}$$

where $\boldsymbol{H} \triangleq \partial \boldsymbol{J}/\partial \boldsymbol{q} \in \boldsymbol{R}^{n\times n\times 6}$ is called the Hessian, and it can be regarded as an $n \times n$ matrix whose elements are six-dimensional vectors. Let the linear block and the angular block of $\boldsymbol{H}$ be represented by $\boldsymbol{H}_p \triangleq \partial \boldsymbol{J}_p/\partial \boldsymbol{q} \in \boldsymbol{R}^{n\times n\times 3}$ and $\boldsymbol{H}_o \triangleq \partial \boldsymbol{J}_o/\partial \boldsymbol{q} \in \boldsymbol{R}^{n\times n\times 3}$ respectively. Then, ${}^0\bar{\boldsymbol{v}}_n$ and ${}^0\bar{\boldsymbol{\omega}}_n$ are represented as follows:

$${}^0\bar{\boldsymbol{v}}_n = \dot{\boldsymbol{q}}^T \boldsymbol{H}_p \dot{\boldsymbol{q}} \tag{7.26}$$

$${}^0\bar{\boldsymbol{\omega}}_n = \dot{\boldsymbol{q}}^T \boldsymbol{H}_o \dot{\boldsymbol{q}} \tag{7.27}$$

First, let us show that $\boldsymbol{H}_p$ is symmetric. From the definition of $\boldsymbol{H}_p$ and eq.(7.14), the (i,j) element vector of $\boldsymbol{H}_p$ when $i \leq j$, is calculated as follows. The following four cases must be considered according to the choice whether each of the i-th and j-th joints is rotational or prismatic.
(i) i-th joint: rotational , j-th joint: rotational

$$\boldsymbol{H}_{pij} = \partial {}^0\boldsymbol{\beta}_j/\partial q_i = {}^0\boldsymbol{\gamma}_i \times {}^0\boldsymbol{\beta}_j; \tag{7.28}$$

(ii) i-th joint: prismatic , j-th joint: prismatic

$$\boldsymbol{H}_{pij} = \partial {}^0\boldsymbol{\beta}_j/\partial q_i = \mathbf{o} = {}^0\boldsymbol{\gamma}_i \times {}^0\boldsymbol{\beta}_j, \tag{7.29}$$

since ${}^0\boldsymbol{\gamma}_i = \mathbf{o}$;
(iii) i-th joint: rotational , j-th joint: prismatic

$$\boldsymbol{H}_{pij} = \partial {}^0\boldsymbol{\beta}_j/\partial q_i = {}^0\boldsymbol{\gamma}_i \times {}^0\boldsymbol{\beta}_j; \tag{7.30}$$

(iv) i-th joint: prismatic , j-th joint: rotational

$$\boldsymbol{H}_{pij} = \partial {}^0\boldsymbol{\beta}_j/\partial q_i = \mathbf{o} = {}^0\boldsymbol{\gamma}_i \times {}^0\boldsymbol{\beta}_j, \tag{7.31}$$

since ${}^0\boldsymbol{\gamma}_i = \mathbf{o}$. The cases (iii) and (iv) occur only when $i < j$.

Similarly, when $i > j$, the (i,j) element of $\boldsymbol{H}_p$ can be calculated as follows:

(i) i-th joint: rotational , j-th joint: rotational

$$\begin{aligned}\boldsymbol{H}_{pij} &= \partial^0\boldsymbol{\beta}_j/\partial q_i = \partial({}^0\boldsymbol{\gamma}_j \times {}^0\boldsymbol{h}_{j-1})/\partial\theta_i \\ &= {}^0\boldsymbol{\gamma}_j \times \left(\frac{\partial}{\partial\theta_i}{}^0\boldsymbol{h}_{i-1}\right) = {}^0\boldsymbol{\gamma}_j \times ({}^0\boldsymbol{\gamma}_i \times {}^0\boldsymbol{h}_{i-1}) \\ &= {}^0\boldsymbol{\gamma}_j \times {}^0\boldsymbol{\beta}_i = \boldsymbol{H}_{pji};\end{aligned} \tag{7.32}$$

(ii) i-th joint: prismatic , j-th joint: prismatic

$$\begin{aligned}\boldsymbol{H}_{pij} &= \partial^0\boldsymbol{\beta}_j/\partial q_i = \mathbf{o} \\ &= {}^0\boldsymbol{\gamma}_j \times {}^0\boldsymbol{\beta}_i = \boldsymbol{H}_{pji},\end{aligned} \tag{7.33}$$

since ${}^0\boldsymbol{\gamma}_j = \mathbf{o}$;

(iii) i-th joint: rotational , j-th joint: prismatic

$$\begin{aligned}\boldsymbol{H}_{pij} &= \partial^0\boldsymbol{\beta}_j/\partial q_i = \mathbf{o} \\ &= {}^0\boldsymbol{\gamma}_j \times {}^0\boldsymbol{\beta}_i = \boldsymbol{H}_{pji},\end{aligned} \tag{7.34}$$

since ${}^0\boldsymbol{\gamma}_j = \mathbf{o}$;

(iv) i-th joint: prismatic , j-th joint: rotational

$$\begin{aligned}\boldsymbol{H}_{pij} &= \partial^0\boldsymbol{\beta}_j/\partial q_i = \partial({}^0\boldsymbol{\gamma}_j \times {}^0\boldsymbol{h}_{j-1})/\partial d_i \\ &= {}^0\boldsymbol{\gamma}_j \times \left(\frac{\partial}{\partial d_i}{}^0\boldsymbol{h}_{j-1}\right) = {}^0\boldsymbol{\gamma}_j \times {}^0\boldsymbol{z}_{i-1} \\ &= {}^0\boldsymbol{\gamma}_j \times {}^0\boldsymbol{\beta}_i = \boldsymbol{H}_{pji}.\end{aligned} \tag{7.35}$$

These result shows that $\boldsymbol{H}_p$ is symmetric. Consequently, from eq.(7.26), eq.(7.21) is proved as follows:

$$\begin{aligned}{}^0\bar{\boldsymbol{v}}_n &= \sum_{i=1}^{n}\sum_{j=1}^{n}\boldsymbol{H}_{pij}\dot{q}_i\dot{q}_j \\ &= \sum_{i=1}^{n}\boldsymbol{H}_{pii}\dot{q}_i^2 + 2\sum_{i=2}^{n}\sum_{j=1}^{i-1}\boldsymbol{H}_{pji}\dot{q}_j\dot{q}_i\end{aligned}$$

$$
\begin{aligned}
&= \sum_{i=1}^{n}[(2^0\boldsymbol{\omega}_{i-1} + {}^0\boldsymbol{\gamma}_i\dot{q}_i) \times {}^0\boldsymbol{\beta}_i\dot{q}_i] \\
&= \sum_{i=1}^{n}[({}^0\boldsymbol{\omega}_{i-1} + {}^0\boldsymbol{\omega}_i) \times {}^0\boldsymbol{\beta}_i\dot{q}_i] \\
&= \sum_{i=1}^{n} {}^0\boldsymbol{\xi}_i \qquad (7.36)
\end{aligned}
$$

On the other hand, the angular block $\boldsymbol{H}_o$ is not symmetric. It is calculated as follows:
(i) i-th joint: rotational , j-th joint: rotational

$$
\boldsymbol{H}_{oij} = \partial^0\boldsymbol{\gamma}_j/\partial q_i = \begin{cases} {}^0\boldsymbol{\gamma}_i \times {}^0\boldsymbol{\gamma}_j & (i < j) \\ \mathbf{o} & (i \geq j) \end{cases} ; \qquad (7.37)
$$

(ii) i-th joint: prismatic , j-th joint: prismatic,
(iii) i-th joint: rotational , j-th joint: prismatic, and
(iv) i-th joint: prismatic , j-th joint: rotational

$$
\boldsymbol{H}_{oij} = \partial^0\boldsymbol{\gamma}_j/\partial q_i = \begin{cases} \mathbf{o} = {}^0\boldsymbol{\gamma}_i \times {}^0\boldsymbol{\gamma}_j & (i < j) \\ \mathbf{o} & (i \geq j) \end{cases} , \qquad (7.38)
$$

since ${}^0\boldsymbol{\gamma}_i = \mathbf{o}$ or ${}^0\boldsymbol{\gamma}_j = \mathbf{o}$.

Therefore, from eq.(7.27), eq.(7.22) is proved as follows:

$$
\begin{aligned}
{}^0\bar{\boldsymbol{\omega}}_n &= \sum_{i=1}^{n}\sum_{j=1}^{n} \boldsymbol{H}_{oij}\dot{q}_i\dot{q}_j \\
&= \sum_{i=1}^{n}\sum_{j=1}^{i-1}({}^0\boldsymbol{\gamma}_j \times {}^0\boldsymbol{\gamma}_i)\dot{q}_j\dot{q}_i \\
&= \sum_{i=1}^{n}({}^0\boldsymbol{\omega}_{i-1} \times {}^0\boldsymbol{\gamma}_i\dot{q}_i) \\
&= \sum_{i=1}^{n} {}^0\boldsymbol{\eta}_i \qquad (7.39)
\end{aligned}
$$

In eqs.(7.36) and (7.39), ${}^0\boldsymbol{\omega}_0 = \mathbf{o}$ is considered.

7.4.3 Computation of ID

The Newton-Euler recursive algorithm by Luh et al.[54] is well known as the most efficient algorithm for inverse dynamics. The algorithm is characterized by the fact that the physical values are calculated in the link coordinates. However, for finding the computational duplication, it seems to be more efficient if the physical values are described in the base coordinates, because the computations of DK and IK in the previous subsections are performed in the base coordinates. In this subsection, we formulate a new algorithm of ID by representing the physical values of each link in the base coordinates and transforming the force and moment applied to each link into the equivalent force and moment at the hand tip.

First, the linear and angular accelerations of the i-th link are obtained by the following equation:

$$ {}^0\dot{\boldsymbol{v}}'_i = {}^0\dot{\boldsymbol{v}}'_{i-1} + {}^0\boldsymbol{\beta}_i\ddot{q}_i + {}^0\boldsymbol{\xi}_i \tag{7.40} $$

$$ {}^0\dot{\boldsymbol{\omega}}_i = {}^0\dot{\boldsymbol{\omega}}_{i-1} + {}^0\boldsymbol{\gamma}_i\ddot{q}_i + {}^0\boldsymbol{\eta}_i \tag{7.41} $$

Eqs.(7.40) and (7.41) can be derived from eqs.(7.7), (7.14), (7.21) and (7.22) by regarding $\dot{q}_j = \ddot{q}_j = 0$ for $j = i+1, \ldots, n$. It should be noted that ${}^0\boldsymbol{v}'_i$ is the linear acceleration of the i-th link which reference point is converted to the origin of the n-th link frame. Therefore, ${}^0\dot{\boldsymbol{v}}'_i$ can be interpreted as the linear acceleration of the hand tip when joints from $(i+1)$-th to the n-th are rigidly fixed as shown in **Fig.7.6**. Eqs.(7.40) and (7.41) are mathematically equivalent to the differentiation of eqs.(7.19) and (7.20) with respect to time, but it is not straightforward to derive eqs.(7.40) and (7.41) from these equations.

The linear acceleration at the gravity center of the i-th link is calculated by

$$ {}^0\dot{\hat{\boldsymbol{v}}}_i = {}^0\dot{\boldsymbol{\omega}}_i \times {}^0\hat{\boldsymbol{t}}_i + {}^0\boldsymbol{\omega}_i \times [{}^0\boldsymbol{\omega}_i \times {}^0\hat{\boldsymbol{t}}_i] + {}^0\dot{\boldsymbol{v}}'_i + {}^0\tilde{\boldsymbol{g}}, \tag{7.42} $$

where ${}^0\hat{\boldsymbol{t}}_i$ is the position vector from the origin of the n-th link frame to the gravity center of the i-th link which is calculated as follows:

$$ {}^0\hat{\boldsymbol{t}} = {}^0\hat{\boldsymbol{s}}_i - {}^0\boldsymbol{h}_i \tag{7.43} $$

$$ {}^0\hat{\boldsymbol{s}}_i = {}^0\boldsymbol{A}_i{}^i\hat{\boldsymbol{s}}_i \tag{7.44} $$

The last term of eq.(7.42) is necessary for considering the gravity effect. Accordingly, the equation of motion of the i-th link is represented as follows:

$$ {}^0\boldsymbol{F}_i = m_i {}^0\dot{\hat{\boldsymbol{v}}}_i \tag{7.45} $$

$$ {}^0\boldsymbol{N}_i = {}^0\boldsymbol{A}_i {}^i\widehat{\boldsymbol{I}}_i {}^i\boldsymbol{A}_0 {}^0\dot{\boldsymbol{\omega}}_i + {}^0\boldsymbol{\omega}_i \times [{}^0\boldsymbol{A}_i {}^i\widehat{\boldsymbol{I}}_i {}^i\boldsymbol{A}_0 {}^0\boldsymbol{\omega}_i] \tag{7.46} $$

Eqs.(7.40) through (7.46) are computed recursively from $i = 1$ to n. These equations corresponds to the forward part of the recursive algorithm by Luh et al. Hereafter, the backward part of the algorithm is considered. By representing the backward part of Luh's algorithm in the base coordinates, we obtain

$$ {}^0\boldsymbol{f}_i = {}^0\boldsymbol{f}_{i+1} + {}^0\boldsymbol{F}_i, \tag{7.47} $$

$$ {}^0\boldsymbol{n}_i = {}^0\boldsymbol{n}_{i+1} + {}^0\boldsymbol{p}_i^* \times {}^0\boldsymbol{f}_{i+1} + ({}^0\boldsymbol{p}_i^* + {}^0\hat{\boldsymbol{s}}_i) \times {}^0\boldsymbol{F}_i + {}^0\boldsymbol{N}_i, \tag{7.48} $$

and

$$ \tau_i = \begin{cases} {}^0\boldsymbol{n}_i^T {}^0\boldsymbol{z}_{i-1} + b_i\dot{\theta}_i = {}^0\boldsymbol{n}_i^T {}^0\boldsymbol{\gamma}_i + b_i\dot{\theta}_i & \text{(ifR)} \\ {}^0\boldsymbol{f}_i^T {}^0\boldsymbol{z}_{i-1} + b_i\dot{d}_i = {}^0\boldsymbol{f}_i^T {}^0\boldsymbol{\beta}_i + b_i\dot{d}_i & \text{(ifP)} \end{cases} . \tag{7.49} $$

Of course, it is possible to calculate the joint driving force/torque by using eqs.(7.47) through (7.49). But, we will derive a new algorithm so that it may have more common computations. Let the force ${}^0\boldsymbol{F}_i$ and the moment ${}^0\boldsymbol{N}_i$ exerting on the gravity center of the i-th link be transformed equivalently to the force ${}^0\boldsymbol{F}_i'$ and the moment ${}^0\boldsymbol{N}_i'$ exerting at the origin of the n-th link frame. The relationship is described as follows:

$$ {}^0\boldsymbol{F}_i' = {}^0\boldsymbol{F}_i \tag{7.50} $$

$$ {}^0\boldsymbol{N}_i' = {}^0\boldsymbol{N}_i + {}^0\hat{\boldsymbol{t}}_i \times {}^0\boldsymbol{F}_i \tag{7.51} $$

Then, the equilibrium equations of force and moment at the i-th joint corresponding to eqs.(7.47) and (7.48) are represented as follows:

$$ {}^0\boldsymbol{f}_i = {}^0\boldsymbol{f}_{i+1} + {}^0\boldsymbol{F}_i' \tag{7.52} $$

$$ \begin{aligned} {}^i\boldsymbol{n}_i &= {}^0\boldsymbol{n}_{i+1} + {}^0\boldsymbol{p}_i^* \times {}^0\boldsymbol{f}_{i+1} + {}^0\boldsymbol{h}_{i-1} \times {}^0\boldsymbol{F}_i' + {}^0\boldsymbol{N}_i' \\ &= {}^0\boldsymbol{h}_{i-1} \times {}^0\boldsymbol{f}_i + {}^0\boldsymbol{n}_{i+1} + {}^0\boldsymbol{N}_i' - {}^0\boldsymbol{h}_i \times {}^0\boldsymbol{f}_{i+1} \end{aligned} \tag{7.53} $$

where eq.(7.52) was considered to derive eq.(7.53). When the i-th joint is rotational, the following equation is obtained by substituting eq.(7.53) into eq.(7.49).

$$\begin{aligned}
\tau_i &= {}^0\boldsymbol{\gamma}_i^T({}^0\boldsymbol{h}_{i-1} \times {}^0\boldsymbol{f}_i + {}^0\boldsymbol{n}_{i+1} + {}^0\boldsymbol{N}_i' - {}^0\boldsymbol{h}_i \times {}^0\boldsymbol{f}_{i+1}) \\
&\quad + b_i\dot{\theta}_i \\
&= {}^0\boldsymbol{\gamma}_i^T \left({}^0\boldsymbol{h}_{i-1} \times \sum_{k=i}^{n+1} {}^0\boldsymbol{F}_k' + \sum_{k=i}^{n+1} {}^0\boldsymbol{N}_k' \right) + b_i\dot{\theta}_i \\
&= \left(\sum_{k=i}^{n+1} {}^0\boldsymbol{F}_k' \right)^T ({}^0\boldsymbol{\gamma}_i \times {}^0\boldsymbol{h}_{i-1}) + {}^0\boldsymbol{\gamma}_i^T \sum_{k=i}^{n+1} {}^0\boldsymbol{N}_k' + b_i\dot{\theta}_i \\
&= {}^0\boldsymbol{\beta}_i^T \sum_{k=i}^{n+1} {}^0\boldsymbol{F}_k' + {}^0\boldsymbol{\gamma}_i^T \sum_{k=i}^{n+1} {}^0\boldsymbol{N}_k' + b_i\dot{q}_i \qquad (7.54)
\end{aligned}$$

Similarly, when the i-th joint is prismatic, the following equation is obtained by substituting eq.(7.52) into eq.(7.49).

$$\begin{aligned}
\tau_i &= {}^0\boldsymbol{\beta}_i^T({}^0\boldsymbol{f}_{i+1} + {}^0\boldsymbol{F}_i') + b_i\dot{d}_i \\
&= {}^0\boldsymbol{\beta}_i^T \left(\sum_{k=i}^{n+1} {}^0\boldsymbol{F}_k' \right) + b_i\dot{d}_i \\
&= {}^0\boldsymbol{\beta}_i^T \sum_{k=i}^{n+1} {}^0\boldsymbol{F}_k' + {}^0\boldsymbol{\gamma}_i^T \sum_{k=i}^{n+1} {}^0\boldsymbol{N}_k' + b_i\dot{q}_i \qquad (7.55)
\end{aligned}$$

In eqs.(7.54) and (7.55), the external force ${}^0\boldsymbol{f}_{n+1}$ and moment ${}^0\boldsymbol{n}_{n+1}$ are represented as ${}^0\boldsymbol{F}_{n+1}'$ and ${}^0\boldsymbol{N}_{n+1}'$ respectively. Both eqs.(7.54) and (7.55) can be regarded that the i-th element of the joint driving force/torque vector calculated by the following equation:

$$\boldsymbol{\tau} = \boldsymbol{J}^T[\ {}^0\boldsymbol{F}_i^{*T}\ \ {}^0\boldsymbol{N}_i^{*T}\ ]^T + \mathrm{diag}(b_i)\dot{\boldsymbol{q}} \qquad (7.56)$$

where ${}^0\boldsymbol{F}_i^*$ and ${}^0\boldsymbol{N}_i^*$ are defined by

$${}^0\boldsymbol{F}_i^* = \sum_{k=i}^{n+1} {}^0\boldsymbol{F}_k', \qquad (7.57)$$

$${}^0\boldsymbol{N}_i^* = \sum_{k=i}^{n+1} {}^0\boldsymbol{N}_k'. \qquad (7.58)$$

Eq.(7.56) is similar to the static relation between the external force/moment and joint force/torque. Eq.(7.56) can be interpreted as the computation of the balancing force/torque at the i-th joint against the external force/moment ${}^0\boldsymbol{F}_i^*$ and ${}^0\boldsymbol{N}_i^*$ exerted at the hand tip in addition to the viscous friction term at the joint axis. The force/moment ${}^0\boldsymbol{F}_i^*$ and ${}^0\boldsymbol{N}_i^*$ changes their values as the subscript i decreases from n to 1. This situation corresponds to the fact that the total force and moment at a link are supported only by the lower joints than that link. From eqs.(7.54) through (7.58), the i-th joint force/torque is calculated by the following equations:

$$\tau_i = {}^0\boldsymbol{\beta}_i^T {}^0\boldsymbol{F}_i^* + {}^0\boldsymbol{\gamma}_i^T {}^0\boldsymbol{N}_i^* + b_i\dot{q}_i \tag{7.59}$$

$${}^0\boldsymbol{F}_i^* = {}^0\boldsymbol{F}_{i+1}^* + {}^0\boldsymbol{F}_i' \tag{7.60}$$

$${}^0\boldsymbol{N}_i^* = {}^0\boldsymbol{N}_{i+1}^* + {}^0\boldsymbol{N}_i' \tag{7.61}$$

The initial conditions of eqs.(7.60) and (7.61) are ${}^0\boldsymbol{F}_i^* = {}^0\boldsymbol{f}_{n+1}$ and ${}^0\boldsymbol{N}_i^* = {}^0\boldsymbol{n}_{n+1}$ respectively. The proposed algorithm of ID is the computation using eqs.(7.50), (7.51), and (7.59) through (7.61) instead of (7.47) through (7.49). In this new algorithm, the Jacobian matrix can be used again at the backward part of the ID computation. The computational process is shown in **Fig.7.3**(e).

7.4.4 Consideration of Computational Duplication

In **Fig.7.3**, the equations marked by * mean the equations already calculated in the previous computations. Therefore, they can be regarded as the computational duplication. The basic idea of the unified computation is to eliminate these duplicated calculation marked by *, when DK, IK and ID are computed at the same time in the dynamic control.

Another remarkable point of the proposed unified recursive algorithm is that most of the equations in the algorithms can be used commonly whichever the joint type is rotational or prismatic. Only the differences of the algorithm exist in eqs.(7.15) and (7.16). This characteristic makes easy to code the program for computers especially for the digital signal processors where only low level languages are available.

Table 7.1: The numbers of computations and the duplicated computations†

	Mul.	Add.
${}^0\boldsymbol{r}_p, {}^0\boldsymbol{A}_n$	$34n - 24$	$21n - 18$
$\boldsymbol{J}$	$6n + (34n) + (-24)$	$3n + (21n) + (-18)$
$\dot{\boldsymbol{r}}$	$6n + (40n) + (-24)$	$6n + (24n) - 6 + (-18)$
$\dot{\boldsymbol{J}}\dot{\boldsymbol{q}}$	$12n + (46n) - 6 + (-24)$	$15n + (27n) - 15 + (-21)$
ID	$100n + (58n) - 6 + (-30)$	$91n + (36n) - 16 + (-27)$
ID(Luh)	$129n + (4n) - 18$	$106n - 20$
Total	$158n + (138n) - 36 + (-78)$	$136n + (84n) - 55 + (-66)$
Total(Luh)	$187n + (84n) - 48 + (-48)$	$151n + (48n) - 59 + (-39)$

Rotational joint only, n: DOF, † $n \geq 3$
( ): duplicated computation
Total: using ID, Total(Luh): using ID(Luh)

7.5 Discussion on the Number of Computations

In this section, we show the number of computations necessary for the algorithms proposed in the previous sections and discuss the effect of eliminating the duplicated computation.

Table 7.1 shows the number of arithmetic operations for performing the proposed algorithms, where Add. means the number of additions and subtractions and Mul. means the number of multiplications. And ID indicates the algorithm for inverse dynamics proposed in the previous section and ID(Luh) indicates the recursive Newton-Euler algorithm proposed by Luh et al.[54]. In the table, the numbers with parentheses imply the numbers of duplicated arithmetic operations, and Total and Total(Luh) mean the total number of arithmetic operations corresponding with ID and ID(Luh). In the evaluation of total number of operations, duplicated operations between the computations of $\dot{\boldsymbol{r}}$ and Jacobian matrix are always eliminated because the algorithm of $\dot{\boldsymbol{r}}$ is based on eq.(7.6) and the duplication with the computation of

Table 7.2: Number of arithmetic operations (Mul. and Add.) for $n = 6$

	Mul.		Add.	
	Total	Total(LUh)	Total	Total(Luh)
Case A	1,662	1,530	1,199	1,096
Case B	912	1,074	761	847
Case C	704	630	606	457

Total : using ID
Total(Luh) : using ID(Luh)
Case A : including duplication
Case B : excluding duplication
Case C : excluding duplication and considering $\alpha_i = 0°$ or $\pm 90°$ for the PUMA type manipulators

Jacobian matrix itself is obvious. From the table, one can find that the number of computations for DK, IK, and ID are efficiently reduced by eliminating the duplication. The proposed algorithm for ID requires more computations than the recursive algorithm by Luh et al. when only ID is calculated. However, it has much computational duplication with DK and IK, and the total number of computations becomes smaller than the total number when Luh's algorithm is used.

As for the computation of $\dot{\boldsymbol{J}}\dot{\boldsymbol{q}}$, it can be conventionally obtained from the computation of the hand tip acceleration ${}^n\ddot{\boldsymbol{r}} = [\ {}^n\dot{\boldsymbol{v}}_n^T \quad {}^n\dot{\boldsymbol{\omega}}_n^T\ ]^T$ when $\ddot{\boldsymbol{q}} = \boldsymbol{0}$ and its transformation into the base coordinates, considering eq.(7.7), in the forward part of recursive algorithm of inverse dynamics[60]. Using the method proposed by Mudge et al.[60], it is required 372 multiplications and 306 additions when $n = 6$. On the other hand, the algorithm proposed here requires 318 multiplications and 216 additions where Jacobian matrix can be calculated simultaneously. Therefore, the proposed algorithm of $\dot{\boldsymbol{J}}\dot{\boldsymbol{q}}$ itself is also efficient.

Table 7.2 shows the total number of arithmetic operations in the case when $n = 6$. Case A is the case where the duplicated computations are included. Case B is the case where the duplicated computations are eliminated, and Case C is the case where the duplicated computation

are eliminated and the algorithm is customized for the PUMA type manipulators by considering $\alpha_i = 0°$ or $\pm 90°$. It should be noted that the number of computations of eq.(7.8) for obtaining $\ddot{\boldsymbol{q}}_{adj}$ is not included. The number of computations of eq.(7.8) is evaluated, for example, as 139 multiplications, 6 divisions and 127 additions when $n = 6$ using eq.(7.10) for orientational error representation and Gaussian elimination is applied. **Fig.7.7** is the graph of **Table 7.2**. In the Case B, the total number of computations when the proposed algorithm of ID is used becomes smaller than when the ID algorithm by Luh et al.[54] is used. Comparing to the Case A, the total number of computations can be reduced by 42% multiplications and 33% additions without customizing the algorithms when the duplication is eliminated.

The number of computations becomes smaller when the algorithms are customized for the PUMA type manipulators by considering $\alpha_i = 0°, \pm 90°$ in the Case C. It is interesting that the total number of computations becomes smaller when the ID algorithm by Luh et al. is used than the case when the proposed ID algorithm is used. The reason is explained as follows. While the proposed algorithm uses ${}^0\boldsymbol{A}_i$ and ${}^0\boldsymbol{p}_i^*$ often, the algorithm by Luh et al. uses ${}^{i-1}\boldsymbol{A}_i$ and ${}^i\boldsymbol{p}_i^*$ some of which elements become 1 or 0 by considering $\alpha_i = 0°$ or $\pm 90°$, and the number of computations is reduced. It should be noted that the unified computation is applied to the computations for kinematics even in this case and the duplication in the kinematic computations is eliminated.

7.6 Conclusion

We proposed a unified recursive formulation for DK, IK and ID which are necessary for dynamic trajectory control and dynamic force control of robot manipulators. Among the formulation, the algorithms of $\dot{\boldsymbol{J}}\dot{\boldsymbol{q}}$ and ID are new algorithms. Especially, the algorithm of $\dot{\boldsymbol{J}}\dot{\boldsymbol{q}}$ is efficient even for individual use.

The computational complexity of dynamic control of robot manipulators was reduced by eliminating the duplicated computations in the algorithms. It was shown that 42% of multiplications and 33% of additions are reduced for 6 DOF manipulators. If we assume that the operation time for multiplication and for addition are equal, the total

number of operations for 6 DOF manipulators becomes 1673, and finally, it becomes 1945 by including the computation of (v) which was omitted in this chapter. Therefore, it seems to be possible to perform the dynamic control in $2 \sim 4$ msec if a computer which can execute one operation in $1 \sim 2$ μsec, that is, $0.5 \sim$ 1MFLOPS, is used.

The reduction of the computation in Case B shown in this chapter was realized without customizing algorithms. It indicates that these algorithms are useful for the computation of kinematics and dynamics for any kind of master and slave arms. It would also be useful for developing versatile robot controllers or dynamic simulators which can treat any type of robot manipulators without changing software.

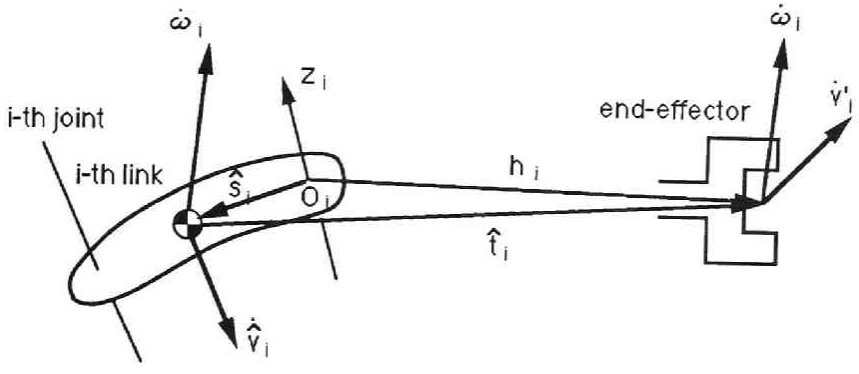

Figure 7.6: Translational acceleration of the i-th link which reference point is converted to the hand tip

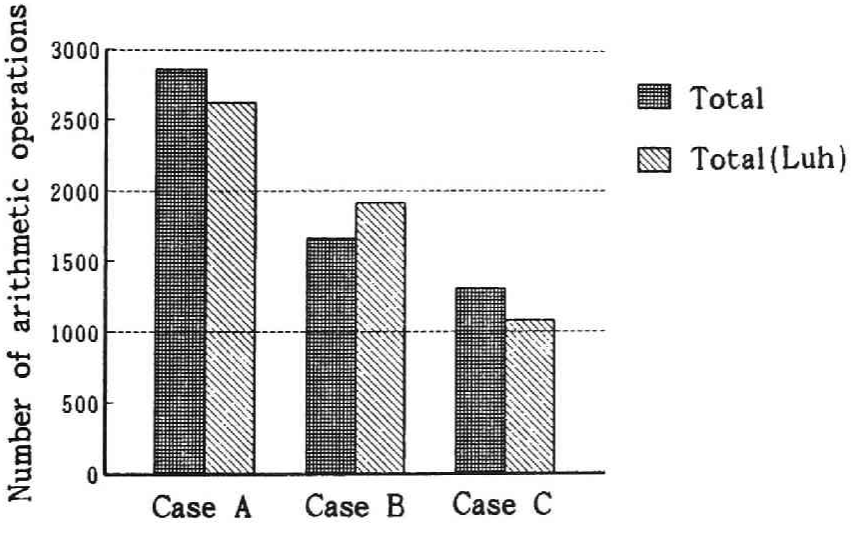

Figure 7.7: Number of arithmetic operations (Add. and Mul.) for $n = 6$

Chapter 8

APPLICATION OF A FLOATING-POINT DSP TO REAL TIME COMPUTATION OF MANIPULATOR CONTROL

8.1 Introduction

In chapter 5, we have shown that the ideal response can be achieved if the dynamic control scheme is applied to both the master and slave arms. In order to realize the dynamic control, it is necessary to execute a huge amount of computations in real time.

Many studies have been done in order to reduce the number of computations. One of the ways to reduce the number of computations is to formulate an efficient computational algorithm. In chapter 7, the unified computational algorithm of kinematics and dynamics was proposed where the duplication of computations is eliminated among DK, IK and ID which must be computed at the same time for the dynamic control to follow a desired trajectory in Cartesian space (resolved acceleration

control[55]).

Even if these efficient algorithms were introduced, it would be difficult for a conventional 16-bit microcomputer in the 8086/8087 class to perform the on-line computation, therefore high speed computers are required. Parallel computation[56] is one of the typical approaches to realize high speed computation with low cost.

In this chapter, the utilization of a floating-point DSP to manipulator control is discussed. The first generation of DSP was based on the fixed-point arithmetic, and a "scaling procedure" was required to avoid large round-off errors in the numerical results. LSI technology advances very rapidly, and recently low-cost floating-point DSPs become commercially available. The floating-point arithmetic eliminates the scaling problem. Mayeda et al.[57] applied a floating-point DSP to the computation of the resolved acceleration control (RAC) of manipulators and showed that its computation time was sufficiently fast (330[μs] for 6 DOF manipulators). However, they treated only the manipulators with parallel or perpendicular rotational joints. Takanashi[82] applied a floating-point DSP to the computation of stiffness control of manipulators.

In this chapter, a 32-bit floating-point DSP (μPD 77230 developed by NEC Corp.) is used for all of the computations required for the resolved acceleration control. To reduce the total number of computations, the unified computational algorithm proposed in chapter 7 is used. It is confirmed that the total computational time for RAC except trigonometric functions becomes 1.06[ms] for a general 6 DOF manipulator.

8.2 Utilization of Floating-Point DSP

8.2.1 μPD77230 Floating-Point DSP

μPD77230 is a floating-point digital signal processor developed by NEC Corporation in 1985. Its specification is shown in **Table 8.1** and its inside block diagram is shown in **Fig.8.1**[65]. μPD77230 has two inner RAMs and a hardware logic floating-point multiplier. The multiplier can execute in parallel with other operation units such as ALU (Arith-

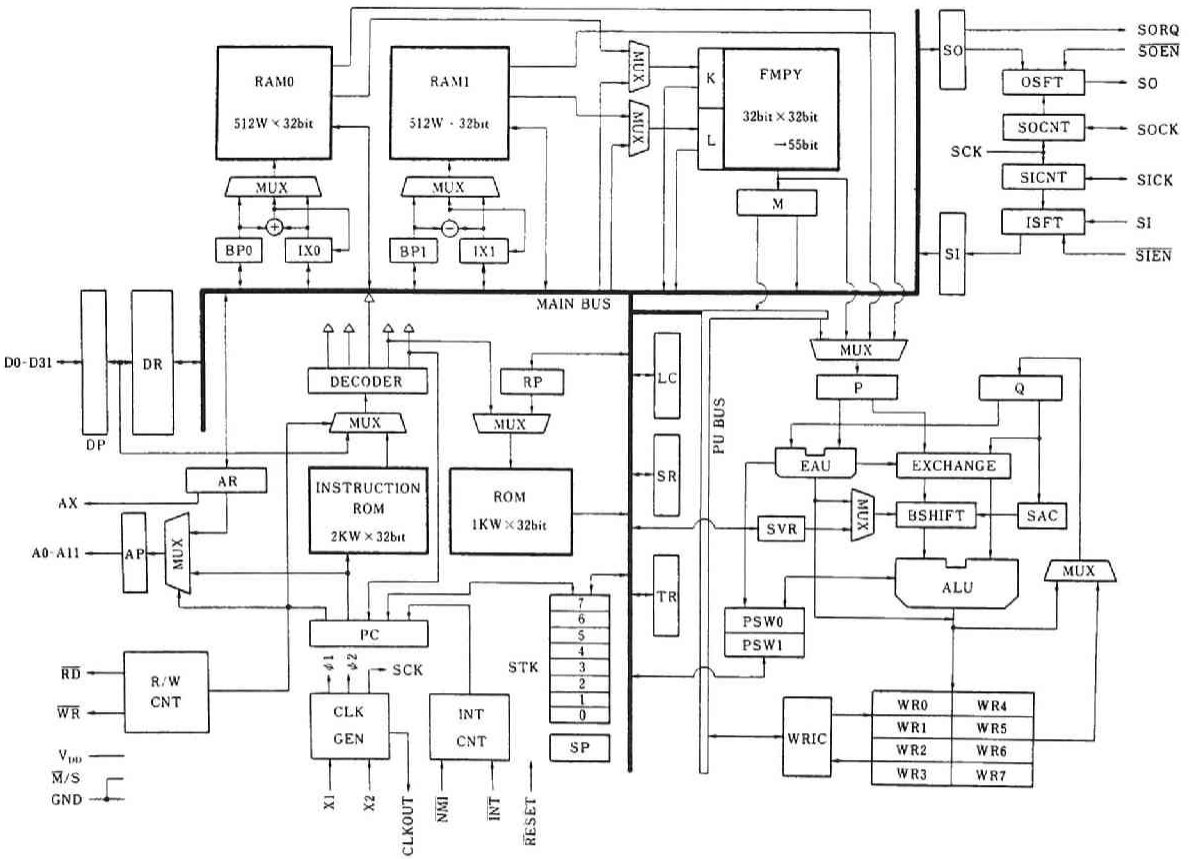

Figure 8.1: Block diagram of μPD77230[65]

Table 8.1: Specification of μPD77230

data length	32-bit floating-point (8-bit exponent + 24-bit mantissa)
instruction cycle	150[ns]
multiplier	(8-bit+24-bit) × (8-bit+24-bit) ⟶ (8-bit+47-bit)
Processing Unit	ALU: 47-bit EAU: 8-bit Barrel Shifter: 47-bit Working Register: 55-bit × 8
RAM	(512[wd] × 32-bit) × 2
external memory	maximum 8[kwd] × 32-bit (4[kwd] for instructions)

metic Logic Unit), and multiply/accumulate operations can be performed very efficiently. μPD77230 has several data buses such as Main Bus, PU Bus and the bus between the RAM and multiplier which realize the parallel data moves. **Fig.8.2** shows an example of the program code for vector product by μPD77230. In one step line, it is possible to describe at most three kinds of operations. In the left side column, arithmetic and logic operations can be specified. In the middle column, "move" operation can be specified, and in the right side column, the management of RAM pointer for RAM addressing can be specified.

At coding the program for μPD77230, it should be noted that the operations are executed in three-stage pipeline process (fetch, decode and execute). Therefore, the result of an operation can be obtained two steps later. Since μPD77230 uses a special data format, data conversion is necessary when the data move is required between μPD77230 and the host computer which uses IEEE format.

8.2.2 Evaluation System

For performance evaluation of the DSP, a commercially available DSP board was used. This board can be inserted into the extension slot

```
ldi     ix0,a_vec                                                   ;
ldi     ix1,b_vec                                                   ;
ldi     bp0,c_vec                                                   ;
nop                                             spcix0  spcix1      ;
clr     wr0                                     incix0  incix1      ;
clr     wr1                                             incix1      ;
clr     wr2     mov     lkr0,ram1       incix0  decix1              ;
addf    wr0,m   mov     lkr0,ram1               decix1              ;
subf    wr0,m   mov     lkr0,ram1       decix0  incix1              ;
norm    wr0                             decix0  incix1              ;
addf    wr1,m   mov     lkr0,ram1               decix1              ;
subf    wr1,m   mov     lkr0,ram1       incix0  decix1              ;
norm    wr1                                                         ;
addf    wr2,m   mov     lkr0,ram1       incix0  incix1              ;
subf    wr2,m                           incix0  incix1 spcbp0       ;
norm    wr2     mov     ram0,wr0        incbp0  incix1              ;
nop             mov     ram0,wr1        incbp0                      ;
nop             mov     ram0,wr2                                    ;
nop                                                                 ;
```

arithmetic operation — "move" operation — addressing and others

Figure 8.2: Example of Program Code of μPD77230

of the personal computer (NEC PC-9801 series) that is used for a host computer. The developed program by the host computer is downloaded to the DSP board. The DSP board has a shared memory of 128kbyte which is accessible by both the DSP and the host computer, and can be used for data moves. In our evaluation system, a personal computer with 80386 CPU (20MHz) is used for the host computer.

8.3 Implementation

8.3.1 Programming

The resolved acceleration control using unified computation proposed in chapter 7 was implemented on μPD77230. Programming language is μPD77230 Macro Assembler.

The computation of the resolved acceleration control is described as follows:

$$\ddot{\boldsymbol{q}}_{adj} = \boldsymbol{J}^{\#}(\ddot{\boldsymbol{r}}_d + \boldsymbol{K}_1(\dot{\boldsymbol{r}}_d - \dot{\boldsymbol{r}}) + \boldsymbol{K}_2(\boldsymbol{r}_d - \boldsymbol{r}) - \dot{\boldsymbol{J}}\dot{\boldsymbol{q}}) \tag{8.1}$$

$$\boldsymbol{\tau} = \boldsymbol{F}_{ID}(\boldsymbol{q}, \dot{\boldsymbol{q}}, \ddot{\boldsymbol{q}}_{adj}, \boldsymbol{f}_{ext}, \boldsymbol{n}_{ext}) \tag{8.2}$$

At first, $\ddot{\boldsymbol{q}}_{adj}$ is obtained by eq.(8.1). The joint driving force $\boldsymbol{\tau}$ to realize $\ddot{\boldsymbol{q}}_{adj}$ is then obtained by eq.(8.2) (Inverse dynamics) where $\boldsymbol{f}_{ext}$ and $\boldsymbol{n}_{ext}$ denote the external force and moment exerted at the hand tip respectively.

For coding the program, all the data areas were assigned to two inner RAM. Multiplication between the two inner RAMs can be performed efficiently, because each RAM data can be moved to the multiplier in parallel. Therefore, each data area should be assigned carefully to either RAM so that two data can go to the multiplier in parallel at each multiplication operation. Moreover, since μPD77230 has only four RAM pointers, each data area should be assigned to each RAM so that these RAM pointers can be used efficiently at each addition operation.

The unified computation was programmed in a recursive manner so that any DOF is available. The program size is about 3kwords. But the capacity of the inner RAM restricts up to 9 DOF. The computation of $\boldsymbol{J}^{\#}$ was replaced by Gaussian Eliminations supposing that the Jacobian

Table 8.2: Computation Time for RAC by μPD77230

Unified Computation	Kinematics	0.20[ms]
	ID	0.33[ms]
Gaussian elimination		0.20[ms]
Data conversion		0.15[ms]
Data move		0.18[ms]
Total		1.06[ms]

matrix is square. Computation by the DSP is realized as the following function-call from the host computer.

$$\text{unify}([\sin\theta_i],[\cos\theta_i],\dot{\boldsymbol{\theta}},{}^0\boldsymbol{f}_{ext},{}^0\boldsymbol{n}_{ext},\boldsymbol{r}_{pd},{}^0\boldsymbol{A}_{nd},\dot{\boldsymbol{r}}_d,\ddot{\boldsymbol{r}}_d,\boldsymbol{\tau});$$

where the present status (the joint position is given by the form of trigonometric functions) and the external force/moment at the hand tip, the desired trajectory (orientation component is given by the orientation matrix) are given and the joint torque vector is returned.

The program is only for manipulators with rotational joints. But, as mentioned in chapter 7, the extension for prismatic joints is possible by only changing the part of the Jacobian matrix computation. And there is no restriction of twist angle of the joint axes.

8.3.2 Computation Time

The execution time for 6 DOF general manipulators was measured actually, and it was 1.06[ms] for one cycle, that would be sufficient speed for the real time computation. **Table 8.2** shows the details of the computation time. It shows that the data moves between the DSP and host computer and the data conversions take much time.

8.3.3 Discussion about Computational Efficiency

The machine cycle of μPD77230 is 150[ns]. If floating-point operations are executed in every cycle, the computational performance becomes

6.67[Mflops]. The peak performance becomes 13.3[Mflops] when multiply/accumulation operations are executed in every cycle where addition and multiplication operations can be computed in parallel.

According to the result of chapter 7, the number of computations for the resolved acceleration control of 6 DOF manipulators is about 2000 additions and multiplications. If the peak performance of 13.3[Mflops] is realized, it can be executed in 150[μs], and even if the performance of 6.67[Mflops] is realized, it can be executed in 0.3[ms].

However, even though we pick up the pure computational parts from **Table 8.2** except the data moves and data conversion, it actually becomes 0.75[ms]. It means that the rate of the pure arithmetic operations in the coded program is only 20% of the peak performance and 40% of the case when either addition or multiplication is executed in every step. The remainder was spent just for data moves and other operations. **Table 8.2** shows that the gaussian elimination takes much time considering the required number of computations. The reason is that the Gaussian elimination contains division operations and a partial pivoting strategy in order to avoid the numerical difficulties at divisions, and these operations at the DSP requires many steps including not only the arithmetic operations but also some other operations.

The required operation except floating-point arithmetic are data moves, normalization, loop processing and data addressing by RAM pointers. Especially, since only two variables can be access in each RAM, it is necessary to save the intermediate result to inner RAM when the calculation is related with many variables, and it spoils the computational efficiency. The time required for data moves and data conversion is also much. Direct input/output of data between the DSP and the manipulator would be better than moving the data through the host computer.

Consequently, the following points would be recommended for DSP architecture in order to improve the computational efficiency.

- More addressing mode of RAM and more RAM pointers (μPD-77230 has only the indirect addressing mode using RAM pointers and has only four pointers.)

- Perfect parallel processing between the arithmetic operations and

data addressing including immediate data loading to the RAM pointers

- Plural data buses between the inner RAMs and the processing units which make possible both loading the next data and saving the previous result at the same time

The improvement of computational efficiency means the improvement of parallelism, and it is unavoidable that the programming becomes complicated more. It depends on the quality of the architecture design of DSP how the computational efficiency can be improved without making the programming style difficult.

8.4 Conclusion

The resolved acceleration control using the unified computation was implemented on floating-point DSP μPD77230. The evaluated execution time was 1.06[ms] for 6 DOF rotational joint manipulators. This would be a sufficient performance for the real time computation. Application of DSP makes possible the real time computation of the uncustomized algorithm where there is no restriction about the twist angle of joint axes. Although we treated manipulators with only rotational joints, it is easy to include the case of prismatic joints as shown in chapter 7.

The utilization of floating-point DSPs solves the scaling problem completely. However, efficiency of the computation is still low comparing to the peak performance of the DSP. DSP was originally designed for digital filtering, and it was not supposed to treat many variables at the same time. It would be desirable to develop a new DSP which has suitable architecture for the manipulator control.

Chapter 9

ON A LINK COORDINATE FRAME ASSIGNMENT FOR SERIAL LINK ROBOT MANIPULATORS

9.1 Introduction

For improving the computational efficiency for the manipulator control, the assignment of link frames is discussed in this chapter. For formulating the kinematics and dynamics of robot manipulators, it is usually necessary to assign a coordinate frame to each link of the manipulator. Well known methods for assigning the link frames are Denavit-Hartenberg (D.H.) method[18] and Craig's method[17].

In this chapter, four types of link frame assignment are defined and the efficiency of assignment is evaluated by the number of computations for the inverse dynamics problem. Lastly, the concept of optimal link frame assignment is proposed.

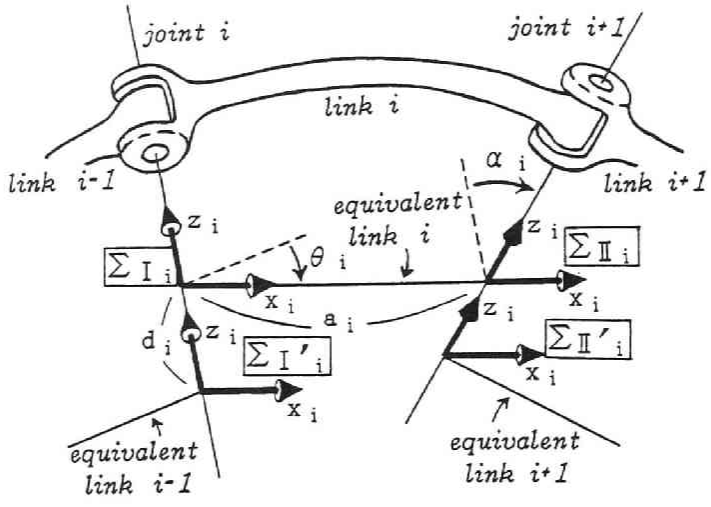

Figure 9.1: Four types of link frames assignment

9.2 Link Coordinate Frames

9.2.1 Four Types of Link Frame Assignment

In the case of serial link manipulators, the kinematic relations can be described by four parameters which are well known as the link parameters in D.H. notation[18][69]. These are *link length* a_i, *twist angle* α_i, *joint length* d_i, and *joint angle* θ_i as shown in **Fig.9.1**.

The efficiency of the D.H. assignment method comes from the following points: (i) z-axis of the frame is aligned with the joint axis; (ii) origin of the frame is set at the cross point between the joint axis and common normal of the joint axes; (iii) x-axis is parallel to the common normal. There are four types of link frames including the D.H. method, which satisfy these three conditions.

For convenience, let a segment between joint i and $i+1$ from the common normal of these two joint axes be called the *equivalent link i*. As shown in **Fig.9.1**, the four types of frames are as follows:

Frame Σ_{I_i}: z-axis is parallel to the joint axis i and the origin is set at the end point of the equivalent link i on the joint axis i;

Frame $\Sigma_{\mathrm{I}'_i}$: z-axis is parallel to the joint axis i and the origin is set at the end point of the equivalent link $i-1$ on the joint axis i;

Frame Σ_{II_i}: z-axis is parallel to the joint axis $i+1$ and the origin is set at the end point of the equivalent link i on the joint axis $i+1$;

Frame $\Sigma_{\mathrm{II}'_i}$: z-axis is parallel to the joint axis $i+1$ and the origin is set at the end point of the equivalent link $i+1$ on the joint axis $i+1$.

Among these link frames, the D.H. method corresponds to Σ_{II_i} and the assignment method defined by Craig[17] corresponds to Σ_{I_i}. It should be noted that $\Sigma_{\mathrm{I}'_i}/\Sigma_{\mathrm{II}'_i}$ cannot be assigned when joint $i/i+1$ is a prismatic joint because the link i frame must be fixed at the link i.

9.2.2 Special Management for Parallel and Prismatic Joints

One of the features of the D.H. assignment method is the efficient management in two cases when the joint is prismatic and when the joint is parallel with the neighboring joint. When the joints i and $i+1$ are parallel, there are infinite number of common normals between them. Two efficient managements are possible in this case.

[Forward/Backward management for parallel joints i and $i+1$]
The equivalent link i is chosen so that $d_i = 0/d_{i+1} = 0$.

The meaning of forward/backward is that the link frames are fixed from the end-effector link to the base link in the case of backward management, whereas the link frames are fixed from the base link to the end link in the case of forward management.

When the joint i is prismatic, the kinematic relation does not change wherever the joint may be moved, as long as the direction of the joint axis is kept in the original direction. Therefore, there are two efficient management for prismatic joints.

[Forward/Backward management for prismatic joints i]

The position of the joint i is moved so that $a_{i-1} = 0/a_i = 0$, $d_{i-1} = 0/d_{i+1} = 0$.

It should be noted that since the joint distance of a prismatic joint is variable, one cannot apply the special management to make this distance zero in both of the above managements. The D.H. assignment method is employing backward managements for both parallel and prismatic joints[69]. The Craig's method is not described specifically but it is employing forward management for both cases[17].

9.3 Evaluation of Computational Efficiency

Rotational transformation from $\Sigma_{X_{i-1}}$ to Σ_{X_i} $(X = \mathrm{I}, \mathrm{I}', \mathrm{II}, \mathrm{II}')$ can be regarded as the combination of θ_i rotation around z-axis and $\alpha_i(\alpha_{i-1})$ rotation around x-axis in all cases. Therefore, the number of computations for rotational transformation are equal.

For position transformation, the relative position vector from the origin of $\Sigma_{X_{i-1}}$ to the origin of Σ_{X_i}, $\boldsymbol{p}_i^*$, is given in each case as follows:

In case of Σ_{I_i}:

$$^{i-1}\boldsymbol{p}_i^* = [\ a_{i-1} \quad -d_i S_{\alpha(i-1)} \quad d_i C_{\alpha(i-1)}\ ]^T; \tag{9.1}$$

In case of $\Sigma_{\mathrm{I}'_i}$:

$$^{i-1}\boldsymbol{p}_i^* = [\ a_{i-1} \quad 0 \quad d_{i-1}\ ]^T; \tag{9.2}$$

In case of Σ_{II_i}:

$$^{i}\boldsymbol{p}_i^* = [\ a_i \quad d_i S_{\alpha(i)} \quad d_i C_{\alpha(i)}\ ]^T; \tag{9.3}$$

In case of $\Sigma_{\mathrm{II}'_i}$:

$$^{i}\boldsymbol{p}_i^* = [\ a_i \quad 0 \quad d_{i+1}\ ]^T, \tag{9.4}$$

where $S_{\alpha(i)}$ and $C_{\alpha(i)}$ mean $\sin\alpha_i$ and $\cos\alpha_i$ respectively. The left superscript of $\boldsymbol{p}_i^*$ represents the coordinates which describes this vector. In eqs.(9.1) through (9.4), the superscript (i or $i-1$) was chosen so that it does not contain θ_i.

Table 9.1: Comparison of the number of computations for inverse dynamics

	ADD.		MUL.	
Σ_{I_i}	$96n-83$	(493)	$122n-92$	(640)
$\Sigma_{I'_i}$	$90n-77$	(463)	$116n-87$	(609)
Σ_{II_i}	$106n-44$	(592)	$133n-44$	(754)
$\Sigma_{II'_i}$	$98n-42$	(546)	$126n-42$	(714)

Rotational joint only, n: DOF, ( ): when $n=6$

Inverse dynamics (ID) problem is one of the representative computations for manipulator control. **Table 9.1** shows the number of computations for the inverse dynamics algorithm proposed by Luh et al.[54] using the four types of link frames. It is noticeable that only the change of link frame assignment affects the computational efficiency. From this result, $\Sigma_{I'_i}$ is the most efficient.

9.4 Optimal Link Coordinate Frame

The efficiency of $\Sigma_{I'_i}$ comes from the fact that one element of $\boldsymbol{p}_i^*$ is always zero and the origin of the frame is located at the end of the equivalent link i, near side to the base frame. The frame Σ_{I_i} also satisfies the second condition. Therefore, considered the first condition, it would be possible to reduce the number of computations by assigning each link frame so that as much elements of $\boldsymbol{p}_i^*$ become zero as possible. Hereafter, we will not fix the assignment rules but choose an appropriate combination between Σ_{I_i} and $\Sigma_{I'_i}$ and also between forward/backward managements. We call this special assignment the optimal frame in the sense that number of zero elements of $\boldsymbol{p}_i^*$ is maximum.

By combining Σ_{I_i} and $\Sigma_{I'_i}$, we obtain $\boldsymbol{p}_i^*$ as follows:

From $\Sigma_{I_{i-1}}$ to Σ_{I_i}:

$$ {}^{i-1}\boldsymbol{p}_i^* = [\ a_{i-1} \quad 0 \quad 0\ ]^T; \tag{9.5} $$

From $\Sigma_{I'_{i-1}}$ to Σ_{I_i}:

$$^{i-1}\boldsymbol{p}_i^* = [\ a_{i-1} \quad -d_i S_{\alpha(i-1)} \quad d_{i-1} + d_i C_{\alpha(i-1)}\ ]^T. \tag{9.6}$$

The Optimal link frame is obtained by the following steps:

(STEP 1) If the manipulator has prismatic joints in a series of m joints from the joint $j+1$ to $j+m$, set appropriate k among $0 \leq k \leq m$ and apply the forward management to the joints from $j+1$ to $j+k$, that is, move these joints together to the origin of the link j frame, and apply the backward management to the joints from $j+k+1$ to $j+m$, that is, move these joints together to the origin of the link $j+m+1$;

(STEP 2) If the manipulator has parallel joints in a series of m' joints from the joint $j'+1$ to $j'+m'$, set appropriate k' among $0 \leq k' \leq m'$ and apply the forward management to the equivalent links from $j'+1$ to $j'+k'$, and apply the backward management to the equivalent links from $j'+k'+1$ to $j'+m'$;

(STEP 3) Up to the step 2, three parameters, a_i, α_i, d_i can be fixed which determine $^{i-1}\boldsymbol{p}_i^*$. But d_i at prismatic joints is variable and will be regarded as nonzero. Then, choose Σ_{I_i} or $\Sigma_{I'_i}$ at each link and obtain $^{i-1}\boldsymbol{p}_i^*$;

(STEP 4) Choose a set of $^{i-1}\boldsymbol{p}_i^*$ $(i = 1 \ldots n)$ which has the most zero elements among the all combinations obtained from the above steps.

Tables 9.2 and **9.3** show the combinations of $^{i-1}\boldsymbol{p}_i^*$ set obtained in the step 3 and the number of computations for ID in case of the PUMA type manipulator and the Stanford type manipulator respectively. In the both tables, type I corresponds to the Craig's assignment method, but there are more efficient assignments which require less number of computations, such as type IV (backward for parallel joint, Σ_{I_i} $(i = 1 \sim 3, 5, 6)$ $\Sigma_{I'_i}$ $(i = 4)$) in the case of the PUMA type, and type III (forward for prismatic joint and backward for parallel joint, Σ_{I_i} $(i =$

Table 9.2: Combination of ${}^{i-1}\boldsymbol{p}_i^*$ for the PUMA type manipulator and the number of computations for ID

Type	${}^1\boldsymbol{p}_2^*$	${}^2\boldsymbol{p}_3^*$	${}^3\boldsymbol{p}_4^*$	${}^4\boldsymbol{p}_5^*$	N	ADD.	MUL.
I	$[\ 0\ \ 0\ \ 0\ ]^T$	$[\ *\ \ 0\ \ *\ ]^T$	$[\ *\ \ *\ \ 0\ ]^T$	$[\ 0\ \ 0\ \ 0\ ]^T$	8	343	429
II	$[\ 0\ \ 0\ \ 0\ ]^T$	$[\ *\ \ 0\ \ *\ ]^T$	$[\ *\ \ 0\ \ 0\ ]^T$	$[\ 0\ \ 0\ \ *\ ]^T$	8	344	431
III	$[\ 0\ \ 0\ \ 0\ ]^T$	$[\ *\ \ 0\ \ 0\ ]^T$	$[\ *\ \ *\ \ *\ ]^T$	$[\ 0\ \ 0\ \ 0\ ]^T$	8	343	427
IV	$[\ 0\ \ 0\ \ 0\ ]^T$	$[\ *\ \ 0\ \ 0\ ]^T$	$[\ *\ \ 0\ \ *\ ]^T$	$[\ 0\ \ 0\ \ *\ ]^T$	8	345	431
V	$[\ 0\ \ *\ \ 0\ ]^T$	$[\ *\ \ 0\ \ 0\ ]^T$	$[\ *\ \ *\ \ 0\ ]^T$	$[\ 0\ \ 0\ \ 0\ ]^T$	8	338	428
VI	$[\ 0\ \ *\ \ 0\ ]^T$	$[\ *\ \ 0\ \ 0\ ]^T$	$[\ *\ \ 0\ \ 0\ ]^T$	$[\ 0\ \ 0\ \ 0\ ]^T$	8	334	420

$*$ means non zero
${}^0\boldsymbol{p}_1^*$ and ${}^5\boldsymbol{p}_6^*$ are $[\ 0\ \ 0\ \ 0\ ]^T$ for every type
N: number of zeros

Table 9.3: Combination of ${}^{i-1}\boldsymbol{p}_i^*$ for the Stanford manipulator and the number of computations for ID

Type	${}^1\boldsymbol{p}_2^*$	${}^2\boldsymbol{p}_3^*$	${}^3\boldsymbol{p}_4^*$	${}^4\boldsymbol{p}_5^*$	N	ADD.	MUL.
I	$[\ 0\ \ 0\ \ 0\ ]^T$	$[\ 0\ \ x\ \ 0\ ]^T$	$[\ *\ \ 0\ \ *\ ]^T$	$[\ 0\ \ 0\ \ 0\ ]^T$	9	336	423
II	$[\ 0\ \ 0\ \ 0\ ]^T$	$[\ 0\ \ x\ \ 0\ ]^T$	$[\ *\ \ 0\ \ 0\ ]^T$	$[\ 0\ \ 0\ \ *\ ]^T$	9	337	425
III	$[\ 0\ \ 0\ \ 0\ ]^T$	$[\ 0\ \ x\ \ 0\ ]^T$	$[\ *\ \ 0\ \ 0\ ]^T$	$[\ 0\ \ 0\ \ 0\ ]^T$	10	329	415
IV	$[\ 0\ \ 0\ \ 0\ ]^T$	$[\ 0\ \ x\ \ *\ ]^T$	$[\ 0\ \ 0\ \ *\ ]^T$	$[\ 0\ \ 0\ \ 0\ ]^T$	9	337	426
V	$[\ 0\ \ 0\ \ 0\ ]^T$	$[\ 0\ \ x\ \ *\ ]^T$	$[\ 0\ \ 0\ \ 0\ ]^T$	$[\ 0\ \ 0\ \ *\ ]^T$	9	337	426
VI	$[\ 0\ \ 0\ \ 0\ ]^T$	$[\ 0\ \ x\ \ *\ ]^T$	$[\ 0\ \ 0\ \ 0\ ]^T$	$[\ 0\ \ 0\ \ 0\ ]^T$	10	329	416
VII	$[\ 0\ \ *\ \ 0\ ]^T$	$[\ 0\ \ x\ \ 0\ ]^T$	$[\ 0\ \ 0\ \ *\ ]^T$	$[\ 0\ \ 0\ \ 0\ ]^T$	9	333	422
VIII	$[\ 0\ \ *\ \ 0\ ]^T$	$[\ 0\ \ x\ \ 0\ ]^T$	$[\ 0\ \ 0\ \ 0\ ]^T$	$[\ 0\ \ 0\ \ *\ ]^T$	9	333	422
IX	$[\ 0\ \ *\ \ 0\ ]^T$	$[\ 0\ \ x\ \ 0\ ]^T$	$[\ 0\ \ 0\ \ 0\ ]^T$	$[\ 0\ \ 0\ \ 0\ ]^T$	10	325	412

x means variable of prismatic joint

$1 \sim 6$)), type VI (backward for prismatic and backward for parallel, Σ_{I_i} ($i = 1, 3 \sim 6$)) $\Sigma_{I'_i}$ ($i = 2$)), and type IX (backward for prismatic and backward for parallel, Σ_{I_i} ($i = 1 \sim 6$))) in the case of the Stanford type. The optimal frames are type VI for the PUMA type and type IX for the Stanford type. The choice of the frames where the set of $\boldsymbol{p}_i^*$ has the most number of zero elements would be reasonable from the evaluation result of the number of computations. If plural sets of ${}^{i-1}\boldsymbol{p}_i^*$ are obtained even at the step 4, like the case of the Stanford type, we should choose one set appropriately based on such an experience rule that we can choose a set which has nonzero elements in ${}^1\boldsymbol{p}_2^*$. **Figs.9.2** and **9.3** show the location of frame by Craig's assignment and the optimal assignment. Especially, it should be noted that the optimal assignment of the PUMA type cannot be obtained unless $\Sigma_{I'_i}$ are introduced.

9.5 Conclusion

In this chapter, the link coordinate frame assignment has been defined as four type of frames and the special management for parallel and prismatic joints are also defined exactly. It has been shown that the Craig's method and new assignment method like $\Sigma_{I'_i}$ are more efficient than D.H. assignment method. The concept of the optimal frame assignment has been proposed. The difference of the number of computations between Craig's method and the optimal method is not so large, but it would be effective when we want to reduce the number of computations as much as possible if the automatic assignment function is realized in the control system or simulator system.

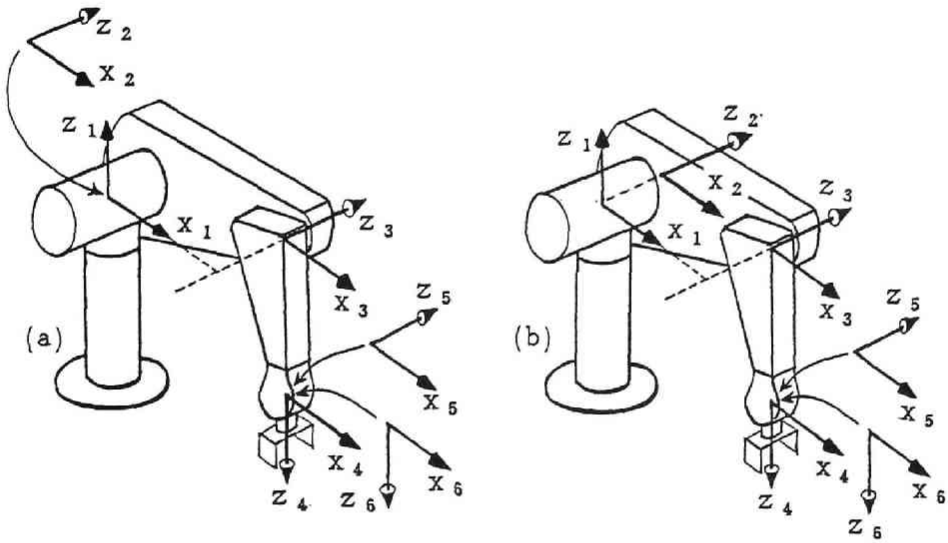

Figure 9.2: The Craig's assignment and the optimal assignment for the PUMA type manipulator:
(a) Craig's assignment (type I);
(b) Optimal assignment (type VI)

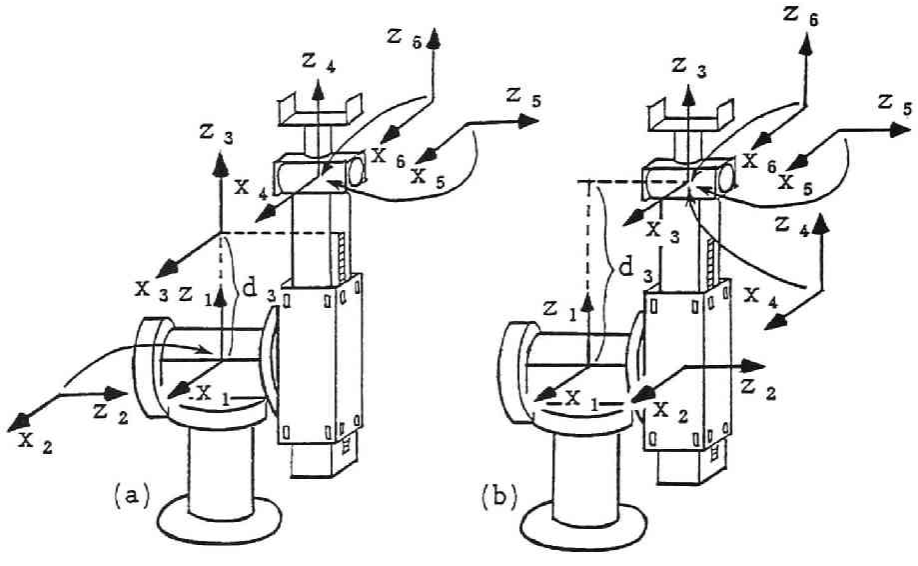

Figure 9.3: The Craig's assignment and the optimal assignment for the Stanford type manipulator:
(a) Craig's assignment (type I);
(b) Optimal assignment (type IX)

Chapter 10

CONCLUDING REMARKS

10.1 Results of this Paper

Teleoperation is an important technology at present and in the future. The use of master-slave bilateral servo manipulators is an effective way for teleoperation because the operator can maneuver the system intuitively with the help of force reflection. In this paper, analysis and design of the master-slave teleoperation system have been discussed.

In the first part, chapters 2 through 6, analysis and design of master-slave systems have been discussed in both a simple one degree-of-freedom (DOF) case and the multiple DOF case. We have shown that on-line compensation of the dynamics of both master and slave arms is necessary for improvement of the system maneuverability. Since no specific desired trajectory is given in advance in teleoperation, on-line compensation of dynamics is required. Concerning the multiple DOF case, the on-line compensation of arm dynamics becomes difficult because dynamics of multi-link mechanisms is complex.

From the viewpoint of the mechanism, master and slave arms are equivalent to robot manipulators. Therefore, efficient computations of manipulator kinematics and dynamics for trajectory control have been discussed in the second part, chapters 7 through 9. Efficient computational algorithms of the robot manipulator, real time computation using DSP and efficient link frame assignments have been discussed. And these results are applicable to the on-line compensation of arm

dynamics in master-slave teleoperation, where no specific desired trajectory is given in advance.

In chapter 2, a simple one degree of freedom system model of the master-slave system has been discussed where both the operator and object dynamics have been considered. Three ideal responses have been defined and the conditions to achieve these ideal responses have been derived. It has been shown that acceleration signals must be used in the control schemes in order to realize the ideal responses. A quantitative performance index has been given based on the concept of ideal responses. It becomes possible to evaluate the performance of system maneuverability quantitatively using the results obtained in this chapter. It would also be a design guide for new control schemes to provide good maneuverability.

In chapter 3, new control schemes for master-slave manipulators have been proposed which can realize the three ideal responses previously defined. These control schemes compensate for the arm dynamics using acceleration signals. Especially, the control scheme that can achieve the ideal response III provides the ideal kinesthetic coupling. It has been shown that, when the proposed control scheme is applied, the system stability is guaranteed in a wider range of operators and objects than in linear systems, based on the concept of network passivity.

In chapter 4, we have proposed a measure for the manipulability of master arms considering operator dynamics by extending the concept of the dynamic manipulability. We have considered the dynamic manipulability of the operator himself without a load as a standard for evaluating the manipulability of master arms. We have also proposed a new index of similarity between the manipulability ellipsoid of the master arm and the dynamic manipulability ellipsoid of operators. We have pointed out that the relative position of the master arm to the operator is an important factor for evaluating the manipulability of master arms as well as the arm design itself.

In chapter 5, the concept of an ideal kinesthetic coupling has been extended to the multiple DOF case. Control schemes which are applicable to different configuration arms have been proposed. Then, control schemes which are applicable only to isomorphic configuration arms have been proposed. Design guides of master and slave arms from various viewpoints have been discussed.

In chapter 6, we designed experimental 3 DOF arms with direct-drive motors based on the design guides shown in chapters 4 and 5. A master-slave system was constructed for the experiments by using the designed arms and a 32-bit personal computer. The validity of the control schemes proposed in chapter 3 for realizing the ideal responses was confirmed experimentally.

In chapter 7, a unified recursive formulation for direct kinematics, inverse kinematics and inverse dynamics has been proposed. The computational complexity of the dynamic control of robot manipulators was reduced by eliminating the duplicated computations in the algorithms. The reduction of the computation shown in this chapter was realized without customizing algorithms.

In chapter 8, the resolved acceleration control using the unified computation was implemented on a floating-point DSP. Execution time was evaluated as 1 msec for 6 DOF general manipulators, which would be a sufficient performance for real time computation.

In chapter 9, the method of link coordinate frame assignment has been defined more generally in order to improve the computational efficiency of kinematics and dynamics. It has also been shown that the new assignment methods are more efficient than the conventional assignment methods. The concept for an optimal frame assignment has been proposed.

The author believes that the results obtained in this paper will contribute to the improvement of the maneuverability of master-slave teleoperation systems and also be useful for telerobot systems in the future.

10.2 Further Problems

Before concluding this paper, we will mention several further problems concerned with teleoperation. The problem that should be mentioned first is the experiment in the multiple DOF case. We cannot practically show the effectiveness of the result in the second part of this paper till we complete the experiment with a multiple DOF master-slave system.

As the next problem, we have to confirm the validity of the proposed evaluation of maneuverability by comparing the quantitative in-

dex with the practical operation feeling in experiments. Of course, the motivation of this study comes from the fact that the evaluation of the practical operation feeling is difficult. And, certainly, the proposed index can evaluate the maneuverability quantitatively based on the idea that an exact replica of the remote side signals would be the most beneficial for the operator. However, if we could find a correlation between the proposed index and the easiness of practical operations, we could prove the validity of the proposed index more.

Another problem is the study of the mechanism of kinesthetic sensations of humans. In this paper, we assumed that an exact replica of the remote side signals would be the most realistic for the operator. However, there is the possibility that the operator could feel *more realistic* and perform the task more efficiently by modifying the signals through the study of the mechanism of human perception, especially kinesthetic sensation. This approach is also important to cope with the limitation of transmission capacity between the master and slave sites or the limitation of actuator capacity of the master arm.

The problem in the future is the addition of autonomy to the slave arm, that is, *telerobotization* of teleoperation systems. The most important point of the master-slave system is its intuitiveness of operation. It is important to keep this intuitiveness when we add autonomy to the system. In the field of computers, GUI (Graphical User Interface) has already become a standard of the man/machine interface, where the operator can intuitively command the computer through a graphic display that imitates a "desk-top". It would be desirable to extend this kind of concept to the telerobot systems. For example, if a repeat motion such as grinding is required, teaching a motion confirming reaction force by a master-slave system would be more intuitive than commanding the motion numerically by a program. Highly maneuverable master-slave systems would play a significant role in this situation.

Last problem to be mentioned is time delay. When the spatial distance becomes large between the master side and the slave side, time delay of the signal transmission cannot be neglected. In the case of teleoperation of robots on the satellite orbit from the ground, the time delay becomes 0.5~2.0 seconds. Communication with exploration robots on another planet such as Mars, takes several minutes or several hours or more. Noyes and Sheridan[66] considered the time delay problem

and developed the predictive display which shows the predicted motion of the slave arm to the operator according to the command from the operator. Conway et al.[16] proposed several concepts such as "time and position clutches", "time ratio control" and "time brakes" as a tele-autonomous system architecture in the presence of time delay. On the other hand, Anderson[4, 5] proposed a new bilateral control scheme which maintains stability even though there is a time delay. However, it is obvious that conventional master-slave teleoperation is of no use when the degree of time delay becomes large. The only way would be to send autonomous robots and supervise them or building a virtual environment at the master side and sending the command obtained from the interaction with this virtual environment.

Development of fully autonomous robots is one of the goals of robotics. However, this approach seems to alienate humans from robots. We believe that the approach of telerobotics from teleoperation can be another goal of robotics aimed at the cooperation and coexistence between humans and robots.

Bibliography

[1] Advanced Robot Technology Research Association,"ADVANCED ROBOT TECHNOLOGY", Report of Large-scale National R & D Project promoted by the Agency of Industrial Science and Technology, Ministry of International Trade and Industry, Japan (1990) (*in Japanese*)

[2] K. Akazawa et al.,"Development of new actuator modeled on mechanical properties of muscles", In *Proceedings, The 24th SICE Annual Conference*, pp.895–896 (1985) (*in Japanese*)

[3] C.H.An et al.,"Experimental Evaluation of Feedforward and Computed Torque Control", In *Proceedings, IEEE International Conference on Robotics and Automation*, pp.165–168 (1987)

[4] R. J. Anderson and M. W. Spong,"Bilateral Control of Teleoperators with Time Delay", IEEE Trans. on Automatic Control, **Vol.34**, No.5, pp.494–501 (1989)

[5] R.J.Anderson and M.W.Spong,"Asymptotic Stability for Force Reflecting Teleoperators with Time Delay", In *Proceedings, IEEE International Conference on Robotics and Automation*, pp.1618–1625 (1989)

[6] T.Arai et al., "Advanced Teleoperation with Configuration Differing Bilateral Master-Slave System," In *Robotics Research The Fourth International Symposium*, pp.163–170, The MIT Press, 1988.

[7] H.Asada, "A Geometrical Representation of Manipulator Dynamics and Its Application to Arm Design", ASME J. Dyn. Sys. Meas. Cont., **Vol.105**, No.3, pp.131–135 (1983)

[8] H.Asada and K.Ogawa, "On the Dynamic Analysis of a Manipulator and Its End Effector Interacting with the Environment", *Proceedings, IEEE International Conference on Robotics and Automation*, pp.751–756 (1987)

[9] C.G.Atkeson, C.H.An and J.M.Hollerbach, "Estimation of Inertial Parameters of Manipulator Loads and Links", International Journal of Robotics Research, **Vol.5**, No.3, pp.101–119 (1986)

[10] C.A.Balafoutis et al.,"Efficient Modeling and Computation of Manipulator Dynamics Using Orthogonal Cartesian Tensors, IEEE Journal of Robotics and Automation, **Vol.4**, No.6, pp.665–676 (1988)

[11] A.K.Bejczy and J.K.Salisbury, "Kinesthetic Coupling Between Operator and Remote Manipulator", In *Proceedings, ASME Computer Technology Conf.*, **Vol. 1**, pp.12–15 (1980)

[12] A.K.Bejczy and M.Handlykken, "Generalization of Bilateral Force-Reflecting Control of Manipulators", In *Proceedings, 4th Ro.man.sy.*,p.242 (1981)

[13] M.Brady et al. ed., "Robot Motion: Planning and Control", MIT Press, (1982)

[14] J.R.Burnett, "Force-Reflecting Servos Add "Feel" to Remote Controls", *Control Engineering*, **Vol.4**, No.7, pp.1269–1274, (1957)

[15] J.E.Colgate and N.Hogan,"Robust Control of Dynamically Interacting Systems", Int. J. Control, **Vol.48**, No.1, pp.65–88 (1988)

[16] L.Conway et al., "Tele-Autonomous Systems: Methods and Architectures for Intermingling Autonomous and Telerobotic Technology, In *Proceedings, IEEE International Conference on Robotics and Automation*, pp.1121–1130 (1987)

[17] J.J.Craig, "Introduction to Robotics", Addison-Wisely, (1986)

[18] J.Denavit and R.S.Hartenberg, "A Kinematic Notation for Lower-Pair Mechanisms Based on Matrices", ASME Journal of Applied Mechanics, **Vol.22**, No.6, pp.215–221 (1955)

[19] J.Dudragne et al., "A Generalized Bilateral Control Applied to Master-Slave Manipulators", In *Proceedings, 20th ISIR*, pp.435–442 (1989)

[20] W.R.Ferrell and T.B.Sheridan, "Supervisory Control of Remote Manipulation", IEEE Spectrum, **Vol.4**, No.10, pp.81–88 (1967)

[21] S.Fujii et al.,"Adaptive Control for Master-Slave Robot Manipulators", In *Proceedings, Japan-USA Symposium on Flexible Automation*, pp.609–616 (1990)

[22] T.Fukuda et al.,"A Study on Bilateral Control of Micro Manipulator", In *Proceedings, The 25th SICE Annual Conference*, pp.715–716, (1986) (*in Japanese*)

[23] K.Furuta et al., "Master-Slave Manipulator Based on Virtual Internal Model Following Control Concept", In *Proceedings, IEEE International Conference on Robotics and Automation*, pp.567–572 (1987)

[24] R.C.Geortz, "Fundamentals of General-Purpose Remote Manipulators", Nucleonics, **Vol.10**, No.11, pp.36–42 (1952)

[25] R.C.Geortz and F.Bevilacqua, "A Force-Reflecting Positional Servomechanism", Nucleonics, **Vol.10**, No.11, pp.43–45 (1952)

[26] R.C.Geortz, "Mechanical Master-Slave Manipulator", Nucleonics, **Vol.12**, No.11, pp.45–46 (1954)

[27] R.C.Geortz and W.M.Thompson, "Electronically Controlled Manipulator", Nucleonics, **Vol.12**, No.11, pp.46–47 (1954)

[28] R.C.Geortz et al., "The ANL Model-3 Master-Slave Electric Manipulator –Its Design and Use in A Cave", In *Proceedings, The*

9th Conference on Hot Laboratories and Equipment, pp.121–142 (1961)

[29] R.C.Geortz, "Manipulator Systems Developed at ANL", In *Proceedings, The 12th Conference on Remote Systems Technology*, pp.117–136 (1964)

[30] R.C.Geortz et al., "ANL Mark E4A Electric Master-Slave Manipulator", In *Proceedings, The 14th Conference on Remote Systems Technology*, pp.115–123 (1966)

[31] E.G.Gilbert and I.J.Ha, "An Approach to Nonlinear Feedback Control with Application to Robotics", IEEE Trans. Systems, Man, and Cybernetics, **Vol.SMC-14**, No.6, pp.879–884 (1984)

[32] M.Handlykken and T.Turner,"Control System Analysis and Synthesis for a Six Degree-of-Freedom Universal Force-Reflecting Hand Controller", In *Proceedings, IEEE International Conference on Decision and Control*, pp.1197–1205 (1980)

[33] B.Hannaford and R.Anderson,"Experimental and Simulation Studies of Hard Contact in Force Reflecting Teleoperation", In *Proceedings, IEEE International Conference on Robotics and Automation*, pp.584–589 (1988)

[34] B.Hannaford,"Stability and Performance Tradeoffs in Bi-Lateral Telemanipulation", In *Proceedings, IEEE International Conference on Robotics and Automation*, pp.1764–1767 (1989)

[35] B.Hannaford,"A Design Framework for Teleoperators with Kinesthetic Feedback", IEEE Journal of Robotics and Automation, **Vol.5**, No.4, pp.426–434 (1989)

[36] K.Hashimoto and H.Kimura, "A New Parallel Algorithm for Inverse Dynamics", The International Journal of Robotics Research, **Vol.8**, No.1, pp.63–76 (1989)

[37] J.D.Hightower and D.C.Smith, "Teleoperator Technology Development", In *Proceedings, 12th Meeting of UJNR/MFP*, pp.43–47 (1983)

[38] S.Hirai and T.Sato, "Direct-drive Master-Manipulator: Design Principles and Characteristics", J. of Robotics Society of Japan, **Vol.5**, No.1, pp.14–18 (1987) (*In Japanese*)

[39] N.Hogan, "Impedance Control : An Approach to Manipulation : Part II Implementation", ASME J. Dyn. Sys. Meas. Cont., **Vol.107**, No.1, pp.8–16 (1985)

[40] J.M.Hollerbach, "A Recursive Lagrangian Formulation of Manipulator Dynamics and a Comparative Study of Dynamics Formulation Complexity", IEEE Trans. Systems, Man, and Cybernetics, **Vol.SMC-10**, No.11, pp.730–736 (1980)

[41] J.M.Hollerbach and G.Sahar, "Wrist-Partitioned Inverse Kinematic Accelerations and Manipulator Dynamics, The International Journal of Robotics Research, **Vol.2**, No.4, pp.61–76 (1983)

[42] B.K.P.Horn and M.H.Raibert, "Configuration Space Control, Industrial Robot, June, pp.69–73 (1978)

[43] Inoue et al., "6-axis Bilateral Control of an Articulated Manipulator Using a Cartesian Master Arm, J. of Robotics Society of Japan, **Vol.6**, No.1, pp.75–82 (1988) (*In Japanese*)

[44] K.Ioi and K.Nakashima, "Design and Development of Master-arm with Homogeneous Mass of Inertia Tensor for Any Direction", Trans. of JMSE (Part C), **Vol.55**, No.509, pp.222–226 (1989) (*In Japanese*)

[45] E.G.Johnsen and W.R.Coliss, "Teleoperators and Human Argumentation", An AEC-NASA Technology Survey, NASA SP-5047, (1967)

[46] M.E.Kahn, "The Near-Minimum-Time Control of Open-Loop Articulated Kinematic Chains", Stanford Artificial Intelligence Laboratory, AIM 106, December (1969)

[47] T.Kanade, P.K.Khosla and N.Tanaka, "Real Time Control of CMU Direct-Drive Arm II Using Customized Inverse Dynamics", In *Proceedings, The 23rd IEEE Conference on Decision and Control*, pp.1345–1352, (1984)

[48] H.Kasahara and S.Narita, "Parallel Processing of Robot Arm Control Computation on a Multi-microprocessor System", IEEE Journal of Robotics and Automation, **Vol.1**, No.2 (1985)

[49] H.Kazerooni et al.,"Telefunctioning: An Approach to Telerobotic Manipulations", In *Proceedings, American Control Conference*, pp.2778–2783 (1990)

[50] H.Kawasaki and K.Nishimura, "Parameter Identification of Robot Manipulators", Trans. SICE, **Vol.22**, No.1, pp.76–83 (1986) (*In Japanese*)

[51] W.Khalil and C.Chevallereau, "An Efficient Algorithm for the Dynamic Control of Robots in the Cartesian Space", In *Proceedings, The 26th IEEE Conference on Decision and Control*, pp.582–588, (1987)

[52] P.K.Khosla and T.Kanade, "Experimental Evaluation of Nonlinear Feedback and Feedforward Control Schemes for Manipulators", The International Journal of Robotics Research, **Vol.7**, No.1, pp.18–28 (1988)

[53] T.Koga,"Transmission Networks", Corona Co.Ltd. (1978) (*in Japanese*)

[54] J.Y.S.Luh, M.W.Walker and R.P.C.Paul, "On-Line Computational Scheme for Mechanical Manipulators", ASME Journal of Dynamic Systems, Measurement and Control, **Vol.102**, pp.69–76 (1980)

[55] J.Y.S.Luh, M.W.Walker and R.P.C.Paul, "Resolved Acceleration Control of Mechanical Manipulators", IEEE Trans. Automatic Control, **Vol.AC-25**, No.3, pp.468–474 (1980)

[56] J.Y.S.Luh and C.S.Lin, "Scheduling of Parallel Computation for a Computer Controlled Mechanical Manipulator", IEEE Trans. Systems, Man, and Cybernetics, **Vol.SMC-12**, No.2, pp.214–234 (1982)

[57] H.Mayeda, K.Kusamoto and k.Ohashi, "Robot Controller with Digital Signal Processor for the Resolved-Acceleration Control", In *Proceedings, USA-Japan Symposium on Flexible Automation*, pp.147–152, (1988)

[58] F.Miyazaki et al.,"A New Control Methodology Toward Advanced Teleoperation of Master-Slave Robot System", In *Proceedings, IEEE International Conference on Robotics and Automation*, pp.997–1002 (1986)

[59] T.Miyasaki and S.Hagiwara,"Development of a 6 D.O.F. Kinematically Different Master-Slave Servomanipulator System with Stereoscopic Television System", In *Proceedings, USA-Japan Symposium on Flexible Automation*, pp.425–431 (1988)

[60] T.N.Mudge and J.L.Turney, "Unifying Robot Arm Control, IEEE Trans. Industry and Application, **Vol.IA-20**, No.6, pp.1554–1563 (1984)

[61] Y.Nakamura, "A Necessary and Sufficient Condition for Manipulation Force Applicability of Robot Manipulators", Journal of Robotics Society of Japan, **Vol.4**, pp.3–9 (1986) (*in Japanese*)

[62] Y.Nakamura and H.Hanafusa, "Task Priority Based Redundancy Control of Robot Manipulators", Robotics Research: The Second International Symposium, MIT Press, Cambridge Mass, pp.155–162, (1985)

[63] Y.Nakamura and H.Hanafusa, "Inverse Kinematic Solutions with Singularity Robustness for Robot Manipulator Control", Robotics and Manufacturing Automation (PED-Vol.15), ASME, New York, pp.193–204 (1985)

[64] A.Nagai and K.Matsushima, "On the Remote Mini Manipulator –Control of Its Arm and Gripper–", Trans. SICE, **Vol.16**, No.1, pp.91–97 (1980) (*In Japanese*)

[65] NEC Co., "μPD77230 User's Manual", (1985) (*in Japanese*)

[66] M.Noyes and T.B.Sheridan, "A Novel Predictor for Telemanipulation through a Time Delay", In *Proceedings, 20th Annual Conference on Manual Control* (1984)

[67] D.E.Orin and W.W.Schrader, "Efficient Computation of the Jacobian for Robot Manipulators, International Journal of Robotics Research, **Vol.3**, No.4, pp.66–75 (1984)

[68] K.Osuka et al., "PD-Type Two-Stage Robust Tracking Control for Robot Manipulators", In *Proceedings, USA–Japan Symposium on Flexible Automation*, pp.153–160 (1988)

[69] R.P.C.Paul, "Robot Manipulators: Mathematics, Programming and Control", MIT Press, (1981)

[70] R.P.C.Paul, "Manipulator Cartesian Path Control", IEEE Trans. on Systems, Man, and Cybernetics, **Vol.SMC-9**, pp.702-711 (1979)

[71] D.L.Pieper, "The Kinematics of Manipulators under Computer Control", Ph.D. Thesis, Department of Computer Science, Stanford University (1968)

[72] G.J.Raju,"Operator Adjustable Impedance in Bilateral Remote Manipulation", Ph.D. Thesis, Man-Machine Systems Laboratory, MIT (1988)

[73] G.J.Raju,"Design Issues in 2-port Network Models of Bilateral Remote Manipulation", In *Proceedings, IEEE International Conference on Robotics and Automation*, pp.1316–1321 (1989)

[74] G.J.Raju,"An Experiment in Bilateral Manipulation with Adjustable Impedance", In *Proceedings, Japan-USA Symposium on Flexible Automation*, pp.395–399 (1990)

[75] M.Renaud, "Quasi-Minimal Computation of the Dynamic Model of a Robot Manipulators Utilizing the Newton-Euler Formulations and the Notion of Augmented Body, In *Proceedings, IEEE International Conference on Robotics and Automation*, pp.1677–1682 (1987)

[76] T.Sato and S.Hirai, "MEISTER: A Model Enhanced Intelligent and Skillful Teleoperational Robot System", Robotics Research –The Fourth International Symposium–, The MIT Press, pp.155–162 (1988)

[77] T.B.Sheridan,"Telerobotics", In *Proceedings, The 10th IFAC World Congress on Automatic Control*, pp.103–717 (1987)

[78] W.M.Silver, "On the Equivalence of Lagrangian and Newton-Euler Dynamics for Manipulators", The International Journal of Robotics Research, **Vol.1**, No.2, pp.60–70 (1982)

[79] S.Tachi et al., "Tele-existence (I): Design and Evaluation of A Visual Display with Sensation of Presence", In *Proceedings, 5th International Symposium on Theory and Practice of Robots and Manipulators (CISM-IFToMM RoManSy '84)*, pp.245–254 (1984)

[80] S.Tachi and H.Arai., "Study on Tele-existence (II): Three-dimensional Color Display with Sensation pf Presence", In *Proceedings, '85 International Conference on Advanced Robotics (ICAR'85)*, pp.345–352 (1985)

[81] S.Tachi and T.Sakaki, "Impedance Controlled Master Slave Manipulation System –Part I: Basic Concept and Application to the System with Time Delay", J. of Robotics Society of Japan, **Vol.8**, No.3, pp.241–252 (1990) (*In Japanese*)

[82] N.Takanashi et al.,"A High-Sample-Rate Robot Control System Using a DSP Based Numerical Calculation Engine, In *Proceedings, IEEE International Conference on Systems, Man and Cybernetics*, pp.1168–1173 (1989)

[83] K.Takase, "Generalized Decomposition and Control of a Motion of a Manipulator", Trans. SICE, **Vol.12**, pp.62–68 (1976) (*in Japanese*)

[84] K.Takase, "Fundamental Mathematics for Manipulators –An Approach to Kinematics and Dynamics on the basis of Vector Notation–", Journal of Robotics Society of Japan, **Vol.1**, pp.131–138, 217/223 (1983) (*in Japanese*)

[85] R.H.Tayler, "Planning and Execution of Straight Line Manipulator Trajectories", IBM Journal of Research and Development, **Vol.23**, pp.424–436 (1979)

[86] M.Thomas and D.Tesar, "Dynamic Modeling of Serial Manipulator Arms, ASME J. pf D.S.M.C., **Vol.104**, pp.218–228 (1972)

[87] J.J.Uicker, "On the Dynamic Analysis of Spatial Linkages Using 4 by 4 Matrices", Ph.D. Thesis, Department of Mechanical Engineering and Astronautical Sciences, Northwestern University (1965)

[88] T.Yoshikawa, "Dynamic Manipulability of Robot Manipulators", In *Proceedings, IEEE International Conference on Robotics and Automation*, pp.1033–1038 (1985)

[89] T.Yoshikawa, "Dynamic Hybrid Position/Force Control of Robot Manipulators –Description of Hand Constraints and Calculation of Joint Driving Force", Journal of the Robotics Society of Japan, **Vol.3**, pp.531–537 (1985) (*in Japanese*)

[90] L.T.Wang and B.Ravani, "Recursive Computations of Kinematic and Dynamic Equations for Mechanical Manipulators, IEEE J. of Robotics and Automation, **Vol.RA-1**, No.3, pp.124–131 (1985)

[91] D.E.Whitney, "Resolved Motion Rate Control of Manipulators and Human Prostheses", IEEE Trans. Man-Machine Systems, **Vol.MMS-10**, pp.47–53 (1969)

[92] D.E.Whitney, "The Mathematics of Coordinated Control of Prostheses and Manipulators", ASME Journal of Dynamic Systems, Measurement, and Control, **Vol.94**, pp.303–309 (1972)

Published Papers by the Author

Chapter 2:

T.Yoshikawa and Y.Yokokohji, "Analysis of Maneuverability and Stability for Master-Slave System", In *Proceedings, USA–Japan Symposium on Flexible Automation*, pp.433–440 (1988)

Y.Yokokohji and T.Yoshikawa, "Control of Master-Slave Manipulators for Object Teleperception", In *Preprints, 5th International Symposium of Robotics Research*, pp.17–24 (1989)

Y.Yokokohji and T.Yoshikawa, "Maneuverability of Master-Slave Telemanipulation Systems", Trans SICE, **Vol.26**, No.5, pp.572–579, (1990) (*In Japanese*)

Chapter 3:

Y.Yokokohji and T.Yoshikawa, "Bilateral Control of Master-Slave Manipulators for Ideal Kinesthetic Coupling", Trans SICE, **Vol.27**, No.1, pp.56–63 (1991) (*In Japanese*)

Chapter 4:

Y.Yokokohji and T.Yoshikawa, "Manipulability of master arms considering operator dynamics", Trans SICE, **Vol.26**, No.7, pp.818–825 (1990) (*In Japanese*)

Y.Yokokohji and T.Yoshikawa, "Manipulability of master arms considering operator dynamics", In *Proceedings of the 1990 Japan-U.S.A. Symposium on Flexible Automation –A Pacific Rim Conference–*, pp.35–40, July 9–13, 1990, Kyoto, JAPAN

Chapter 5:

Y.Yokokohji and T.Yoshikawa,"Bilateral Control of Master-Slave Manipulators for Ideal Kinesthetic Coupling", In *Proceedings of IEEE International Workshop on Intelligent Robots and Systems '90: IROS'90*, pp.355–362, July 3–6, 1990, Tsuchiura, Ibaraki, JAPAN

Chapter 7:

Y.Nakamura, H.Hanafusa, Y.Yokokohji and T.Yoshikawa, "Efficient Computation and Kinematic Representation for Robot Manipulator Simulation, In *Proceedings, The 15th ISIR*, pp.1059–1066 (1985)

Y.Nakamura, Y.Yokokohji, H.Hanafusa and T.Yoshikawa, "Unified Recursive Formulation of Kinematics and Dynamics of Robot Manipulators", In *Proceedings, Japan-USA Symposium on Flexible Automation*, pp.53–60 (1986)

Y.Nakamura, Y.Yokokohji, H.Hanafusa and T.Yoshikawa, "Unified Com-

putation of Kinematics and Dynamics of Robot Manipulators", Trans SICE, **Vol.23**, No.5, pp.71–78 (1987) (*In Japanese*)

Chapter 8:

T.Yoshikawa, Y.Nakamura and Y.Yokokohji, "Application of DSP to Real Time Computation for Dynamic Control of Robot Manipulators", Journal of the Robotics Society of Japan, **Vol.6**, No.3, pp.175–183 (1988) (*in Japanese*)

T.Yoshikawa, Y.Nakamura and Y.Yokokohji, "Application of DSP to Real Time Computation for Dynamic Control of Robot Manipulators", Advanced Robotics, **Vol.5** (*to appear*)

Chapter 9:

T.Yoshikawa and Y.Yokokohji, "On a Link Coordinate Frame Assignment for Serial Link Robot Manipulators", Trans SICE, **Vol.24**, No.12, pp.1343–1345 (1988) (*In Japanese*)